THE UNIVERSITY
of EDINBURGH

Investigating macrophage heterogeneity and function during acute liver injury

Dyana Markose

Degree of Doctor of Philosophy

The University of Edinburgh

2020

Abstract

Acetaminophen-induced liver injury (AILI) is the leading cause of acute liver failure (ALF) in Western Europe and USA. In ALF patients the intrinsic regenerative capacity of the liver is overwhelmed by massive hepatocellular death. Current treatment for AILI is limited to *N*-Acetylcysteine (NAC), the therapeutic potential of NAC decreases dramatically during the later stages of AILI and liver transplantation becomes the sole option. More potent therapies which promote liver regeneration which negates the need for transplantation is urgently required. Previous studies in both humans and animal models have highlighted monocytes and macrophages are key regulators of liver regeneration following AILI, due to their dynamic nature during AILI their therapeutic manipulation has proven to be challenging. In this thesis, using a murine model of AILI, I show specific hepatic leucocytes populated the liver at distinct phases of AILI, at the time of maximal liver regeneration macrophages represented the most dominant subset in the liver. Phenotypic characterisation of the three distinct macrophages populations: Kupffer cells (KCs), Ly6C^{Hi} monocytes and Ly6C^{Lo} monocyte derived macrophages (MDMs) indicated injury induced heterogeneity, particularly in the Ly6C^{Lo} MDMs.

Droplet-based single cell RNA sequencing (scRNA-seq) was employed to interrogate monocyte and macrophage heterogeneity during liver regeneration, in an unbiased manner. Unsupervised clustering of mononuclear phagocytes from uninjured and post-AILI livers generated four distinct injury specific monocyte/MDM clusters. Gene ontology enrichment analysis indicated distinct functional roles for each cluster. Using newly identified marker genes, the heterogeneity within the Ly6C^{Lo} MDMs was validated in wild type and macrophage reporter mice. During maximal liver regeneration two distinct Ly6C^{Lo} MDMs populated the liver, they were defined as: CD63+ MHCII- and CD63- MHCII- MDMs. Identification of CD63+ MHCII- and CD63- MHCII- MDMs in the liver following CCl_4 but not partial hepatectomy suggested it is an inflammation-induced phenotype. Experiments in CCR2 deficient mice

indicated both macrophage subsets are a progeny of bone-marrow derived circulating monocytes. Localization of CD63+ macrophages to areas of resolving liver necrosis, adjacent to proliferating hepatocytes and their increased phagocytic capacity suggested a pro-repair role for CD63+ MHCII- MDMs.

Additionally, scRNA-seq of circulating monocytes indicated AILI resulted in transcriptional pre-programming of circulating monocytes into an inflammatory phenotype, prior to their entry into the liver. These results support the notion that both circulating and hepatic monocytes and macrophages are highly dynamic and utilization of scRNA-seq in combination with traditional techniques such as flow cytometry and immunohistochemistry has facilitated the delineation of macrophage heterogeneity during liver regeneration. Further studies in mouse models and in humans are required to investigate the functional significance of these cells *in vivo*.

Lay Summary

The liver has an exceptional capacity to regenerate after various different injuries such as alcohol, drugs, and viruses. However, following overwhelming injury the regenerative capacity of the liver is diminished resulting in liver failure and if left untreated this can cause death. This is often seen in the case of acetaminophen (APAP) poisoning. APAP is an over the counter drug, commonly taken as a pain killer and in western countries like the UK, APAP poisoning is the commonest cause of acute (sudden and unexpected) liver failure. Past research in the field has shown macrophages can promote both liver regeneration and liver failure after APAP poisoning. However, we have not been able to identify which specific type of macrophage can help the liver regenerate and which type contribute to liver failure. This is because macrophages are like chameleons, their appearance (phenotype) and function are influenced by their environment. The aim of my research is to pinpoint the macrophage subset that drive live regeneration and understand the mechanism behind this process in order to manipulate these cells as a treatment for patients suffering from APAP poisoning.

By the time patients are admitted to the hospital from APAP poisoning, their liver has already began shutting down and the high degree of cell death makes it difficult to study macrophages in humans. For this reason, I used a mouse model, where I controlled the timing and dose of APAP and took out macrophages from the liver when there is less death and more repair to study their genetic-make up. Genes make proteins and proteins defines what a macrophage looks like, where they go, and what they do. To do this, I used a method called single cell RNA sequencing (scRNA-seq), this allowed me to study the hundreds and thousands of genes a single macrophage is expressing and then do this for thousands of macrophages. By doing this I was able to find a specific type of macrophage, that populated the liver at the time of repair, with the ability to eat dead cells. Using genetically modified mice, with fluorescent macrophages, I saw that these macrophages were infiltrating

the liver from the blood stream, to localise specifically to the areas of death, neighbouring regenerating liver cells.

To summarise, a specific type of macrophage involved in clearing up dead cells was found in the liver at the time of repair. Future studies are needed to see how important these cells are and whether they help the liver repair by clearing up dead liver cells, paving the way for new liver cells to grow. These findings will allow us to develop macrophage-based cell treatments for patients suffering from liver failure.

Signed Declaration

I declare that this thesis has been composed solely by myself and that it has not been submitted, in whole or in part, in any previous application for a degree. The work presented is entirely my own, some experiments were carried out in collaboration with colleagues in my research group. Where this is the case, I have acknowledged it in text.

.....

Dyana Markose

Acknowledgements

This thesis came to reality with help and support from many individuals and I express my sincerest gratitude to each and every one of them. Firstly, I would like to thank my supervisors Prof. Neil Henderson and Prof. Jeffery Pollard, for their advice and support throughout this project. To my primary supervisor Neil, who welcomed me into his research group and introduced me to the world of single cell- I thank you for your endless inspiration and encouragement for the past four years. Many thanks to my secondary supervisor Jeff, for guiding me through the project with his wealth of knowledge on macrophages. A special mention to Dr. Prakash Ramachandran for his mentorship and constant support with experimental design and troubleshooting which has been instrumental to my progression.

I would like to thank all past and present members of the Henderson and Pollard research groups for their advice and assistance. In particular John Wilson Kanamori, without his bioinformatic expertise this project would not have been possible. Thanks also to Kylie Conroy, Ross Dobie, Elena Dora, Stephen Greenhalgh, Beth Henderson, Laura Kitto, Prasad Palani Velu and Jordan Portman all of whom have been ever so supportive and provided me with: technical assistance, much needed comic relief, intellectual and not so intellectual discussions and plenty of baked goods to get me through the hardships of the PhD.

Thanks to the support and guidance provided by the QMRI Flow Cytometry and Cell Sorting Facility staff Shonna Johnston, Will Ramsay and Mari Pattison, who have taken the time to not only assist but also teach me. A huge thank you to Jon Henderson, who goes above and beyond what he is asked off to care for our animals and to provide technical assistance.

I would like to acknowledge the Medical Research Council for the financial support towards pursuing this PhD, thank you to the Tissue Repair PhD programme directors and organisers for giving me the invaluable opportunity

to learn from experts, advance my education and contribute to the wider scientific community.

I am grateful to all my friends for their moral support. Namely, Lizzie Reynolds and Yasrab Raza, my oldest friends who saw me through nine years of University, even from a distance. Thanks to Isabel Bravo, Luke Way, Lisa Kelly, Nikolay Ogryzko, David Taggart, Ross Mills, Natasha Gibson, Lucy Remnant, Ollie Kay and Sash Kay for making me feel at home in Edinburgh.

Finally, I am extremely grateful to my parents and my brother, all my achievements are the result of the sacrifices made by them and for that I dedicate this thesis to you.

Abbreviations

ACLF	acute on chronic failure
ADGRE	adhesion G protein-coupled receptors, subfamily E
AILI	acetaminophen induced liver injury
ALF	acute liver failure
ALT	alanine aminotransferase
APAP	acetaminophen
APC	antigen presenting cell
AST	aspartate aminotransferase
ATP	adenosine triphosphate
BM	bone marrow
C	caudate
CCL2	C-C motif chemokine ligand 2
CCl4	carbon tetrachloride
CCR2	C-C chemokine receptor type 2
cDC	conventional DC
cDNA	complementary DNA
CDP	common dendritic cell precursor
CLEC4F	C-type lectin domain family 4 member F
cMoP	common monocyte precursor
CMP	common myeloid precursor
CSF1	colony stimulating factor 1
CSF1R	colony stimulating factor 1 receptor
CX3CR1	CX3C chemokine receptor 1
CXCL2	C-X-C motif chemokine ligand 2
CXCR2	C-X-C chemokine receptor type 2
CYP2E1	cytochrome P450 isoform 2E1
DAMP	damage associated molecular pattern
DAM	damage-associated microglia
DAPI	4’,6-diamindino-2-phenylindole
DC	dendritic cell

DE	differentially-expressed
DNA	deoxyribonucleic acid
ECM	extracellular matrix
EGF	epidermal growth factor
eGFP	enhanced green fluorescent protein
EGFR	epidermal growth factor receptor
FACS	fluorescence-activated cell sorting
GAS6	growth arrest specific 6
gDNA	genomic DNA
GFP	green fluorescent protein
GLDH	glutamate dehydrogenase
GMP	granulocyte-monocyte precursor
GPNMB	glycoprotein nonmetastatic melanoma B
HGF	hepatocyte growth factor
HLA-DR	human leukocyte antigen – DR isotype
HMGB1	high-mobility group box 1
HNF4	hepatocyte nuclear transcription factor alpha
HSC	hepatic stellate cell
ICAM-1	intercellular adhesion molecule 1
IFN	interferon
IL	interleukin
IVC	inferior vena cava
KC	kupffer cell
KO	knockout
LL	left lateral
LPS	lipopolysaccharide
LSEC	liver sinusoidal endothelial cell
Ly6C	lymphocyte antigen 6 complex
MDM	monocyte-derived macrophage
MDP	monocyte-macrophage dendritic cell precursor
MerTK	MER proto-oncogene, tyrosine kinase
MHCII	major histocompatibility complex II

mitDNA	mitochondrial DNA
MP	mononuclear phagocyte
MPS	mononuclear phagocyte system
mRNA	messenger RNA
NAC	N-acetyl cysteine
NAFLD	non-alcoholic fatty liver disease
Nalp3	NACHT, LRR and PYD domains-containing protein 3
NAPQI	N-acetyl-p-benzoquinoneimine
NASH	non-alcoholic steatohepatitis
NF-κB	nuclear factor kappa light chain enhancer of activated B cells
NGS	next generation sequencing
NK	natural killer
NKT	natural killer T
NO	nitric oxide
NPC	non-parenchymal cell
pDC	plasmacytoid DC
PHx	partial hepatectomy
PRR	pattern recognition receptor
PtdSer	phosphatidylserine
RAGE	receptor for advanced glycation end products
RL	right lateral
RNA	ribonucleic acid
ROS	reactive oxygen species
RT	reverse transcription
ScRNA-seq	single cell RNA sequencing
SIRS	systemic inflammatory response syndrome
SLPI	secretory leucocyte protease inhibitor
STAT3	signal transducer and activator of transcription 3
T3	triodothronine
TF	transcription factor
TGF	transforming growth factor
TIMD4	T-cell immunoglobulin and mucin domain-containing protein 4

TLR	toll-like receptor
TNF	tumour necrosis factor
TNF-R1	tumour necrosis factor receptor 1
TRM	tissue resident macrophage
UMI	unique molecular identifier
VEGF	vascular endothelial growth factor

Table of Contents

Abstract ..... *i*

Lay Summary ..... *iii*

Signed Declaration ..... *v*

Acknowledgements ..... *vi*

Abbreviations ..... *viii*

Table of Contents ..... *xii*

List of Figures and Tables ..... *xv*

1 Introduction *1*

1.1 Liver disease - a global clinical burden **1**

1.2 Liver architecture **5**

1.3 Liver regeneration **7**

1.4 Models of acute liver injury and regeneration **7**

1.4.1 Partial hepatectomy (PHx) 8

1.4.2 Hepatotoxins to model liver regeneration and failure 11

1.4.3 Mechanisms of AILI 12

1.5 Factors influencing liver regeneration **14**

1.5.1 Growth factors and cytokines 14

1.5.2 Inflammation and Immune dysfunction 17

1.6 Liver as an immunological organ **19**

1.7 Role of immune cells during acute liver injury **21**

1.7.1 Lymphocytes 21

1.7.2 Granulocytes 23

1.7.3 Mononuclear phagocyte system 24

1.7.4 Role of MPs during acute liver injury and regeneration 36

1.8 Single-cell RNA sequencing **46**

1.8.1 Cell capture and mRNA extraction 46

1.8.2 cDNA amplification and library preparation 47

1.8.3 Sequencing 48

1.8.4 Data Analysis 48

1.8.5 Novel findings using scRNA-seq 49

1.8.6 Choice of single-cell RNA sequencing method to study heterogeneity 51

1.9 Hypothesis **54**

1.10 Aims and objectives **54**

2 Materials and Methods *55*

2.1 Mice **55**

2.2 Genotyping of genetically modified mice **55**

2.3 Murine models of liver regeneration 56
2.3.1 AILI 56
2.3.2 CCl_4 57
2.3.3 PHx 57
2.4 5-Ethynyl-2'-deoxyuridine (EdU) administration 58
2.5 Serum biochemistry 58
2.6 Hepatic non-parenchymal cell (NPC) isolation 58
Protocol 1 59
Protocol 2 60
2.7 Systemic leucocyte isolation and generation of single cell suspension 60
2.8 In vivo phagocytosis assay 61
2.9 *Ex vivo* PhagoGreen assay 61
2.10 Flow cytometry and fluorescence-activated cell sorting 62
2.10.1 Gating strategy 62
2.11 Tissue fixation and preparation 67
2.12 Immunofluorescence 67
2.12.1 HNF4α / EdU 68
2.12.2 F4/80 / EdU 68
2.12.3 CLEC4F / TIMD4 69
2.12.4 CD63 / MacGreen / EdU 69
2.12.5 IL7R / MacGreen / EdU 69
2.13 Histology staining 70
2.14 Image capture 71
2.15 Image quantification 71
2.16 Droplet-based scRNA-seq 72
2.17 Bioinformatics analysis of scRNA-seq data 76
2.17.1 Pre-processing 76
2.17.2 Dimensionality reduction, clustering, and DE analysis 76
2.17.3 Defining cell lineage signatures 77
2.17.4 Inferring pseudotemporal dynamics 78
2.18 Statistical Analysis 78
3 Characterisation of leucocyte dynamics during murine model of liver regeneration 79
3.1 Introduction 79
3.1.1 Aims 82
3.2 Results 83
3.2.1 Characterisation of hepatocyte death and proliferation during AILI 83
3.2.2 Hepatic leucocytes show a dynamic response during AILI 86
3.2.3 Ly6C^{Lo} MDMs represents the most expanded macrophage subset in the liver during maximal liver regeneration 90
3.2.4 Injury specific phenotypic changes indicate heterogeneity within the macrophage subsets during AILI 95

3.2.5 Systemic changes following AILI 97
3.2.6 Leucocyte dynamics following partial hepatectomy 101

3.3 Discussion 106

4 Single cell sequencing of mononuclear phagocytes cells during liver regeneration 113

4.1 Introduction 113
4.1.1 Aims 115

4.2 Results 116
4.2.1 Tissue digest optimisation 116
4.2.2 Methodology for scRNA-seq of hepatic and systemic leucocytes 120
4.2.3 Quality control and cell filtering post-sequencing 126
4.2.4 Unsupervised clustering of hepatic and systemic leucocytes 126
4.2.5 Annotation of leucocyte lineages in the scRNA-seq dataset 130
4.2.6 Investigating heterogeneity within the mononuclear phagocyte compartment 135
4.2.7 APAP induces transcriptional changes in the circulating monocyte compartment 143

4.3 Discussion 145

5 Validation of scRNA-seq results to identify injury specific monocyte and macrophage subsets during AILI 152

5.1 Introduction 152
5.1.1 Aims 154

5.2 Results 155
5.2.1 Validation of conventional dendritic cell clusters 155
5.2.2 Validation of kupffer cell clusters 159
5.2.3 Identification of phenotypic heterogeneity in the Ly6C^{Hi} monocytes during AILI 163
5.2.4 Identification of phenotypic heterogeneity within the Ly6CLo MDMs during AILI 167
5.2.5 Validation of Ly6C^{Lo} MDM heterogeneity using macrophage reporter mice 170
5.2.6 CD63+ MHCII- MDMs expand during the regenerative phase of the AILI 178
5.2.7 CD63+ MHCII- MDMs show enhanced phagocytic capacity 181
5.2.8 Origin of CD63+ MHCII- macrophages 184
5.2.9 Identification of Ly6C^{Lo} MDM heterogeneity in other models of acute liver injury 188

5.3 Discussion 191

6 Discussion 198

6.1 Future Work 207

7 Appendices 211

8 Bibliography 225

List of Figures and Tables

Figure 1.1 Standardised UK under-65 mortality rates (1970-2010) 3
Figure 1.2 Worldwide aetiologies of Acute Liver Failure (ALF) 4
Figure 1.3 Liver regeneration following partial hepatectomy (PHx) 10
Figure 1.4 Regulatory role of immune cells in the liver during homeostasis 20
Figure 1.5 Leucocyte involvement in the necroinflammatory phase of AILI 43
Figure 1.6 Leucocyte involvement in the repair phase of AILI 44
Figure 1.7 Old dogmas versus new insights on macrophages during murine models of liver injury 45
Figure 1.8 Characteristics of common single cell RNA sequencing methods 53

Figure 2.1 Schematic of 10X Chromium workflow 73
Figure 2.2 Schematic of reaction workflow inside the GEMs 74
Figure 2.3 Schematic of cDNA library construction 75

Figure 3.1 Assessment of liver injury following AILI 85
Figure 3.2 Assessment of hepatocyte proliferation following AILI 86
Figure 3.3 Flow cytometric characterization of the temporal dynamics of hepatic non-parenchymal cells following AILI 88
Figure 3.4 Changes in leucocyte numbers over the course of AILI 89
Figure 3.5 Analysis of the different subsets of macrophages during AILI 93
Figure 3.6 Kupffer cells following AILI do not disappear but localize to centrilobular areas of injury and repair 94
Figure 3.7 Injury specific phenotypic changes in macrophages following AILI 96
Figure 3.8 Changes in the circulating leucocytes following AILI 99
Figure 3.9 Changes in the circulating monocyte numbers and phenotype following AILI 100
Figure 3.10 Comparison of changes in hepatic leucocyte responses following PHx and AILI 103
Figure 3.11 Comparison of changes in hepatic macrophage responses following PHx and AILI 104

Figure 3.12 Comparison of changes in systemic leucocyte response following PHx and AILI 105

Figure 4.1 Liver digestion protocols for isolating NPCs 118
Figure 4.2 Optimisation of liver digestion protocols for scRNA-Seq 119
Figure 4.3 Methodology for scRNA-seq of hepatic and circulating leucocytes 122
Figure 4.4 Representative results from cDNA analysis for scRNA-seq samples 125
Figure 4.5 Cell filtering metrics used for quality control 128
Figure 4.6 Unsupervised clustering of hepatic and systemic leucocytes 129
Figure 4.7 Annotation of clusters based on gene signature analysis 132
Figure 4.8 Endothelial cluster with macrophage markers 133
Figure 4.9 Proportional changes and transcript metrics for leucocyte lineages 134
Figure 4.10 Unsupervised clustering of mononuclear phagocytes 137
Figure 4.11 Proportional changes and transcript metrics for mononuclear phagocyte lineages 138
Figure 4.12 Differential gene expression analysis of mononuclear phagocytes 141
Figure 4.13 Transcriptomic analysis of circulating monocytes 144

Figure 5.1 Methodology and gating strategy for flow cytometric validation of tissue MP clusters from scRNA-seq analysis 156
Figure 5.2 Identification of cDC1 cells in uninjured and APAP livers 157
Figure 5.3 Identification of cDC2 cells in uninjured and APAP livers 158
Figure 5.4 Identification of KCs and MDMs 161
Figure 5.5 Phenotypic characterisation of KCs 162
Figure 5.6 Identification of Ly6C^{Hi} monocytes and Ly6C^{Lo} MDMs in uninjured and APAP livers 164
Figure 5.7 Validating heterogeneity in the Ly6C^{Hi} monocytes in uninjured and APAP livers 166
Figure 5.8 Identification of two distinct subsets of Ly6C^{Lo} MDMs populating the liver during the repair phase of AILI 169
Figure 5.9 Validation of MDM clusters in MacGreen^{GFP} mice 172

Figure 5.10 Localization of CD63+ MDMs to repairing areas of the liver at 48hrs post-APAP 173
Figure 5.11 Localization of IL7R+ MDMs to repairing areas of the liver at 48hrs post-APAP 174
Figure 5.12 Validation of MDM clusters in CX3CR1$^{GFP/+}$ mice 175
Figure 5.13 Validation of CX3CR1$^{GFP/+}$ expression in CD63+ MDMs 176
Figure 5.14 Identification of CX3CR1+ CD63+ MDMs and CX3CR1- CD63+ MDMs in the regenerative niche of the liver at 48hrs post-APAP 177
Figure 5.15 Dynamics of CD63+ MHCII- and CD63- MHCII- MDMs during AILI 179
Figure 5.16 Phenotypic characterization of Ly6C^{Lo} MDMs 180
Figure 5.17 Optimisation of *ex vivo* phagocytosis assay 182
Figure 5.18 *In vivo* and *ex vivo* assessment of phagocytosis in macrophages 183
Figure 5.19 Computational analysis of differentiation trajectories in MP cluster via Velocyto 186
Figure 5.20 Assessing the origin to CD63+ MHCII- and CD63- MHCII- MDMs using CCR2 deficient mice 187
Figure 5.21 Characterizing the Ly6C^{Lo} MDM compartment on CD63 and MHCII expression in PHx and CCl_4 models of liver injury 190

Table 1.1 Ligands and receptors involved in efferocytosis 35
Table 2.1 Primer sequences used for genotyping of CCR2-/- mice 56
Table 2.2 Antibodies used for flow cytometry and FACS 65
Table 2.3 Antibodies used for Immunohistochemistry 70
Table 4.1 Pre-sequencing quality control metrics 124
Table 4.2 Post-sequencing information on the scRNA-seq samples 127

Appendix 1 Comparison of histology stains to visualize liver architecture 211
Appendix 2 Gating strategy for the identification of hepatic leucocytes following acute liver injury 212
Appendix 3 Gating strategy for the identification of systemic leucocytes following acute liver injury 213
Appendix 4 Gene signature analysis 214
Appendix 5 Top 10 differentially expressed genes

identified for MP clusters 0-12 216
Appendix 6 t-SNE visualization of top markers genes identified for Kupffer clusters: 0, 8. 220
Appendix 7 t-SNE visualization of top marker genes for MDM clusters 222
Appendix 8 t-SNE visualization of top marker genes for cDC1 and cDC2 clusters 223
Appendix 9 t-SNE visualization of top marker genes for monocyte clusters 224

1 Introduction

1.1 Liver disease - a global clinical burden

Worldwide, liver disease accounts for approximately two million deaths a year (Asrani *et al.*, 2019). While we have made massive strides in lowering mortality from many life-threatening conditions, mortality associated with liver diseases has continued to rise inexorably since the 1970s (Figure 1.1) (Williams and Horton, 2013). In the UK, liver disease is estimated to overtake ischemic heart disease as the leading cause of years of working life lost (Williams *et al.*, 2018).

Acute liver failure (ALF) is a clinical syndrome initiated via hepatocyte death overwhelming the regenerative capacity of liver, leading to the rapid development of hepatic encephalopathy, coagulopathy and jaundice, and culminating in multi-organ failure and death (Bernal and Wendon, 2013). In contrast to chronic liver disease, where damage culminates overtime to cause liver failure, acute liver failure (ALF) is characterized by rapid deterioration of hepatic function, without any pre-existing liver disease. Though not as major a global concern as chronic liver disease, the mortality and morbidity rates associated with ALF are significant. The aetiologies of ALF vary demographically, with viral infections the predominant cause in developing countries (Figure 1.2): hepatitis A and E, typically transmitted by ingestion of contaminated food or water, and hepatitis B transmitted through infected bodily fluids (Bernal, Lee, *et al.*, 2015). The most common cause of ALF in the developed world is drug-induced liver injury, primarily via acetaminophen (APAP) overdose (Figure 1.2). APAP-induced liver injury (AILI) accounts for 60% of ALF cases in the UK and 50% of the cases in USA (Bernal and Wendon, 2013; Bernal, Lee, *et al.*, 2015). Rarer cases of ALF may be caused by idiosyncratic drug reaction, hepatic ischemic insults, autoimmune hepatitis, hypoxia-induced liver injury, acute Budd-Chiari syndrome, or Wilson disease (Bernal and Wendon, 2013). Additionally, liver failure may also be caused by

acute-on-chronic liver failure (ACLF), where ALF occurs in patients with underlying liver disease or undiagnosed cirrhosis. The mortality rates associated with ACLF are higher than those seen with chronic liver disease (Bernal, Jalan, *et al.*, 2015; Sarin and Choudhury, 2016)

Implementation of vaccination policies and improved sanitation have reduced the incidence of viral-induced ALF in developed countries, whereas the incidence of drug-induced ALF, particularly from APAP overdose, has increased (Bernal, Lee, *et al.*, 2015). This can be attributed to ease of accessibility: APAP is readily purchased over the counter. Many cases occur after intentional ingestion of large doses from suicide attempts; accidental overdose from “therapeutic misadventure” is also common, when APAP is not taken as directed (Zimmerman and Maddrey, 1995). Regardless of the nature of liver injury (acute, chronic or acute-on-chronic) the regenerative capacity of the liver is severely compromised, and if left untreated this may result in death. The only current therapeutic remedy for AILI is N-acetylcysteine (NAC) administration, which has the potential to reduced hepatotoxicity by 30% (El-Serafi *et al.*, 2018), but as NAC targets the initial stages of AILI it is most effective when given within 8-10 hours after APAP overdose. Unfortunately, many patients are late-presenting; in these instances, there are no alternative strategies available to prevent APAP-induced ALF (Nelson and Kowdley, 2010; Hu *et al.*, 2015).

Curative treatment for end-stage liver disease and liver failure are limited to liver transplantation. Ever-increasing demand for donor livers outweighs the availability of donor-matched organs; coupled with life-long dependency on immunosuppression medications, this is far from ideal (Asrani *et al.*, 2019). This has put an emphasis on the development of potent therapies that promote liver regeneration and negate the need for transplantation.

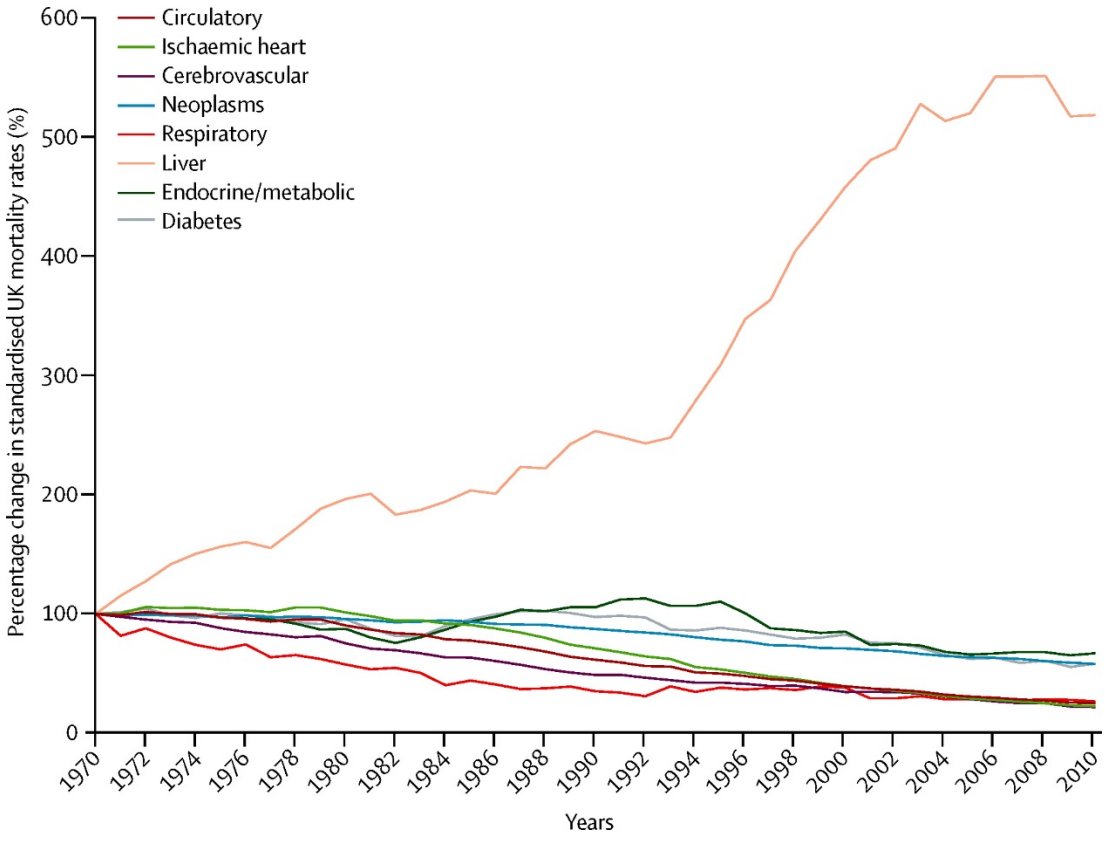

Figure 1.1 Standardised UK under-65 mortality rates (1970-2010). Reprinted from Williams et al., 2013.

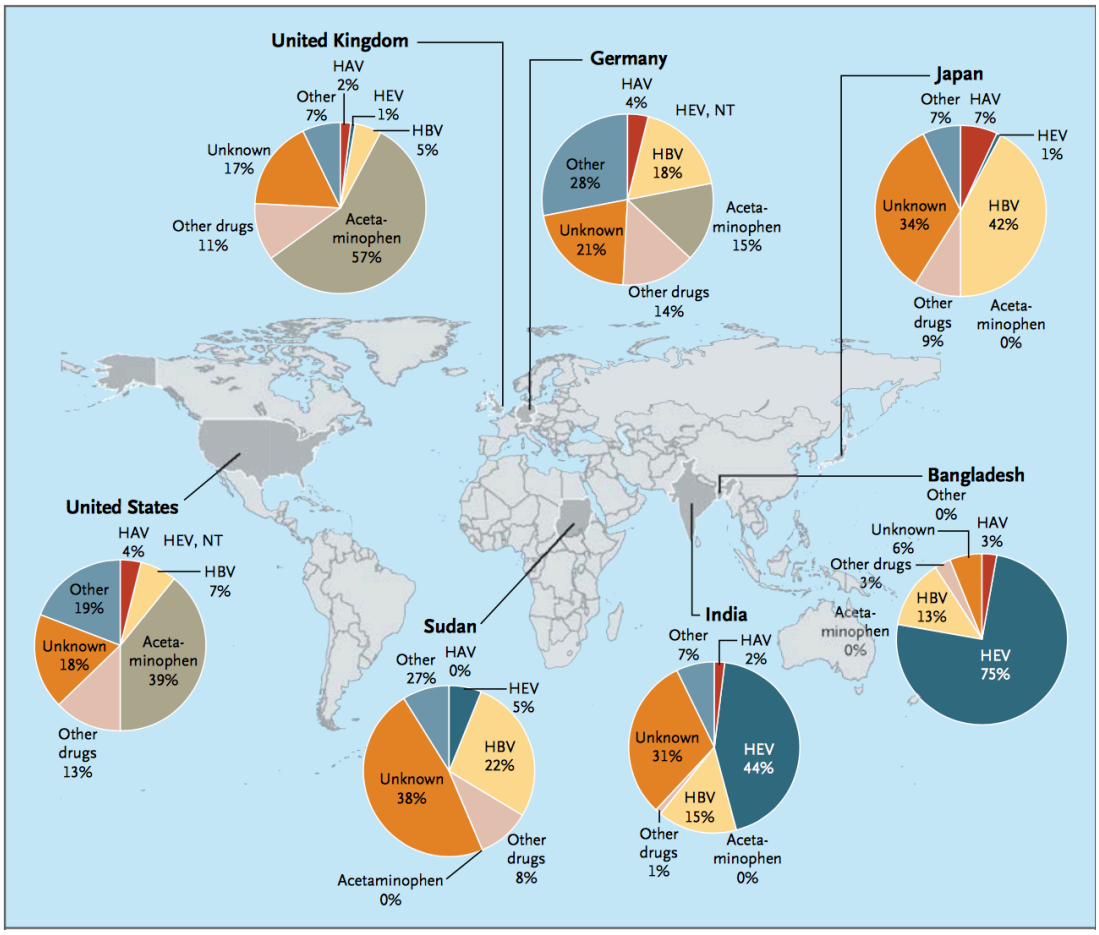

Figure 1.2 Worldwide aetiologies of Acute Liver Failure (ALF). (HAV) Hepatitis A Virus, (HEV) Hepatitis E Virus, (HBV) Hepatitis B Virus and (NT) not tested. Reprinted from Bernal and Wendon, 2013.

1.2 Liver architecture

The liver is the largest internal organ in the body, responsible for a myriad of functions including metabolic homeostasis of carbohydrates, lipids and proteins, storage of nutrients, bile secretion, metabolism and detoxification of harmful toxins and immunoregulation (Trefts, Gannon and Wasserman, 2017). It is segmented into two major lobes (right and left) and two minor lobes (caudate and quadrate). The lobes are further divided into hexagonal microscopic lobules, centred on branches of the hepatic vein (central vein) and bordered on the periphery by the “portal triad”, composed of branches of the hepatic artery, hepatic portal vein and bile duct (Stanger, 2015).

The primary liver parenchymal cells are hepatocytes, responsible for executing liver function and contributing up to 80% of liver mass; the remaining 20% is contributed to by non-parenchymal cells (NPC). Hepatocytes are arranged as cords that radiate from central vein to lobule perimeter. Cords of hepatocytes are separated by small capillaries called sinusoids, and the space between hepatocytes and adjacent sinusoids is called the Space of Disse. The Space of Disse is characterized by extra cellular matrix (ECM) components and contains blood plasma and hepatic stellate cells (HSCs) (Stanger, 2015). HSCs are NPCs that have a role in vitamin A and fat storage during homeostasis; during liver pathogenesis they are activated and transform into ECM-secreting cells called myofibroblasts, which contribute to fibrosis (Trefts, Gannon and Wasserman, 2017). The remaining NPCs are located in the sinusoids and includes Liver Sinusoidal Endothelial Cells (LSECs) lining the insides of sinusoids, Kupffer cells (KCs) and a wide spectrum of other immune cells such as Natural Killer (NK) Cells, Dendritic Cells (DCs) and T cells that circulate in the sinusoidal lumen (Gao, 2016).

The liver lobule receives blood flow from two independent sources. The hepatic portal vein supplies the lobule with two-thirds of its blood flow, enriched with nutrients drained from the gastrointestinal tract and spleen. The remaining oxygenated blood flow comes from the hepatic artery (Jenne and Kubes,

2013). Arterial and venule blood disseminate through the liver via a meshwork of sinusoids before draining into the central vein and Inferior Vena Cava (IVC). Fenestrated LSECs facilitate efficient exchange of oxygen and nutrients between the sinusoids and hepatocytes.

The biliary network transports bile produced primarily by hepatocytes, to the bile canaliculi and then to bile ductules within the portal triad via the canals of Hering, for storage in the gall bladder before draining into the duodenum. Bile ducts are lined with liver parenchymal cells called cholangiocytes, which are epithelial cells that modulate bile secretion (Bloomston and Misih, 2010).

The liver lobule represents the structural unit of the liver, but the functional unit of the liver is known as the hepatic acinus, visualized by the porto-central axis which runs from the portal triad to the central vein (Kietzmann, 2017). Hepatocyte distribution along the porto-central axis shows functional specialization, a phenomenon known as metabolic zonation (Kietzmann, 2017). Zone 1 contains hepatocytes closer to the portal ducts (periportal) specialized for functions such as gluconeogenesis, urea production and cholesterol synthesis; as they are surrounded by oxygen-rich blood, periportal hepatocytes are generally more resistant to damage (Kietzmann, 2017). Hepatocytes closer to the central vein (zone 3; pericentral), are responsible for glycolysis, lipogenesis, and cytochrome P-450-based drug detoxification. The intermediary zone (zone 2) contains hepatocytes that lie in between zone 1 and 3 (Macaulay *et al.*, 2016). Zonation has been shown to be dynamic, controlled by a combination of hemodynamic factors including oxygen gradient, reactive oxygen species and Wnt/β-catenin signaling. Metabolic zonation can influence liver injury patterns seen during liver pathologies (Trefts, Gannon and Wasserman, 2017).

1.3 Liver regeneration

Mechanisms of cellular regeneration vary across tissues of the body. Epithelial tissues such as the intestine and the skin possess distinct stem cell pools, which contributes to high cellular turnover in these tissues during homeostasis. Conversely, tissues such as the heart and the brain show minimal turnover. Regeneration in the liver is context-dependent; in mammals during steady-state there is minimal cellular turnover (roughly 1-2% of hepatocytes in cell cycle), and cells have an average life span of 200-300 days (MacDonald, 1961). Following injury the liver exhibits a remarkable regenerative capacity, a potential evolutionary adaptation brought about by its anatomical location and function where it is frequently exposed to ingested toxins from the GI tract (Stanger, 2015). This regenerative capacity is not limited to toxin-induced injuries, for example following the removal of tissue the liver can fully regenerate to its original mass in the span of a week in rodents and within 60 days in humans (Nagasue *et al.*, 1987; Michalopoulos, 2017). When the proliferative ability of mature hepatocytes is blocked (senescence), either experimentally or during chronic liver diseases, hepatic progenitor cells (HPCs) located in the canals of Hering have been shown to give rise to hepatocytes and ductular cells (Lu *et al.*, 2015; Stanger, 2015). However the most common mechanism of liver regeneration, and the focus of this body of work, is proliferation of fully-differentiated hepatocytes (Stanger, 2015). Liver regeneration is a complex process, and injury initiation to cellular regeneration encompasses a multitude of events including involvement from different cell types, growth factors and cytokines. We rely on animal models to study this phenomenon *in vivo*.

1.4 Models of acute liver injury and regeneration

Pre-clinical rodent models represent an ideal system to study the cellular and molecular mechanisms at play during liver injury, regeneration and progression of liver failure. Reliable and highly reproducible models of liver regeneration have been developed, where liver injury can be induced in a

timely manner via chemical or surgical methods (Forbes and Newsome, 2016). Recent advancements in transgenic technology, such as the development of fluorescent reporter mice, has allowed the interrogation of specific cells, molecules or pathways involved in liver injury and regeneration (Greenhalgh, Conroy and Henderson, 2015).

1.4.1 Partial hepatectomy (PHx)

One of the most widely used and well-described models of liver regeneration is partial hepatectomy (PHx), whereby two-thirds or 70% of the liver is surgically resected (Mitchell and Willenbring, 2008) (Figure 1.3a). PHx was developed by Higgins and Anderson in 1931 and has become a standardized procedure in rodents for the study of liver regeneration, popular for two main reasons. First, the process of liver regeneration post-PHx is mediated by crosstalk between the hepatic parenchymal and non-parenchymal cells with minimal involvement from any necrotic or acute inflammatory processes (Figure 1.3b). Second, the multilobular structure of the rodent liver makes a “clean” removal feasible, with regeneration initiated immediately after the resection and completed approximately within 7-10 days in mice. Liver regeneration following PHx is achieved through compensatory hyperplasia, in which remnant lobes enlarge through parenchymal and NPC proliferation until the original mass of the liver is reached (Figure 1.3).

The series of events which are involved in this process can be broadly categorized into three distinct phases: (1) initiation or priming of hepatocytes, (2) proliferation of hepatocytes, (3) termination of hepatocyte proliferation. Initiation events involve rapid upregulation of more than 100 genes, promoting production of growth factors and mitogenic signalling pathways required for hepatocytes to switch from their homeostatic, quiescent state to a proliferative state (Michalopoulos, 2007). The proliferation phase consists of both parenchymal (hepatocytes and cholangiocytes) and NPC proliferation, where the former precedes the latter (Taub, 2004). In mice, four continuous waves of

hepatocyte replication are required to restore lost hepatocytes and reconstitute liver mass. Hepatocyte proliferation starts in the periportal areas of the liver and proceeds to the pericentral areas, peaking 36-48h post-PHx (Zou *et al.*, 2012). Paracrine signalling between hepatocytes and NPCs is crucial in orchestrating liver regeneration following PHx (Taub, 2004); during the early stages of liver regeneration, NPCs secrete many growth factors needed for hepatocyte priming and proliferation. NPCs then proliferate during the later stages of regeneration, around 48-72hrs post-PHx, when additional growth factors such as vascular endothelial growth factor (VEGF) are required to promote endothelial proliferation and vascular sprouting, so as to establish normal liver architecture (Michalopoulos, 2017).

To avoid carcinogenesis, hepatocyte proliferation needs to be terminated once the liver has re-gained structural and functional capacity. A small wave of hepatocyte apoptosis is seen at the end of DNA synthesis, highlighting the intrinsic capacity in the liver, termed as the “hepatostat”, to sense and prevent over-shooting of the regenerative response (Sakamoto *et al.*, 1999). As in the initiation phase, termination of liver regeneration following PHx is mediated by numerous factors, but these are not well-characterized. Nevertheless, key factors and signalling pathways have been highlighted, such as transforming growth factor β (TGF-β). TGF-β signalling can significantly suppress liver regeneration following PHx by inhibiting cell cycle genes in hepatocytes, promoting apoptosis of hepatocytes and inactivating hepatocyte mitogens (Michalopoulos, 2007, 2017)

Studying liver regeneration in the context of PHx has highlighted the major growth factors, signalling pathways and molecules necessary for liver growth. Importantly, PHx does not reflect hepatic and extrahepatic manifestations such as necrosis, inflammation and fibrosis evident in human acute liver injury, where liver regeneration may be compromised. To address this, liver injury models more relevant to human pathologies have been developed.

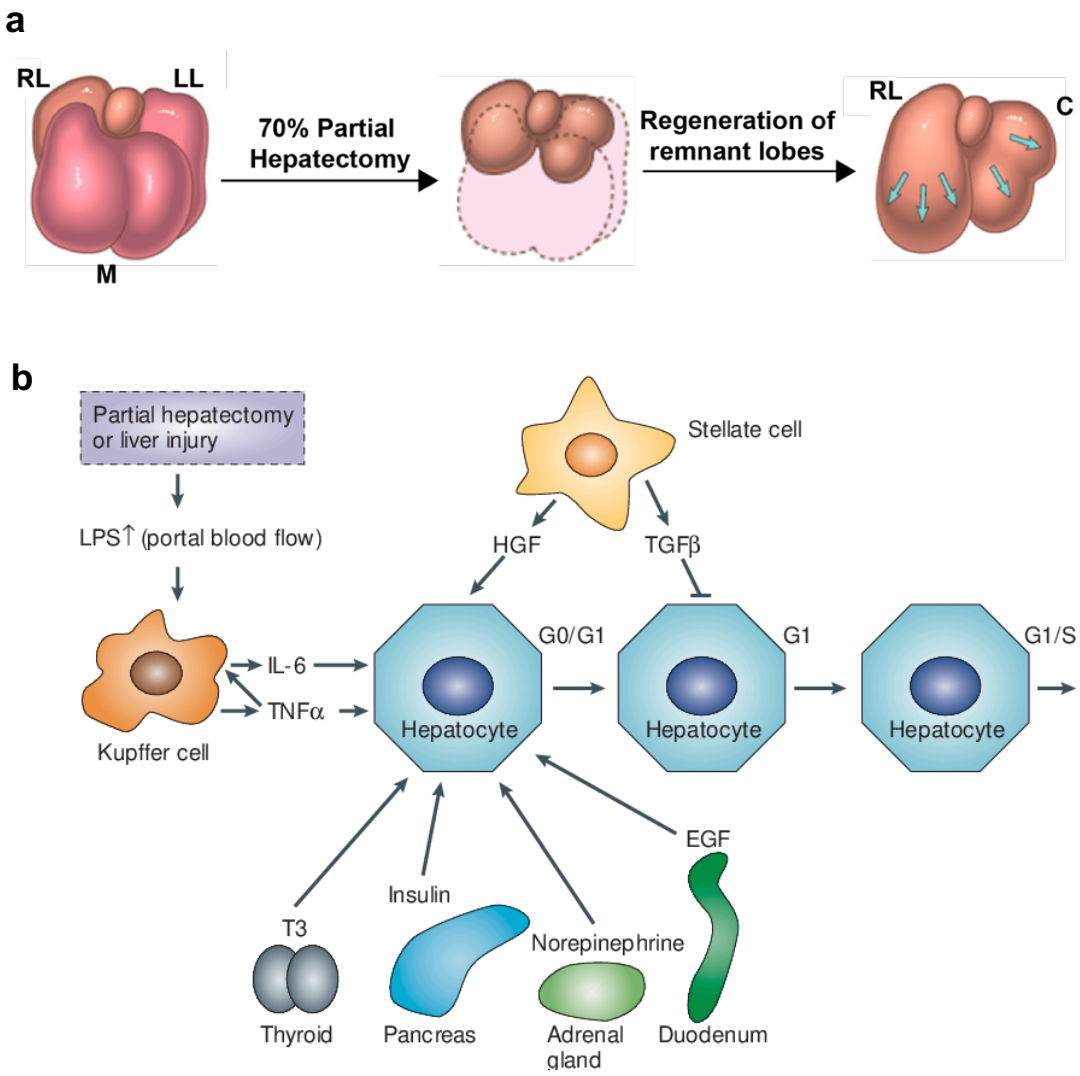

Figure 1.3 Liver regeneration following partial hepatectomy (PHx). (a) 70% PHx model of regeneration is established via removal of median (M) and left lateral (LL) lobes, the remnant right lateral (RL) and caudate (C) lobes enlarge via compensatory hyperplasia, until the original liver mass is reached. Reprinted from Goss, (1992). **(b)** Tissue injury activates hepatic NPCs (Kupffer cells, stellate cells) via upregulation of lipopolysaccharides (LPS). NPCs release pro-mitogenic factors: interleukin-6 (IL-6), tumour necrosis factor α (TNF-α), hepatocyte growth factor (HGF), and various factors from other cells and tissues are also released: epidermal growth factor (EGF), insulin, norepinephrine, triodothronine (T3). The released factors stimulate hepatocyte proliferation by promoting cell cycle entry ($G_0 \rightarrow G_1$), once the original mass is reached hepatocyte proliferation halts via transforming growth factor β (TGFβ) mediated signalling, restoring a quiescent state in hepatocytes. Reprinted from Taub, (2005).

1.4.2 Hepatotoxins to model liver regeneration and failure

Researchers have relied on hepatotoxins for experimental models of ALF, each with individual advantages and disadvantages. A wide range of hepatotoxins such as thioacetamide, galactosamine and carbon tetrachloride (CCl_4) have been used to induce massive hepatocyte death, either directly or indirectly. However, the murine model of acetaminophen-induced liver injury (AILI) represents the most widely used system to study liver regeneration in the context of acute liver injury.

Administrating a single dose of APAP can initiate hepatocyte necrosis and elevation in liver enzyme levels (AST, aspartate aminotransferase; ALT, alanine aminotransferase) similar to that seen in humans. Moderate doses of APAP (200-400mg/kg) can be administered to recapitulate a regenerative response, whereas severe doses of APAP (600mg/kg and above) can inhibit liver regeneration and can be used to model ALF (Bhushan *et al.*, 2014). One main disadvantage of the AILI model is lack of reproducibility, as injury extent and temporal dynamics of cellular and molecular events can vary between mice. Some of this variation has been attributed to factors such as genetic background, sex and age of the mice, fasting period, and routes of administration and dose of APAP (Mossanen and Tacke, 2015). Mice bred on different genetic backgrounds show differences in the extent of liver injury; for example, C57BL/6 mice exhibit enhanced liver injury in comparison to BALB/c mice, and even within C57BL/6 mice sub-strains display differential susceptibility to APAP (Mossanen and Tacke, 2015; Duana *et al.*, 2016). Female mice are more resistant to APAP hepatotoxicity, irrespective of their genetic background; therefore most studies use male mice (Mohar *et al.*, 2014; Mossanen and Tacke, 2015). These factors must be controlled to identify meaningful and biologically relevant changes occurring during AILI.

1.4.3 Mechanisms of AILI

In therapeutic doses, APAP is mainly metabolized through sulfation and glucuronidation. A small proportion is metabolized by cytochrome P450 isoform 2E1 (CYP2E1), which leads to the formation of toxic metabolite N-acetyl-p-benzoquinoneimine (NAPQI). NAPQI is quenched by endogenous glutathione, preventing hepatotoxicity (Yan *et al.*, 2018). During APAP overdose, sulfation and glucuronidation pathways are saturated, and as a result the P450 cytochrome oxidase enzyme system is relied upon for APAP metabolism. Consequently, the rate of NAPQI production exceeds glutathione production, leading to glutathione depletion and accumulation of NAPQI in hepatocytes. Covalent binding of NAPQI to cellular and mitochondrial proteins results in mitochondrial dysfunction, oxidative stress, peroxynitrite formation and initiation of stress signalling pathways leading to hepatocyte necrosis. AILI-induced necrosis occurs primarily in pericentral hepatocytes (Zone 3) due to their high expression of CYP2E1 enzymes (Jaeschke, Xie and Mcgill, 2014).

AILI is bi-phasic, where the primary stage is characterized by a series of necro-inflammatory events (Figure 1.5). Dying hepatocytes release damage associated molecular patterns (DAMPs) such as high-mobility group box 1 (HMGB1) and heat shock protein-70. DAMPs activate NPCs such as KCs via toll-like receptors (TLRs), which release various inflammatory cytokines and chemokines to recruit peripheral leucocytes (immune cells) into the liver. Additionally, release of proteolytic enzymes like calpains from necrotic hepatocytes creates a milieu that promotes further death and inflammation (Limaye *et al.*, 2003).

This primary stage is followed by a repair phase, in which hepatocytes close to necrotic zones proliferate and replace dead cells; additionally, proliferation in NPCs and other recruited cells is also seen (Figure 1.6) (Jaeschke, Xie and

Mcgill, 2014; Zigmond *et al.*, 2014). The cellular and molecular mechanisms underpinning liver regeneration following AILI is wildly different to that in PHx, perhaps unsurprising considering the differences in mode of injury. In AILI, hepatocyte proliferation depends on other events such as attenuation of liver injury via resolution of inflammation and clearance of necrotic and apoptotic debris (Triantafyllou *et al.*, 2017). Therefore, unlike in PHx, the term “liver regeneration” in the context of AILI extends beyond hepatocyte proliferation. Nevertheless, following efficient repair, liver architecture and function is restored in rodent models of AILI within 7 days.

In circumstances where liver regeneration fails, AILI progresses to ALF. Of note, NAC (the current therapy for AILI) replenishes glutathione; while this prevents further hepatocyte damage from occurring, it has very little effect on pre-established hepatocyte necrosis and hepatic and systemic events that precede ALF. These events include heightened liver injury, systemic and hepatic inflammation and inhibition of hepatocyte proliferation, which accumulates to hepatic encephalopathy, multi-organ failure and death (Bernsmeier, Antoniades and Wendon, 2014).

Mechanisms of CCl_4 induced liver injury

CCl_4 is a solvent primarily used in generating an experimental model of liver fibrosis. Like APAP, CCl_4 is metabolized in the liver by the cytochrome P450 system, to form trichloromethyl peroxy free radicals. These free radicals react with nucleic acids, protein and lipids in hepatocytes, leading to lipid peroxidation, mitochondrial dysfunction, membrane dysfunction, all of which ultimately lead to hepatocyte death (Scholten *et al.*, 2015). The subsequent events that follow hepatocyte death are analogous to those seen in AILI, whereby DAMPs released by dying hepatocytes, such as HMGBI, activate NPCs which initiate a hepatic and systemic inflammatory response resulting in the recruitment of immune cells into the liver (Dai *et al.*, 2018). Repeated occurrence of these events can lead to fibrosis, which is established via

chronic iterative administration of CCl_4 (Ramachandran *et al.*, 2012; Scholten *et al.*, 2015). Since most studies use CCl_4 in the context of establishing fibrosis to reflect a chronic liver injury scenario, from herein this literature review will focus on AILI.

1.5 Factors influencing liver regeneration

1.5.1 Growth factors and cytokines

Growth factors driving liver regeneration can either directly induce or indirectly promote hepatocyte proliferation. The primary hepatocyte mitogens are hepatocyte growth factor (HGF) and epidermal growth factor (EGF). HGF receptor cMET and EGF receptor EGFR on hepatocytes are activated within 30 minutes to an hour post-PHx (Stolz *et al.*, 1999); combined elimination of cMET and EGFR signalling completely abolishes liver regeneration, prevents restoration of liver mass and leads to liver decompensation (Paranjpe *et al.*, 2016). EGFR and cMET are activated following AILI within 15 minutes and 3 hours respectively (Bhushan *et al.*, 2014, 2017); abolishment of EGFR alone results in complete inhibition of compensatory hepatocyte proliferation, progression of liver injury and decreased survival in mice (Bhushan *et al.*, 2017).

Cytokines such as interleukin(IL)-6, tumour necrosis factor α (TNFα) and IL-4 have been identified to act as hepatocyte mitogens (Selzner *et al.*, 2003). These cytokines do not have the ability to directly induce hepatocyte proliferation, like HGF and EGF, however they promote hepatocyte proliferation indirectly and their inhibition can impair regenerative response. IL-6 and TNFα regulate liver regeneration following PHx by promoting hepatocyte entry from G_0 into G_1, via STAT3 and NF-κB signalling respectively (Michalopoulos, 2007). IL-6 deficient mice display increased necrosis and mortality rate following PHx, and IL-6 injections have been shown to rescue this phenotype (Cressman *et al.*, 1996). TNF-α mediated NF-κB signalling

occurs mainly through TNF-receptor1 (TNFR1) on hepatocytes; TNFR1 knockout (KO) mice exhibit a regenerative defect rescued by IL-6 injection. This suggests a redundancy in cytokine mediated signalling during liver regeneration (Yamada *et al.*, 1997).

Cytokines have also been shown to promote liver regeneration following AILI. TNF-R1 KO mice following AILI show extensive necrosis and decreased liver regeneration, with reduced expression of cell cycle genes like cyclin D and A and STAT3 signalling. However, it is unclear whether TNF-R1 KO mice are more susceptible to APAP, which could explain the increase in liver injury. Similar to PHx, IL-6 has also been heavily implicated in liver regeneration following AILI, with elevated serum levels. IL-6 KO mice show attenuated regenerative capacity, without differences in initial liver necrosis and serum ALT levels. IL-6 administration in these mice prior to APAP overdose was able to restore efficient regenerative response (James *et al.*, 2003). While there is evidence to suggest IL-6 signalling is pro-mitogenic, IL-6 signalling alone does not promote liver regeneration. A study in which incremental doses of APAP was used to identify the key pathways active during AILI highlighted the IL-6/STAT3 pathway to be significantly elevated in mice which received moderate doses (300mg/kg) and also which in mice which received severe doses (600mg/kg) of APAP (Bhushan *et al.*, 2014). Similar to PHx there is crosstalk between IL-6/STAT3 and TNF-α/NF-κB pathways during AILI, which was highlighted in TNFR1 KO mice where inhibition of TNF-α signalling also resulted in delayed STAT 3 activation (Chiu *et al.*, 2003). Bhushan et al. (2014) highlighted the NF-κB pathway to be downregulated in animals receiving severe doses of APAP (600mg/kg) where liver regeneration was inhibited, whereas in mice in which successful regeneration took place, the NF-κB pathway was active (Bhushan *et al.*, 2014).

Several signalling pathways observed during development are also upregulated during liver regeneration. Following PHx there is rapid induction of both Wnt/β-catenin and Notch pathways within 15mins-3hrs post-PHx

(Michalopoulos, 2007). Wnt/ β-catenin signaling promotes upregulation of key cell cycle genes such as Cyclin D1, involved in G_1 to S phase transition during cell cycle. In the absence of β-catenin, hepatocyte proliferation following PHx is delayed but not abolished, again indicating redundancy during liver regeneration (Tan *et al.*, 2006; Sekine *et al.*, 2007). Inducible deletion of Notch-1 in hepatocytes causes delayed hepatocyte proliferation following PHx; notch signalling is also important for endothelial regeneration (Wang *et al.*, 2009). The Wnt/β-catenin pathway has been associated with promoting liver regeneration during AILI, with the downstream targets of β-catenin signalling (cyclin-D1) downregulated following administration of severe doses of APAP where liver regeneration was inhibited (Bhushan *et al.*, 2014). Studies in β-catenin KO mice in the context of AILI have been challenging due to differences in APAP metabolism resulting in reduced liver injury. However, β-catenin KO mice receiving equitoxic dose of APAP show deficient liver regeneration (Apte *et al.*, 2009). In line with this, β-catenin activation correlated with increased levels of spontaneous liver regeneration in APAP-induced ALF patients (Apte *et al.*, 2009).

In a very recent study, Bird et al (2018) demonstrated that TGF-β-driven hepatocyte senescence (permanent cell cycle arrest) inhibits liver regeneration following AILI. Administration of TGFβ receptor 1 inhibitor in mice receiving a lethal dose of APAP showed striking improvement in their clinical symptoms. Additionally, they also showed inhibition of hepatocyte senescence and increased hepatocyte proliferation in the peri-necrotic area (Bird *et al.*, 2018). This has highlighted the therapeutic potential of inhibiting TGF-β signalling for liver pathologies where regeneration is inhibited. However, considering the role that TGF-β signalling has in preventing tumorigenesis, this has to be approached with caution (Yang *et al.*, 2006).

1.5.2 Inflammation and Immune dysfunction

Sterile inflammation is a key feature of AILI, and a response required to combat overwhelming parenchymal death and initiate the repair process. Crucially, the resolution of inflammation is also key for successful liver repair. Persistent hepatic and systemic inflammation are features of many acute and chronic liver pathologies. There is strong evidence to suggest that mortality from ALF correlates with the presence of systemic inflammatory response syndrome (SIRS), a condition sharing striking similarities to sepsis, featuring systemic inflammation, immune dysfunction and extra-hepatic organ failure (Bernsmeier *et al.*, 2015; Triantafyllou *et al.*, 2018). Numerous targets have been identified to promote inflammation during AILI.

AILI triggers local inflammation through the release of DAMPs from necrotic hepatocytes, which overrides hepatic tolerogenic mechanisms. DAMPs such as high mobility group box 1 (HMGB1), adenosine triphosphate (ATP), heat shock protein 70, mitochondrial DNA (mitDNA) are detected by KCs and other NPCs via various TLRs (2, 4, 9) and the receptor for advanced glycation end products (RAGE) recognition receptor, initiating pro-inflammatory signalling (Scaffidi, Misteli and Bianchi, 2002; Martin-Murphy, Holt and Ju, 2010). Genomic DNA (gDNA) and mitDNA from necrotic-release have been detected in systemic circulation of ALF patients and in experimental models of AILI, suggesting a role for DAMPs in promoting SIRS and multiorgan dysfunction (Marques *et al.*, 2012). DNA release from necrotic hepatocytes have the capacity to guide neutrophils to the areas of injury via the TLR9/NF-κB pathway, where they promoted inflammation. Blocking this interaction via DNA removal or through ablation of TLR9 significantly reduced systemic inflammation, neutrophil recruitment and liver injury (Marques *et al.*, 2015).

Similarly, mice lacking HMGB1 were protected from a lethal dose of APAP, and humanized antibodies to HMGB1 attenuated AILI in mice more effectively

than NAC (Lundbäck *et al.*, 2016). DAMP recognition by immune cells via TLR9 and TLR4 pathway can activate molecular complexes called inflammasomes. The NACHT, LRR and PYD domains-containing protein 3 (Nalp3) inflammasome has been implicated in promoting hepatotoxicity during AILI by promoting the activation and secretion of potent pro-inflammatory mediators IL-1β and IL-18 (Imaeda *et al.*, 2009; Woolbright and Jaeschke, 2017b; Bachmann, Pfeilschifter and Mühl, 2018). Blocking inflammasome formation, either via TLR9 antagonism or blocking IL-18 activity, was shown to ameliorate hepatotoxicity during AILI (Imaeda *et al.*, 2009; Bachmann, Pfeilschifter and Mühl, 2018).

Activated NPCs also release a range of chemotactic factors, called chemokines, which guide and recruit circulatory leucocytes to necrotic areas. KCs are the major producer of C-X-C ligand 2 (CXCL2) and C-C ligand 2 (CCL2), involved in the recruitment of neutrophils and monocytes respectively (Ishida *et al.*, 2006; Zimmermann, Trautwein and Tacke, 2012). CXCL2 binding to its receptor CXCR2 inhibited neutrophil accumulation in the liver following AILI, which in turn dampened liver injury and inflammation (Marques *et al.*, 2012). Similarly, inhibiting CCL2 interaction with CC receptor 2 (CCR2) led to reduced monocyte infiltration and attenuation of liver injury and inflammation (Mossanen *et al.*, 2016). ALF patients often show increased levels of chemokine ligands (namely CCL2) in their serum, and this has been attributed to poor prognosis (discussed further in sections below) (Antoniades *et al.*, 2012; Mossanen *et al.*, 2016). As a result, blocking chemokine ligand-receptor interaction and or inhibiting chemokine release has become a therapeutic target for the treatment of AILI (Mota *et al.*, 2017).

There is a wealth of evidence implicating inflammation in the progression of liver injury, but crucially it is also needed for driving liver repair through chemokine-mediated recruitment of various leucocytes into the liver. Leucocytes regulate liver injury and regeneration and their dysfunction can drive mortality and morbidity in ALF patients. For instance, circulating

neutrophils and monocytes have significantly impaired capacity to respond to pathogens during ALF, a feature often seen in patients with worst outcomes from APAP poisoning (Antoniades *et al.*, 2008; Taylor *et al.*, 2013; Bernsmeier *et al.*, 2015; Moore *et al.*, 2017). The role of leucocytes in regenerating liver has been studied both in the context of PHx and AILI; the majority of existing data is on myeloid cells, especially macrophages, however lymphocytes have also been shown to be modulators of liver regeneration.

1.6 Liver as an immunological organ

The liver is a highly immunological organ, harbouring a rich reservoir of innate and adaptive immune cells essential for immunoregulatory functions (Jenne and Kubes, 2013). Portal blood flow supplied by the hepatic vein contains a spectrum of gut contents including pathogens, non-self-antigens from nutrients and gut microbiota. The immune network in the liver forms a “firewall” between these gut contents and systemic circulation (Balmer *et al.*, 2014). The hepatic immune network includes KCs, dendritic cells, NK cells, NKT cells, T cells; during steady-state conditions they function to maintain tolerance against harmless non-self-antigens whilst rapidly removing harmful pathogens (Figure 1.4) (Jenne and Kubes, 2013; Heymann and Tacke, 2016).

KCs are strategically positioned in the liver sinusoids and are equipped with various pattern-recognition receptors (PRRs), complement receptors required to recognize and capture non-self-antigens (Heymann and Tacke, 2016). Following binding, KCs are activated and pathogens are phagocytosed and eliminated in the phagolysosomes, thus preventing their dissemination (Surewaard and Kubes, 2017). Activated KCs can release various pro-inflammatory cytokines to activate NK cells and promote cytotoxic responses towards bacterial and viral pathogens (Salazar-Mather, Orange and Biron, 1998; Lauwerys *et al.*, 2000). Most importantly, during homeostasis these events are tightly controlled to avoid evoking a systemic immune response (Heymann and Tacke, 2016). KC response to lipopolysaccharide (LPS), a common bacterial PAMP often found on non-pathogenic commensal bacteria,

is a perfect example of this. In response to physiological concentrations of LPS, KCs readily produce interleukin (IL)-10 which suppresses T cell activation via downregulation of MHC class II expression on LSECs and DCs (Knoll *et al.*, 1995).

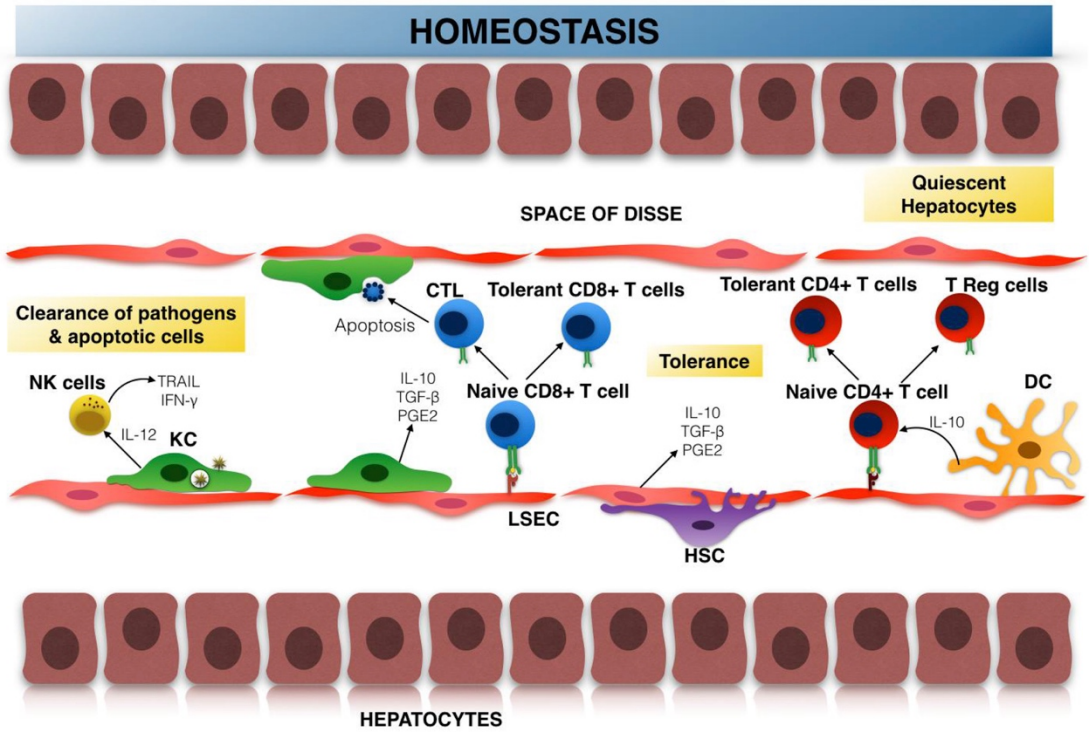

Figure 1.4 Regulatory role of immune cells in the liver during homeostasis. APCs such as KCs, DCs, and LSECs flank the sinusoids, capturing and removing circulating non-self-antigens and commensal bacteria. They modulate T cell responses via releasing immunosuppressive mediators (IL-10, TGFβ and PGE2) to promote and tolerogenic state in the liver. Microbial pathogens detected via KCs are eliminated by NK cell derived TRAIL/IFN-γ mechanisms. Abbreviations: APCs, Antigen presenting cells; CTL, cytotoxic T cells; DC, dendritic cells; HSC, hepatic stellate cells; IFN-γ, interferon-gamma, IL, interleukin; KC, Kupffer cells; LSEC, liver sinusoidal endothelial cells; NK, natural killer cells; PGE2, prostaglandin E2; TGF-β, transforming growth factor-β; TRAIL, Tumour necrosis factor-related apoptosis inducing ligand. Reprinted from Markose et al (2018).

1.7 Role of immune cells during acute liver injury

1.7.1 Lymphocytes

Lymphocytes constitute approximately 25% of hepatic NPCs, including both innate and adaptive lymphocytes. Innate lymphocytes in the liver can be broadly categorised into NK cells and NKT cells. Hepatic NK cells are phenotypically and functionally different from conventional NK cells found in circulation; in fact they resemble innate lymphoid cells (ILCs); a subset of cells with an immunoregulatory phenotype, found on mucosal surfaces (Heymann and Tacke, 2016). During homeostasis NK cell activity is suppressed, partly via KC-derived IL-10, but following infection or injury they are activated. Through the release of cytolytic enzymes like perforin, granzyme and interferon gamma (IFN-γ) mediated signalling, NK-cells can eliminate non-self-antigens and viral infected and tumour-transformed cells (Heymann and Tacke, 2016).

NKT cells on the other hand are cells which share phenotypical similarities with both NK cells and T cells. In the context of PHx NK/NKT cells interact with KCs to release pro-mitogenic cytokines TNF-α, IL-6, HGF and IL-4 and also directly secrete IL-22 to promote liver regeneration (Hosoya *et al.*, 2013). Thus far none of the existing studies in the field has been able to faithfully and precisely investigate the role of NK and NKT cells in promoting injury and regeneration the context of AILI. A hepatoprotective role for NK/NKT cells during AILI in early studies has been attributed to DMSO, a widely used solvent for APAP. While there is no evidence to show that NK/NKT directly influence liver injury and regeneration following AILI, IFN-γ released by activated NK cells is a promoter of tissue injury and inflammation following AILI (Ishida *et al.*, 2002). Following hepatic focal sterile injury, invariant NKT cells were shown to have a wound healing phenotype via IL-4 secretion, which polarised macrophages to a pro-reparative phenotype and promoted hepatocyte proliferation (Liew, Lee and Kubes, 2017).

Adaptive lymphocytes (T and B cells) perform immunoregulatory functions in the liver during homeostasis, and following injury or infection they have the capacity to initiate inflammatory responses (Zhang *et al.*, 2013). Hepatic T cells may be localised to the portal tracts and parenchyma of the liver, and are distinct from circulating T cells (Collins *et al.*, 1996). Of the two major T cell subtypes, CD4+ T (T helper) cells are responsible for modulating pro-inflammatory and inflammatory responses and CD8+ T (cytotoxic T) cells perform MHC-I mediated effector functions against intracellular pathogens (Heymann and Tacke, 2016). CD4+ T cells interact with MHCII on antigen presenting cells (APCs) and shape immune responses, and are subdivided into four different subtypes (TH_1, TH_2, TH_{17} and regulatory T_{Reg} cells) based on their activation states (Heymann and Tacke, 2016). Recently a small population of non-classical T cells were identified in the liver, termed γδ-T cells. Increased mortality, observed in RAG1 deficient (T and B cell deficient) mice following PHx, highlights the requirement for adaptive lymphocytes in promoting liver regeneration. T cell-derived lymphotoxin (LT) (also known as TNFSF1; a member of the TNF super-family) was shown to promote hepatocyte proliferation directly and via the IL-6 pathway in the context of PHx; this response was seen in both CD4+ and CD8+ T cells but not in γδ-T cells, indicating functional heterogeneity within T cell populations during liver regeneration (Tumanov *et al.*, 2009).

During AILI, CD4+ T (TH_1) cells contribute towards liver injury via IFNγ production; conversely, T_{Reg} subsets were shown to promote an anti-inflammatory phenotype in the liver. Depletion of T_{Reg} cells amplified inflammation, which was reversed following adoptive transfer of T_{Reg} cells. T_{H1} and T_{H2} balance is crucial during AILI (Wang *et al.*, 2015), demonstrated by increase hepatoxicity in T_{H1}-dominant C57B/6 mice in comparison to T_{H2}-dominant BALB/c mice (Masubuchi, Sugiyama and Horie, 2009). Expression of proinflammatory cytokines TNF-α and IL-6 was elevated in T_{H1}-dominant mice, whilst mitogenic cytokine IL-6 was upregulated in T_{H2}-dominant mice.

T_{H17} cells have also been implicated in the progression of inflammation during AILI via IL-17 signalling, which results in the release of pro-inflammatory cytokines and neutrophil-mobilizing chemokines (Zhu and Uetrecht, 2013). Collectively, these results indicate T cell subsets show functional difference during AILI, which can influence progression and resolution of hepatic injury.

1.7.2 Granulocytes

One of the early responders to liver injury are neutrophils; necrosis-derived DAMPs, pro-inflammatory mediators such as TNF-β and IL-1β released from KCs and CXCL2-CXCR2 interaction can all recruit neutrophils to necrotic sites (Wang *et al.*, 2013; Marques *et al.*, 2015). Recently, TLR2 and calprotectin proteins S100A8 and S100A9 were identified as key regulators of hepatic chemokine CXCL-2 and neutrophil recruitment during AILI (Moles *et al.*, 2014). Neutrophils populate the liver during the early stages of AILI and have a dual role. Neutrophil infiltration can exacerbate inflammation and liver injury during the early necroinflammatory phase, through release of tissue-damaging molecules like nitric oxide (NO), reactive oxygen species (ROS), proteolytic enzymes and through driving inflammatory pathways TLR9/NF-κB and IL-33/ST2 (Ishida *et al.*, 2006; Liu *et al.*, 2006; Marques *et al.*, 2015; Yang *et al.*, 2019). Therefore, depleting neutrophil recruitment and function during the early stages phase of AILI can dampen liver injury (Marques *et al.*, 2012). Crucially, neutrophils also drive liver repair, as depleting neutrophils during the later stages of AILI reduces liver regenerative capacity (Yang *et al.*, 2019). Neutrophils are professional phagocytes, capable of removing necrotic debris; their timely recruitment to the liver when hepatocyte necrosis is extensive suggests they may have a role in promoting clearance of debris. Interactions between neutrophils and other leucocytes also influence liver repair: during AILI, clearance of apoptotic neutrophils can induce a pro-repair phenotype in macrophages, and recently neutrophil-derived ROS has also been suggested to drive this polarisation (Graubardt *et al.*, 2017; Yang *et al.*, 2019). Furthermore, ALF patients show impaired bactericidal function in their

circulating neutrophils, whereby complement activity, ROS production and the ability to phagocytose is significantly compromised (Wyke *et al.*, 1982; Altin *et al.*, 1983; Taylor *et al.*, 2013). The role of cytokines in promoting hepatocyte proliferation during acute liver injury was highlighted in previous sections. Neutrophil interaction with ICAM-1 has been shown to promote the release of pro-mitogenic cytokines TNF-α and IL-6 by KCs, following PHx. Goh et al. (2013) demonstrated that recruited eosinophils are a major source of IL-4, and that IL4-IL4r signalling promoted hepatocyte proliferation during CCl_4 induced acute liver injury and following PHx. Eosinophil-deficient mice display ~50% reduction in their regenerative capacity following PHx and acute CCl_4 injury (Goh *et al.*, 2013). In keeping with this, eosinophilia was associated with favourable outcomes in patients suffering from drug-induced liver injury (Bjornsson, Kalaitzakis and Olsson, 2007).

Currently there is no known role for basophils in the context of liver injury and liver regeneration. Mast cells have been implicated in a wide range of biliary injuries such as primary biliary cholangitis and bile duct obstruction; perhaps not surprising as they are localised mainly to the portal tract in the liver (Jarido *et al.*, 2017).

1.7.3 Mononuclear phagocyte system

The mononuclear phagocyte system (MPS) was formed in 1969 to collectively classify cells with shared ability to phagocytose and a common ontogeny from bone-marrow derived precursors (Hume, 2006). The MPS comprises of macrophages, monocytes and dendritic cells (DCs) and perhaps the most studies cells in the MPS during tissue repair are macrophages. Macrophages were initially identified by Elie Metchnikoff in 1883 as phagocytes with the ability to capture and engulf dead cells and harmful pathogens, thus giving rise to the concept of cellular immunity (Guilliams, Mildner and Yona, 2018). Since then, distinct macrophage populations have been identified in different tissues of the body (tissue resident macrophages; TRMs) with specialised roles. For

example, alveolar macrophages in the lung are responsible for removing inhaled particles and pathogens, osteoclasts reside in the bone and have a role in bone resorption, and microglia in the brain function to eliminate dead neurons, microbes, and protein aggregates which may endanger the central nervous system (Colonna and Butovsky, 2017). Kupffer cells represent the largest population of TRMs, with a range of functions extending beyond providing innate immunity, including iron and lipid metabolism (Scott and Guilliams, 2018). Given their key roles in tissue development, homeostasis and inflammation macrophages have been termed as a “cell for all seasons”. Their involvement in a wide range of inflammatory and malignant pathologies have identified them as key therapeutic targets (Ginhoux *et al.*, 2016). In order to fully understand their therapeutic potential, you need to appreciate the complex biology of macrophages, which includes their origin, activation states and functions.

1.7.3.1 Origin and maintenance of tissue resident macrophages

For a long time it was believed that all macrophages originated from circulating monocytes from common myeloid precursor (CMP) cells in foetal liver and bone marrow during embryonic and adult haematopoiesis (Ginhoux and Jung, 2014). Bone marrow (BM) haematopoietic stem cells differentiate into CMPs, which diverge into either GMP (granulocyte-monocyte precursor) for the neutrophil differentiation pathway or MDP (monocyte-macrophage DC precursor). The MDP population is believed to make a binary decision to either differentiate into DC-restricted CDP (common DC precursor), giving rise to tissue DCs, or monocyte-restricted progenitor cMoP (common monocyte precursor) giving rise to circulating monocyte precursors (Hettinger *et al.*, 2013; Ginhoux and Jung, 2014).

Circulating monocyte precursors were thought to continuously replenish all TRMs in various tissues across the body, but this concept was challenged by a series of studies in the early 20th century, which redefined macrophage ontogeny and indicated heterogeneity within the MPS. Studies showed

replenishment of various TRMs following their depletion occurring independently of bone marrow-derived circulating monocytes (Merad *et al.*, 2002; Ajami *et al.*, 2007; Ginhoux *et al.*, 2010). Additionally, parabiosis and BM-chimera experiments which can trace circulating monocyte mixing and differentiation to macrophages suggested tissue-dependent bone-marrow contribution to TRM maintenance (Guilliams *et al.*, 2013; Hashimoto *et al.*, 2013; Tamoutounour *et al.*, 2013; Bain *et al.*, 2014; Epelman *et al.*, 2014). TRMs such as microglia, Langerhans cells, and alveolar macrophages self-maintain independent of circulating precursors (Ginhoux *et al.*, 2010; Yona *et al.*, 2013; Gomez Perdiguero *et al.*, 2015). Conversely, TRM populations in the gut and dermis show contribution from BM-derived circulating precursors (Hashimoto *et al.*, 2013; Bain *et al.*, 2014). Yona et al. (2013) took advantage of the broad expression of CX3CR1 by cells in the MPS and performed fate mapping of MPs using a conditional CX3CR1 promoter driven Cre recombinase system. Their findings showed that Kupffer cells (KCs), in addition to lung alveolar macrophage, microglia and splenic macrophages, are established during embryogenesis prior to the generation of HSCs and self-maintain with no contribution from circulating blood monocytes during adulthood (Yona *et al.*, 2013). Although circulatory monocytes have the capacity to give rise to macrophages in tissues such as the liver, brain, and lungs during inflammation, these macrophages are usually ephemeral (Yona *et al.*, 2013).

Despite differences in origin, TRMs and their MPS counterparts share several common characteristics in addition to their phagocytic capacity. The development of MPS cells is regulated by PU.1, which in turn is regulated by RUNX1 (Ginhoux *et al.*, 2010). PU.1 regulates the early stages of myeloid cell development, where high concentration of PU.1 levels were shown to promote macrophage and DC development whereas low levels of PU.1 are needed for B cell development (DeKoter and Singh, 2000; Carotta *et al.*, 2010). The proliferation and differentiation of MPs (monocytes, DCs and macrophages) are regulated by colony stimulating factor 1 (CSF1) and interleukin (IL)-34,

signalling via a common receptor, CSF1R (Hume and MacDonald, 2012; Gow *et al.*, 2014). Indeed, *CSF1R* is one of the major target genes of PU.1. Osteopetrotic (op/op) mice which show constitutive deficiency for Csf1 show significant reduction in circulating monocytes, macrophage populations. The severe phenotypical defects including loss of teeth, male and female infertility, and increased bone mass in these mice highlights the trophic functions of macrophages (Dai *et al.*, 2002; Pollard, 2009). Similar phenotypes are observed in CSF1R knock out (KO) mice, which rarely live beyond a few weeks of age and show complete loss of Langerhans cells and microglia (Pollard, 2009).

Creation of MacGreen mice in which the expression of enhanced green fluorescent protein (eGFP) is under control of the *Csf1r* promoter allows the visualisation of MPs, especially macrophages, across different tissues (Sasmono *et al.*, 2003). Modification to the Csf1r promoter enables selective interrogation of macrophages without neutrophil labelling, and MacBlue mice have been developed where certain TRMs such as KCs are not labelled (Sauter *et al.*, 2014). Additional core macrophage genes and proteins include CX3CR1, Fc receptors (CD64), *Adgre1* (F4/80). These are expressed by the majority of macrophage populations, and expression of these proteins is used in the identification of macrophages across various tissue (T'Jonck, Guilliams and Bonnardel, 2018).

TRMs including KCs also acquire tissue-specific identities to perform specific functions, and this adaptation is controlled by many transcriptional factors. ID3 has been identified as a regulator of KC development (Mass *et al.*, 2016); similarly PPAR-γ and GATA6 are important to the development and maintenance of alveolar macrophages (Schneider *et al.*, 2014) and peritoneal macrophages (Okabe and Medzhitov, 2014), respectively. Tissue-specific programming of macrophages gives rise to a unique transcriptional profile, and TRM-specific markers such as TIMD4 have been identified to selectively study these cells (Thornley *et al.*, 2014; Fujiyama *et al.*, 2018; Shaw *et al.*, 2018).

CLEC4F has recently been identified as a KC-specific marker (Scott *et al.*, 2016). Scott et al. (2016) demonstrate the niche-dependent capacity of circulating monocytes to acquire TRM identity, selectively depleting KCs and showing that circulating monocytes gave rise to macrophages with a similar gene expression profile to KCs and the capacity to self-maintain for as long as four months. A similar phenotype was observed in *Zeb2*-/- mice, in which KCs are absent due to their dependency on *Zeb2*; BM-derived circulating monocytes gave rise to KCs in these mice, supporting niche competition (Scott *et al.*, 2018).

1.7.3.2 Circulating monocytes as precursors to macrophages

The capacity of circulating monocytes to infiltrate the liver and differentiate into macrophages is a common feature seen during liver injury and inflammation, and this process does not require niche availability. The chemokine signals derived from the inflammatory response to tissue injury are detected by circulating monocytes, resulting in transmigration of specific subsets of monocytes to the site of injury. Circulating monocytes were thought to be a homogenous population, however, phenotypic characterization of monocytes using multi-parametric flow cytometry identified heterogeneity within the both human and murine monocyte populations. In humans CD14 and CD16 expression is used to identify monocytes, with CD14+ $CD16^-$ monocytes (classical monocytes) accounting for 80-90% of the total monocyte pool and the remainder comprised of CD14+ CD16+ monocytes (intermediate) and $CD14^{Lo}$ CD16+ (non-classical) monocytes (Patel *et al.*, 2017). Murine monocytes are broadly identified by flow cytometry, firstly based on their expression of CD115 (CSF1R), CD11b and lymphocyte antigen 6C (Ly6C). In depth-characterisation of murine monocyte populations was made possible by the generation of a $CX3CR1^{GFP}$ reporter mouse, in which fluorescent protein expression (GFP) was driven by the *CX3CR1* locus. Two main subsets of monocytes have been identified and characterized: classical monocytes defined as $Ly6C^{Hi}$ ($CX3CR1^{Int}$ $CCR2^+$ $CD62L^+$ $CD43^{Lo}$) and non-classical monocytes as $Ly6C^{Lo}$ ($CX3CR1^{Hi}$ $CCR2^{Lo}$ $CD62L^-$ $CD43^+$). A third intermediary

subset ($Ly6C^{Int}$) has been described based on CD11b expression; transcriptomic analysis revealed $Ly6C^{Hi}$ and $Ly6C^{Lo}$ monocytes to be homogenous, whereas $Ly6C^{Int}$ monocytes are heterogeneous (Mildner *et al.*, 2017).

$Ly6C^{Hi}$ monocytes are short lived (18 hours), with their primary function to respond to chemokines released following inflammation, namely CCL2 (monocytes chemotactic protein-1; MCP-1), and to migrate to sites of injury and inflammation (Serbina and Pamer, 2006). $Ly6C^{Hi}$ monocytes are often called inflammatory monocytes, based on their capacity to readily release pro-inflammatory cytokines in the site of injury. At the site of inflammation $Ly6C^{Hi}$ monocytes are highly plastic and depending on micro-environmental cues act as precursors of inflammatory and restorative monocyte-derived macrophages (MDMs).

$Ly6C^{Lo}$ circulating monocytes on the other hand are long lived (~2 days in mice and 7 days in humans) (Patel *et al.*, 2017; Guilliams, Mildner and Yona, 2018). Intravital imaging studies of $CX3CR1^{GFP/+}$ mice revealed $Ly6C^{Lo}$ monocytes as custodians of the vasculature in the steady state, where they crawl along the luminal side of the endothelium (Auffray *et al.*, 2017), carry out effector functions such as scavenging micro particles and maintain endothelial cell integrity (Carlin *et al.*, 2013). $Ly6C^{Lo}$ monocytes were also shown to have an active role during tissue injury; for example, injury induced by irritants, aseptic wounding and peritoneal infection with *Listeria monocytogenes* (*Lm*) resulted in rapid extravasation (within 1 hour) of $Ly6C^{Lo}$ monocytes. During *Lm* infection, $Ly6C^{Lo}$ monocytes were shown to initiate an inflammatory response, producing cytokines such as TNF-α. They also upregulated various TLRs, scavenger receptors and chemokines involved in the recruitment of other immune cells, and exhibited a TF profile that specified macrophage differentiation (Auffray, Sieweke and Geissmann, 2009). This response was transient, with $Ly6C^{Lo}$ monocytes shortly replaced by $Ly6C^{Hi}$ monocytes. Studies have shown a role for $Ly6C^{Lo}$ monocytes in tissue injury and repair,

with Nahrendorf et al. 2007 demonstrating that during myocardial injury there is an initial recruitment of Ly6C^{Hi} monocytes with phagocytic, proteolytic and inflammatory functions, followed by infiltration of Ly6C^{Lo} monocytes which promoted tissue restoration through matrix remodelling and angiogenesis (Nahrendorf *et al.*, 2007). A similar phenomenon was seen in the context of muscle regeneration following necrosis, whereby inflammatory Ly6C^{Hi} monocytes populated the areas of injury in the initial phase, which was followed by an increase in Ly6C^{Lo} monocytes with an anti-inflammatory phenotype. The authors of this study postulated that instead of a secondary infiltration, Ly6C^{Hi} monocytes differentiated into Ly6C^{Lo} monocytes (Arnold *et al.*, 2007). These studies collectively show that Ly6C^{Lo} monocytes have the capacity to respond to tissue injury, differentiate into macrophages and participate in tissue repair process. However, the temporal dynamics of Ly6C^{Lo} infiltration, their origin and phenotype are injury dependent.

As with TRM a set of transcription factors (TFs) and growth factors determine commitment towards monocyte lineage. The role of PU.1 and CSF1R has been discussed previously; additionally IRF8, GATA2 and KLF4 have been identified as critical in myeloid lineage differentiation, with deletion of these TFs resulting in reduced peripheral monocyte numbers (Guilliams, Mildner and Yona, 2018). Recent studies have highlighted that the canonical MDP-cMoP-monocyte developmental pathways can be bypassed during inflammation, and that GMPs (granulocyte-monocyte precursors) can give rise to monocytes (Yáñez *et al.*, 2017). Ly6C^{Hi} monocytes derived from GMPs during LPS-induced inflammation exhibit a distinct gene expression signature showing upregulation of neutrophil-related genes (Yáñez *et al.*, 2017). Similarly, a distinct monocyte subset derived from granulocyte precursors, named segregated nucleus-containing atypical (SatM) Ly6C^{Lo} monocytes, were shown to populate the lung during inflammation and identified as driving fibrosis (Satoh *et al.*, 2017).

1.7.3.3 DCs and Macrophages- a complex relationship

When dendritic cells (DCs) were first identified they were characterized as cells with a stellate morphology, lacking capacity for phagocytosis but with a unique ability to present antigens to naïve T cells. However, increasing evidence demonstrating their phagocytic capacity, in addition to other shared similarities to macrophages and monocytes, led to their inclusion in the MPS (Hume, 2006). DCs are a heterogeneous group of cells, and assessment of surface markers facilitates the characterization and identification of different DC subsets including classical or conventional DCs (cDCs) and plasmacytoid DCs (pDCs); murine cDCs are further divided into two major lineages, cDC1 and cDC2 (Guilliams, Mildner and Yona, 2018). cDCs are short lived cells specialized to carry out innate immune responses, enabled via high phagocytic and cytokine-producing activity. They are also efficient in antigen processing and presenting and in regulating T cell responses. In comparison, pDCs are long lived, present in the BM and in all peripheral organs, and are specialized to rapidly secrete type 1 interferons (IFN I) in response to viral infections resulting in T cell priming (Patricia Fitzgerald-Bocarsly, Dai and Singh, 2008). pDCs can also act as APCs and can modulate T cell responses (Geissmann *et al.*, 2010).

Currently it is a challenge to distinguish between DCs and macrophages, due to overlapping expression of surface molecules. Both cDCs and pDCs are derived from distinct precursors in the bone marrow (CDPs), independent of monocyte precursors (cMoP) (Paul *et al.*, 2015; Guilliams, Mildner and Yona, 2018). DCs show dependency on growth factor Flt3 (Auffray, Sieweke and Geissmann, 2009), and therefore Flt3 expression has been used to define DCs. Notably, DCs also depend on CSF1, a monocyte/macrophage differentiation factor, and CS1FR KO mice exhibit deficiency in DC numbers. Recent studies have revealed that monocytes have the capacity to differentiate into DCs (Mildner *et al.*, 2017) during steady state condition and inflammation (Menezes *et al.*, 2016). Two independent studies report that a subset of Ly6C^{Hi}

monocytes can give rise to monocyte-derived DCs (m-DCs), expressing DC-related genes *Cd209a* and *MHCII* in steady state conditions (Menezes *et al.*, 2016; Mildner *et al.*, 2017). In one of the studies these monocyte precursors were defined as Ly6C^{Int} monocytes (Mildner *et al.*, 2017). Following inflammatory stimuli Ly6C^{Hi} monocytes have also been shown to give rise to DCs, expressing TNF-α, iNOS, and reactive oxygen species; these cells have been termed TipDCs (Serbina, Shi and Pamer, 2012). To add complexity, in the context of inflammation monocyte-derived macrophages (MDMs) can upregulate CD11c and MHCII, classic DC markers, in addition to classical macrophage markers like F4/80, CD64 and MerTK (Guilliams, Mildner and Yona, 2018). Monocyte-derived DC populations are distinct to cDC and pDC subsets, and their development and maintenance is independent of CDPs and FLT3 (Serbina, Shi and Pamer, 2012; Menezes *et al.*, 2016; Mildner *et al.*, 2017) However, it remains unclear whether m-DCs and MDMs represent ontogenically distinct entities, regulated by a distinct TF or gene program, or highly dynamic cells with the capacity to acquire a multitude of phenotypical and functional characteristics in response to their micro environmental signals (Guilliams, 2014).

1.7.3.4 Macrophage activation states

While the MPS framework has facilitated our understanding of tissue phagocyte biology, it promotes the assumption that all phagocytes are homogenous regarding their origin and function. Previous sections have highlighted heterogeneity within monocytes and DCs; here I will focus on the plasticity exhibited by the macrophages.

The ability of macrophages to change their phenotype in response to their environment was demonstrated in the early 1990s, when researchers observed differences in macrophage phenotype in response to IL-4 versus interferon gamma (IFN-γ) and/or LPS. Following this, the M1 (classically activated) and M2 (alternatively activated) model was introduced by Mills et al., (2000) to define the two different macrophages responses. *In vitro*

polarization of macrophages to M1 and M2 phenotypes highlighted their potential to regulate their phenotype and thus function in response to environmental stimuli (Mills *et al.*, 2000). M1 macrophages activated by IFN-γ and or LPS release various pro-inflammatory mediators such as nitric oxide, TNF-α and IL-1, and exhibit the necessary phenotype for pathogen killing, whereas M2 macrophages display a wound healing phenotype upregulating MHCII molecules, arginase-1 and scavenger receptors in response to IL-4 and IL-13. Importantly, these dichotomous states represent the extremes of a continuum which is not representative of *in vivo* macrophage responses. In depth transcriptomic analyses of human macrophages cultured with an array of stimuli including various cytokines, fatty acids and TLR ligands revealed a spectrum of macrophage activation states, extending beyond the M1 and M2 polarization model (Xue *et al.*, 2014). Tumour-associated macrophages (TAMs) show bidirectional transformation between anti-inflammatory and immunosuppressive phenotypes *in vivo* (Mantovani *et al.*, 2002; Watkins *et al.*, 2007). In the context of tissue injury, macrophages are educated by endogenous stimuli, such as DAMPs from dying cells, chemokine and cytokines released from neighbouring cells, and are also capable of self-regulating based on autocrine signals. As a result, macrophages show an incredible level of plasticity, changing their phenotype and thus their function depending on ever-changing microenvironmental cues. One such activation state exhibited by macrophages promoting tissue repair is phagocytosis.

1.7.3.5 Phagocytic properties of macrophages

MPs are unified by their ability to phagocytose; phagocytosis is defined as the cellular uptake of particulates >5 μM in size within a plasma-membrane envelope (Hochreiter-Hufford and Ravichandran, 2013). The mechanisms in place for internalization of particles <0.5 μM in size is referred to as endocytosis or pinocytosis. Phagocytosis is an integral part of the innate immune system, required to remove microbial pathogens, non-self-antigens and dead cells (Ravichandran and Lorenz, 2007). It begins with internalization of particulates, which are then processed within a membrane-bound vesicle

referred to as the phagosome. Phagosomal fusion to acidic lysosome structures results in the degradation of the particulates (Kinchen and Ravichandran, 2008). Phagocytosis can be further defined by their target: bacteria and yeasts are internalized through scavenger receptors present on macrophages, while complement or Fc receptors can facilitate the removal of microorganisms (Hochreiter-Hufford and Ravichandran, 2013). The uptake of apoptotic or necrotic material is referred to as efferocytosis and is a complex process requiring a specific set of secreted factors and cell surface receptors. Efferocytosis is a critical mechanism during homeostasis for the removal of necrotic and apoptotic debris, with around 200 billion cells being turned over a day and also during tissue injury, to clear apoptotic and necrotic bodies (Hochreiter-Hufford and Ravichandran, 2013).

Efferocytosis is initiated through the release of soluble factors called “find-me” signals by the dying cell. These signals establish a chemotactic gradient which guides phagocytes towards the dying cell (Ravichandran and Lorenz, 2007). There have been several different “find-me” signals reported, which are recognized by specific receptors on the phagocytes: lysophosphatidyl-choline (LPC), sphingosine 1-phosphate (S1P), fractalkine (CX3CL1), and the nucleotides ATP and UTP, sensed by receptors G2A, S1P1-5, CX3CR1 and P2Y2, respectively (Koizumi *et al.*, 2007; Hochreiter-Hufford and Ravichandran, 2013). Once the phagocytes are near the dying cell, “eat me” signals presented by the apoptotic cells facilitate their phagocytic uptake, whilst avoiding ‘friendly fire’ of live cells in the vicinity. A range of “eat me” signals have been described in the literature, including phosphatidylserine (PtdSer), oxidized low-density lipoprotein (LDL)-like moiety, ICAM3, bound opsonins such as thrombospondin and complement C1q. Phagocytes possess numerous receptors capable of recognizing these “eat me” signals (Table 1.1), and can also secrete bridging molecules such as MFG-E8, growth-arrest-specific 6 (Gas6) and proteins S which can facilitate phagocytosis via binding to PtdSer on the dying cell (Li, 2012).

Table 1.1 Ligands and receptors involved in efferocytosis (Hochreiter-Hufford and Ravichandran, 2013)

Phagocytic Receptors	"Eat me" Targets
CD36	Thrombospondin
LRP1/CD91	C1q complement
CD14	ICAM3
Scavenger receptors	Oxidized LDL
Tyro-3-Axl-Mer family, e.g. MerTK	PtdSer (via bridging molecules)
PtdSer receptors: TIMD4, BAI1, Stabilin-2, RAGE	PtdSer

The interaction of phagocytes and apoptotic target leads to cytoskeletal rearrangements in the phagocytes resulting in internalization of the corpse in a membrane envelope called phagosome. For efferocytosis to be complete the internalized particles need to be trafficked into a series of increasingly acidified membrane-bound structures culminating in particle degradation; a process called phagosomal maturation. Acidification of the phagosome can be used as a readout for successful phagosome maturation (Kinchen and Ravichandran, 2008). Defects in phagosomal maturation can have consequences during tissue injury: in a model of kidney ischemia reperfusion injury, defects in glycoprotein nonmetastatic melanoma B (GPNMB), a phagocytic protein that regulates phagosomal trafficking and degradation, led to an increase in apoptotic cellular debris and increased mortality in mice compared to wild type counterparts (Li, Castano, Hudson, Nowlin, S. L. Lin, *et al.*, 2010). In concordance, Campana et al. (2017) demonstrated that following AILI, GPNMB-deficient mice had extended necrotic areas compared to wildtype mice; IL-6 treatment improved phagocytosis in these mice via the IL6-STAT3 pathway. The authors also showed that successful efferocytosis promoted the differentiation of $Ly6C^{Hi}$ inflammatory monocytes to $Ly6C^{Lo}$ MDMs (Campana *et al.*, 2018).

1.7.4 Role of MPs during acute liver injury and regeneration

1.7.4.1 DCs

DCs have been shown to promote liver regeneration following PHx. Administration of Flt3l in the context of PHx promotes expansion of DCs and significantly increased liver regeneration (Castellaneta *et al.*, 2006). Modulation of T cell responses by DCs during PHx to promote anti-inflammatory milieu that facilitates liver regeneration (Castellaneta *et al.*, 2006). During AILI, DC depletion via diphtheria toxin (CD11c-DTR) promoted hepatotoxicity and increased mortality in mice in mice (Connolly *et al.*, 2011). The mechanisms by which DCs suppress injury and promote repair in this setting has not be fully elucidated. It was shown that rather than numerical changes, AILI induced phenotypical changes in DCs, which resulted in increased production of IL-6, TNF-α and CCL2 (Connolly *et al.*, 2011). Another presumed mechanism by which they exert a pro-reparative phenotype is by negatively regulating NK activation and promoting neutrophil apoptosis. Furthermore, Flt3l treatment caused expansion of hepatic DCs and reduced hepatotoxicity following AILI (Connolly *et al.*, 2011). The main drawback to these studies is the lack of DC specific markers, conventional markers such as MHCII and CD11c are also expressed on macrophages, especially during inflammation (Guilliams, Mildner and Yona, 2018). The Flt3l experiments would suggest that DCs are important in modulating liver regeneration, but currently it remains challenging to draw specific conclusions on their specific role.

1.7.4.2 Monocytes and macrophages

Kupffer cells (KCs) represent the predominant tissue resident macrophage (TRM) population in the liver during homeostasis, accounting for 20% of the NPC population (Heymann and Tacke, 2016). KCs have been identified based on their expression of core macrophage receptors such as F4/80 and CD64,

in addition to TRM-specific receptors including CLEC4F and TIMD4, but do not express CX3CR1, expressed by most other MPs (Scott *et al.*, 2016). They are derived embryonically and self-maintain with minimal contribution from the bone marrow. During homeostasis KCs function as sentinels, capturing and destroying food antigens and microbial pathogens. They also have a role in lipid and cholesterol metabolism (Scott and Guilliams, 2018). The remaining TRM population in the liver are liver capsular macrophages (LCMs), expressing macrophage markers, CD64, CSF1R, F4/80 but not KC marker TIMD4, which indicates that these cells are distinct from KCs (Sierro *et al.*, 2017). Unlike KCs, LCMs rely on circulating monocytes for replenishment; they reside in the liver capsule and combat bacterial load from the peritoneum by promoting neutrophil recruitment (Sierro *et al.*, 2017).

Both KCs and recruited macrophages have been shown to drive liver regeneration. Following PHx, KCs promote hepatocyte proliferation via IL-6 and TNF-α release; inhibiting or depleting KCs resulted in significantly reduced numbers of proliferating hepatocytes (Selzner *et al.*, 2003). Liver regeneration is also impaired in the absence of $CCR2^{+}$ circulating monocytes, suggesting these cells might have a distinct role during PHx (Nishiyama *et al.*, 2015; Wyler *et al.*, 2016). The main caveat to these studies is they have not used KC-specific markers to delineate the TRM from infiltrating macrophages ((Nishiyama *et al.*, 2015; Wyler *et al.*, 2016).

Three distinct macrophage subsets have been identified to populate the liver during AILI, based on a combination of cell surface markers expression:

- KCs (TIMD4+ CLEC4F+ $F4/80^{Hi}$ $CD11b^{Lo}$ $CX3CR1^{Lo}$ $CCR2^{Lo}$)
- $Ly6C^{Hi}$ monocytes (TIMD4- CLEC4F- $F4/80^{Lo}$ $CD11b^{Hi}$ $CX3CR1^{Int}$ $CCR2^{Hi}$)
- $Ly6C^{Lo}$ MDMs[1] (TIMD4- CLEC4F- $F4/80^{Hi}$ $CD11b^{Int}$ $CX3CR1^{Hi}$ $CCR2^{Int}$)

[1] $Ly6C^{Lo}$ MDMs are also referred to as $Ly6C^{Lo}$ MoMFs. These terms are used interchangeably in the literature.

These subsets of macrophages behave dynamically during AILI (Figure 1.5, 1.6). During the necroinflammatory phase of AILI various DAMPs released by necrotic hepatocytes are recognized by KCs via DAMP-sensing receptors (TLR4, TLR9, RAGE, P2X7), which initiates a range of signalling cascades. KCs secrete pro-inflammatory mediators such as TNF-α, reactive oxygen species and various chemokines (CCL2, CXCL2), which amplifies the inflammatory signal and results in the recruitment of bone-marrow derived immune cells into the liver. KCs were linked to promoting inflammation during AILI through the release of pro-inflammatory mediators such as IL-6, IL1β, and TNFα, and their ablation resulted in reduced liver necrosis and improved survival rate (Fisher *et al.*, 2013). On the other hand, KCs have also been associated with promoting tissue repair following AILI through the release of IL-6 IL-10, IL-18 and various complement molecules, and their complete elimination increased hepatocyte necrosis (Ju *et al.*, 2002). Both studies relied on clodronate liposomes or gadolinium chloride to deplete or inhibit KCs respectively, and both mechanisms are not specific to KCs and can target other phagocytic cells. This also indicates that KCs behave dynamically during AILI, promoting inflammation during the necroinflammatory phase whilst mediating liver repair in the later stages (Figure 1.5, 1.6).

Zigmond et al. (2014) report that KC numbers are depleted during the early stages of AILI (~24-48hrs post-APAP), but that at 72hrs post-APAP their numbers are re-established via local proliferation without any BM-derived monocyte contribution. The significance of “KC disappearance” is currently unknown; it could be a result of cell death, of migration, or of macrophage plasticity following AILI. Transcriptomic profiling of KCs during the later stages of AILI (72hrs post-APAP) revealed that KCs express a wide array of scavenger receptor genes that can promote phagocytosis and extracellular matrix remodelling genes. They have also been identified as major producers of IL-6 which can drive hepatocyte proliferation (Ju *et al.*, 2002; Zigmond *et al.*, 2014)

BM-derived circulating Ly6C^{Hi} monocytes play a crucial role following AILI, with recruitment into the liver heavily dependent on the CCR2/CCL2 axis. CCR2 deficient mice (CCR2-/-) show marked reduction in hepatic Ly6C^{Hi} monocytes (Mossanen *et al.*, 2016; Yang *et al.*, 2019). Circulating monocyte Ly6C^{Hi} monocyte (CCR2+) infiltration occurs as early as 6hrs post-AILI (Zigmond *et al.*, 2014), and once in the liver they form dense cellular clusters around necrotic areas (Mossanen *et al.*, 2016). Ly6C^{Hi} monocytes show increased expression of a wide range of proinflammatory genes including *Nos1*, *Ptgs2*, TLRs (*Tlr2, Tlr4, Tlr5, Tlr8, Tlr9*), LPS receptor *Cd14*, chemokines (*Ccl2, Ccl3, Ccl6*) and neutrophil recruitment genes (S100A8/9, LCN). During later phases, Ly6C^{Hi} monocytes acquire a pro-reparative phenotype and differentiate into ephemeral Ly6C^{Lo} MDMs, exhibiting a gene profile associated with phagocytosis (Celc4d, Clec4e, Clec5a, CD93) and ECM remodelling (MMP8, ADAM8) (Zigmond *et al.*, 2014). BM-derived Ly6C^{Lo} MDMs exhibit some phenotypical similarity to KCs such as the expression of markers including F4/80 and CD64, however the pro-restorative molecular signature displayed by KCs and Ly6C^{Lo} MDMs are very distinct (Zigmond *et al.*, 2014). Of note, a population of peritoneal macrophages marked by GATA6 was shown to infiltrate the liver during thermal and CCl_4-induced acute liver injury. GATA6+ macrophages migrated via the liver visceral endothelium rather than the vasculature and promoted wound healing and liver regeneration (Wang and Kubes, 2016). The contribution of these cells to AILI is currently unknown.

Ly6C^{Hi} monocytes have been shown to be drivers of both liver injury and repair during AILI (Figure 1.5, 1.6). Mossanen et al. (2016) demonstrated that during the necroinflammatory phase (6hrs-12hrs) CCR2-/- mice lacking Ly6C^{Hi} monocytes and Ly6C^{Lo} MDMs show attenuated liver injury, where ALT levels and hepatocyte necrosis is markedly reduced in CCR2-/- mice in comparison to wild type mice. The authors further show via adoptive transfer experiments that early infiltration of Ly6C^{Hi} monocytes can aggravate liver injury (Mossanen *et al.*, 2016). In the clinical setting, monocytopenia coupled with high levels of

serum CCL2 confers a poor prognosis in ALF patients, suggesting that increased monocyte infiltration is a feature of worsened outcome (Antoniades *et al.*, 2012). In line with this, patients show increased levels of hepatic CCR2+ monocytes in the necrotic areas of the liver, expressing S100A9, indicating a proinflammatory phenotype (Antoniades *et al.*, 2012; Mossanen *et al.*, 2016). Based on this, inhibitors of CCR2 have been suggested as a potential therapeutic intervention for patients suffering from acute liver injury (Mossanen *et al.*, 2016).

Conversely, there is evidence to show that Ly6C^{Hi} monocytes can promote liver repair. In addition to pro-inflammatory genes, Ly6C^{Hi} monocytes also display a gene signature associated with wound healing (*Agr1, Chil3l3, IL4ra, TNFSF14*), angiogenesis (Vegfa, Sema4d, Hif1a, Plaur) and extracellular matrix remodeling (ECM) genes (*MMP18, ADAM8*) (Zigmond *et al.*, 2014; Graubardt *et al.*, 2017). Several studies report liver injury is higher in CCR2-/- mice in comparison to wildtype mice, where this observation is made during the repair phase of AILI (24hrs-48hrs) (Yang *et al.*, 2019). At this time CCR2-/- mice exhibit increased ALT levels, extensive hepatocyte necrosis, increased number of apoptotic cells around the necrotic areas and more importantly, marked reduction in proliferating hepatocytes (Hogaboam *et al.*, 2000; Zigmond *et al.*, 2014; Yang *et al.*, 2019). This highlights that temporal cues can influence macrophage phenotype during AILI. For example, there is an interplay between neutrophils, Ly6C^{Hi} monocytes and LyC6^{Lo} MDMs during AILI that regulates macrophage phenotype and promotes liver repair. Neutrophil-derived reactive oxygen species provide cues for Ly6C^{Hi} monocytes differentiation to Ly6C^{Lo} MDMs (Yang *et al.*, 2019). There is evidence to show that Ly6C^{Hi} monocytes regulate neutrophil activity and promote their apoptosis, and apoptotic-neutrophil clearance is carried out by Ly6C^{Lo} MDMs. Transcriptomic analysis of Ly6C^{Lo} MDMs during the repair phase of AILI (72hrs post-APAP) show expression of a unique set of apoptotic cell bridge molecules and receptors required for efferocytosis (Graubardt *et al.*, 2017). Based on these data, infiltrating monocytes and their progeny are

highly dynamic, exhibiting potential to both promote and inhibit liver repair following AILI.

Investigating the precise mechanisms by which macrophages promote liver injury and repair can facilitate the discovery of specific targets. An example of this is the recent discovery of MerTK+ macrophages populating the liver during the repair phase of ALF in both humans and mice. In this study, secretory leucocyte protease inhibitor (SLPI) induced MerTK expression on both KCs and Ly6C^{Lo} MDMs, which was shown to drive liver repair by promoting neutrophil apoptosis and subsequent clearance (Triantafyllou *et al.*, 2017). Interestingly, ALF patients showed elevated numbers of both hepatic and systemic MerTK+ HLA-DR^{Hi} cells, characterised by supressed innate and enhanced efferocytic/phagocytic responses (Bernsmeier *et al.*, 2015; Triantafyllou *et al.*, 2017). The immunoregulatory phenotype exhibited by circulating MerTK+ HLA-DR^{Hi} monocytes supresses the innate immune response, which increases susceptibility to infections in these patients. In this context, blocking the activity of MerTK+ HLA-DR^{Hi} monocytes was reported to be beneficial (Bernsmeier *et al.*, 2015). Clearly, the balance between immunoregulatory and pro-inflammatory macrophages and monocyte phenotype influences disease progression in ALF patients (Antoniades *et al.*, 2006; Bernsmeier, Antoniades and Wendon, 2014; Bernsmeier *et al.*, 2015; Triantafyllou *et al.*, 2017). Whilst an immunoregulatory phenotype is favourable in the liver to promote efferocytosis and drive liver repair, an inflammatory phenotype is needed in the systemic circulation to combat infections (Bernsmeier *et al.*, 2015; Triantafyllou *et al.*, 2018).

Overall these data highlight that embryonically-derived KCs, BM-derived monocyte precursors (Ly6C^{Hi} monocytes) and their progeny (Ly6C^{Lo} MDMs) are key regulators of liver regeneration following AILI (Figure 1.5, 1.6). Given the recent developments in macrophage ontogeny and activation states, we need to rethink our strategy for identifying macrophage-based therapeutic targets (Figure 1.7). Previous studies in the context of AILI and other types of

acute liver injury have heavily relied on known biology and broadly classified macrophages into KCs, Ly6C^{Hi} monocytes and Ly6C^{Lo} MDMs for subsequent gene expression and functional studies (Zigmond *et al.*, 2014; Ju and Tacke, 2016; Mossanen *et al.*, 2016; Graubardt *et al.*, 2017). While this has given us some insights into their role during AILI, their capacity to promote both liver injury and repair indicates heterogeneity within these broadly classified subsets.

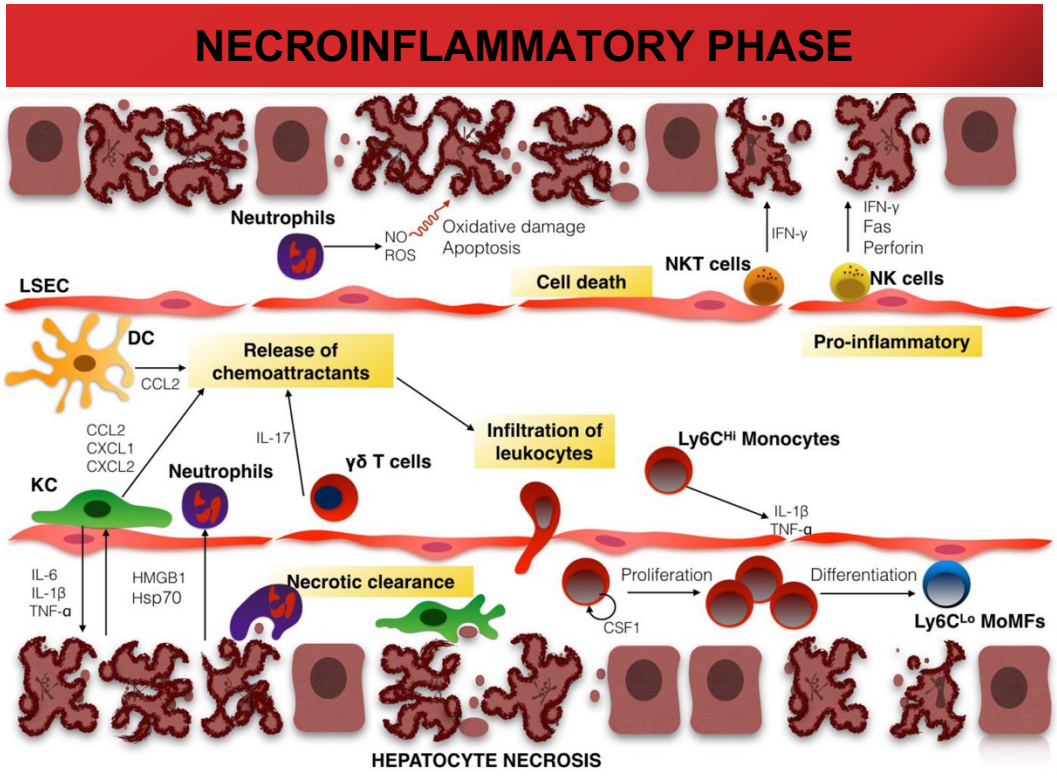

Figure 1.5 Leucocyte involvement in the necroinflammatory phase of AILI. Early stages of AILI is characterised by significant hepatocyte necrosis. DAMPs (HMGB1, Hsp70) released from necrotic materials activates liver resident leucocytes (KCs, DCs, γδ T cells) which causes pro-inflammatory cytokine (IL6, TNF-α, IL-1β) and chemokine (CCL2, CXCL1, CXCL2, IL-17) release. Chemokine-mediated leucocyte infiltration one of the key characteristics during this phase. Liver injury can be exacerbated by Ly6C^{Hi} monocytes (IL-1β TNF-α mediated mechanisms), neutrophils (ROS and NO mediated mechanisms), NKT and NK cells (IFN-γ, Fas and Perforin mediated mechanisms). Liver repair responses are initiated via necrotic clearance, proliferation and differentiation of pro-inflammatory Ly6C^{Hi} monocytes to pro-reparative Ly6C^{Lo} MDMs (MoMFs). Adapted from Markose et al. (2018)

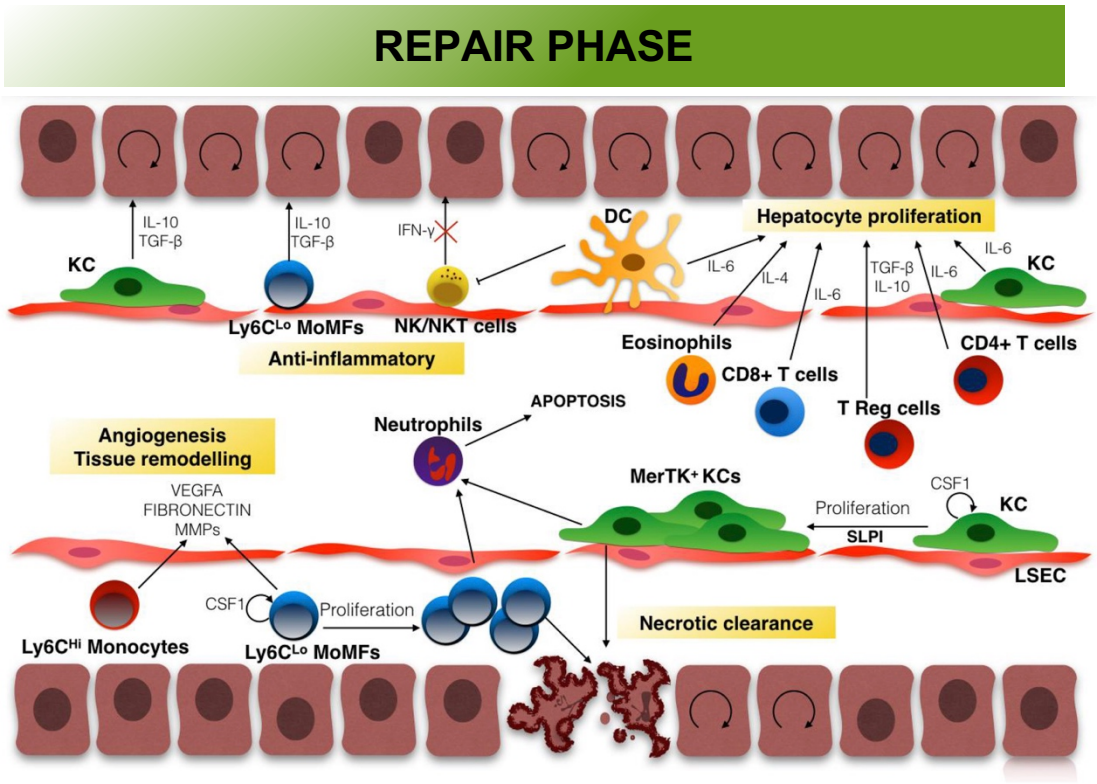

Figure 1.6 Leucocyte involvement in the repair phase of AILI. Inflammation is dampened via Ly6C^{Hi} monocyte mediated neutrophil apoptosis. Mediators such as SLPI drives the reprogramming macrophages to an efferocytic phenotype. Various efferocytic receptors such as MerTK, expressed by Ly6C^{Lo} MDMs (MoMFs) and KCs facilitates apoptotic neutrophil clearance. Cytokines released via leucocytes promote an anti-inflammatory milieu and drives hepatocyte proliferation. Ly6C^{Hi} monocytes and Ly6C^{Lo} MDMs promote angiogenesis and ECM remodelling and collectively these events result in restoration of normal liver architecture. Adapted from Markose et al. (2018)

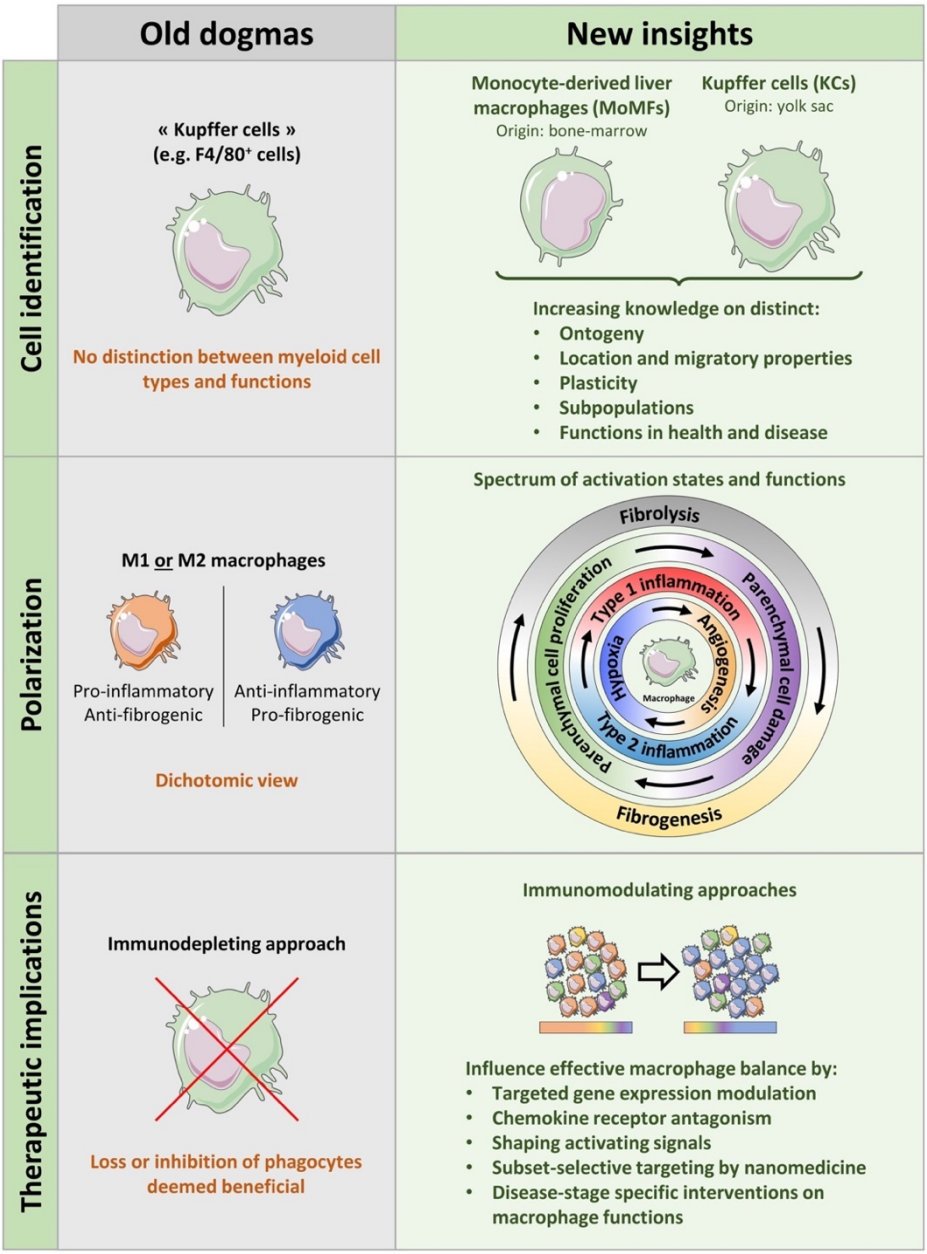

Figure 1.7 Old dogmas versus new insights on macrophages during murine models of liver injury. Cell identification: hepatic macrophages have gone from broad F4/80 classification to CLECF4 and TIMD4 expression delineating yolk sac derived KCs from bone marrow derived Ly6C^{Lo} MDMs (MoMFs). Polarisation: rather than a dichotomous M1 (pro-inflammatory) M2 (anti-inflammatory) phenotype macrophages during liver injury are heterogenous exhibiting spectrum of activation states**.** Therapeutic implications: broad immunodepleting approaches will lead to loss of pro-reparative macrophages shifting focus to immunomodulating approaches for identifying therapeutic target to treat liver diseases. Reprinted from Guillot and Tacke, (2019).

1.8 Single-cell RNA sequencing

Gene expression studies guide researchers to gain insight into the transcriptome of cells, from which they may infer protein expression, phenotype and cellular function. The advent of Next Generation Sequencing (NGS) enabled RNA analysis via sequencing of complementary Deoxyribonucleic Acid DNA (cDNA), a method referred to as Ribonucleic Acid (RNA) sequencing. RNA sequencing (RNA-seq) eliminates limitations posed by hybridization-based microarrays and Sanger sequencing-based approaches (Kukurba and Montgomery, 2015); for example DNA is simultaneously sequenced and detected base-by-base, in real time, with low background signal and with no requirement of prior sequence knowledge.

Conventional bulk population RNA-seq analyses expression of RNA from an ensemble of many cells, providing genomic measures for a sample that may mask heterogeneity within cell populations. Conversely, single-cell RNA sequencing (scRNA-Seq) allows interrogation of RNA expression in individual cells. This facilitates the identification of rare subtypes and vital cell-to-cell variability in heterogeneous cell populations, which would otherwise be masked in population-averaged measurements generated through bulk RNA-seq. ScRNA-seq is a multistep process, following the same basic principles of RNA-seq, whereby cells are isolated and lysed, messenger RNA (mRNA) is captured which is then reverse transcribed into cDNA, followed by cDNA amplification and library generation for sequencing.

1.8.1 Cell capture and mRNA extraction

Cells of interest can be captured via both low-throughout and high-throughput methods. Techniques such as micro pipetting and laser capture microdissection give precise control over specific cells and areas of tissue isolated for sequencing, however these methods are labour-intensive and limit the number of cells that may be isolated at a given time (Hwang, Lee and Bang, 2018). Therefore, high-throughput techniques such as fluorescence-

activated cell sorting (FACS), microfluidic and droplet-based systems are current preferred methods for scRNA-seq (Figure 1.8).

FACS allows rapid and accurate isolation of hundreds of thousands of cells in a matter of minutes. Cells of interest can be selected based on size, granularity, fluorescent-tagged cell surface markers and or transgenic reporters. One of the main drawbacks of FACS is that it can induce cell stress and reduce cell viability as cells are passed through pressured streams to generate single cell suspensions (Haimon *et al.*, 2018). To combat this, systems have been developed to isolate cells from peripheral blood based on magnet-conjugated antibodies, without the use of FACS, however these are not feasible for cell isolation from tissues (Hwang, Lee and Bang, 2018).

Droplet-based techniques such as DropSeq, InDrop and 10X Genomics Chromium rely on capturing cells in oil droplets, enabling capture and sequencing of thousands to millions of cells. Currently, this method has the highest throughput of all single-cell platforms, and is usually preferred for detecting rare cell types and investigating heterogeneity (Figure 1.8) (Nguyen *et al.*, 2018; Chen, Ye and Guo, 2019). Additionally, combining FACS with droplet-based systems enables enrichment for populations of interest. Following cell isolation, cells are lysed to capture mRNA, usually via poly(A)+ selection using poly(dT) primers.

1.8.2 cDNA amplification and library preparation

Once mRNA is extracted it is reverse transcribed into cDNA, followed by an amplification step which is crucial as only picograms of mRNA may be captured from an individual cell. There are numerous methods for generating cDNA libraries; for example, methods such as SMART-seq are designed to generate full-length cDNA, while droplet-based methods generate cDNAs with either a 5’ or 3’ bias, which consequently reduces the read depth (See *et al.*, 2018). On the other hand these methods allow cDNA tagging with unique

molecular identifiers (UMIs), specifically marking individual mRNA in a cell, to assist in downstream analysis by removing amplification bias. Droplet-based systems such as 10X Genomics Chromium further tag the cDNA with cellular barcodes to map sequence reads with the cell of origin (See *et al.*, 2018). During the library preparation process, cDNA is fragmented and ligated with primers and adapters for sequencing.

1.8.3 Sequencing

Illumina sequencing represents the most widely used NGS method that relies on Sequencing by Synthesis. Illumina flow cell immobilises cDNA strands via oligonucleotides complement to the ligated adapter oligonucleotides. The flow-cell bound single stranded DNA fragments are amplified through bridge amplification to generate double stranded bridge which is subsequently denatured leaving two single-stranded templates tethered to the Illumina flow cell. Bridge amplification occurs simultaneously for millions of clusters, resulting in massively parallel clonal amplification of all the fragments in the sample. Sequencing occurs through the addition of fluorescently tagged nucleotides and DNA polymerase. The wavelength and fluorescent signal emitted following nucleotide binding to complementary bases in the DNA fragments is used to determine the sequenced base. A library of millions of base sequences is generated in this manner, which may then be aligned to a reference genome to obtain gene expression data in the form of a counts matrix.

1.8.4 Data Analysis

Conventional RNA-seq methods are not suitable for the analysis of scRNA-seq data, due to particular challenges associated with scRNA-seq such as the inherent biological variation between individual cells. Additionally, the degree of “drop-out” events (the presence of zero-inflated counts) is high, owing to the low amount of starting RNA and the inefficiency of RT and amplification

reactions, and this can be further increased by 3' or 5' end bias. While some cells may contain no expression or low expression of certain genes due to biological reasons, in many cases this is a result of technical artefacts (See *et al.*, 2018). Therefore, single-cell computational tools for the analysis of scRNA-seq datasets rely heavily on quality control and normalisation steps to account for technical and biological variability (discussed further in Chapters 2 and 5). These tools also allow for the incorporation of UMIs and cellular barcodes to generate reads, quantify gene expression and map to individual cells. Further algorithms may be used to cluster the cells based on their gene profile, following which differentially-expressed (DE) gene analysis can identify genes to define and annotate clusters. Marker gene identification also facilitates further validation studies (Choi and Kim, 2019). Further downstream analyses such as pseudotime (Haghverdi *et al.*, 2016) and RNA velocity (Manno *et al.*, 2018; Zywitza *et al.*, 2018) can be applied to datasets containing cells on a continuum, and are often used to investigate differentiation trajectories within populations.

1.8.5 Novel findings using scRNA-seq

Since its introduction in 2009, scRNA-seq has revolutionised immunology by allowing the study of immune cells at an unprecedented resolution. This technology has been applied to cell lineages from different tissues and blood during development, homeostasis and disease states in both humans and animal models, which has led to many discoveries (Chen, Ye and Guo, 2019). For instance, using different scRNA-seq platforms, two independent studies identified precursors of dendritic cells (pre-DC) in human peripheral blood (A. Villani *et al.*, 2017; See *et al.*, 2017). In both studies, newly identified marker genes guided the researchers to validate their *in-silico* findings at protein level.

Use of scRNA-seq in pathological conditions can aid the identification of molecular and cellular therapeutic targets in disease. Based on scRNA-seq data a novel disease-associated microglia (DAMs) population was identified in

Alzheimer's disease, and further analysis localised the DAMs in tissue and uncovered the pathways by which they promote disease (Keren-Shaul *et al.*, 2017).

scRNA-seq has also facilitated the creation of cell atlases, mapping the transcriptomes of multiple cell lineages in a given organ. For example, two very recent studies analysing parenchymal and NPCs from human liver using scRNA-seq (MacParland *et al.*, 2018; Aizarani *et al.*, 2019) have generated a human liver cell atlas. Using marker genes identified through scRNA-seq, both studies recapitulate known zonation of hepatocytes, but also highlight zonation of endothelial cells in the liver. Furthermore, these studies have revealed heterogeneity within what was believed to be a homogenous population and identified novel cell types. MacParland et al (2018) identified two transcriptionally distinct KC populations showing functional differences, one enriched for pathways relating to tolerance whilst the second was enriched for pathways relating to inflammation. A novel discovery of bipotent epithelial progenitor populations in the adult human liver was made by Aizarani et al. (2019). Efforts are already underway to combine these studies and others to establish a "human cell atlas", identifying all cell types in the human body, and no doubt this will have a significant impact in the field of biomedicine (Regev *et al.*, 2017).

Two studies recently revealed novel findings in monocytes and macrophage dynamics in the context of non-alcoholic fatty liver disease (NAFLD) (Krenkel *et al.*, 2019; Xiong *et al.*, 2019). scRNA-seq of NPCs from healthy and non-alcoholic steatohepatitis (NASH; a form of NAFLD) mouse livers revealed the emergence of NASH-associated macrophages, which the authors defined as TREM2+ macrophages, conserved in human disease as well. In concordance, unpublished data from the Henderson lab has also identified a subpopulation of scar associated macrophages, defined as TREM2+ CD9+, showing a pro-fibrogenic phenotype in cirrhotic human livers (Ramachandran et al. in press). Krenkel et al. (2019) utilised a murine model of NAFLD and scRNA-seq to

show transcriptional re-programming of monocytes to a unique inflammatory phenotype (NAFLD myeloid phenotype) in the bone marrow, characterised by downregulation of calprotectin genes. This NAFLD monocyte phenotype was shown to be stable; following adoptive transfer they dampened AILI in recipient mice (Krenkel *et al.*, 2019). These studies highlight the power of scRNA-seq in identifying novel, injury-specific signatures and cell types during chronic liver injury, that can be therapeutically manipulated. To date, however, no studies have looked at the transcriptional changes in monocytes and macrophages during acute liver injury at single-cell resolution.

1.8.6 Choice of single-cell RNA sequencing method to study heterogeneity

There are a wide range of methods and platforms available to investigate the transcriptome of cells at a single-cell level (Figure 1.8). The variety of methods can be technically categorised into two groups: full-length methods (SMART-seq and Fluidigm C1) and molecular tag-based methods (MARS-seq and 10X Genomics Chromium). Full-length methods allow the whole transcriptome to be sequenced, providing an increased number of mappable reads (~400-7000 genes/cell), and facilitating allelic gene expression analysis and isoform discovery. On the other hand, they restrict the digital quantification of transcripts, as they do not incorporate UMIs and restrict the number of cells sequenced per run (~96-384). Molecular tag-based methods preferentially sequence either the 3' or 5' end of the transcript, incorporating UMIs to facilitate multiplexing of the sample and thereby improving throughput and precise gene expression quantification. The main caveat of tag-based methods is the 3' or 5' bias impacting overall sensitivity (~500-1500 genes/cell), and a high rate of "dropout events". Nonetheless, given that the number of cells sequenced per run can range to the tens of thousands using droplet-based systems such as the 10X Chromium Genomics platform, it is often more suitable for the identification of rare cell-types.

To reliably dissect the heterogeneity of monocytes and macrophages I felt it necessary to sequence a large number of cells. Therefore, I utilised a droplet-based method using the 10X Genomics Chromium platform.

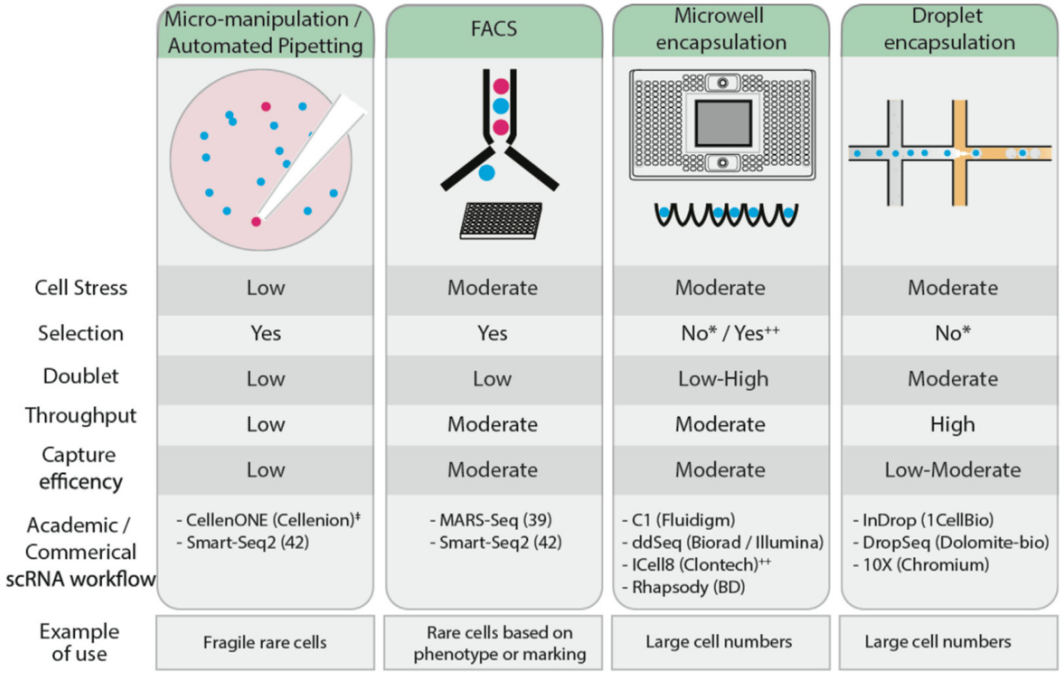

Figure 1.8 Characteristics of common single cell RNA sequencing methods. Reprinted from Nguyen et al, (2018).

1.9 Hypothesis

Unidentified monocyte and macrophage subpopulations exist during acute liver injury, that are key regulators of liver repair

1.10 Aims and objectives

The overall aim of this body of work is to employ scRNA-seq in an unbiased manner to investigate heterogeneity in circulating and hepatic monocyte and macrophage populations during homeostasis and following AILI

My experimental objectives to test this hypothesis are as follows:

- Characterise the systemic and hepatic leucocyte response following acute liver injury

- Perform scRNA-seq of systemic and hepatic monocytes and macrophages in an unbiased manner to study their dynamics and heterogeneity during AILI

- Validate scRNA-seq findings at protein level and *in vivo* to identify distinct injury- and repair-regulating subsets of monocytes and macrophages

2 Materials and Methods

2.1 Mice

Wild-type C57BL/6J mice (CD45.2^{+}) were purchased from Charles River. MacGreen^{GFP}, CX3CR1^{GFP} and CCR2$^{-/-}$ mice were obtained from Prof. Jeffery Pollard (Secondary supervisor). All mice were maintained on a C57BL/6J background and bred under specific pathogen-free conditions at the University of Edinburgh. All experiments were done on male mice, aged between 8-14 weeks, following approval by the University of Edinburgh Veterinary Scientific Services and were conducted under UK Home Office Legislation, following ethical guidelines.

2.2 Genotyping of genetically modified mice

Genotyping of MacGreen^{GFP} and CX3CR1^{GFP} lines were performed by flow cytometry. Blood samples (40μl) were obtained from the tail vein of the animals, then resuspended in 1mL of PBS, followed by centrifugation at 300g for 5mins at 4°C, before resuspending in 400μl of phosphate-buffered saline (PBS). GFP protein fluorescence were detected on Attune NxT flow cytometer (Thermo Fisher Scientific). CCR2-/- genotyping was performed by Sheila Webb, lab manager to Prof. Pollard, via polymerase chain reaction (PCR), the primer sequences and PCR end product information is shown in Table 2.1.

Table 2.1 Primer sequences used for genotyping of CCR2-/- mice

	Primer Sequences	**PCR Product (bp)**
CCR2 wild type Fw	CCACAGAATCAAAGGAAATGG	494
CCR2 wild type Rw	CACAGCATGAACAATAGCCAAG	
CCR2 Knockout R Neo	CCTTCTATCGCCTTCTTGACG	390

2.3 Murine models of liver regeneration

Three models of liver regeneration were used throughout the course of this project. Acetaminophen Induced Liver injury (AILI), Carbon tetrachloride (CCl_4) induced liver injury and Partial Hepatectomy (PHx). Following the induction of injury, all animals were assessed twice daily until the end of the experiment, any animals showing signs exceeding the severity limit were humanely killed.

2.3.1 AILI

Acetaminophen (APAP; Sigma-Aldrich, A7085) was dissolved at 10mg/mL of sterile PBS (Gibco; 14190250). Mice were fasted for 12 hours prior to intraperitoneal administration APAP at a dose of 300mg/kg. Animals had access to water throughout the experiment, food was returned with APAP administration. To avoid hypothermia animals were housed in a heated cabinet at 27°C for the first 24 hours. Aged-matched uninjured littermate controls were used for all experiments. Animals were humanely killed by CO_2 induction at stated timepoints after APAP administration.

2.3.2 CCl_4

For the CCL_4 acute inflammatory model, mice were once injected intraperitoneally with carbon tetrachloride (CCl_4, 1μl/g; Sigma; 289116) diluted 1:3 in olive oil (Sigma; O1514). Control animals received pure olive oil and standard checks were performed twice daily until the end of the experiment. Animals were humanely killed by CO_2 induction stated timepoints after CCl_4 administration.

2.3.3 PHx

All surgeries were performed by me with assistance from Dr. Kylie Conroy. Mice were kept under anesthetised by inhalation of 2% isoflurane (Abbott) mixed with 2L/min oxygen flow and kept on a heated mat during surgery and recovery. Eye lubricant was applied (Viscotears Liquid Gel, Alcon Laboratories (UK) Ltd). Warmed, sterile 0.9% saline (25mL/kg, Braun, Sodium Chloride 0.9% w/v Intravenous Infusion BP) and buprenorphine (0.1mg/kg, Ceva, Vetergesic), diluted to 0.03mg/mL in sterile water for injection was administered subcutaneously pre-operatively and post-operatively.

Two-thirds partial hepatectomy (PHx) was performed as previously described in Mitchell and Willenbring, 2014. A midline abdominal skin and muscle incision was made, the median and left lateral lobes were exteriorised, ligated with 1.5M braided silk (SMI, 8015) individually and then excised. Followed by exteriorisation, ligation and excision of left lateral lobe. The abdominal incision was closed via a continuous suture of 1.5M polyglactin 910 (Ethicon, Vicryl, W9067). Surgical clips (Biochrom, 9mm Autoclips, 52-3748) were used to close the skin. Animals were humanely killed by CO_2 induction stated timepoints after PHx surgery.

2.4 5-Ethynyl-2'-deoxyuridine (EdU) administration

To label proliferating cells, 5-Ethynyl-2'-deoxyuridine powder (EdU, Sigma-Aldrich, 900584) dissolved in sterile PBS (Thermo Fisher Scientific, 14190-250) at 2.5mg/mL, was injected intra-peritoneally at 50mg/kg, 3 hours prior to humane killing.

2.5 Serum biochemistry

Whole blood was collected from the inferior vena cava (IVC), immediately after post-mortem and allowed to clot at room temperature for 30 minutes. Serum was obtained by twice centrifuging the blood at 10000g for 5 minutes. Samples were frozen at -20°C until analysis. Serum alanine transaminase (ALT), aspartate aminotransferase (AST), glutamate dehydrogenase (GLDH) and albumin measurements were analysed at the Shared University Research Facilities within the Queen's Medical Research Institute, according to a standard protocol. This was performed using commercial kits (Alpha Laboratories Ltd) and Cobas Fara centrifugal automated chemistry analyser (Roche Diagnostics).

2.6 Hepatic non-parenchymal cell (NPC) isolation

Mouse livers were perfused *in situ* with ice cold PBS via the Inferior Vena Cava (IVC), portal vein was cut to allow the release of perfusion PBS, until the liver was blanched. The liver was excised while and weighed. The right lobe and the caudate lobes were dissected and weighed and immediately placed in ice cold PBS for flow cytometric analysis, while the remaining lobes were processed accordingly for immunohistochemistry. The livers were mechanically chopped into small fragments with a razor blade, and then two different digestion protocols were followed for isolation of NPCs. Falcon, polypropylene conical centrifuge tubes (Corning) were used for centrifugation of the samples, despite the protocol. All samples were kept on ice unless

stated otherwise, centrifugation for protocol 1 was performed at 4°C, 300g for 5 minutes and protocol 2 at 4°C, 400g for 7 minutes.

Protocol 1 (adapted from Lynch *et al*., 2018)

NPCs were isolated for all flow cytometry experiments in chapter 3 and chapter 5 and specified experiments in chapter 4 following a protocol described in Lynch et al., 2018, with slight modifications. Following mechanical chopping, liver tissue was enzymatically digested in Roswell Park Memorial Institute (RPMI, Gibco, 21875034) 1640 medium, containing a cocktail of: 0.8mg/mL collagenase V (Sigma, C9263-1G), 0.625mg/mL collagenase D (Roche, 11088882001), 1mg/ml dispase (Gibco, 17105-041), and 30μg/mL DNase (Roche, 101104159001). Enzymatic digestion was performed at 37°C for 18 minutes with agitation (240 r.p.m).

Following digestion the cell suspension was strained through a 100μm filter (EASYstrainer Greiner Bio-One, 542000), along with RPMI, and centrifuged. The resultant supernatant was removed, and cell pellet was resuspended in RPMI and centrifuged again. Following this, resultant supernatant was removed, and the cell pellet was lysed for erythrocytes by 3 minutes incubation with 10% RBC lysis buffer (Biolegend, 420301) in dH2O. Cells were resuspended in 3mL of PEB buffer, containing PBS (Thermo Fisher Scientific, 14190-094), 2% Foetal Bovine Serum (Thermo Fisher Scientific, 10500-064), and 2mM EDTA (Sigma-Aldrich, E5134) and centrifuged. After the supernatant was discarded, the resultant cell pellet was resuspended in PEB buffer, filtered through a 35μm nylon mesh (Corning, 352235) 5mL tube. A 6μL aliquot was taken for cell counting, cells/mL count was obtained on a TC-20 cell counter (Bio-Rad), using trypan blue as a live dead marker, and the rest of the sample was centrifuged to obtain a pellet. Based on the cell count, the sample was resuspended in appropriate volume of PEB buffer to plate 2 million cells in a 96-well plate. The cells were blocked in 10% mouse serum (Sigma-Aldrich,

M5905) and 1% CD16/32 (Biolegend, 101302), for 10 minutes at 4°C prior to antibody staining.

Protocol 2 (adapted from Mederacke *et al*., 2015)

NPCs were isolated to generate single cell suspensions for single cell RNA sequencing by following protocol. After mechanical mincing, the liver was enzymatically digested in Hank's Balanced Salt Solution (HBSS, Gibco, 14170112) containing 0.53 Wunsch Units/mL collagenase B (Roche, 11088807001), 10mg/mL Pronase (Sigma, P5147) and 0.25mg/mL DNase 1 (Roche, 10104159001) at 37°C for 15 minutes with agitation (240 r.p.m). Following this, strained through 120μm nybolt mesh, along with PEB buffer, containing PBS, Thermo Fisher Scientific, 14190-094), 2% low endotoxin Foetal Bovine Serum (Thermo Fisher Scientific, 10082139), and 2mM EDTA (Sigma-Aldrich, E5134) and DNase (0.02mg/ml). A syringe plunger was used to gently push through any undigested tissue. Then centrifuged, resultant supernatant was removed, cell pellet was lysed for erythrocytes by 3 minutes incubation with 10% RBC lysis buffer (Biolegend, 420301) in dH2O. Following this, cells were resuspended in PEB buffer with DNase and centrifuged, supernatant was discarded, and cell pellet was resuspended in 2mL of PEB buffer and passes through a 35μm nylon mesh (Corning, 352235). The samples for relevant controls was decanted, cells were centrifuged, and the supernatant was discarded. The cells were blocked in 10% mouse serum (Sigma-Aldrich, M5905) and 1% CD16/32 (Biolegend, 101302) for 10 minutes at 4°C prior to antibody staining.

2.7 Systemic leucocyte isolation and generation of single cell suspension

At the time of harvest, whole blood (100-200μL) was collected from the IVC, into 0.5mM EDTA solution, on ice. Erythrocytes were lysed by incubation with 10% Red Blood Cell (RBC) lysis buffer (Biolegend, 420301) in dH2O for 5 minutes, resuspended in PEB buffer (same composition as for hepatic NPC

isolation, low endotoxin FBS was used for scRNA-seq experiments), followed by centrifugation at 4°C, 300g for 5 minutes. The supernatant was removed, and cell pellet was lysed again by resuspending in 10% RBC lysis buffer in dH2O for 5 minutes, followed by centrifugation at 4°C, 300g for 5 minutes, before resuspending in PEB buffer and centrifuging the cell suspension. After the resulting supernatant was removed, the cell pellets were resuspended in 1mL of PEB buffer and filtered through 35μm nylon mesh (Corning, 352235). Followed by a wash by centrifugation, the residual supernatant was removed, and the cells were incubated with live/dead stain (Zombie UV, Biolegend, 423107), at a concentration of 1:100 in PBS, for 15 minutes at room temperature. Cells were washed in PEB buffer, then blocked in 10% mouse serum (Sigma-Aldrich, M5905) and 1% CD16/32 (Biolegend, 101302) for 10 minutes at 4°C and labelled with antibodies for 20 minutes at 4°C. Followed by two washes in PEB buffer, before overnight fixation in 100μl of fixation and permeabilization buffer (1:3 to diluent, eBioscience, 00-5523), at 4°C. After fixation, cells were washed twice with perm/wash buffer (eBioscience, 00-5523) and resuspended in PEB buffer for acquisition on the flow cytometer.

2.8 In vivo phagocytosis assay

In vivo labelling of phagocytic cells using PKH26 red fluorescent cell linker (PKH, Sigma-Aldrich, PKH26PCL) was performed as previous described in Campana et al., 2018. PKH26 was dissolved in diluent solution provided in the commercial kit, at a 1 in 100 dilution. To label phagocytic cells 100μL of dissolved PKH solution was injected intravenously, 16hrs prior to humane killing. The fluorescence was detected in cells of interest via flow cytometry.

2.9 *Ex vivo* PhagoGreen assay

Ex vivo labelling of phagocytic cells was performed using pH sensing smart fluorescent probes: PhagoGreen and PhagoRed (Vázquez-Romero *et al.*, 2013; Fernández and Vendrell, 2016). Both fluorescent probes were acquired

from Dr. Marc Vendrell. Cells were incubated with 100μL of PhagoGreen (at concentrations of: 50nM, 100nM, 150nM, 200nM) and PhagoRed (at concentrations of: 150nM, 200nM, 250nM, 300nM) for 30 minutes at 4°C. Cell labelling with PhagoGreen, and PhagoRed was done after live/dead staining, prior to blocking and surface antibody staining.

2.10 Flow cytometry and fluorescence-activated cell sorting

For flow cytometry or fluorescence-activated cell sorting (FACS), cells were isolated and following blocking, they were incubated with primary antibodies for 20 minutes at 4°C. Antibodies and fluorophore combinations varied depending on the staining combination, all antibodies and conjugates and their catalogue numbers are shown in Table 2.2. Flow cytometry compensations were set up using single stained beads (UltraComp eBeads, Thermo Fisher Scientific, 01-2222-42). Compensations for PKH, PhagoGreen, PhagoRed and intrinsic fluorescent reports (GFP) was set up using single stained cells. Controls for gating included 'fluorescence-minus-one' samples. Cell viability was assessed using the following live/dead stains: DAPI (1:100 dilution, Invitrogen, D3571), which was added immediately prior to cytometry or sorting, Zombie UV (Biolegend, 423107) and Zombie NIR (Biolegend, 423105), added prior to blocking, at a concentration of 1:100 in PBS and incubated with cells for 15 minutes at room temperature, in the dark. Cell sorting for scRNA-seq was performed on FACSAria II (BD Biosciences). Flow cytometry acquisition was performed on LSRFortessa (BD Biosciences) and Aurora (Cytek Biosciences) and data was analysed using FlowJo 10.0.8rl software.

2.10.1 Gating strategy

Gating strategy for the detection of different hepatic leucocytes and circulating leucocytes varied depending on the combination of antibodies used in experiments but followed the same initial steps to detect cells, single cells and live cells. The nonparenchymal cell (NPC) population was isolated on forwards

(FSC-A) against side (SSC-A) scatter, following the removal of doublets via FSC-A vs FSC-H. Live cells were isolated based on negative staining of one of the three live dead stains: DAPI, Zombie UV, Zombie NIR. Leucocytes were identified on the positive expression of CD45 in both liver and blood, along with endothelial lineage markers (CD31, ICAM2) in the liver.

For the identification of specific hepatic leucocytes, the following strategy was followed. Cells not belonging to the of the mononuclear phagocyte (conventional dendritic cells, cDC; monocytes, monocyte derived macrophage, MDMs; Kupffer cells, KCs) compartment were identified first. B cells were identified as: CD45+ B220+, T cells as: CD45+ CD11b- CD3+, NK cells as: CD45+ NK1.1+, eosinophils as: CD45+ CD11b+ SiglecF+, Neutrophils as: CD45+ Ly6C+ Ly6G+, plasmacytoid DCs (pDCs) as: CD45+ F4/80- CD11B- B220+ CD11C+. After the removal of lymphocytes and eosinophils, neutrophils and pDCs the different types of MPs were isolated. In chapter 3, cDCs were generally identified as: CD45+ F4/80- CD11b- $MHCII^{Hi}$ $CD11c^{Hi}$ in chapter 3, however following scRNA-seq cDCs were defined further into cDC1 and cDC2 in chapter 5.

For the identification of mononuclear phagocytes (MPs) in chapter 5, the following gating strategy was used. Cells, single cells and live cells were identified as described above. Leucocytes were isolated based on CD45 expression, following this any cells not belonging to the MP system was excluded from the analysis using a dump channel. These included: neutrophils, NK cells, eosinophils, pDCs, B cells, T cells using Ly6G, NK1.1, SiglecF, SiglecH, CD19 and CD3, respectively, all conjugated to the same fluorophore. Following this, cDCs1 cells were identified as: CD45+ $XCR1^{Hi}$ $CD24^{Hi}$ cDC1 and cDC2 cells as:CD45+ $CD11c^{Hi}$ $F4/80^{Lo}$. Hepatic monocytes were identified as: CD45+ $F4/80^{Lo}$ $CD11b^{Hi}$ $Ly6C^{Hi}$ $MHCII^{Lo}$. MDMs were identified as: CD45+ $F4/80^{Int}$ $TIMD4^{Lo}$ $CD11b^{Hi}$ $Ly6C^{Int/Lo}$ $MHCII^{Hi/Lo}$. KCs were identified as: CD45+ $F4/80^{Hi}$ $TIMD4^{Hi}$ $CD11b^{Lo}$. Hepatic monocytes were further defined based on CD62L or CXCR2. MDMs were further defined by

CD63, MHCII, IL7R. Expression of CD36, MerTK, CD24, CD9, CD11c was assessed on KCs and MDMs.

Liver cells were quantified as absolute numbers or proportions of NPCs (represented as % of leucocytes; CD45+ cells, or as % of parent population). Absolute numbers were calculated by expressing each subset as a proportion of leucocytes, then the total number cells in the digested portion of the liver was counted and represented as cells/g of liver, based on the number of cells in the whole sample and the weight of the portion of liver used for flow cytometry.

The gating strategy for the identification of specific circulating leucocytes was similar to that of that of hepatic leucocytes with minor changes. B cell identified as: CD45+ B220+, T cells were identified as: CD45+ CD3+, NK were cells identified as: CD45+ NK1.1+. Eosinophils were identified as: CD45+ CD11b+ SiglecF+. Following this, circulating monocytes were isolated as: CD45+ CD11b+ CD115+ and further defined as Ly6C^{Hi} monocytes (CD45+ CD11b+ CD115+ Ly6C^{Hi}) and Ly6C^{Int} monocytes (CD45+ CD11b+ CD115+ Ly6C^{Int}) and Ly6C^{Lo} monocytes (CD45+ CD11b+ CD115+ Ly6C^{Lo}). Circulating subsets were quantified and represented as a portion of the leucocytes (CD45+ cells) or as absolute counts. Absolute counts were quantified using fluorescent precision count beads (Biolegend, 424902), at a known concentration, added to each sample at a volume of 50μL, immediately before flow cytometry acquisition. The number of beads per mL of whole blood was quantified and cell counts were expressed relative to the number of beads in the sample, to calculate the number of cells per mL of blood.

Table 2.2 Antibodies used for flow cytometry and FACS

Antibody	Fluorophore	Manufacturer	Cat.No.	Dilution
B220	BV421	Biolegend	103239	1:200
CCR2	BV421	Biolegend	150605	1:100
CD115	PE	ThermoFisher	12-1152-82	1:100
CD115	PE/Cy7	Biolegend	135523	1:100
CD11b	BUV737	BD Biosciences	564880	1:100
CD11b	APC/Cy7	Biolegend	101225	1:400
CD11c	PE/CY5	Biolegend	117316	1:400
CD19	BV650	BD Biosciences	115541	1:50
CD209a	BV421	BD Biosciences	747827	1:50
CD24	BV510	Biolegend	101831	1:50
CD3	BV650	BD Biosciences	100229	1:50
CD3	AF488	Biolegend	100212	1:100
CD3	eFluor 450	e-Bioscience	48-0032-82	1:100
CD31	PE/Dazzle	Biolegend	102525	1:100
CD36	AF647	Biolegend	102610	1:400
CD45	BV605	BD Biosciences	563053	1:100
CD45	PE	Biolegend	103105	1:100
CD62L	PE/ Dazzle 594	Biolegend	104447	1:50
CD63	APC	Biolegend	143905	1:100
CD63	PE	Biolegend	143903	1:100
CD64	BV421	Biolegend	139309	1:100
CD9	PerCP/Cy5.5	Biolegend	124817	1:50
CX3CR1	BV711	Biolegend	149031	1:50
CXCR2	PE	Biolegend	149303	1:100
F4/80	BV785	Biolegend	123141	1:100
F4/80	PE/Cy7	Biolegend	123113	1:200
F4/80	APC/Cy7	Biolegend	123117	1:100
ICAM2	AF647	Biolegend	105611	1:100

IL7R	PE/Dazzle 594	Biolegend	135031	1:50
IL7R	APC	Biolegend	135011	1:50
Ly6C	PercpCy5.5	Biolegend	128011	1:400
Ly6C	PE/Dazzle	Biolegend	128043	1:100
Ly6G	AF700	Biolegend	127621	1:200
Ly6G	BV650	Biolegend	127641	1:100
MerTK	APC	Biolegend	151507	1:200
MHCII	AF700	Biolegend	1076121	1:500
NK1.1	BV650	BD Biosciences	108736	1:50
NK1.1	PE/Cy7	Biolegend	108713	1:200
SiglecF	BV650	BD Biosciences	740557	1:50
SiglecF	PE-CF594	BD Biosciences	562757	1:200
SiglecH	BV650	BD Biosciences	747672	1:50
TIMD4	PE/CY7	Biolegend	130009	1:400
XCR1	AF647	Biolegend	148213	1:200

Cat.No: Catalogue number

2.11 Tissue fixation and preparation

Perfused livers were harvested, the median lobes were taken for paraffin-embedding and left lobe was taken for fixed-frozen preparation using Optimal Cutting Temperature (OCT) embedding. For paraffin-embedding, livers were fixed overnight at room temperature in 4% formaldehyde, then transferred into 70% ethanol before embedding in paraffin and sectioning. Liver tissue was sectioned at a thickness of 5-8μm. For OCT embedding, livers were fixed at 4°C in 4% paraformaldehyde for 2 hours, before washing in PBS, dehydrating through serial sucrose gradients (15% for 1 hour and then 30%, overnight at 4°C). Following dehydration, tissue was placed in OCT embedding matrix (Thermo Fisher Scientific, 12678646) and subjected to freezing on dry ice. Sample were stored at -80°C until sectioning. Tissue was sectioned at 5μm, using a cryostat microtome (Bright instruments, 5040).

2.12 Immunofluorescence

Paraffin-embedded tissue sections were dewaxed in xylene, twice for 5 minutes and rehydrated in decreasing concentrations of ethanol (100%,75%, 65%, 2 minutes in each). Washed in dH_2O and where stated heat mediated antigen retrieval was performed by microwaving the tissue in 10mM Sodium Citrate buffer, pH6, for 15 minutes. Endogenous peroxidase activity was inhibited with 3% hydrogen peroxide (10 minutes incubation). For the staining of frozen-fixed tissue there was no additional preparations except the tissue sections were allowed to reach room temperature for 20 minutes, before continuing with the staining protocol. All tissue sections were washed in PBS buffer and blocked using serum block (Biolegend, 927501), primary antibodies and secondary antibodies (Table 2.3) were diluted in antibody diluent (Abcam, ab64211) unless otherwise stated. Negative control section, lacking the primary antibody was used to confirm positive signal for all stains performed.

2.12.1 HNF4α / EdU

This protocol was performed on paraffin-embedded liver sections, prepared as outlined above and 0.5% Triton-X 100 was used for the washes (5 minutes). After performing antigen retrieval and quenching endogenous peroxidase, the tissue was permeabilized using 0.5% Triton-X 100 (Sigma, T8787) in PBS for 20 minutes, at room temperature. Tissue was blocked in protein block for 1 hours, followed by overnight incubation of HNF4α, at 4°C. Tissue was washed twice, then incubated in a drop of anti-mouse polymer ImPRESS (Vector Laboratories, MP-7402-15) for 30 minutes at room temperature, followed by two washes. TSA Plus Cyanine 3 (Perkin Elmer, NEL744001KT-1:1000) was applied for 10 minutes. After twice washing, sections were permeabilised in 0.5% Triton-X100 as before. Click-iT Plus EdU Imaging Kit Alexa Fluor 647 (Thermo Fisher Scientific, C10640) was used to detect incorporation of EdU in cells. EdU detection cocktail was made up as per manufacturer's instructions and tissue sections were incubated with EdU cocktail, for 30 minutes at room temperature and twice washed after staining. Nuclear counterstain was achieved with DAPI (Sigma, D9542) diluted 1:1000 in PBS, sections were incubated for 15 minutes, at room temperature, before mounting in ProLong Gold (Thermo Fisher Scientific, P36930).

2.12.2 F4/80 / EdU

This protocol was performed on fixed-frozen sections, prepared as outlined above. No antigen retrieval was required, tissue sections were washed twice, incubated with protein block for 30 minutes at room temperature. Anti-F4/80 was applied, sections were incubated overnight, at 4°C, followed by two washes in PBS. For Click-iT Plus EdU Imaging sections were permeabilized with 0.5% Triton-x100 for 20 minutes at room temperature, followed by blocking with protein block for 30 minutes, at room temperature. EdU protocol was carried out exactly as above, following EdU staining, sections were counterstained with DAPI before mounting.

2.12.3 CLEC4F / TIMD4

This protocol was performed on fixed-frozen sections, prepared as outlined above and required no antigen retrieval. Sections were washed and blocked described as previously, primary antibodies goat anti-CLEC4F and rat anti-TIMD4 was applied simultaneously, incubated overnight at 4°C. Sections were washed twice in PBS to remove unbound primary antibodies then secondary antibodies: donkey anti-goat 555 and chicken anti-rat 647 were applied for 30 minutes at room temperature. Following this counterstained with DAPI before mounting.

2.12.4 CD63 / MacGreen / EdU

This protocol was performed on fixed-frozen liver sections, from MacGreen ^{GFP} mice, and required no antigen retrieval. Sections were washed and blocked described as previously. As the fixation protocol can weaken the GFP signal, chicken anti-GFP primary antibody was applied, along with rat anti-CD63, sections were incubated overnight at 4°C. Secondary antibodies: horse anti-chicken 488 and goat anti-rat 555 were applied for 30 minutes, at room temperature. Counterstain with DAPI was performed as before, followed by mounting.

2.12.5 IL7R / MacGreen / EdU

This protocol was performed on fixed-frozen liver sections, from MacGreen ^{GFP} mice, and required no antigen retrieval. Sections were washed and blocked described as previously. Chicken anti-GFP and rat anti-IL7R primary antibodies were applied overnight, at 4°C. Secondary antibodies: horse anti-chicken 488 and goat anti-rat 555 were applied for 30 minutes, at room temperature. Counterstain with DAPI was performed as before, followed by mounting.

2.13 Histology staining

To visualize liver architecture, the following histology stains were performed: Hematoxylin and Eosin, Hematoxylin, Masson's trichrome, Picro Sirius Red, and Periodic Acid-Schiff. These stains were performed within the Histology, Immunodetection and Aquila-HistoPlex section of the Shared University Research Facilities within the Queen's Medical Research Institute, according to a standard protocol.

Table 2.3 Antibodies used for Immunohistochemistry

Description	Application	Manufacturer	Catalogue Number	Dilution
Mouse Anti-HNF4α	1°	Perseus Proteomics	pp-H1415-00	1:300
Rat Anti-F4/80	1°	Abcam	Ab6640	1:200
Goat Anti-CLEC4F	1°	R&D Systems	AF2784	1:500
Rat Anti-TIMD4	1°	Biolegend	130002	1:200
Rat Anti-CD63	1°	Biolegend	143901	1:100
Chicken Anti-GFP	1°	Abcam	Ab13970	1:800
Rat Anti-IL7R	1°	Biolegend	121102	1:100
Goat Anti-rat 555	2°	ThermoFisher	A-21434	1:200
Chicken Anti-rat 647	2°	ThermoFisher	A-21472	1:200
Donkey Anti-goat 555	2°	ThermoFisher	A-21432	1:200
Donkey Anti-mouse 555	2°	ThermoFisher	A-31570	1:200
Donkey Anti-chicken 488	2°	Jackson ImmunoResearch	703-545-155	1:200

2.14 Image capture

Brightfield images and fluorescent images of whole tissue sections were captured using the slide scanner AxioScan.Z1 (Carl Zeiss, Oberkochen, Germany) at 20X magnification. Representative images of EdU / F4/80 stains were imaged using a confocal LSM780 microscope (EdU / F4/80 stains), at 40X magnification, fields were chosen at random using the DAPI channel. Thresholds for all the fluorescent channels were set against the negative controls, were kept constant throughout the same experiment. Images were processed and scale bars were added on Zen Blue (Zeiss) software.

2.15 Image quantification

Slide scanned images were imported into a Definiens Tissue Studio workspace (Definiens AG, Munich, Germany) workspace, which is a machine learning platform that facilitates automated image quantification, based on contrast, intensity, and morphological features. The analysis was done with guidance and assistance from Dr. Daniel Soong, a post-doctoral researcher in Prof. Jeffrey Pollard's lab. Tissue artefacts were removed from the analysis via automated segmentation, images were checked manually, to remove any artefacts that were missed by automated analysis.

For the quantification of necrosis (Figure 3.1) random fields were chosen from a selection of training images (at least 4, to account for variations in staining intensity), these fields were segmented, and manually classified as "necrotic" (lighter staining) and "not-necrotic" (brighter staining). After several rounds of training on the randomly selected fields, analysis was performed on the actual images. The images were segmented automatically based on "necrotic" and "non-necrotic" classifications across the whole liver cross-section for all samples. Following the analysis, statistics for total area of the tissue, area of "necrotic" and "non necrotic" was exported.

The immunofluorescence quantification was made up of three stages. In the primary stage ("ROI detection") the tissue was segmented based on stained regions of interest (ROI). The secondary stage consisted of "Cellular analysis" where the DAPI channel was used to detect and segment nuclei. Cellular artefacts were discarded through five-cycles of trained intensity- and morphology-based machine learning; this included incomplete or low-quality cells. In order to detect cells of interest: CLEC4F+ TIMD4+ (Figure 3.2) and HNF4α+ EdU+ (Figure 3.6), cell stimulation was performed based on even growth from the nuclear detection object, cellular objects were then classified based threshold-based positivity appropriate channels. The third and final stage consisted of "Data Export" where statistics for the ROIs was exported. The statistics consisted of single positive, double positive and triple positive cells in per square millimeter of ROI (tissue). In order to quantify the percentage of proliferating hepatocytes (Figure 3.6) the number of DAPI+ HNF4α+ EdU+ cells were divided by DAPI+ HNF4α+ cells (total number of hepatocytes) and then multiplied by 100.

2.16 Droplet-based scRNA-seq

Single cells were processed through the Chromium™ Single Cell Platform using the Chromium™ Single Cell 3' Library and Gel Bead Kit v2 (10X Genomics, PN-1200237) and the Chromium™ Single Cell A Chip Kit (10X Genomics, PN-120236) as per manufacture's protocol. As 10X is a fully commercial system, the exact primer and adapter sequences are not available. This section will contain a brief overview of the procedure (Figure 2.1).

Single cells were sorted via FACS into PBS + 2% FBS, washed twice and counted using TC20 (Bio-Rad). 10,769 cells and 10X reagents were added to one lane of the 10X microfluidics chip, 10X gel beads into another and Oil into the third lane. The cells were then partitioned into Gel Beads in Emulsion in the Chromium ™ instrument (Figure 2.1), where cell lysis and barcoded reverse transcription of RNA occurred (Figure 2.2), followed by amplification,

fragmentation and 5′ adaptor and sample index attachment (Figure 2.3). Libraries were sequenced on an Illumina HiSeq 4000.

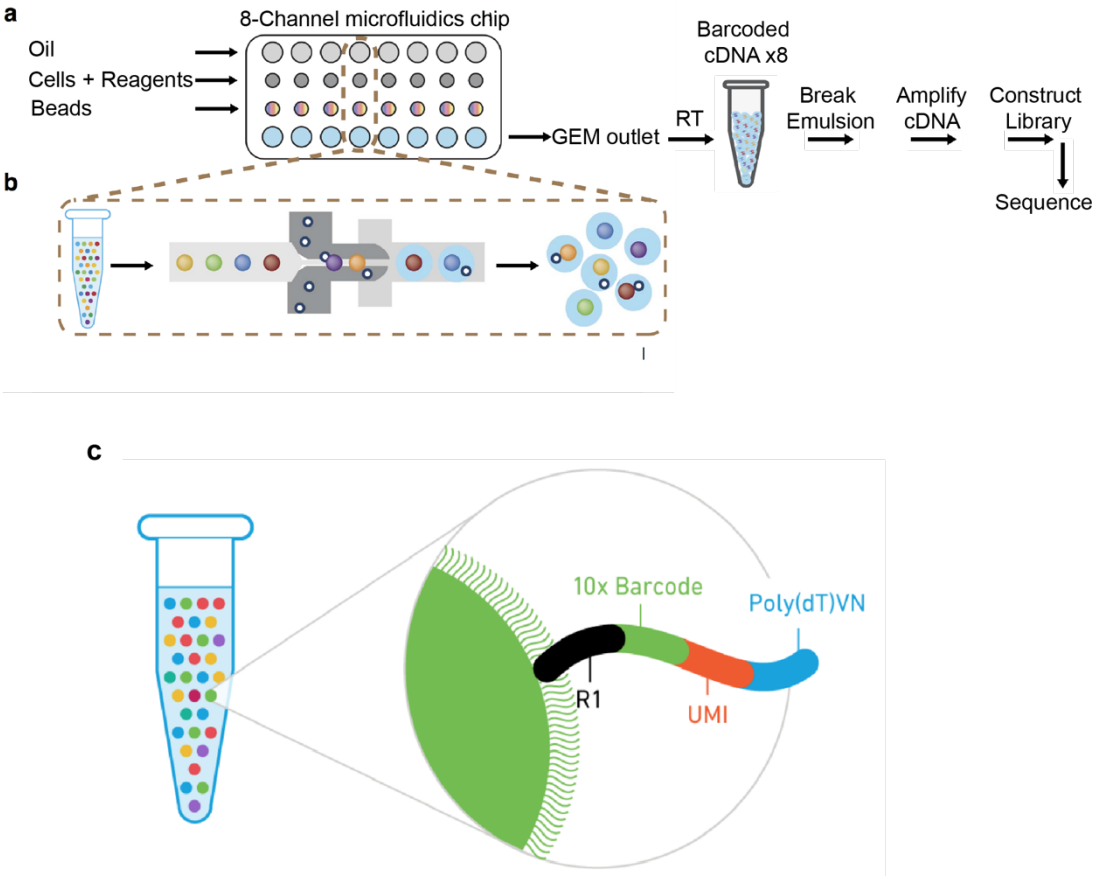

Figure 2.1 Schematic of 10X Chromium workflow. (**a**) Cells with reagents loaded in one channel of the microfluidic chip combines with Gel beads to form Gel beads in EMulsion (GEMs). Reverse transcription (RT) occurs inside the GEM, emulsions are lysed, and cDNA is pooled for amplification and library construction in bulk. (**b**) GEM formation. Gel bead containing primers and barcoded oligonucleotides are first mixed with cells and reagents and then subsequently partitioned into an oil droplet at a microfluidic junction. A successful GEM will contain single gel bead attached to one cell inside an oil droplet. (**c**) Composition of Gel beads. Each gel bead contains barcoded oligonucleotides containing Illumina adapters, unique 10X cellular barcodes, unique molecular identifiers (UMIs) and oligo dTs, required to prime RT of polyadenylated RNAs. (a,b) Adapted from Zheng et al. (2017), (c) Reprinted from 10X Genomics.

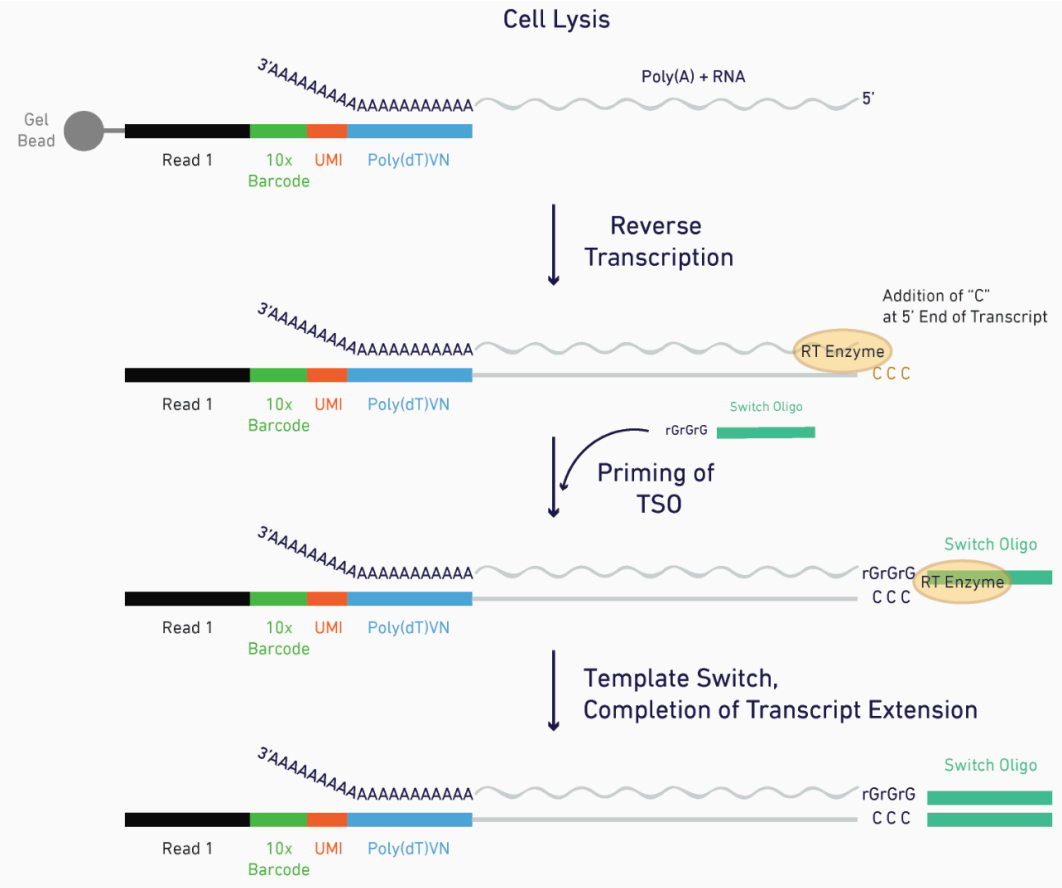

Figure 2.2 Schematic of reaction workflow inside the GEMs. Captured cells inside the GEM lyses, Gel bead dissolves, releasing the oligo primers into the aqueous environment. The contents of GEM (lysed cell components, master mix reagents, oligos) are incubated in a reverse transcription reaction to generate full-length, barcoded cDNA from poly A-tailed mRNA transcripts. Primed by barcoded Gel bead oligo, reverse transcriptase performs a template switch to a template oligo at the 5' end of the transcript. Reprinted from 10X Genomics.

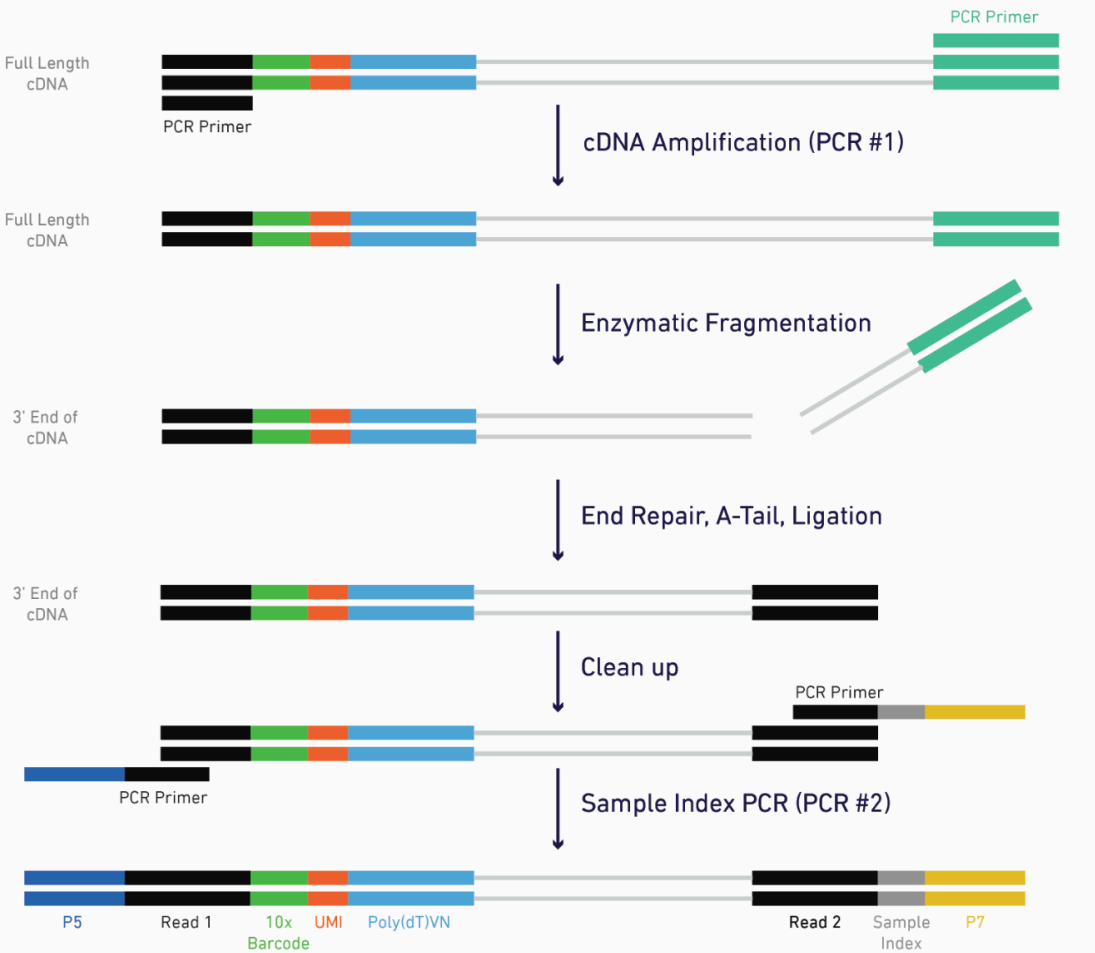

Figure 2.3 Schematic of cDNA library construction. Following RT, the GEMs are lysed, pooling single-stranded, barcoded cDNA molecules from every cell. cDNA is amplified by bulk PCR, followed by Enzymatic Fragmentation and size selection for the optimized generation of the sequencing libraries. During library construction Read 2 is added by Adapter ligation. During the Sample Index PCR Illumina P5 and P7 sequences, and sample index sequences are added. The finished library construct will contain P5, P7, Read 1 and Read 2 sequences for Illumina bridge amplification and sequencing, in addition to 10x barcode and UMI used during data analysis. Reprinted from 10X Genomics.

2.17 Bioinformatics analysis of scRNA-seq data

The analysis described below was carried out in collaboration with Dr. John Wilson-Kanamori, post-doctoral bioinformaticist in the Henderson group.

2.17.1 Pre-processing

FASTQ files, as retrieved from the sequencing facility, were aligned to the mm10 (Ensembl 84) mouse reference genome using the Cell Ranger v2.1.0 Single-Cell Software Suite from 10X Genomics, and cell-containing partitions and associated UMIs estimated to create a counts matrix per sample. Genes expressed in fewer than three cells in a sample were excluded, as were cells that expressed fewer than 300 genes or mitochondrial gene content >10% of the total UMI count, prior to merge integration of all samples into one dataset. To create normalised expression values, cell counts in the dataset were adjusted by dividing the UMI count per gene with the total UMI count in the corresponding cell (E_n), and log-transformed by calculating $\ln(10^4 * E_n + 1)$. To create relative expression values, variation in normalised UMI counts between cells was regressed according to a negative binomial model, before scaling and centring the result by subtracting the mean expression of each gene and dividing by its standard deviation.

2.17.2 Dimensionality reduction, clustering, and DE analysis

Unsupervised (SNN graph-based) clustering and differential gene expression analyses were performed using the *Seurat* R package v2.3.0[75]. The SNN graph was constructed using between 4 and 16 principal components as determined by dataset variability shown in principal components analysis (PCA); the resolution parameter to determine the resulting number of clusters was also tuned accordingly.

In total, scRNA-seq data from 4 murine liver samples and 4 murine blood samples was analysed and presented here. Initial clustering was performed

on all 8 scRNA-seq datasets (2x uninjured liver tissue, 2x uninjured blood, 2x APAP liver tissue, 2x APAP blood), with the aim of identifying 1) populations of liver-resident and circulating cells and 2) contaminating circulatory cells within datasets generated from liver tissue digests, so as to remove them from downstream analysis. Upon further clustering followed by signature analysis (described below), the post-processed liver-resident dataset was interrogated for cell lineages. The mononuclear phagocyte lineage (MP) was isolated and re-analysed as above to identify robust lineage subpopulations. At this stage clusters expressing more than one unique lineage signature in more than 25% of their cells from the dataset were removed as probable doublets.

All heatmaps, tSNE / UMAP visualisations, violin plots, and dot plots were produced using *Seurat* functions in conjunction with the *ggplot2*, *pheatmap*, and *grid* R packages. tSNE / UMAP visualisations were constructed using the same number of principal components as the associated clustering. Differential gene expression analysis was conducted in *Seurat* using the Wilcoxon rank sum test to assess significance. Genes with a log-fold change of at least 0.25 and expression in at least 10% of cells in the cluster under comparison were retained and the rest were excluded. Gene ontology enrichment analysis was performed on the positive genes which were differentially expressed using PANTHER 13.1 (pantherdb.org).

2.17.3 Defining cell lineage signatures

For each cell we obtained a signature score across a curated list of known marker genes per cell lineage in the liver (Appendix 4). This signature score was defined as the geometric mean of the normalised expression of the associated signature genes in that cell. Lineage signature scores were scaled from 0 to 1 across the dataset, and the score for each cell with signature less than a given threshold (the mean of said signature score across the entire dataset) was set as 0.

2.17.4 Inferring pseudotemporal dynamics

To generate potential pseudotemporal trajectories, we used the *velocyto* R package v0.6.0 (Manno *et al.*, 2018) to estimate cell velocities from the ratio of their spliced and unspliced mRNA content. We generated annotated spliced and unspliced reads from the 10X BAM files via the *dropEst* pipeline, before calculating gene-relative velocity using kNN pooling with k=25, fitting gene offsets with a gamma fit on the top/bottom 2% expression quantiles and determining slope gamma with the full range of cellular expression. We visualised the resulting aggregate velocity fields (using Gaussian smoothing on a regular grid) on the appropriate visualisation as generated previously.

2.18 Statistical Analysis

All non-bioinformatics data was analysed using Microsoft Excel for macOS (version 16.28) and GraphPad Prism 8 for macOS (version 8.3.0). All the graphs are shown as the mean +/- standard error of the mean (SEM) of all the individual data from repeated experiments, as indicated in the figure legend. Statistical analysis was done using GraphPad Prism 8 for macOS (version 16.28) as described in the corresponding figures. Significant values: *$P \leq 0.05$, **$P \leq 0.01$, ***$P \leq 0.001$, ****$P \leq 0.0001$

3 Characterisation of leucocyte dynamics during murine model of liver regeneration

3.1 Introduction

Acetaminophen (APAP) is an over-the-counter drug that is widely used as an analgesic. Overdose of APAP represents the commonest cause of acute liver failure (ALF) in western countries (Bernal and Wendon, 2013). APAP induced liver injury (AILI) is a multiphasic process, the initial phase is often described as necroinflammatory, where overwhelming hepatocyte necrosis releases damage associated molecular patterns (DAMPs), leading to the activation of resident non-parenchymal cells (NPCs) (Woolbright and Jaeschke, 2017a). The activated NPCs release various proinflammatory and chemotactic molecules, which results in rapid infiltration of circulating inflammatory leucocytes into the liver, which further propagates inflammation. This is followed by the repair phase where the resident and recruited cells promote liver regeneration via the resolution of inflammation, hepatocyte proliferation, angiogenesis and matrix remodelling (Markose *et al.*, 2018). In ALF patients there is a prolonged pro-inflammatory phase which fails to resolve, consequently, liver regeneration is severely compromised (Triantafyllou *et al.*, 2018). Previous studies using murine models of AILI have demonstrated the importance of different leucocytes in regulating liver injury and repair following AILI (Markose *et al.*, 2018). The majority of the studies focus on monocytes and macrophages, because of their capacity to regulate inflammation and tissue repair. Their involvement in the clinical setting has also been highlighted by many studies, where monocyte and macrophage dysfunction positively correlates with poor prognosis in ALF patients (Antoniades *et al.*, 2008; Moore *et al.*, 2017). Due to their inherent plasticity where they exhibit a spectrum of activation states, influenced by various environmental cues (Guilliams and van de Laar, 2015), their therapeutic manipulation has been challenging.

In the murine model of AILI, monocytes/macrophages populating the liver can be categorized into three distinct subsets: Kupffer cells (KCs), Ly6C^{Hi} monocytes and Ly6C^{Lo} monocyte-derived macrophages (Ly6C^{Lo} MDMs) (Holt, Cheng and Ju, 2008; Zigmond *et al.*, 2014). In an uninjured liver, KCs account for 80% of the hepatic macrophage pool and self-replenish without contribution from bone marrow-derived circulating monocytes and their progeny (Yona *et al.*, 2013; Gomez Perdiguero *et al.*, 2015). Following APAP overdose and hepatic injury circulating Ly6C^{Hi} monocytes infiltrate the liver in a CCR2/CCL2 dependent manner (You *et al.*, 2013; Mossanen *et al.*, 2016). Ly6C^{Hi} monocytes dominate the necroinflammatory phase and subsequently undergo transcriptional reprogramming towards a pro-reparative phenotype, commonly identified through downregulation of Ly6C, hence referred to as Ly6C^{Lo} MDMs (Ramachandran *et al.*, 2012; Zigmond *et al.*, 2014; Graubardt *et al.*, 2017). Another feature of AILI that studies have observed is the depletion in KC numbers during the necroinflammatory phase, Zigmond et al. (2014) demonstrated their numbers are re-established through local proliferation in the repair phase. Most of the work in the field has relied on cell surface markers to identify and define these cells via flow cytometry and immunohistochemistry. KCs have been defined as: CD68^{+} F4/80^{Hi} CD11b^{Lo}; Ly6C^{Hi} monocytes as CCR2^{Hi} CX3CR1^{Lo} F4/80^{Lo} CD11b^{Hi} Ly6C^{Hi}; and Ly6C^{Lo} MDMs are defined as CCR2^{Lo} CX3CR1^{Hi} F4/80$^{Int/Lo}$ CD11b^{Hi} Ly6C^{Lo} (You *et al.*, 2013; Zigmond *et al.*, 2014; Graubardt *et al.*, 2017; Triantafyllou *et al.*, 2017). Recently, CLEC4F and TIMD4 have been identified as unique markers of resident macrophages, the former is found exclusively on KCs (Beattie *et al.*, 2016; Scott *et al.*, 2016).

Despite the distinct differences in immune cell composition and marker expression between rodents and humans (Heymann and Tacke, 2016), analysis of liver and blood from ALF patients has identified analogous monocyte and macrophage subsets with similar activation states, reported in murine models of AILI. Both resident macrophages (CD68+) and MDMs (MAC387+) are actively involved in the injury and repair process following AILI

and can been seen localized around the injury areas (Antoniades *et al.*, 2012; Triantafyllou *et al.*, 2017). Existence of both pro-inflammatory macrophages (Mossanen *et al.*, 2016) and pro-reparative macrophages with an immunoregulatory phenotype (Triantafyllou *et al.*, 2017) have been identified in the livers of ALF patients. In addition to the hepatic immune response, the systemic immune response can also influence the outcome for ALF patients (Antoniades *et al.*, 2012; Mossanen *et al.*, 2016; Triantafyllou *et al.*, 2018). In parallel to marked hepatic monocyte infiltration, ALF patients exhibit significant monocytopenia with reduced HLA-DR expression on monocytes, a molecule required to carry out antigen presentation functions, critical to innate immunity (Antoniades *et al.*, 2006, 2012). They were also shown to have reduced inflammatory classical monocytes ($CD14^{++}$ $CD16^{+}$) and increased immunoregulatory intermediate monocytes ($CD14^{+}$ $CD16^{+}$), promoting peripheral immunosuppression (Antoniades *et al.*, 2012; Moore *et al.*, 2017). These features increase the risk of infections, which is associated with adverse clinical outcome (Antoniades *et al.*, 2012; Moore *et al.*, 2017).

Macrophages have also been identified as key players in other models of liver injury, both chronic and acute (Selzner *et al.*, 2003; Xu *et al.*, 2007; Ramachandran *et al.*, 2012; Campana *et al.*, 2018). Partial hepatectomy (PHx) is an example of an acute liver injury model that is commonly used to study the mechanisms of liver regeneration. Surgical removal of 70% of the liver results in complete regeneration of the remnant lobes within 7-10 days in murine subjects (Michalopoulos, 2007). Although leucocytes have not been investigated as extensively in PHx model as they have been in AILI, there are some reports of their involvement in liver regeneration following PHx. Both KCs and infiltrating macrophages were shown to influence liver regeneration following PHx but the methods of distinguishing KCs from infiltrating macrophages are not as reliable as the studies focusing on AILI (Selzner *et al.*, 2003; Nishiyama *et al.*, 2015). Studying leucocyte responses during liver regeneration in different models of liver injury could tell us if macrophages and other leucocytes have either an inherent post-injury response to regulate liver

regeneration or whether their response is unique to the type of insult. Identification of differences and commonalities in leucocyte behavior could be key to targeting them in a clinical setting.

There are some conflicting views on whether monocytes/macrophages promote or hinder liver regeneration. Some studies report that KCs and infiltrating monocytes/macrophages have a pro-inflammatory role that might hinder liver regeneration and promote hepatotoxicity (Michael *et al.*, 1999; You *et al.*, 2013; Mossanen *et al.*, 2016; Bird *et al.*, 2018; Zhang *et al.*, 2018). Whereas other studies highlight the importance of macrophages in promoting liver repair and hepatocyte proliferation through enhanced phagocytic capabilities (Triantafyllou *et al.*, 2017) and release of mitogenic factors such as IL-6, IL-10, IL-4, IL-13 (Bourdi *et al.*, 2002; Ju *et al.*, 2002; Yee *et al.*, 2007; Ryan *et al.*, 2012). It has become apparent that these cells are very dynamic, exhibiting temporal changes in their function and phenotype. Additionally, macrophage phenotype and function can be influenced by other leucocytes such as neutrophils (Graubardt *et al.*, 2017; Yang *et al.*, 2019). Therefore, studying the temporal changes in macrophages during the different phases of AILI, in relation to other leucocytes and hepatocytes can facilitate better understanding of these cells and identify specific therapeutic targets (Graubardt *et al.*, 2017; Yang *et al.*, 2019).

3.1.1 Aims

- To characterise the temporal dynamics of liver injury and repair following AILI
- To investigate the hepatic and systemic leucocyte response over the course of AILI
- To numerically and phenotypically characterise monocytes and macrophage populations following AILI
- To identify pro-repair macrophage subsets promoting liver regeneration
- To compare the similarities and differences in leucocyte responses following PHx and AILI

3.2 Results

3.2.1 Characterisation of hepatocyte death and proliferation during AILI

In experimental models, the extent of the injury and the regenerative process that follows AILI can be influenced by multiple factors including the strain of mice, the dose and route of APAP administration (Mossanen and Tacke, 2015). My colleagues in the Henderson lab have previously optimised the dose of APAP for mice bred on a C57BL/6 background, which gives a considerable degree of liver injury with minimal mortality. Based on this, a regenerative murine model of acute liver injury was generated by administration of APAP at a dose of 300mg/kg via a single intraperitoneal (*i.p*) injection.

To fully understand the dynamics of both parenchymal and non-parenchymal cells during the different phases of AILI, I performed a time-course experiment and obtained liver tissue and blood for further analysis (Figure 3.1a). APAP overdose is reported to initiate liver injury, via hepatocyte necrosis (Martin-Murphy, Holt and Ju, 2010). A comparison between various histology stains of the liver showed Periodic Acid Schiff (PAS) to be the optimal stain. The PAS stain demonstrates glycogen, as hepatocytes are glycogen rich it can be used as an indirect measure of hepatocyte death. The necrotic (lighter staining) area is clearly distinct from healthy liver tissue had (stronger staining), facilitating quantification of necrosis (Appendix 1). PAS staining showed APAP overdose induced centrilobular hepatocyte necrosis (Figure 3.1b). Quantification of necrotic area across the whole liver cross-sections demonstrated hepatocyte necrosis peaked as early as 6hrs post-APAP induction (Figure 3.1c), around 45% of the liver lobule is necrotic at this timepoint. The necrotic area decreased at a fast rate, with very minimal necrosis from 48hrs onwards (Figure 3.1c). Serum was analysed for Alanine transaminase (ALT), Aspartate transaminase (AST) and Glutamate dehydrogenase (GLDH) to evaluate the

extent of liver damage (McGill, 2016). As these enzymes are found within hepatocytes, therefore their elevated levels in the serum indicates hepatocyte death and liver injury. Serum ALT and AST peaked at 6hrs post-APAP and significantly reduced at 48hrs post-APAP and returned to baseline by 72hrs (Figure 3.1d, Figure 3.1e). GLDH levels peaked later on in the time course at 24hrs in the same animals, and stayed elevated during the repair phase at 48hrs, 72hrs, therefore GLDH could be used as an indicator of liver injury in the later timepoints of AILI (Figure 3.1f).

Having established the peak liver injury timepoints (6hrs-24hrs), I sought to characterise the dynamics of liver regeneration following AILI. Hepatocyte proliferation was used as an indicator of liver regeneration. In order to assess proliferation, mice were given 5-Ethynyl-2'-deoxyuridine (EdU), a nucleoside analogue to thymidine, 3 hours prior to harvest. Hepatocyte nuclear factor-4-alpha (HNF4α) was used as a marker for identifying hepatocytes and 4',6-diamindino-2-phenylindole (DAPI), a stain that potently binds to adenine-thymine region of deoxyribonucleic acid (DNA), was used as a nuclear counterstain to identify all cells. EdU^+ HNF4α^+ $DAPI^+$ cells across whole liver cross sections were quantified to asses hepatocyte proliferation. Hepatocytes are quiescent under homeostatic conditions, the loss of parenchymal cells following APAP overdose promotes the remaining hepatocytes to proliferate to replace the dead cells (Figure 3.2a). Hepatocyte proliferation is localised to centrilobular regions, the percentage of proliferating hepatocytes at 48hrs and 72hrs post-APAP are significantly increased (Figure 3.2a, b, n=5-9, two independent experiments). Hepatocyte proliferation is still elevated at 120h, 144h (Figure 3.2b), when necrosis and serum ALT/AST levels have returned to baseline and liver architecture is comparable to an uninjured liver (Figure 3.1).

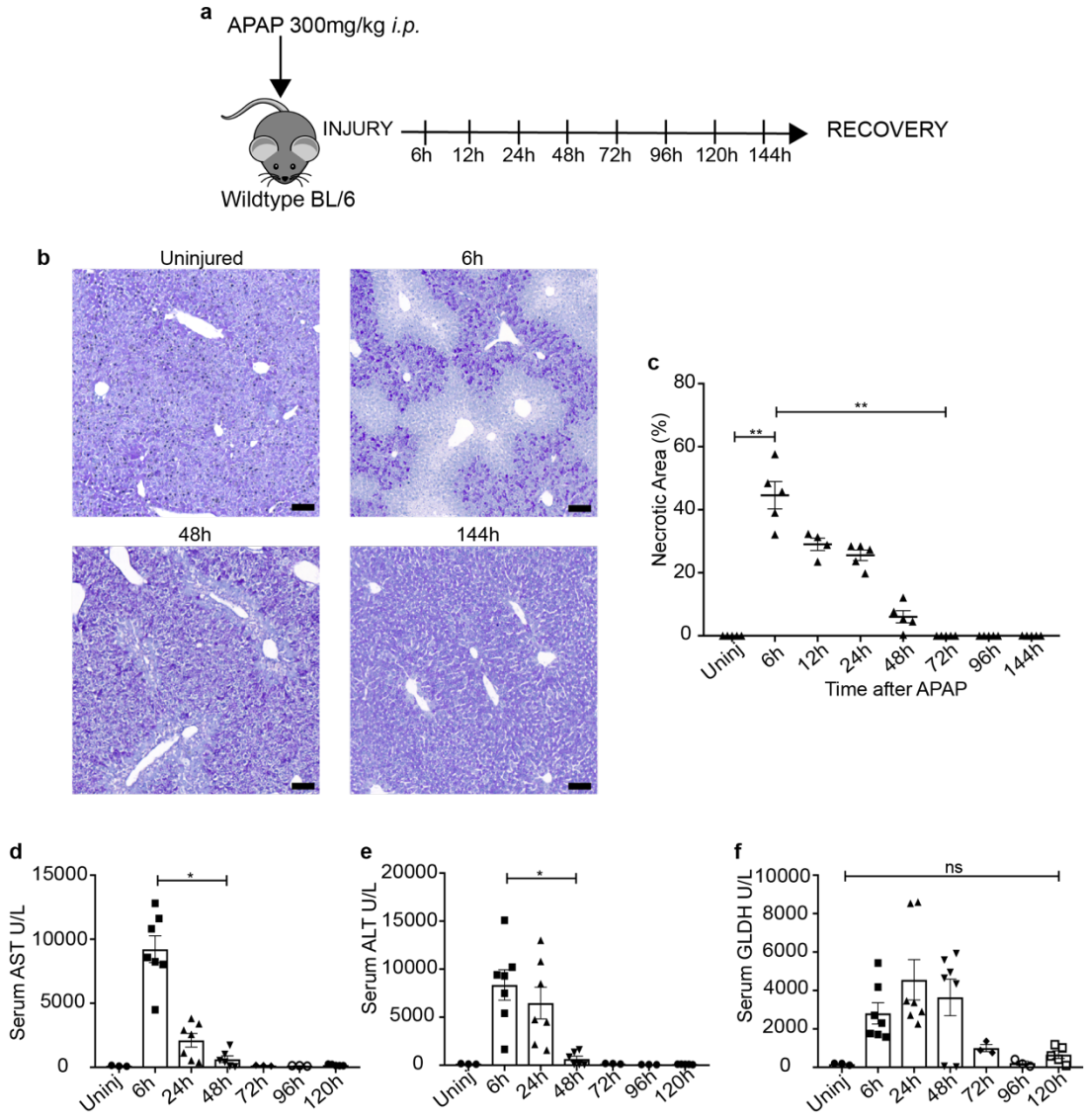

Figure 3.1 Assessment of liver injury following AILI. (**a**) Schematic of the experimental design to study the temporal dynamics of parenchymal and non-parenchymal cells following APAP overdose; i.p., intraperitoneal. (**b**) Representative images of Periodic acid-Shiff (PAS) staining of whole liver-cross sections. (**c**) Quantitation of % necrotic area based on PAS staining for control (uninjured) and post-APAP animals (Scale bar=100μm). Measurement of serum AST (**d**), ALT (**e**), GLDH (**f**) levels for uninjured and post-APAP animals. (c) Data acquired from two independent experiments, n=5 per group, One-way ANOVA with Dunn's multiple comparisons test. (d,e,f) Data acquired from two independent experiments, n=3-7 per group, One-way ANOVA with Dunn's multiple comparisons test. All data shown as Mean±S.E.M. *$P \leq 0.05$, **$P \leq 0.01$.

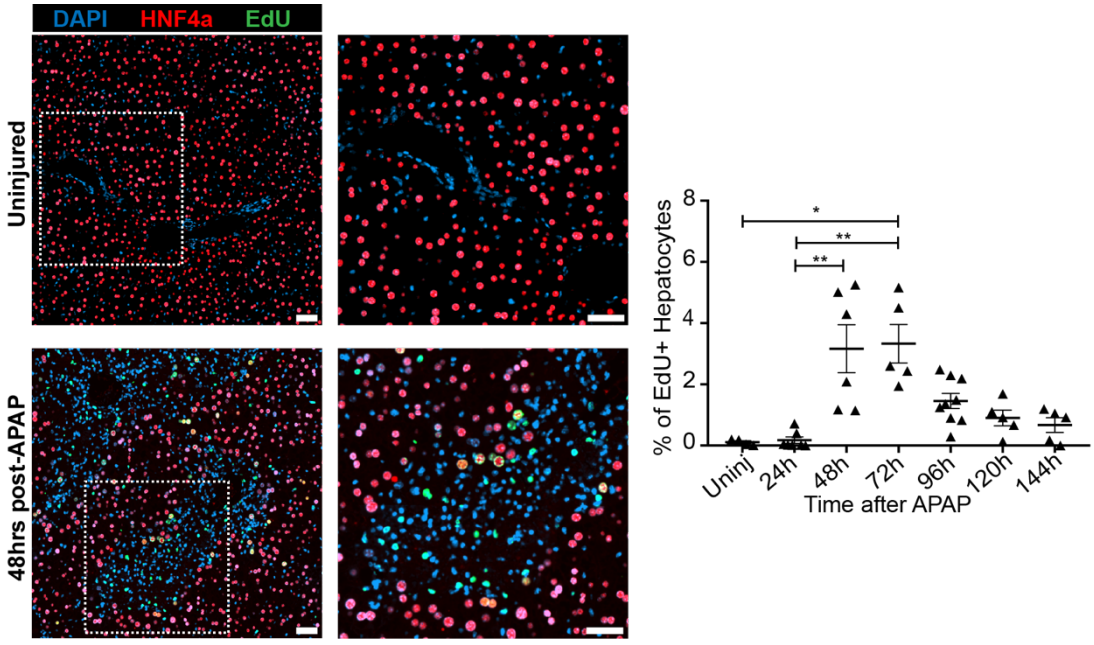

Figure 3.2 Assessment of hepatocyte proliferation following AILI. Representative images of immunofluorescence staining of whole liver cross sections for DAPI (blue); HNF4a (red) and EdU (green) for uninjured and 48hrs-post APAP animals (Scale bar=50μm) and quantitation of % of proliferating hepatocytes (DAPI+ HNF4α+EdU+) over the time course of AILI and for uninjured animals. Data acquired from two independent experiments, n=4-9 per group, One-way ANOVA with Dunn's multiple comparisons test. Data shown as Mean±S.E.M. *$P \leq 0.05$, **$P \leq 0.01$.

3.2.2 Hepatic leucocytes show a dynamic response during AILI

Following the assessment of liver injury and repair, I assessed the broad changes in the hepatic leucocyte populations during the different phases of AILI. To do this a previously reported NPC enriching liver digestion protocol was used (Bain *et al.*, 2016; Lynch *et al.*, 2018). A comprehensive flow cytometry panel consisting of lineage specific cell surface markers was devised to simultaneously isolate different lineages of leucocytes over the course of AILI (Appendix 2). Using the cell surface markers: CD45 and CD31, the NPCs were divided into three compartments: leucocytes ($CD45^+/CD31^-$), endothelial cells ($CD45^-/CD31^+$) and other NPCs ($CD45^-/CD31^-$) (Figure 3.3a).

Hepatic NPCs such as stellate cells and biliary cells, which are not identified through CD45 and CD31 expression may contribute to the “other NPCs” fraction. The number of leucocytes and “other NPCs” are both greatly elevated in both the injury and repair phase (from 6hrs to 120h), whereas endothelial cells decreased following APAP overdose at 12hrs, followed by an increase at 72hrs (Figure 3.3b).

Using cell surface markers shown in Appendix 2 I was able to identify and characterize majority of the leucocytes in uninjured and post-APAP livers. As this was done within one panel, it allowed me to see the dynamic changes in all the main leucocyte subsets throughout the course of AILI. The relatively small numbers of cells, termed “others” might account for basophils, mast cells and innate lymphoid cells (Figure 3.3c; see gating strategy in Appendix 2). Once the cells were annotated, I investigated how AILI affected the leucocyte numbers throughout the time course (n=5-10, from two independent experiments). Assessing the hepatic leucocyte composition, demonstrated that macrophages, T cells and B cells make up majority of the immune cells in an uninjured liver (Figure 3.3c). Following injury, a significant increase in neutrophil, macrophage and eosinophil numbers were observed (Figure 3.3c). APAP induced expansion of neutrophils in the liver at 6, 12 and 24hrs, followed by their decline from 48hrs onwards (Figure 3.4). A similar increase is seen with macrophages at 12hrs, however unlike neutrophils they stay elevated during the later timepoints (Figure 3.3c, 3.4). Expansion of eosinophils occurred much later at 72hrs-post APAP, which also marks peak hepatocyte proliferation (Figure 3.2, 3.4). There were no significant changes in the numbers of T cells, B cells, NK cells, conventional dendritic cells (cDCs) or plasmacytoid dendritic cells (pDCs) (Figure 3.4). This experiment highlighted that the temporal dynamics of different leucocytes varied during AILI and importantly, macrophages represented the most expanded subset of hepatic leucocytes during the inflammatory phase and the repair phase during AILI (Figure 3.3c, 3.4).

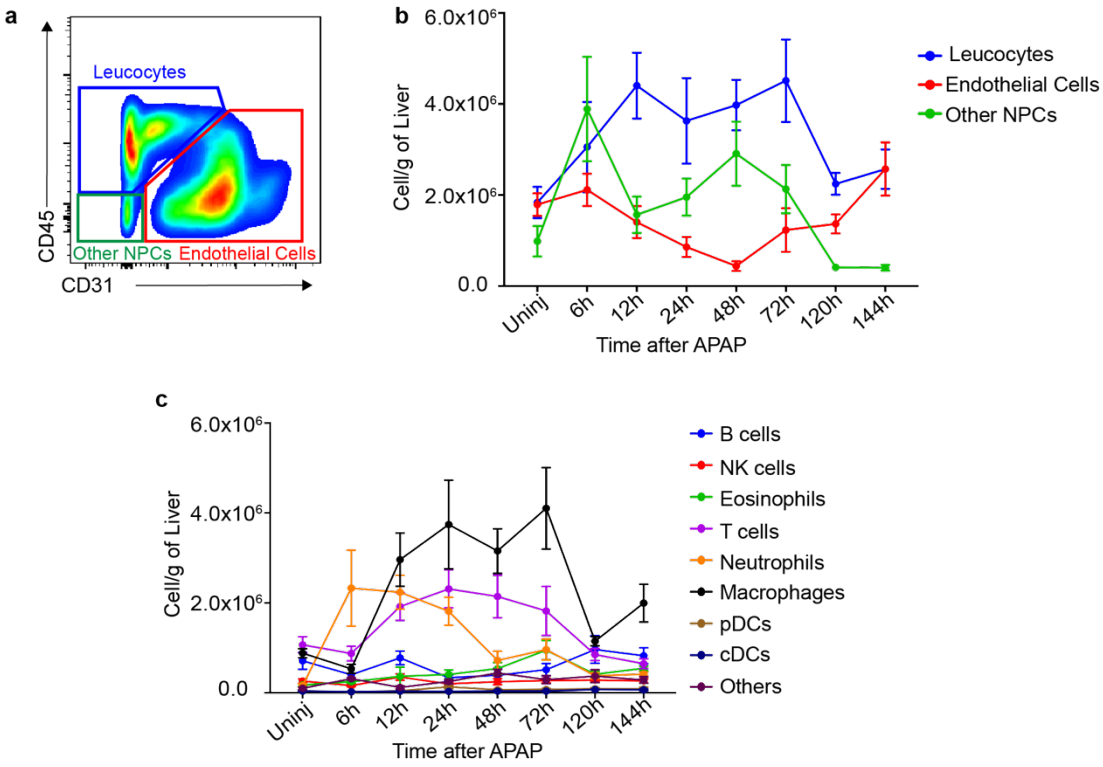

Figure 3.3 Flow cytometric characterization of the temporal dynamics of hepatic non-parenchymal cells following AILI. (**a**) Gating strategy used for the identification of leucocytes, endothelial cells and other hepatic non-parenchymal cells, based on CD45 and CD31 cell surface expression. (**b**) Changes in the absolute number of leucocytes, endothelial cells and other non-parenchymal cells in the liver during AILI. (**c**) Proportional changes in the hepatic leucocyte compartment during AILI. Data acquired from three independent experiments, n=5-10 per group. Data shown as Mean±S.E.M.

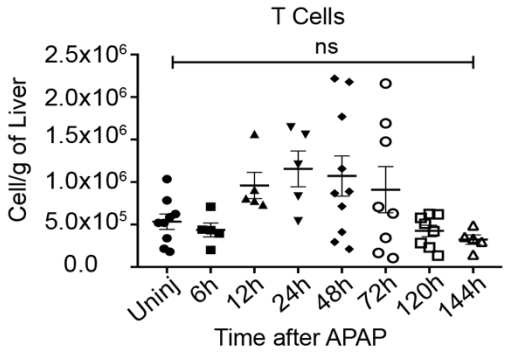
T Cells
ns
Cell/g of Liver
2.5x10⁶
2.0x10⁶
1.5x10⁶
1.0x10⁶
5.0x10⁵
0.0
Uninj
6h
12h
24h
48h
72h
120h
144h
Time after APAP

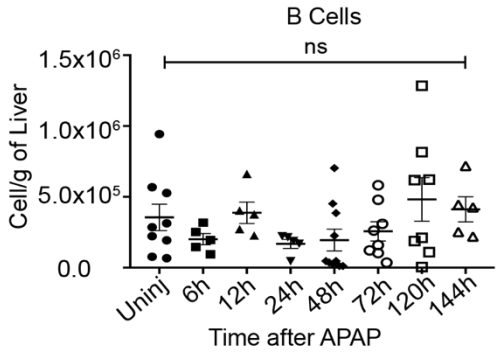
B Cells
ns
Cell/g of Liver
1.5x10⁶
1.0x10⁶
5.0x10⁵
0.0
Uninj
6h
12h
24h
48h
72h
120h
144h
Time after APAP

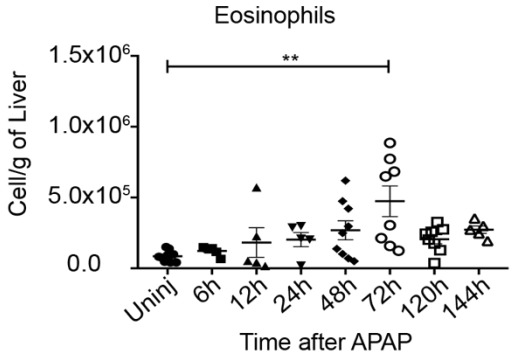
Eosinophils
**
Cell/g of Liver
1.5x10⁶
1.0x10⁶
5.0x10⁵
0.0
Uninj
6h
12h
24h
48h
72h
120h
144h
Time after APAP

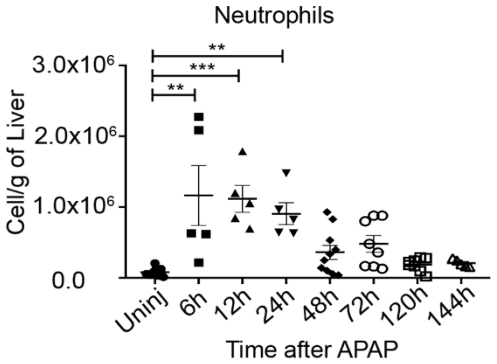
Neutrophils
**
***
**
Cell/g of Liver
3.0x10⁶
2.0x10⁶
1.0x10⁶
0.0
Uninj
6h
12h
24h
48h
72h
120h
144h
Time after APAP

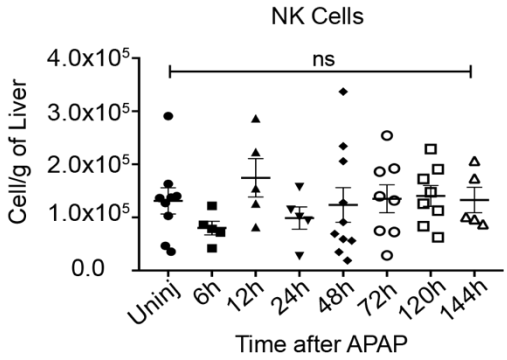
NK Cells
ns
Cell/g of Liver
4.0x10⁵
3.0x10⁵
2.0x10⁵
1.0x10⁵
0.0
Uninj
6h
12h
24h
48h
72h
120h
144h
Time after APAP

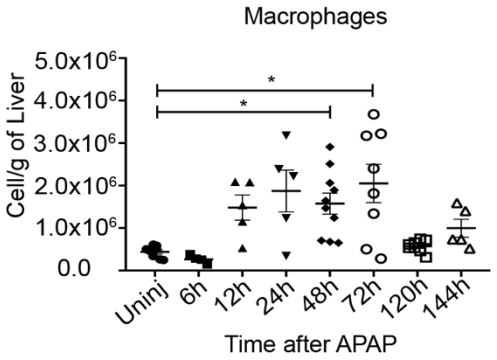
Macrophages
*
*
Cell/g of Liver
5.0x10⁶
4.0x10⁶
3.0x10⁶
2.0x10⁶
1.0x10⁶
0.0
Uninj
6h
12h
24h
48h
72h
120h
144h
Time after APAP

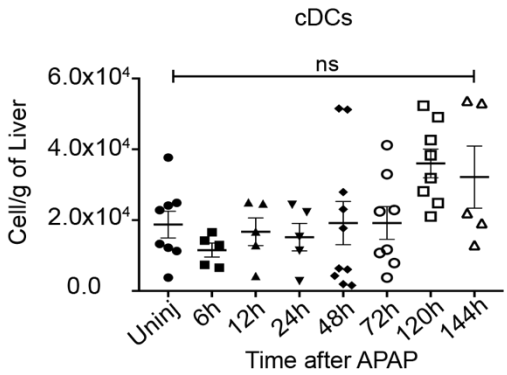
cDCs
ns
Cell/g of Liver
6.0x10⁴
4.0x10⁴
2.0x10⁴
0.0
Uninj
6h
12h
24h
48h
72h
120h
144h
Time after APAP

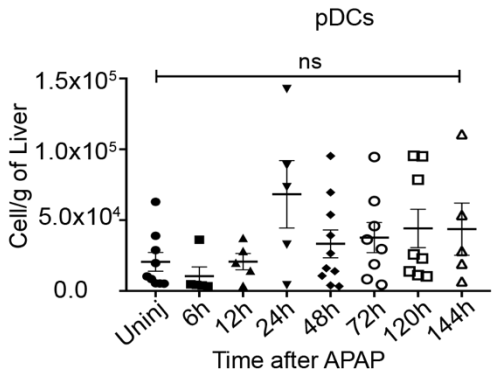
pDCs
ns
Cell/g of Liver
1.5x10⁵
1.0x10⁵
5.0x10⁴
0.0
Uninj
6h
12h
24h
48h
72h
120h
144h
Time after APAP

Figure 3.4 Changes in leucocyte numbers over the course of AILI. Flow cytometric identification and quantitation of changes in the number of different types of hepatic leucocytes during stated timepoints following AILI. Data acquired from three independent experiments, n=5-10 per group, One-way ANOVA with Dunn's multiple comparisons test. All data shown as Mean±S.E.M.
$^{**}P \leq 0.01$, $^{***}P \leq 0.001$.

3.2.3 Ly6C^{Lo} MDMs represents the most expanded macrophage subset in the liver during maximal liver regeneration

Following a broad characterisation of all leucocytes during AILI, I focused specifically on monocytes and macrophages. A series of experiments were performed to characterize macrophage topography and phenotype. Immunofluorescent staining for F4/80, a cell surface glycoprotein commonly used as a murine pan-macrophage marker, showed that under homeostatic conditions macrophages are distributed throughout the liver parenchyma. However, at 48hrs post-APAP there is a population of F4/80+ DAPI+ cells localised around centrilobular areas of hepatic injury and repair (Figure 3.5a). EdU staining also demonstrated that under steady state conditions macrophages did not proliferate however, at 48hrs post-APAP EdU+ F4/80+ cells were seen around the centrilobular areas, indicating that these cells proliferate specifically in the areas of injury and repair (Figure 3.5a).

As previously discussed, macrophages involved in AILI are broadly categorised into three different subsets: Kupffer cells (KCs), infiltrating monocytes and monocyte-derived macrophages (MDMs). Previous studies have utilised transgenic reporter mice (CCR2^{RFP} and CX3CR1^{GFP} mice) to assess the contribution of infiltrating monocytes/macrophages in AILI. My aim here was to see how these cells changed in a wild type C57BL/6 mouse. In order to do this, I used F4/80 and CD11b (an integrin, used as a murine pan-monocyte/macrophage marker) to isolate macrophages by flow cytometry. Following this, TIMD4, a phosphatidylserine receptor which has been reported to exclusively mark resident macrophages, was used to identify KCs (Scott *et*

al., 2016). Ly6C expression was used to define the infiltrating cells as Ly6C^{Hi} monocytes (F4/80^{Lo} CD11b^{Hi} TIMD4^{-}) and Ly6C^{Lo} MDMs (F4/80^{Hi} CD11b^{Int} TIMD4^{-}) (Ramachandran *et al.*, 2012; Scott *et al.*, 2016) (Figure 3.5b).

There are dynamic changes in the three subsets of monocytes/macrophages. Uninjured liver is composed predominantly of KCs (F4/80^{Hi} CD11b^{Lo} TIMD4^{+}), following injury KC numbers significantly decreased (Figure 3.5c, d). Previous studies have reported significant reduction in KCs at 24hrs post-APAP via flow cytometry (Zigmond et al., 2014), here it occurs as early as 6 h post APAP induction and their numbers were re-established at 72hrs and then subsequently peaked at 144hrs (Figure 3.5d). To confirm the KC disappearance seen by flow cytometry I performed immunohistochemistry staining for TIMD4 and CLEC4F (a KC specific C-type lectin receptor) in both uninjured and 48hrs post-APAP livers (Scott *et al.*, 2016). Interestingly, there was no reduction in KCs (TIMD4+ CLECF4+ DAPI+ cells) at 48hrs, as seen with flow cytometry. Quantification of KCs (TIMD4+ CLEC4F+ DAPI+ cells) within a liver cross-section of a whole lobule revealed KCs are significantly increased at 48hrs compared to uninjured livers (Figure 3.6). There were also topographical differences, where a proportion of KCs in post-APAP liver were localised to centrilobular region, whereas in the uninjured liver they are distributed throughout the parenchyma with no obvious zonation (Figure 3.6).

Infiltration of circulating monocytes is a characteristic feature of liver injury, here infiltration of Ly6C^{Hi} monocytes can be seen as early as 12hrs post-APAP and they continued to expand between 12-24hrs, which marks the necroinflammatory phase of AILI. After 24hrs there is a reduction in Ly6C^{Hi} monocytes, in parallel the number of hepatic Ly6C^{Lo} MDMs increased (Figure 3.5). Based on flow cytometric analysis Ly6C^{Lo} MDMs represent the predominant macrophage subset in the liver during maximal regeneration (48hrs-72hrs) and their numbers returned back to near baseline at 144h (Figure 3.5). Recent reports shows that neutrophils, Ly6C^{Hi} monocytes and Ly6C^{Lo} MDMs, spatially and temporally coincide at distinct phases of AILI and

an interplay between these cells can regulate neutrophil apoptosis and polarisation of Ly6C^{Hi} monocytes and Ly6C^{Lo} MDMs (Graubardt *et al.*, 2017; Yang *et al.*, 2019). I investigated the dynamics of these cells and found that neutrophil numbers declined from 12hrs onwards, when the Ly6C^{Hi} monocytes peaked in the liver, followed by a significant decline of both Ly6C^{Hi} monocytes and Neutrophils which was paralleled by an increase in Ly6C^{Lo} MDMs (Figure 3.5g). This would fit with the existing data that Ly6C^{Hi} monocytes promote neutrophil apoptosis, and neutrophils in turn can mediate phenotypic conversion of Ly6C^{Hi} monocytes to Ly6C^{Lo} MDMs (Graubardt *et al.*, 2017; Yang *et al.*, 2019). Contrary to the observation made by Graubardt et al, (2017), in which neutrophil numbers were still elevated in the liver at 48hrs, and then subsequently declined at 72hrs, here, their decline occurred at an earlier timepoint (24hrs) (Figure 3.5g). This discrepancy may be due to the differences in the strain of mice used and the gating strategy followed to isolate neutrophils, Ly6C^{Hi} monocytes and Ly6C^{Lo} MDMs.

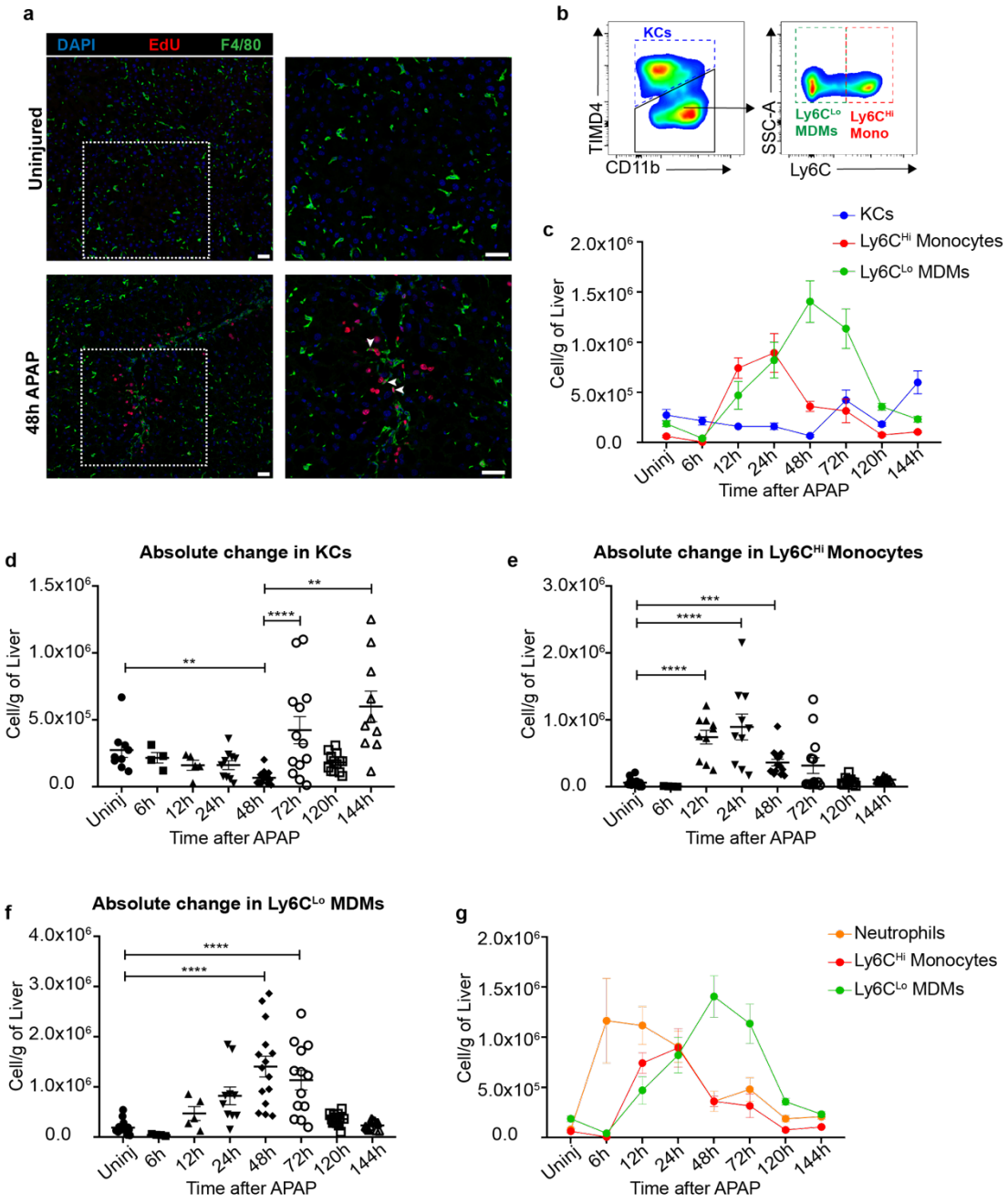
a
DAPI
EdU
F4/80
Uninjured
48h APAP
b
KCs
TIMD4
CD11b
SSC-A
Ly6C
Ly6C^Lo MDMs
Ly6C^Hi Mono
c
KCs
Ly6C^Hi Monocytes
Ly6C^Lo MDMs
Cell/g of Liver
Time after APAP
Uninj
6h
12h
24h
48h
72h
120h
144h
d
Absolute change in KCs
e
Absolute change in Ly6C^Hi Monocytes
f
Absolute change in Ly6C^Lo MDMs
g
Neutrophils
Ly6C^Hi Monocytes
Ly6C^Lo MDMs

Figure 3.5 Analysis of the different subsets of macrophages during AILI. (**a**) Representative Immunofluorescence micrograph of uninjured and 48hrs-post APAP livers, staining of F4/80 (green), DAPI (blue) and EdU (Red) indicates that macrophages localize and expand around areas of injury during the regenerative phase (48hrs) (Scale bar=50μm, white arrows indicate F4/80+ EdU+ DAPI+ cells). (**b**) Gating strategy for the identification of resident and infiltrating macrophages via flow cytometry. (**c**) Temporal dynamics of KCs, Ly6C^{Hi} monocytes and Ly6C^{Lo} MDMs during AILI. Absolute changes in KCs (**d**), Ly6C^{Hi} monocytes (**e**) and Ly6C^{Lo} MDMs (**f**) numbers quantified via flow cytometry at stated timepoints following APAP overdose. (**g**) Temporal dynamics of Ly6C^{Hi} monocytes and Ly6C^{Lo} MDMs and Neutrophils during AILI. Data acquired from three independent experiments, n=5-10 per group, One-way ANOVA with Dunn's multiple comparisons test. Data shown as Mean±S.E.M, * $P \leq 0.05$, ** $P \leq 0.01$, *** $P \leq 0.001$, **** $P \leq 0.0001$.

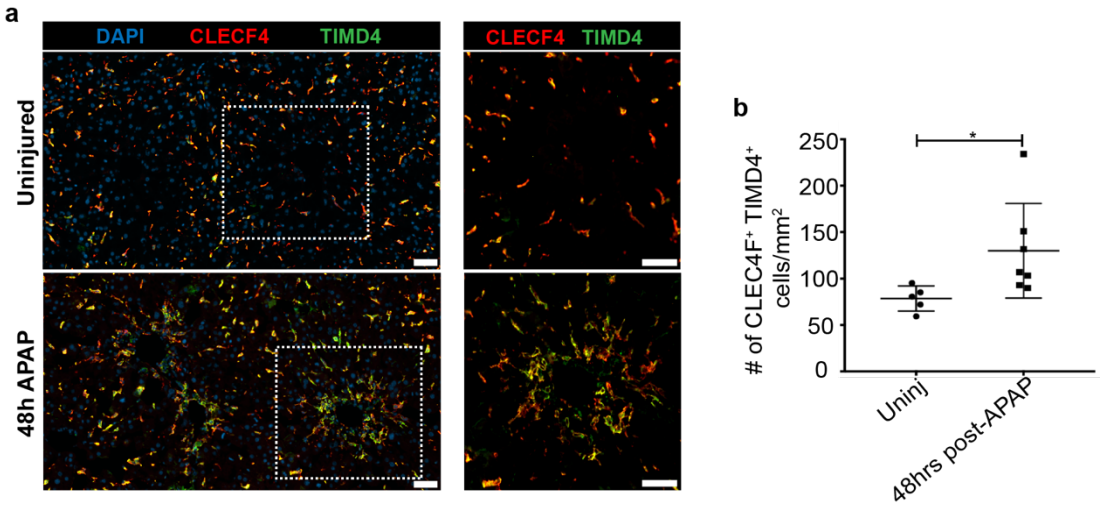

Figure 3.6 Kupffer cells following AILI do not disappear but localize to centrilobular areas of injury and repair. (**a**) Representative Immunofluorescence micrograph of uninjured and 48hrs-post APAP livers, shows the topographical changes in KCs identified via staining of TIMD4 (green), CLEC4F (red) and DAPI (blue) (Scale bar=50μm). (**b**) Quantitation of TIMD4+ CLEC4F+ DAPI+ cells across the whole liver lobule cross-section, identified through immunofluorescence. Data acquired from two independent experiments, n=5-7 per group. Mann-Whitney, nonparametric t-Test. Data shown as Mean±S.E.M, * $P \leq 0.05$.

3.2.4 Injury specific phenotypic changes indicate heterogeneity within the macrophage subsets during AILI

KCs, Ly6C^{Hi} monocytes and Ly6C^{Lo} MDMs were further analysed for their expression of a major histocompatibility complex class II (MHCII), a molecule required to process and present antigens, and CD11c, an integrin with a role in antigen uptake and activation. MHCII and CD11c are commonly used to define dendritic cells (DCs) but also reported to be on macrophages during inflammation (Yu *et al.*, 2016). Plasmacytoid DCs and conventional DCs were removed from this analysis on the basis of B220 and CD11c expression and lack of F4/80 expression (Appendix 2). Focussing on KCs, in an uninjured liver majority are MHCII+/CD11c- or MHCII-/CD11c-, a relatively small proportion of KCs are MHCII+/CD11c+. Following injury MHCII expression is downregulated, at 48hrs most of the KCs are MHCII-/CD11c- and by 144hrs the expression of MHCII and CD11c on KCs were comparable to uninjured setting (Figure 3.7a).

There are minimal phenotypic changes in the Ly6C^{Hi} monocytes, almost all of them are MHCII-/CD11c-, suggesting these cells are immature (Figure 3.7b). On the other hand, Ly6C^{Lo} MDMs undergo major phenotypic changes following AILI. Varying expression of MHCII and CD11c in Ly6C^{Lo} MDMs revealed a high degree of heterogeneity within these cells. On the basis of MHCII and CD11c, in an uninjured liver Ly6C^{Lo} MDMs can defined as three main subsets: MHCII-/CD11c-, MHCII+/CD11c- and lastly, MHCII+/CD11c+, which represents the most dominant subset (figure 3.7c). Following injury both MHCII-/CD11c- and MHCII+/CD11c+ subsets expand and most critically there is an emergence of a fourth subset of cells, which are MHCII-/CD11c+. These three subsets expand considerably at 48hrs and 72hrs, during maximal liver regeneration (Figure 3.7c). These phenotypic changes appeared to be transient, the expression of MHCII and CD11c on the Ly6C^{Lo} MDMs at 144hrs is basal levels (Figure 3.7c).

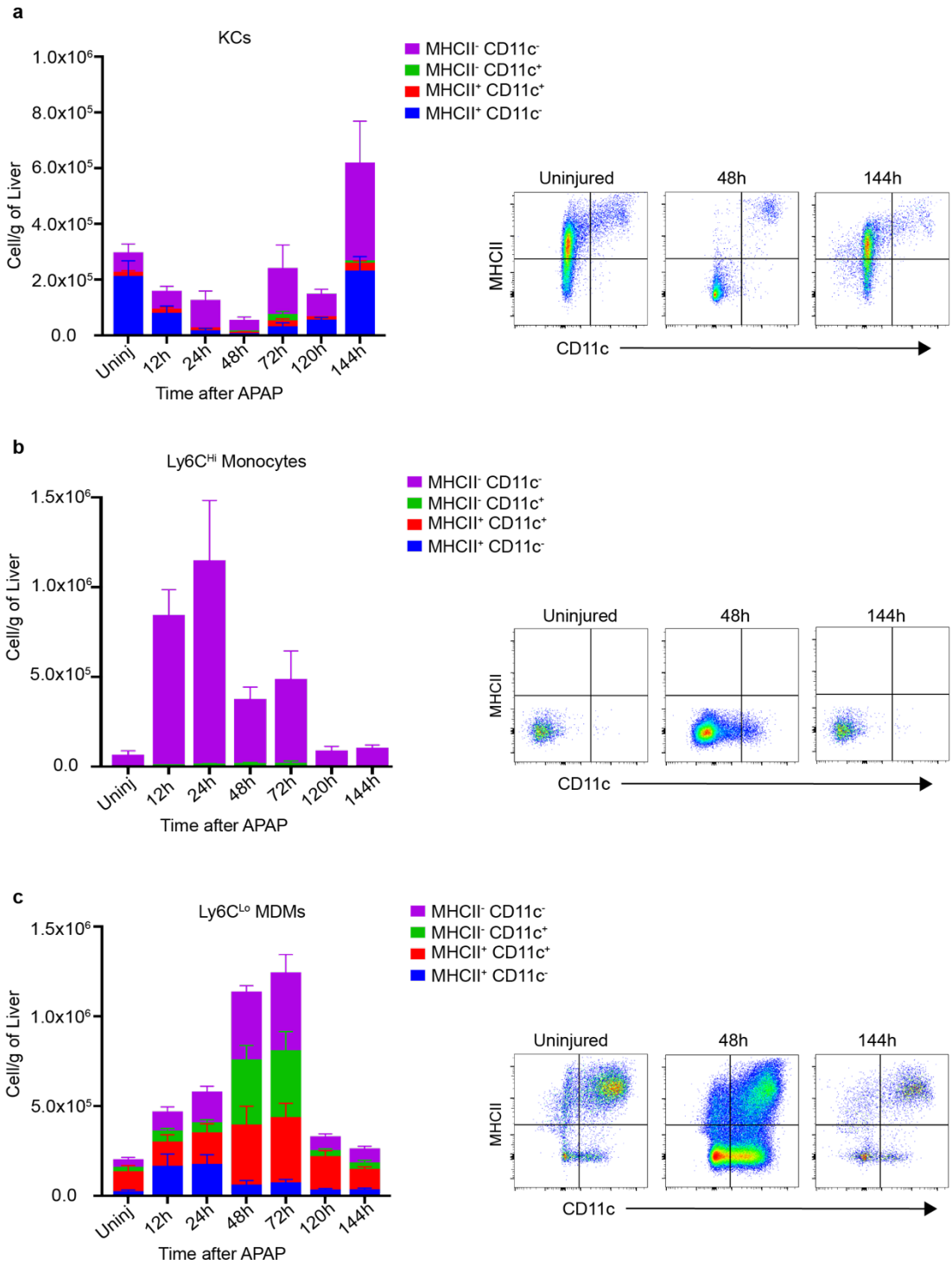

Figure 3.7 Injury specific phenotypic changes in macrophages following AILI. Phenotypic characterization of KCs (**a**), Ly6C^{Hi} Monocytes (**b**) and Ly6C^{Lo} MDMs (**c**) based on the expression of MHCII and CD11c via flow cytometry. Data acquired from three independent experiments, n=5-10 per group. Data shown as Mean±S.E.M

3.2.5 Systemic changes following AILI

AILI induces dynamic changes in the hepatic leucocyte populations, there is a dramatic increase in the number of non-resident cells, especially in the monocyte/macrophage compartment (Figure 3.3, 3.5). I was interested in investigating whether these changes are also reflected in the systemic leucocyte compartment. In order to do this, blood from uninjured and injured mice at specific timepoints following APAP overdose was obtained and circulating leucocytes were immunophenotyped via flow cytometry (n=3-5; See appendix 3 for gating strategy).

Circulating Neutrophils (Ly6G+ CD11b+) were significantly elevated at 6hrs-post APAP (Figure 3.8), corresponding to their increase in the liver at the same timepoint (Figure 3.4). Their relative numbers stayed elevated until 48hrs and then decreased to basal levels. Circulating monocytes on the other hand (CD11b+ CD115+) increased significantly at 12hrs following AILI (Figure 3.8), in parallel with their increase in the liver (Figure 3.4). NK cells proportionally decreased at 6 and 12hrs, however this was not significant. The percentage of B cells and T cells decreased at 12h before increasing at 72h, however this changed was not significant (Figure 3.8).

Three phenotypically distinct circulating murine monocyte subsets have been identified: Ly6C^{Hi} monocytes (CD14^{Hi} CD16- in humans), Ly6C^{Int} monocytes (CD14^{Int} CD16+ in humans) and Ly6C^{Lo} monocytes (CD14^{Lo} CD16+ in humans) (Mildner *et al.*, 2017; Patel *et al.*, 2017; Guilliams, Mildner and Yona, 2018). Numerical and phenotypical changes in these subsets have been associated with patient prognosis following APAP-induced ALF (Antoniades *et al.*, 2006, 2012; Abeles *et al.*, 2012; Moore *et al.*, 2017). Currently there is no data on how these cells respond during specific phases of AILI in mice, therefore, I investigated the changes in these subsets in mouse blood following AILI. Monocytes (CD115+ CD11b+) were identified as circulating mononuclear cells, and then subdivided on their expression of Ly6C and

CD11c, I subdivided the circulating monocytes into Ly6C^{Hi}, Ly6C^{Int} and Ly6C^{Lo} (Mildner *et al.*, 2017) (Figure 3.9a). During the necroinflammatory phase (6hrs-12hrs) the percentage of circulating Ly6C^{Hi} monocytes and Ly6C^{Int} monocytes increased significantly (Figure 3.9b 3.9c), this coincides with the increased influx of Ly6C^{Hi} monocytes into liver (Figure 3.5e). Ly6C^{Hi} monocytes are precursors of Ly6C^{Lo} monocytes in blood, their rapid infiltration into the liver could explain the decline in circulating Ly6C^{Lo} monocytes (Figure 3.9c). Previous studies have associated reduced expression of HLA-DR, a major histocompatibility complex class II (MHCII) receptor on monocytes with ALF disease severity (Antoniades *et al.*, 2006, 2012; Abeles *et al.*, 2012; Moore *et al.*, 2017). Therefore, I was interested to see if there were any changes in the expression of MHCII on circulating monocytes in the murine model of AILI. AILI induced upregulation of MHCII on Ly6C^{Int} monocytes but not Ly6C^{Hi} and Ly6C^{Lo} monocytes (Figure 3.9d). Further studies are required to increase the power of these experiments.

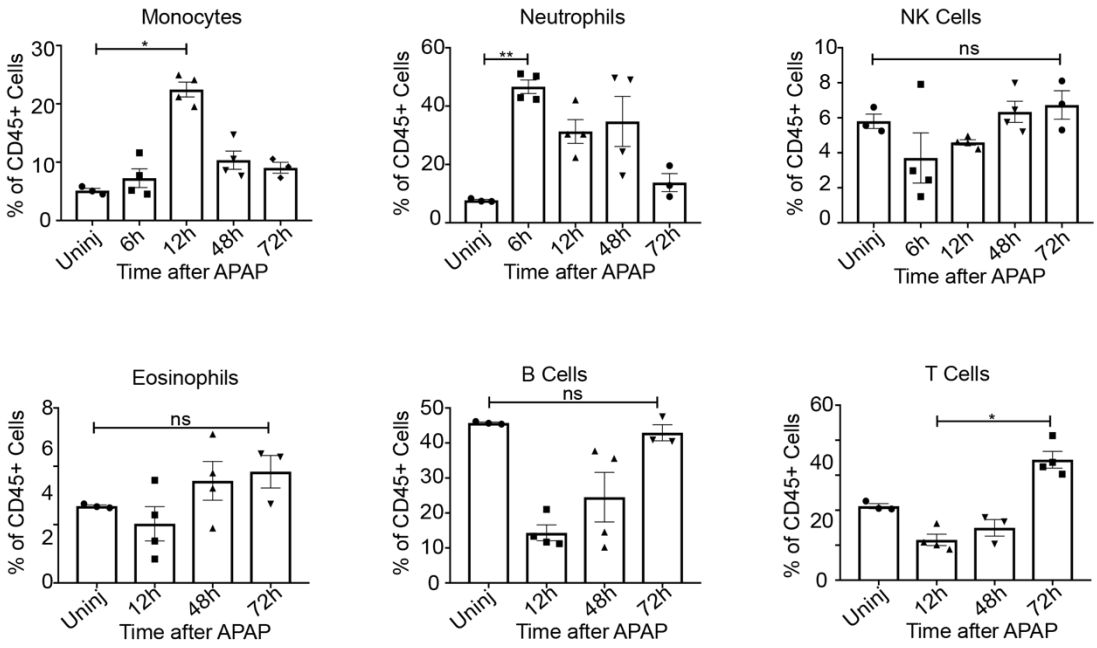

Figure 3.8 Changes in the circulating leucocytes following AILI. The number of circulating monocytes, neutrophils, NK cells, eosinophils, B cells and T cells at stated timepoints following AILI**.** Data acquired from a single experiment, n=3-4 per group. One-way ANOVA with Dunn's multiple comparisons test. Data shown as Mean±S.E.M. * $P \leq 0.05$, ** $P \leq 0.01$.

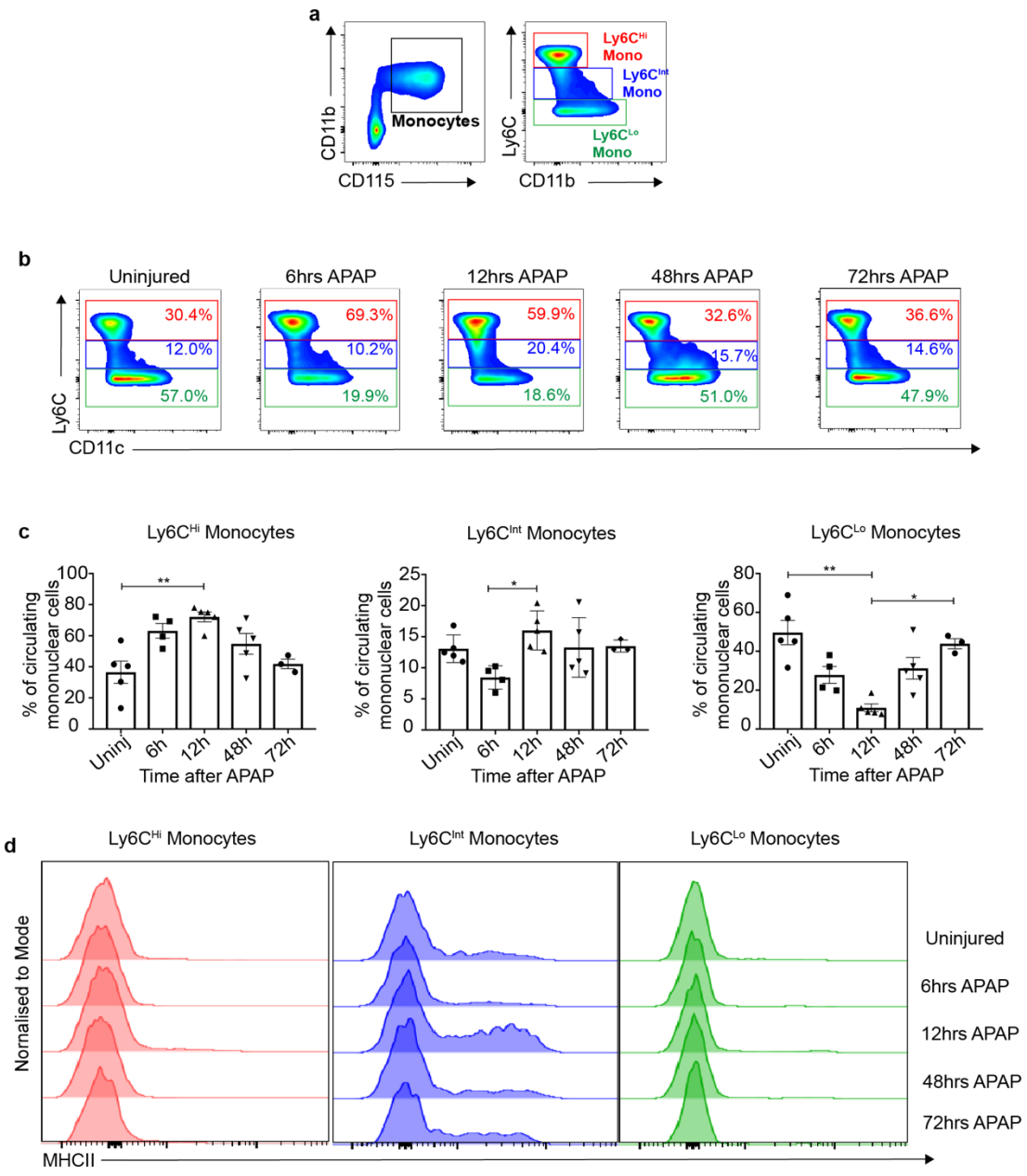

Figure 3.9 Changes in the circulating monocyte numbers and phenotype following AILI. (**a**) Gating strategy used to identify Ly6C^{Hi}, Ly6C^{Int} and Ly6C^{Lo} monocytes from murine blood following AILI. Representative flow cytometry plots (**b**) and quantitation of the percentage of monocyte subsets (**c**) at specific timepoints following APAP overdose, compared to uninjured animals. (**d**) Expression of MHCII on Ly6C^{Hi}, Ly6C^{Int} and Ly6C^{Lo} monocytes at stated time points following APAP induction, compared to uninjured group. Data acquired from a single experiment, n=3-5 per group. One-way ANOVA with Dunn's multiple comparisons test. Data shown as Mean±S.E.M.* $P \leq 0.05$, ** $P \leq 0.01$.

3.2.6 Leucocyte dynamics following partial hepatectomy

Partial hepatectomy (PHx) is a commonly used surgical model of liver regeneration. In comparison to AILI, leucocytes in the context of PHx have not been extensively characterized. Past studies have focused on specific leucocytes such as macrophages and T cells to show they promote liver regeneration following PHx (Tumanov *et al.*, 2009; Nishiyama *et al.*, 2015) however, the broad leucocyte response following PHx has not been previously studied. Thus, I investigated the hepatic and systemic leucocyte composition following PHx and compared it to AILI and uninjured conditions.

Here, wildtype C57BL/6 mice underwent 70% PHx (see methods for more details), liver and blood were obtained from these mice and leucocytes were immunophenotyped using flow cytometry. Previous studies from the Henderson lab performed by Dr. Kylie Conroy showed that 48hrs represents peak hepatocyte proliferation following PHx in C57BL/6 mice, therefore, all immunophenotyping of leucocytes following PHx were done at this time point. In order to account of technical variability and reliably compare any changes between PHx and AILI, livers from 48hrs post-APAP were analysed alongside uninjured livers.

Using the same surface markers and gating strategy shown in Appendix 2, hepatic leucocytes were identified via flow cytometry and their numbers were quantified. Leucocyte numbers changed minimally following 70% PHx, during peak liver regeneration, the relative proportion of leucocytes in PHx group were similar to uninjured conditions (Figure 3.10a). The most significant changes were observed with the number of pDCs, which increased post-PHx compared to AILI and Uninjured livers. Although there is a slight expansion in B cells, NK cells, neutrophils, macrophages and cDCs there changes were not significant (Figure 3.10b). To see if there are any changes within the macrophage subsets, KCs (TIMD4+ F4/80^{Hi} CD11b^{Lo}), Ly6C^{Hi} monocytes (F4/80^{Lo} CD11b^{Hi} Ly6C^{Hi}) and Ly6C^{Lo} MDMs (F4/80$^{Int/Lo}$ CD11b^{Hi} Ly6C^{Lo}) were

identified. The macrophage compartment in PHx was comparable to uninjured livers, the changes are not as significant as seen post-APAP (Figure 3.11). Flow cytometric characterisation of circulating leucocytes (See appendix 3 for gating strategy) following PHx showed that the proportion of systemic leucocytes post-PHx were comparable to basal levels, whereas post-APAP the neutrophil and monocytes numbers are increased and lymphocyte (T cells and B cells) numbers significantly reduced (Figure 3.12a, b).

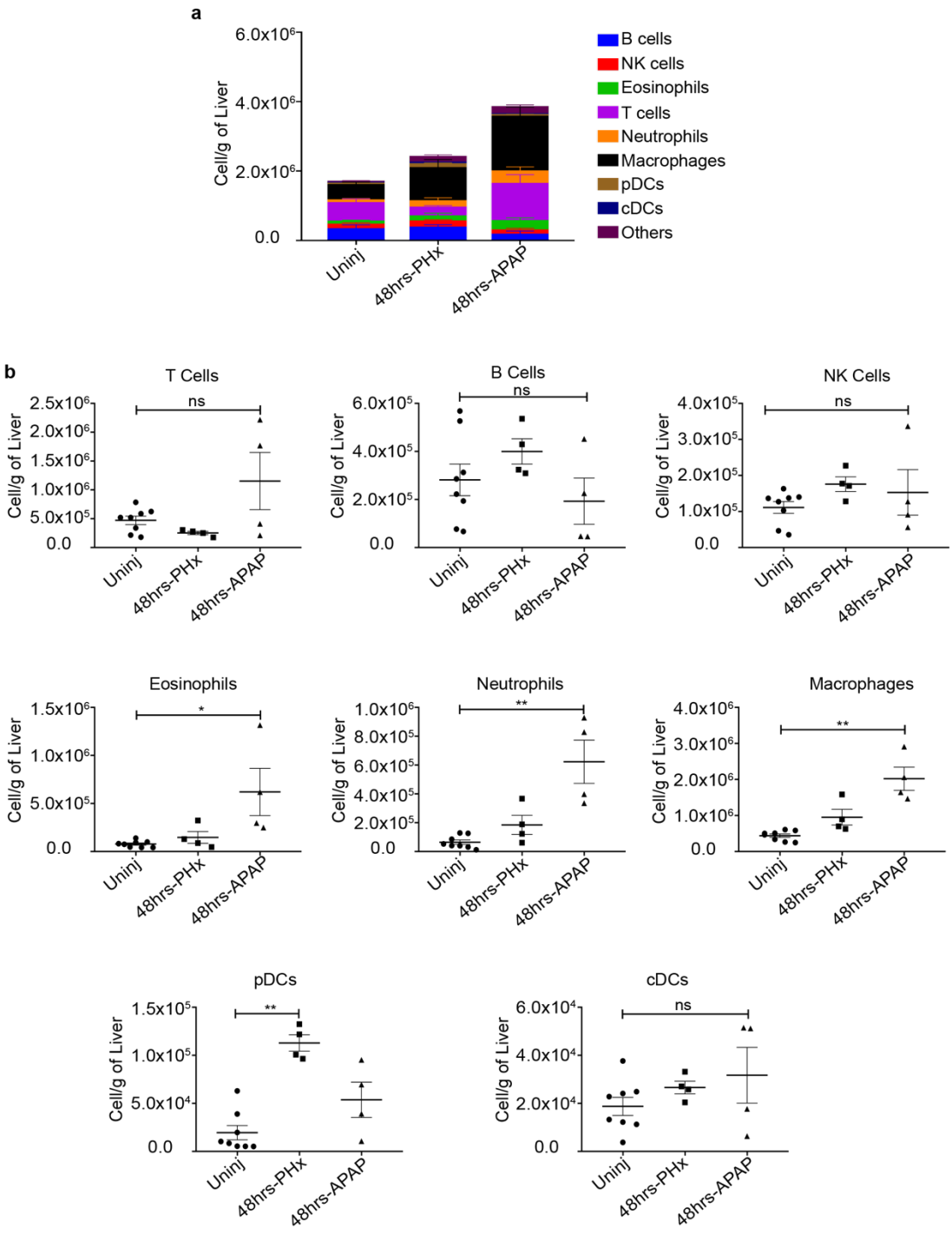

Figure 3.10 Comparison of changes in hepatic leucocyte responses following PHx and AILI. (**a**) Proportional changes in the absolute number of hepatic leucocytes following 48hrs post- PHx and AILI compared to uninjured animals. (**b**) Quantitation of different types of leucocytes following 48hrs post-PHx and AILI compared to uninjured animals. Data acquired from a single experiment, n=4-8 per group. One-way ANOVA with Dunn's multiple comparisons test. Data shown as Mean±S.E.M. * $P \leq 0.05$, ** $P \leq 0.01$.

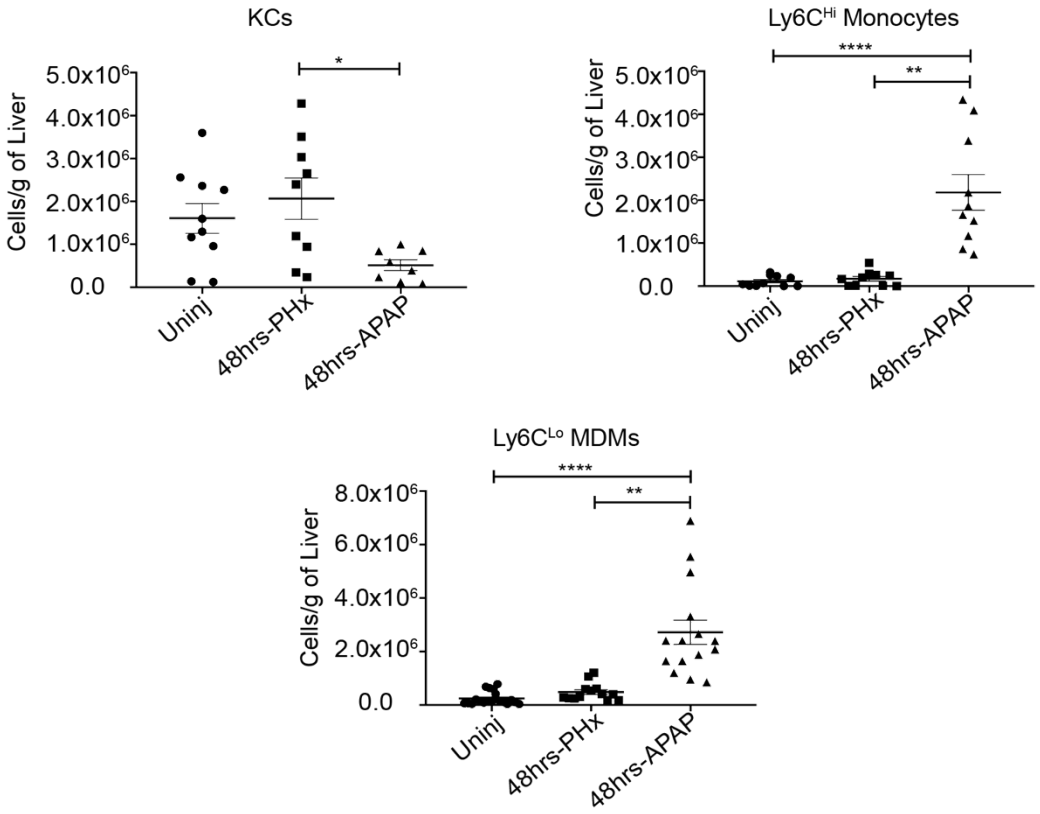

Figure 3.11 Comparison of changes in hepatic macrophage responses following PHx and AILI. Quantitation of KCs, Ly6C^{Hi} monocytes and Ly6C^{Lo} MDMs following 48hrs post-PHx and AILI compared to uninjured animals.
Data acquired from four independent experiments, n=10 per group. One-way ANOVA with Dunn's multiple comparisons test. Data shown as Mean±S.E.M. * $P \leq 0.05$, ** $P \leq 0.01$, **** $P \leq 0.0001$.

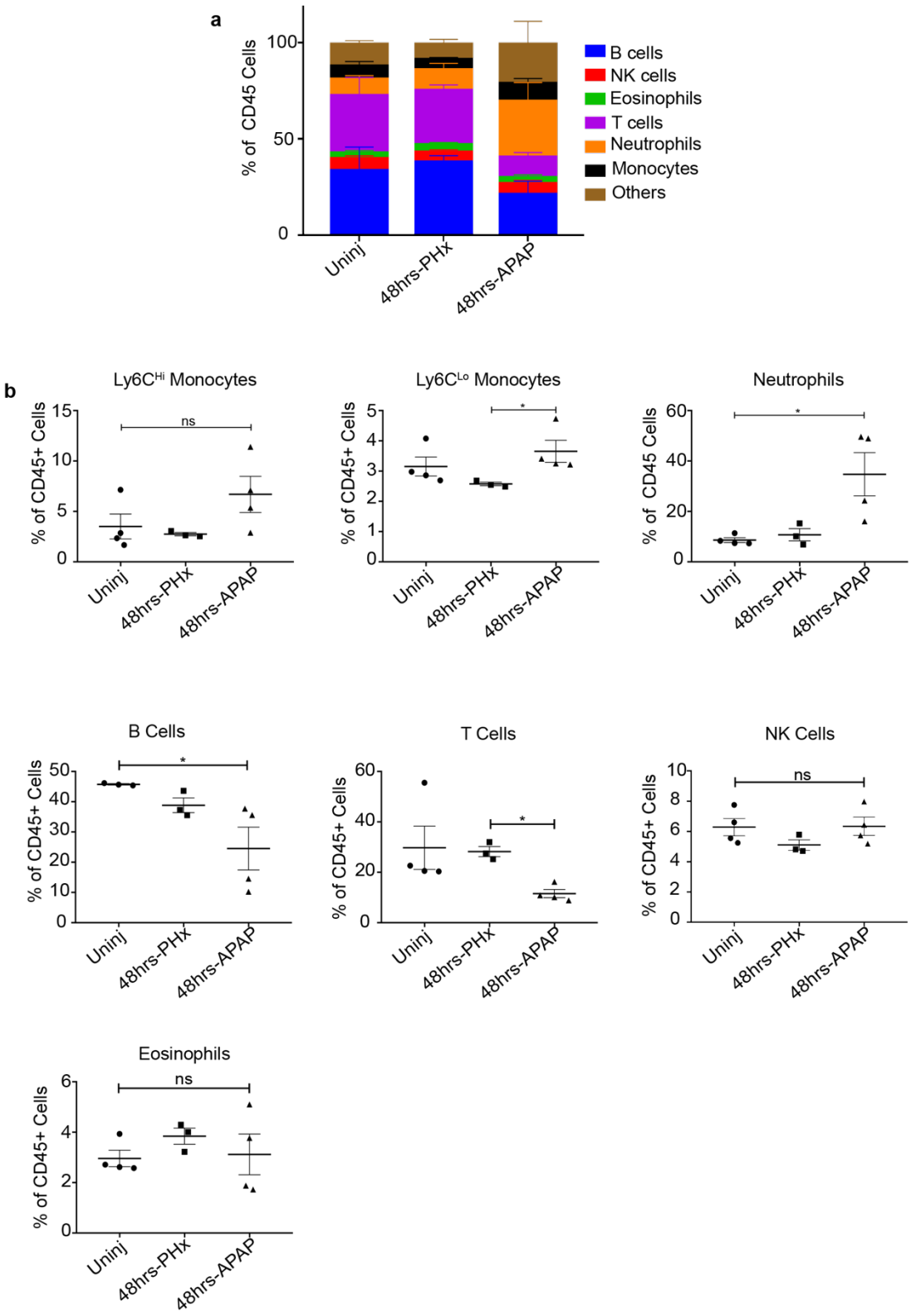
a
% of CD45 Cells
100
50
0
B cells
NK cells
Eosinophils
T cells
Neutrophils
Monocytes
Others
Uninj
48hrs-PHx
48hrs-APAP
b
Ly6C^Hi Monocytes
Ly6C^Lo Monocytes
Neutrophils
B Cells
T Cells
NK Cells
Eosinophils
% of CD45+ Cells
% of CD45 Cells
ns
*

Figure 3.12 Comparison of changes in systemic leucocyte response following PHx and AILI. (**a**) Proportional changes in the % of leucocytes (CD45+ cells) following 48hrs post- PHx and AILI compared to uninjured animals. (**b**) Quantitation of different types of circulating leucocytes following 48hrs post-PHx and AILI compared to uninjured animals. Data acquired from single experiment, n=3-4 per group. One-way ANOVA with Dunn's multiple comparisons test. Data shown as Mean±S.E.M. * $P \leq 0.05$.

3.3 Discussion

In this chapter I have extensively characterised the temporal dynamics of parenchymal and non-parenchymal cells (NPCs) during AILI. Based on detection of liver enzymes (ALT, AST, GLDH) in the serum and necrosis quantitation, I established that liver injury peaks between 6-24hrs (Figure 3.1). Previous studies have relied on cell cycle markers and cell size to detect proliferating hepatocytes (Singhal, Ganey and Roth, 2012; Bird *et al.*, 2018), here I used HNF4α, as a positive marker for hepatocytes, in conjunction with EdU to demonstrate peak regeneration occurs between 48-72hrs post-APAP (Figure 3.2).

Previous studies looking at the leucocyte response during AILI have either focused on specific lineages or partitioned the immune response into innate and adaptive (You *et al.*, 2013; Zigmond *et al.*, 2014; Graubardt *et al.*, 2017; Yang *et al.*, 2019). Here, I wanted to get a global picture of the leucocyte response in the liver during AILI. Using a comprehensive flow cytometry panel, I managed to isolate almost all immune cell types in the liver (Appendix 2, Figure 3.3). The "others" group represents cells which were unidentified, however their numbers are relatively low and based on the literature they could be mast cells, basophils and innate lymphoid cells, further analysis using appropriate markers is needed to confirm this. Leucocytes show a dynamic response following APAP overdose, different lineages expanding at specific timepoints during AILI.

Neutrophils represent the first responders following injury, their numbers are elevated both in the blood and liver during the injury/inflammatory phase (6hrs-24hrs) (Figure 3.4). Neutrophils are professional phagocytes responsible for clearance of necrotic debris, however, they also promote inflammation therefore their appropriate clearance is required for the resolution of inflammation and initiation of the repair process (Graubardt *et al.*, 2017). In line with this, neutrophil numbers decline from 24hrs onwards (Figure 3.4). A caveat to looking at broad leucocyte responses is that you lose resolution within lineages. For instance, there is a huge variation in T cells especially during the repair phase (48-72hrs), probably due to distinct T cells (CD4+, CD8+, T_{REG} cells) behaving differently. Additional markers are required to confirm if there are any significant changes within T cell subsets (Wang *et al.*, 2015). Elevation in eosinophils coincides with peak hepatocyte proliferation, eosinophil derived IL4 has been to promote liver regeneration following acute liver injury (Goh *et al.*, 2013), implying a similar role here. Interestingly, although liver architecture at 144hrs is comparable to uninjured conditions (Figure 3.1b, c) hepatocyte proliferation and leucocyte numbers are still above basal levels (Figure 3.2, 3.3c), suggesting that homeostasis is not completely restored at this timepoint and immune cell response is long lasting. The most striking finding was that macrophages represented the most expanded immune cell type in the liver during the repair phase (Figure 3.4).

AILI induced dynamic changes in macrophage numbers, phenotype and location (Figure 3.5, Figure 3.6, Figure 3.7). Using F4/80, CD11b, TIMD4 and Ly6C I was able to identify KCs, Ly6C^{Hi} monocytes and Ly6C^{Lo} MDMs (Figure 3.5c) (Zigmond *et al.*, 2014). Flow cytometric analysis demonstrated that uninjured liver is composed predominantly of KCs (F4/80^{Hi} CD11b^{Lo} TIMD4+) however following APAP induction KC numbers are depleted (Figure 3.5c, d). Depletion of tissue resident macrophages following inflammatory stimuli has been widely reported, both in the context of liver injury (Ramachandran *et al.*, 2012; Zigmond *et al.*, 2014; Blériot *et al.*, 2015; Ju and Tacke, 2016) and also in other tissues such as the peritoneum (Cassado, D'Império Lima and

Bortoluci, 2015). Zigmond et al., 2014 showed KCs number are depleted at 24hrs post-APAP, followed by their self-replenishment at 72hrs. The flow cytometry experiments here are in agreement with this observation (Figure 3.5c, d). Interestingly, the immunofluorescence staining data at 48hrs post-APAP suggests that "KC disappearance reaction" is a technical artefact, resulting from a failure to liberate these cells from the liver tissue. TIMD4+ CLEC4F+ cells (KCs) were seen in the tissue at 48hrs post-APAP, furthermore their numbers increase significantly post-injury when compared to basal conditions (Figure 3.6a, b). KCs are sessile cells, found within the sinusoids, following APAP there is a subset of KCs localised around the central vein, where you would expect hepatocyte necrosis and proliferation (Figure 3.1, 3.2, 3.6). This data suggests that there is a subpopulation of KCs which migrate towards areas of injury. A very recent study has suggested "macrophage disappearance reaction" during peritonitis is a result of coagulation (Zhang *et al.*, 2019). Flow cytometric analysis showed administration of heparin to mice with peritonitis liberated significantly more tissue resident macrophages (TRMs), whilst the no heparin group with peritonitis had reduced number of TRMs. Through intravital imaging the authors revealed following bacteria induced inflammation peritoneal macrophages were more adherent and formed clots to combat bacterial load more effectively and this was mediated by coagulation factor V (Zhang *et al.*, 2019). It would be interesting to see if heparin administration can liberate more KCs at 48hrs-post APAP.

As discussed previously, depletion studies show that KCs are crucial in liver repair post-APAP (Ju *et al.*, 2002), however, their precise role in promoting this remains to be investigated. Microarray data reports that KCs from 72hrs post-APAP livers have a similar transcriptional profile to KCs from uninjured livers (Zigmond *et al.*, 2014), however this is not to say they might have functional differences. Analysis of MHCII and CD11c expression on KCs following APAP overdose demonstrated downregulation of MHCII on KCs, suggesting a switch towards a more immature phenotype. Tissue resident macrophages in the kidney downregulate MHCII following acute injury, a phenotypic switch to be

akin to that seen on developmental macrophages, and the authors postulated that this downregulation might serve as immunoregulatory mechanism to prevent chronic inflammation (Lever *et al.*, 2019). A similar functionally important switch might be happening here. It is also important to note that from 6hrs-48hrs we are only liberating a fraction of KCs populating the liver during AILI. Therefore, future experiments which focus on optimisation of digestion protocols facilitating their liberation from the liver is necessary in dissecting their role during AILI. Intravital imaging (IVM) studies of the liver following AILI and other forms of sterile injury has revealed dynamic role of leucocytes such as neutrophils and macrophages (Marques *et al.*, 2015; Liew, Lee and Kubes, 2017). Given the current challenges associated with relying on flow cytometry to study KCs during AILI, future studies should use IVM to visualize KCs *in vivo*. Either using injectable fluorescently conjugated antibodies to TIMD4 and CLEC4F or using a KC reporter mice (Scott *et al.*, 2016) will allow KC labelling *in vivo*. However, currently there is no evidence to suggest that TIMD4 and CLEC4F exclusivity to KCs is maintained during injury and inflammation (Scott *et al.*, 2016). Although unlikely, considering their inherent plasticity infiltrating macrophages could gain expression of these markers. An inducible cre/lox system based on either TIMD4 or CLEC4F is required to faithfully lineage trace KCs during AILI.

Previous studies have demonstrated a key role for bone marrow derived monocytes and their progeny in regulating liver injury and repair during AILI. Authors have used transgenic mouse models to show infiltration of CCR2+ monocytes into the liver during the inflammatory phase and their differentiation into $CCR2^{Lo}$ $CX3CR1^{Hi}$ macrophages during the resolution phase (You *et al.*, 2013; Zigmond *et al.*, 2014; Mossanen *et al.*, 2016; Graubardt *et al.*, 2017). To study their dynamics in a wild type mouse I relied on differential expression of Ly6C, in combination with standard markers F4/80 and CD11b. $CCR2^{Hi}$ monocytes were defined as: $F4/80^{Lo}$ $CD11b^{Hi}$ $TIMD4^{-}$ $Ly6C^{Hi}$ and the $CX3CR1^{Hi}$ monocyte derived macrophages were defined as $F4/80^{Lo}$ $CD11b^{Hi}$ $TIMD4^{-}$ $Ly6C^{Lo}$.

In parallel with neutrophil infiltration into the liver, APAP induced significant increase in Ly6C^{Hi} monocytes (Figure 3.5c,e), infiltration of circulating Ly6C^{Hi} monocytes into the liver is a characteristic feature of liver injury and inflammation (Tacke and Zimmermann, 2014). Ly6C^{Hi} monocytes and neutrophils are the most dominant leucocytes in the liver during the inflammatory phase. These cells have the capacity to promote injury and inflammation during AILI, but also facilitate the repair process (You *et al.*, 2013; Zigmond *et al.*, 2014; Mossanen *et al.*, 2016; Graubardt *et al.*, 2017; Yang *et al.*, 2019). Ly6C^{Hi} monocytes have a role in regulating neutrophil function and clearance to promote the generation of pro-reparative Ly6C^{Lo} MDMs (Graubardt *et al.*, 2017). The temporal dynamics between these cells were also demonstrated here (Figure 3.5g). Notably, Ly6C^{Lo} MDMs are the principle macrophage subset in the liver during the regenerative phase (Figure 3.5c, f) and phenotypical characterisation of Ly6C^{Lo} MDMs macrophages using antigen presenting markers: MHCII and CD11c suggests these broadly classified cells are more heterogenous than we currently appreciate (Figure 3.6c). At 48 and 72hrs post-APAP (maximal liver repair), three distinct subsets of Ly6C^{Lo} MDMs (MHCII- CD11c-, MHCII- CD11c+ and MHCII+ CD11c+) expanded, a more detailed analysis of macrophages at a higher resolution will aid in dissecting this heterogeneity (Figure 3.6c).

It is widely accepted that circulating Ly6C^{Hi} monocytes are the main responders following tissue injury (Ramachandran *et al.*, 2012; Zigmond *et al.*, 2014). However, Ly6C^{Lo} monocytes are also capable of rapidly infiltrating into damaged tissues and have been shown to differentiate into macrophages with tissue repair and remodeling properties (Auffray, Sieweke and Geissmann, 2009). The data presented in this chapter shows that AILI leads to significant changes in systemic leucocyte composition. Circulating Ly6C^{Hi} monocytes are increased at 12hrs, coinciding with their accumulation in the liver (Figure 3.9c). Suggesting that during AILI, Ly6C^{Hi} monocytes have a more prominent role. Transcriptional profiling of circulating monocytes have shown that Ly6C^{Int}

monocytes are more heterogenous than Ly6C^{Hi} and Ly6C^{Lo} monocytes (Mildner *et al.*, 2017). The varying levels of MHCII expression on these cells and their proportional increase following injury, suggests that they might also be functionally more heterogenous during AILI (Figure 3.9d). These observations demonstrate that APAP induces numerical and phenotypical changes in the circulating monocyte subsets. Whether circulating monocytes during AILI have a dichotomous differentiation potential and function remains unknown. Studying the transcriptome of these cells during AILI may give us more insight into the functional relevance of these changes. Other significant changes included an increase in circulating neutrophils and reduction in lymphocytes, especially T cells, during the inflammatory phase (12hrs), which returned back to baseline levels during the repair phase (Figure 3.8). Neutrophilia and lymphocytopenia are both clinical features often observed in patients suffering from APAP poisoning, when they are initially admitted to the hospital, which resolves back to normal once they recover from the liver injury (Moore *et al.*, 2017).

Hepatic and systemic leucocyte numbers between PHx and AILI indicated leucocyte composition at 48hrs-post PHx was comparable to uninjured livers. Unlike AILI, there was a lack of involvement from inflammatory cells such as neutrophils and Ly6C^{Hi} monocytes (Figures 3.10 and 3.12). Perhaps this is unsurprising given the “clean” nature of the injury which induces regeneration in the remnant lobes, without any necrotic materials, DAMPs and other signals required to initiate an inflammatory response (Michalopoulos, 2007; Martin-Murphy, Holt and Ju, 2010). Nevertheless, given the role for macrophages in regulating liver regeneration following PHx (Selzner *et al.*, 2003; Nishiyama *et al.*, 2015; Wyler *et al.*, 2016), I expected macrophages to change numerically. To my surprise there were no significant changes in both KCs and infiltrating macrophages (Figure 3.11). I cannot ignore that dynamics of liver regeneration following PHx might vary in comparison to AILI. Therefore, analysis of a single timepoint may be insufficient and time course experiments are needed before drawing any conclusions. We know that KC-derived IL-6 and TNF-α promotes

hepatocyte proliferation following PHx and depletion studies have indicated that both KCs and infiltrating macrophages are necessary for hepatocyte proliferation following PHx, therefore phenotypic and functional differences in these cells are likely to drive liver regeneration (Selzner *et al.*, 2003; Nishiyama *et al.*, 2015; Wyler *et al.*, 2016). The number of hepatic pDCs increased significantly following PHx, compared to uninjured and APAP groups (Figure 3.10). A pro-regenerative role for DCs following PHx has been highlighted, but the authors did not delineate pDCs from cDCs, to pinpoint the key player (Castellaneta *et al.*, 2006).

Overall, this body of work enabled me to see the global changes in the parenchymal and leucocyte compartments over the course of AILI. I have characterised liver injury and repair process following AILI to pinpoint 6-24hrs as the necroinflammatory phase, 48hrs-144hrs as the repair phase, in which 42hrs and 72hrs represent timepoints where hepatocyte proliferation is the most significant. Some of the findings here are in concordance with the existing literature such as dynamics seen between neutrophils, Ly6C^{Hi} monocytes and Ly6C^{Lo} MDMs. Importantly, I have also embarked upon novel observations, which warrants further study. Namely the dynamic changes in the KCs at 48hrs-post APAP and the phenotypic heterogeneity within the Ly6C^{Lo} MDMs during the repair phase of AILI (48hrs-72hrs post-APAP).

4 Single cell sequencing of mononuclear phagocytes cells during liver regeneration

4.1 Introduction

Gene expression changes occurring following AILI have been studied using microarray and bulk RNA sequencing techniques and distinct gene expression profiles for monocytes/macrophages have been identified, facilitating their delineation into three main subtypes: Kupffer cells (KCs), Ly6C^{Hi} monocytes, Ly6C^{Lo} monocytes derived macrophages (MDMs) (Togo *et al.*, 2004; Zigmond *et al.*, 2014; Mossanen *et al.*, 2016; Graubardt *et al.*, 2017). However, there is considerable evidence to suggest functional heterogeneity within these broadly classified subsets, especially Ly6C^{Lo} MDMs, during liver regeneration following AILI (Chapter 3).

The transcriptional profiling of single immune cells can facilitate the identification of subtle but crucial heterogeneity within cell populations, which would be masked in population-averaged measurements generated through bulk-RNA sequencing or microarrays. Single-cell mRNA sequencing (scRNA-seq) is a powerful tool to systematically dissect heterogeneity within these cells types and characterize the transcriptome of individual cells. It has been successfully employed to discover new immune cell types, cell states, and novel molecular pathways in healthy and diseased tissues (Grün *et al.*, 2015; Macaulay *et al.*, 2016; A.-C. Villani *et al.*, 2017; C. Zheng *et al.*, 2017; Miragaia *et al.*, 2019). For example, a recent study used scRNA-seq to identify heterogeneity in hepatic macrophages in humans, and reported two distinct subsets of KCs in homeostasis, showing different functional capabilities (MacParland *et al.*, 2018). ScRNA-seq has an advantage over traditional methods using conventional cell surface markers and single-cell qPCR, as it doesn't heavily rely on pre-defined surface markers.

The process of scRNA-seq can be condensed into five stages:

1) Isolation and lysing single cells from tissue of interest
2) Reverse transcription (RT) to select for mRNA
3) cDNA amplification and Library preparation
4) Sequencing
5) Analysis

Isolation of immune cells from the liver can be challenging; cell types such as macrophages can become adherent to tissue following injury. Currently there is no consensus on the methods used to generate single cell suspensions of murine liver leucocytes (Blom *et al.*, 2009; Ramachandran *et al.*, 2012; Zigmond *et al.*, 2014; Bain *et al.*, 2016; Mossanen *et al.*, 2016). Most macrophage tissue dissociation protocols use a combination of mechanical and enzymatic digestion methods. The number and duration of spins, the composition and selection of enzymes used, and filtering steps can all influence cell purity and yield and can therefore bias the proportion of cell types to be analysed (Lynch *et al.*, 2018). The single cell suspension needs to be generated in an efficient manner, taking the shortest time possible to minimize cell stress to yield viable cells which are a representative “snapshot” of the *in vivo* setting. Isolated cells can be processed through steps 2-4 outlined above by different sequencing protocols, varying in transcript coverage, sequencing depth, strand specificity and positional bias. Droplet-based scRNA-seq permits 3’ mRNA counting, although limited in information on the full transcriptome, it allows you to sequence thousands of single cells per sample (G. X. Y. Zheng *et al.*, 2017; Ziegenhain *et al.*, 2017). This system has been used to uncover rare cell types and dissect heterogeneity in various tissues (Grün *et al.*, 2015; Camp *et al.*, 2017). The inclusion of unique molecular identifiers (UMIs) to samples in this method can reduce these technical variabilities introduced by RT efficiency, temperature differences, differences in sequencing depth and amplification bias etc. In addition, cells are passed through quality control

steps at various stages of the process, to ensure poor quality libraries are discarded from the downstream analysis. A large part of scRNA-seq is the bioinformatic analysis of the vast amount of transcriptomic data generated and there are a wide range of computational tools available which are used to answer specific biological questions (Rostom *et al.*, 2017).

This chapter outlines the methodology used for scRNA-seq of leucocytes an unbiased manner during liver regeneration, following AILI. The includes optimisation of cell isolation protocol and gating strategy used to select viable leucocytes for scRNA-seq and the post-sequencing quality control metrics used to filter misrepresented cells. Following this, the results from the computational analysis of scRNA-seq of leucocytes and mononuclear phagocytes (MPs) are presented via a range of visualisations graphs (t-SNE, heatmaps, violin plots, dot plots).

4.1.1 Aims

- To develop an efficient method to generate viable single cell suspensions of macrophages from murine liver
- To develop a strategy for the scRNA-seq of hepatic and systemic myeloid cells
- To analyse and interpret the scRNA-seq results via computational methods

4.2 Results

4.2.1 Tissue digest optimisation

A collagenase-based protocol reported in Lynch et al., 2018 (Protocol 1), which is efficient in isolating murine hepatic macrophages was used in chapter 3 to characterize leucocyte dynamics during AILI. However, the data from chapter 3 demonstrates that this protocol, along with others protocols reported in the literature, are inefficient in isolating KCs at specific timepoints during AILI (You *et al.*, 2013; Zigmond *et al.*, 2014), especially at 48hrs post-APAP (Figure 3.6). In order to address this issue, I compared the protocol used in Lynch et al, 2018 (Protocol 1) to a pronase based protocol standardly used in the Henderson lab for mesenchymal cell liberation from murine liver (Mederacke *et al.*, 2015) (Protocol 2) (Figure 4.1).

Previous work in the lab by Dr. Ross Dobie, Dr. Prakash Ramachandran and Dr. Jamie Smith demonstrated the requirement for pronase in the isolation of mesenchymal and leucocytes from cells from fibrotic livers, kidney and lung (data not shown). Therefore, I tested whether this protocol could improve the efficiency of leucocytes isolation, especially the number of KCs from murine livers following injury. To do this, livers from C57BL/6 mice (uninjured and injured) were harvested, liver lobules were weighed and partitioned equally to be processed following either protocol 1 or protocol 2. The cells were then stained for surface markers using the same concentration of antibodies and cell populations were analysed via flow cytometry. It is important to note that though pronase based enzymatic digestion protocols can be efficient at liberating non-parenchymal cells from the liver, they do cleave off certain cell surface proteins. Consequently, this limits the range of cell-surface markers that can be used for flow cytometry analysis. After several iterations, a leucocyte flow cytometry panel consisting of markers that survive a pronase-based digestion was developed and used for comparison between protocol 1 and 2.

The protocols differed in duration by a minute between tissue harvest and flow cytometry stages (Figure 4.1). Analysis of DAPI+ cells showed that protocol 2 yielded significantly more viable cells than protocol 1 (Figure 4.2b). The proportion of leucocytes isolated was consistently high (~80%) from both protocols, with negligible differences between them (Figure 4.2a). Since the main goal was to gain information of hepatic macrophages, I wanted to see if there were any differences in the number of macrophages isolated with protocol 1 and 2 from an injured liver (Figure 4.2c). There was increased variance in the percentage of macrophages (F4/80+ CD11b+) isolated from both protocols, with no significant differences between protocols (Figure 4.2c). As TIMD4 is cleaved by pronase, I relied on F4/80 and CD11b expression to identify KCs and MDMs. On average Protocol 2 isolated more KCs, whereas Protocol 1 isolated more MDMs, from an injured liver, but these differences were not significant (Figure 4.2d).

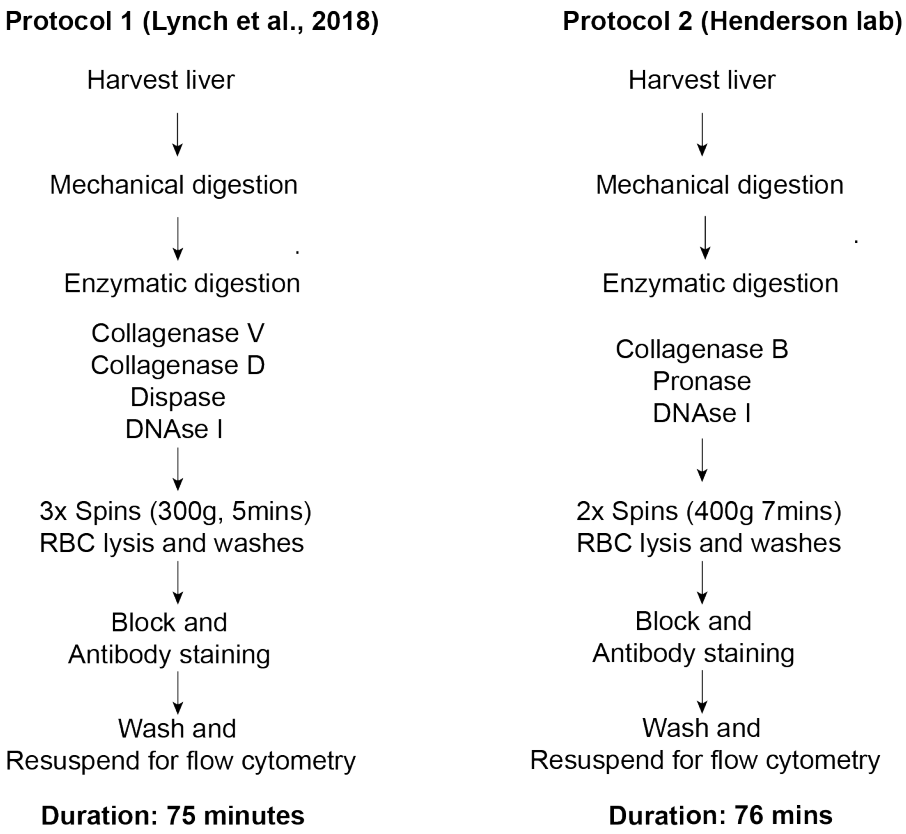

Figure 4.1Liver digestion protocols for isolating NPCs. Comparison of main steps and duration of protocol 1 and protocol 2 from liver harvest to flow cytometry.

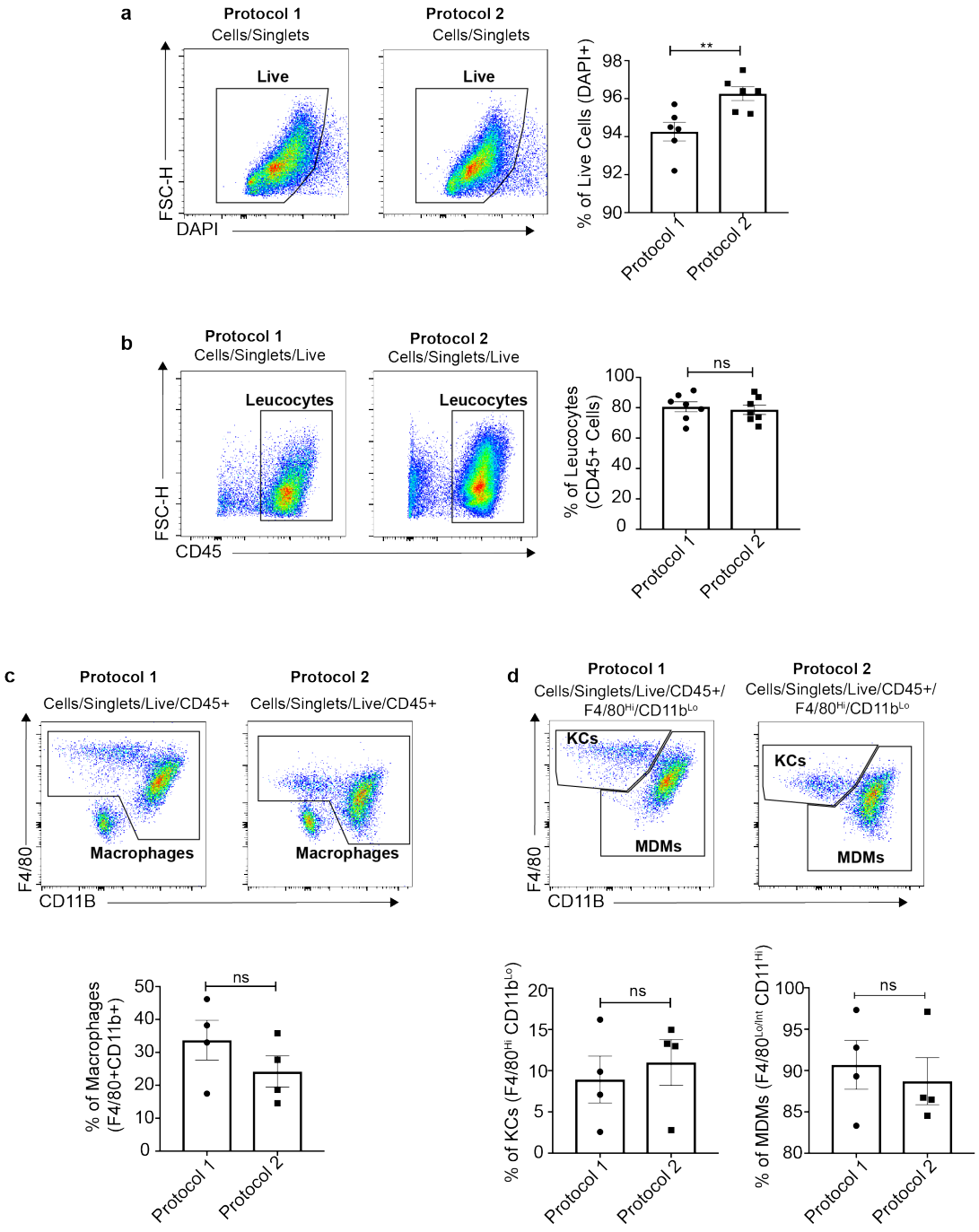

Figure 4.2 Optimisation of liver digestion protocols for scRNA-Seq. (**a**) Comparison of viability of cells between protocol 1 and 2. Comparison of leucocyte (**b**), macrophage (**c**) liberation between protocol 1 and 2. (**d**) Fraction of KCs (F4/80^{Hi} CD11b^{Lo}) and MDMs (F4/80$^{Lo/Int}$ CD11b^{Hi}) liberated from injured liver, from protocol 1 and 2; represented as percentage of total macrophages. (a,b) Data acquired from two independent experiments (c,d) Data acquired from single experiment, n=4-7 per group. Mann-Whitney nonparametric t-Test. Data shown as Mean±S.E.M. ***P*≤0.01.

To summarise there were insignificant differences in leucocyte or macrophage liberation from inflamed livers between protocol 1 and protocol 2. Overall protocol 2 generated significantly more viable cells, therefore a pronase-based protocol (protocol 2) was deemed more appropriate for the scRNA-seq experiment. Additionally, protocol 2 was previously employed by members in the Henderson lab to perform scRNA-seq of mesenchymal cells at 48hrs-post APAP. Therefore, in the hopes of amalgamating these datasets with this particular body of work to gain insight into the interplay between these cells in regulating liver repair following AILI, I decided to proceed with protocol 2 to generate single-cell preparations of murine liver leucocytes for scRNA-seq.

4.2.2 Methodology for scRNA-seq of hepatic and systemic leucocytes

As discussed previously AILI is a dynamic, with distinct phases. The hepatic and systemic leucocyte composition changes depending on the phase of AILI. In addition, macrophage phenotype can also vary during AILI (Figure 3.3, 3.5, 3.7). As the main aim of this body of work was to identify pro-reparative subsets by investigating the transcriptomic changes occurring in cells at a single cell resolution, it was important to select a timepoint which represents the repair phase. Based on the data shown in chapter 3 48hrs post-APAP was chosen as the timepoint to perform scRNA-seq. This timepoint represents a phase of AILI with minimal necrosis and significantly high hepatocyte proliferation (Figure 3.1, 3.2). The most dominant leucocytes in the liver at this timepoint are macrophages (Figure 3.3, 3.4). Furthermore, it also represented a timepoint when Ly6C^{Lo} MDMs peaked in the liver and these macrophages display a significant level of heterogeneity (Figure 3.7c).

AILI has been shown to induce systemic changes in the clinical setting which can affect the outcome for patients, despite this, none of the murine studies have interrogated the changes in the circulating leucocyte compartment in a regenerative model of AILI (Antoniades *et al.*, 2012; Moore *et al.*, 2017). The data in the previous chapter highlights numerical and phenotypical changes in

the leucocyte compartment (Figure 3.8, 3.9). Therefore, I performed scRNA-seq analysis of circulating leucocytes from uninjured and 48hr post-APAP animals, to investigate the systemic transcriptomic changes following AILI. Liver and blood cells from the same animal were used for the analysis, to facilitate discrimination between hepatic and circulating leucocytes following sequencing. Liver and blood from paired, uninjured and 48hrs post-APAP C57BL/6 wild type mice were collected, and single cell suspensions were prepared for fluorescence activated cell sorting (FACS). In order to sort cells from the liver, the gating strategy relied on CD45 to detect leucocytes. As pronase cleaves CD31, ICAM 2 was used as substitute endothelial marker. 100,000 CD45+ cells from each liver of uninjured or 48hr post-APAP animals were sorted for scRNA-seq, in an unbiased manner. Studies have reported that a subpopulation of bone marrow-derived liver sinusoidal endothelial cells (LSECs) expressing CD45, to have a key role in promoting liver regeneration following injury (Wang *et al.*, 2012). With the intention of interrogating this population CD45+ ICAM2+ population was also included in the gating (Figure 4.3a, b).

For the blood samples, 50,000 CD45+ cells from uninjured or 48hr post-APAP animals were sorted. My previous data demonstrated at 48hrs-post APAP only ~10% of the circulating leucocytes were monocytes, whereas neutrophils contributed to ~40% of leucocytes (Figure 3.8). In order to dissect monocyte heterogeneity during AILI I needed to enrich for monocytes, therefore, 30% of the sorted cells in each sample represented CD11b+ CD115+ cells (monocytes) and 70% contained the remaining leucocytes (not CD11b+ CD115+) (Figure 4.3c). The average sort time for the liver samples ranged between 5-10 minutes, whereas the blood samples took around 15-20 mins.

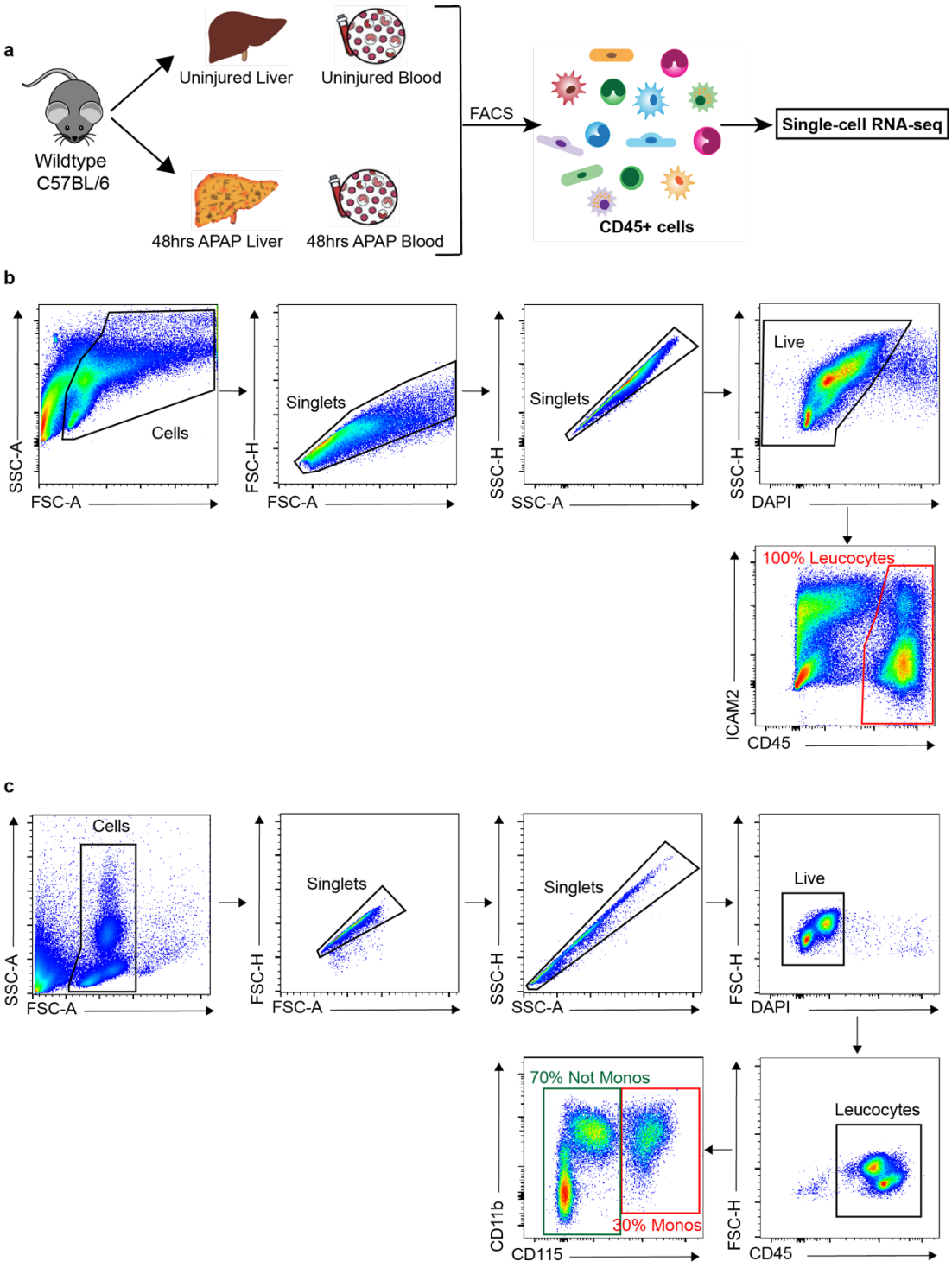

Figure 4.3 Methodology for scRNA-seq of hepatic and circulating leucocytes
(**a**) Schematic of the methodology used for scRNA-seq. Gating strategy used for the FACS for generating viable single cell suspensions of liver (**b**) and blood (**c**) leucocytes. (n=2 for each group).

Before proceeding with the scRNA-seq protocol the quality and quantity of the sorted cells were assessed for all samples (Table 4.1). Cell viability and concentration was measured on a TC20 (Bio-Rad) using trypan blue, which selectively stains dead cells. All of the samples were off excellent quality, with no cell debris or clumps, the cell viability varied between 81-97% depending on the sample (Table 4.1). Following this, cells were loaded onto the 10x Genomics Chromium Single Cell platform, a droplet-based microfluidics system. A protocol generated by 10x genomics was followed (See Methods), with assistance from Dr. Beth Henderson. The uninjured and 48hrs-post APAP liver and blood samples were run in parallel (4 samples in total at a time) to avoid batch effects, the experiment was then repeated on a different day (n=2 for each group).

The official capture rate for this machine is 65%, however previous scRNA-seq experiments performed by researchers in the Henderson lab found the capture rate to be around 30-40%. Therefore, I loaded 10769,000 cells from each of the four groups (Uninjured Liver, APAP Liver, Uninjured Blood, APAP Blood), with the hopes of capturing transcriptomic information from 3000-4000 cells per sample. The GEMs underwent RT and PCR steps to generate 10x barcoded cDNA. Quantification of the cDNA using Qubit (Thermo Fisher) showed the yield varied from 1.41-6.71 ng/μL, between samples; APAP samples generally had more cDNA than uninjured samples (Table 4.1). The 10x system allows successful library construction from cDNA yields as low as ~1-2 ng/μl and all of the samples were within this range, therefore I proceeded with library construction for NGS. Samples were analysed further on a Perkin-Elmer LabChip post library construction. The electropherogram showed sharp peaks, with no evidence of primer dimers or PCR artefacts, which indicated excellent cDNA library quality for all samples (Figure 4.4). The cDNA libraries were sequenced on an Illumina sequencing platform at the Sanger institute and Edinburgh Genomics.

	# Cells sorted	Viability (%)	Cell concentration (/ml)	# Cells loaded	cDNA Concentration (ng/μl)	Library Concentration (ng/μl)
Uninjured Liver 1	100000	85	$0.85x10^6$	10769	1.47	32.27
APAP Liver 1	100000	91	$1.77x10^6$	10769	4.46	28.57
Uninjured Blood 1	50000	81	$0.7x10^6$	10769	1.42	40.46
APAP Blood 1	50000	86	$0.72x10^6$	10769	2.88	30.73
Uninjured Liver 2	100000	97	$1.10X10^6$	10769	4.86	59.13
APAP Liver 2	100000	86	$0.6x10^6$	10769	6.71	50.58
Uninjured Blood 2	50000	96	$0.67x10^6$	10769	3.47	31.46
APAP Blood 2	50000	94	$0.7x10^6$	10769	2.58	38.81

Table 4.1 Pre-sequencing quality control metrics. Number of cells sorted via FACS, viability and concentration of cell post-sort, number of cells loaded onto the 10x machine, cDNA quantification pre and post library construction for each sample.

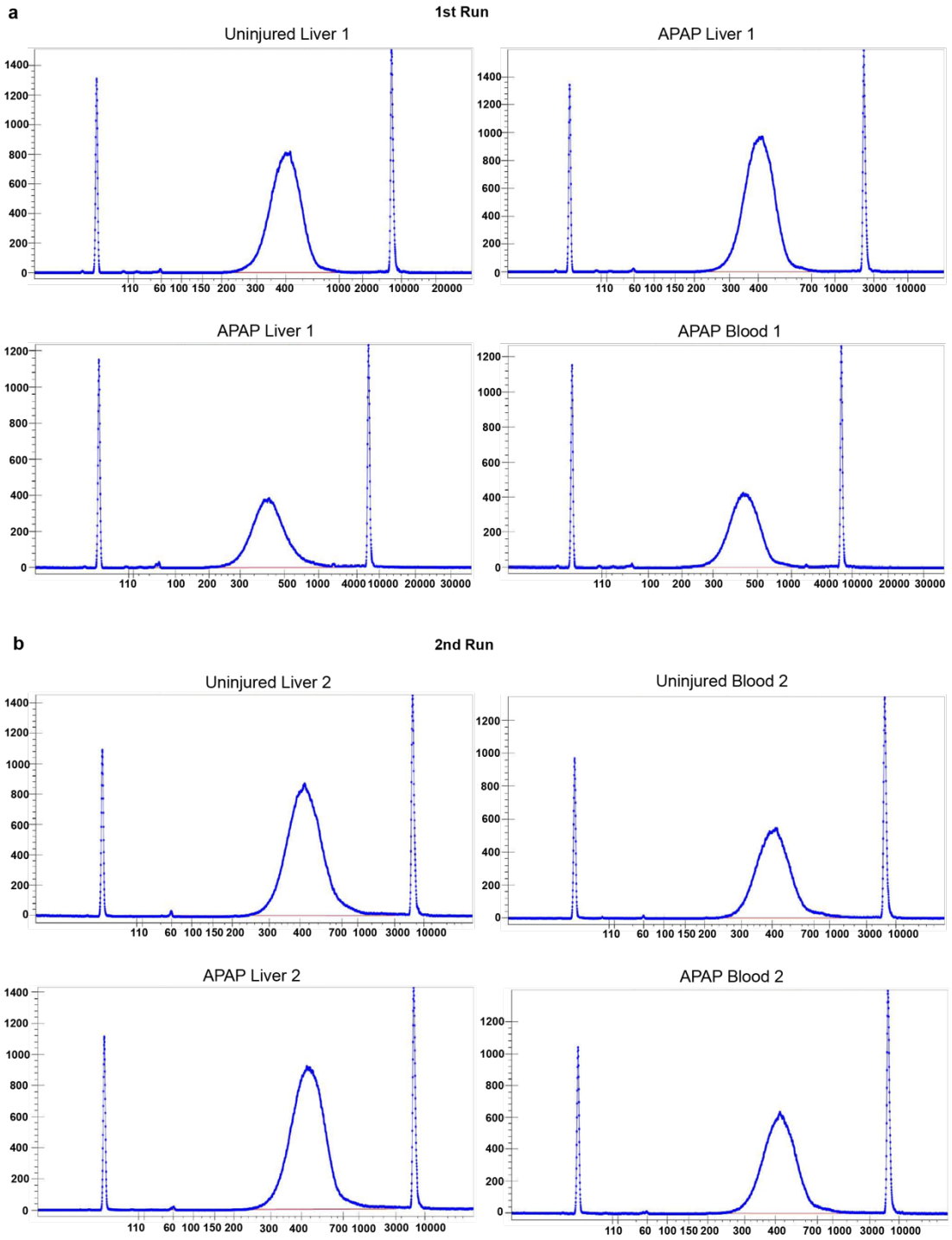

Figure 4.4 Representative results from cDNA analysis for scRNA-seq samples (Uninjured Liver, APAP Liver, Uninjured Blood, APAP Blood) following the 1st run (**a**) and the 2nd run (**b**). The measurement was taken after RT, cDNA amplification and library construction on a 10x genomics chromium technology. DNA fragment size range is depicted on the x-axis (in Base Pairs) and signal intensity (fluorescent units) on the y-axis.

4.2.3 Quality control and cell filtering post-sequencing

Table 4.2 shows the number of cells, genes, and UMIs recovered from each sample after sequencing. The capture efficiency varied between samples (23-61%), the number of genes and UMIs for APAP samples (Liver, Blood) were higher than of Uninjured samples. ScRNA-seq generates a highly complex dataset, the analysis and correct interpretation of this requires a combination of in-depth computational tools and biological expertise. For the computational analysis of the scRNA-seq data I sought the expertise of Dr. John Wilson-Kanamori, a postdoctoral bioinformatician in the Henderson lab. The initial stages of the bioinformatic analysis consisted of quality control (QC) measures, to remove cells with low reads or missing transcripts ("dropout" events). Genes expressed in fewer than three cells in a sample were excluded, along with cells that expressed fewer than 300 genes (Figure 4.5). Cell reads that contained more than 10% of mitochondrial genes were also removed, as this indicated cell stress, cytoplasmic breakdown and cell death (Figure 4.5). Notably, the variation in the number of genes and transcripts (UMIs) between samples is high, indicating heterogeneity. The APAP Liver samples generally had the most transcriptional diversity and activity (Table 4.2, Figure 4.5). After removing the low-quality cells, the 8 datasets were merged, normalized to obtain correct relative gene expression abundances between cells, appropriately scaled and, finally, technical and biological covariates were corrected for by regression based on the number or UMIs.

4.2.4 Unsupervised clustering of hepatic and systemic leucocytes

The resulting 31567 cells from the eight samples (Uninjured Liver; n=2, Uninjured Blood; n=2, APAP Liver; n=2, APAP Blood; n=2) were analysed using Seurat, a publicly available clustering package developed specifically for the analysis of scRNA-seq data. Unsupervised clustering of liver and blood cells from uninjured and 48h post-APAP conditions generated 28 distinct clusters, this was visualized via t-distributed stochastic neighbourhood

embedding (t-SNE) plot (Figure 4.6a). In a t-SNE plot each cell is represented as a single dot and cells with similar gene expression profile cluster together. Labelling the clusters according to the source (Liver or Blood), revealed cells from Liver samples clustered separately from Blood (Figure 4.6b). Further labelling based on the condition of tissue cells were isolated from demonstrated injury specific clusters (3,11,7), composed of cells from APAP samples (Figure 4.6a, c). All clusters expressed CD45 with no contamination from CD45 negative cells, further validating the FACS sort strategy (Figure 4.d). Labelling the cells according the individual sample of origin suggested the transcriptional profile of liver cells changed more dramatically with injury than blood cells (Figure 4.6e). It also indicated there was good reproducibility between the two runs for both liver and blood cells (Figure 4.6e).

Source	Condition	nCell	nGene	nUMI	10x Capture Efficiency (%)
Liver	Uninjured	2495	1858	5041	23
Liver	Uninjured	6572	1994	5335	61
Liver	APAP	3616	2916	11739	34
Liver	APAP	3575	2956	11199	33
Blood	Uninjured	3199	1323	3556	30
Blood	Uninjured	3216	1310	3296	30
Blood	APAP	5199	1467	4035	48
Blood	APAP	3977	1246	3107	37

Table 4.2 Post-sequencing information on the scRNA-seq samples. The table above summarizes the number of cells, total gene and UMI counts generated from scRNA-seq and the capture efficiency of the 10x chromium platform for each sample.

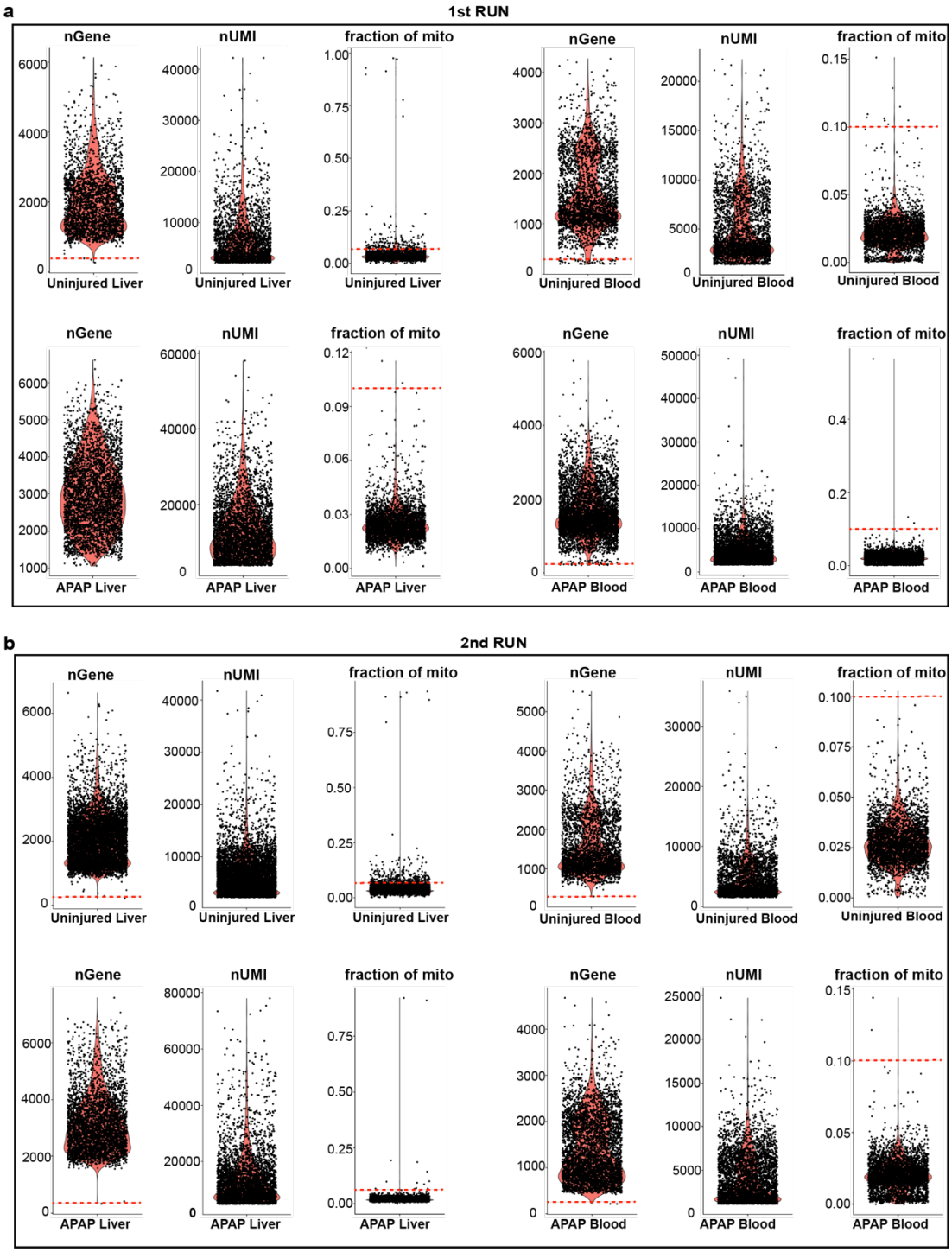

Figure 4.5 Cell filtering metrics used for quality control. Violin plots showing the number of genes, Unique Molecular Identifiers (UMIs) and fraction of mitochondrial RNA per cell for the 1st run (**a**) and the 2nd run (**b**). Black dots indicate a cell and the red dotted line represents the cut off parameter used to remove "low quality" cells based on number of genes and mitochondrial RNA content in each cell.

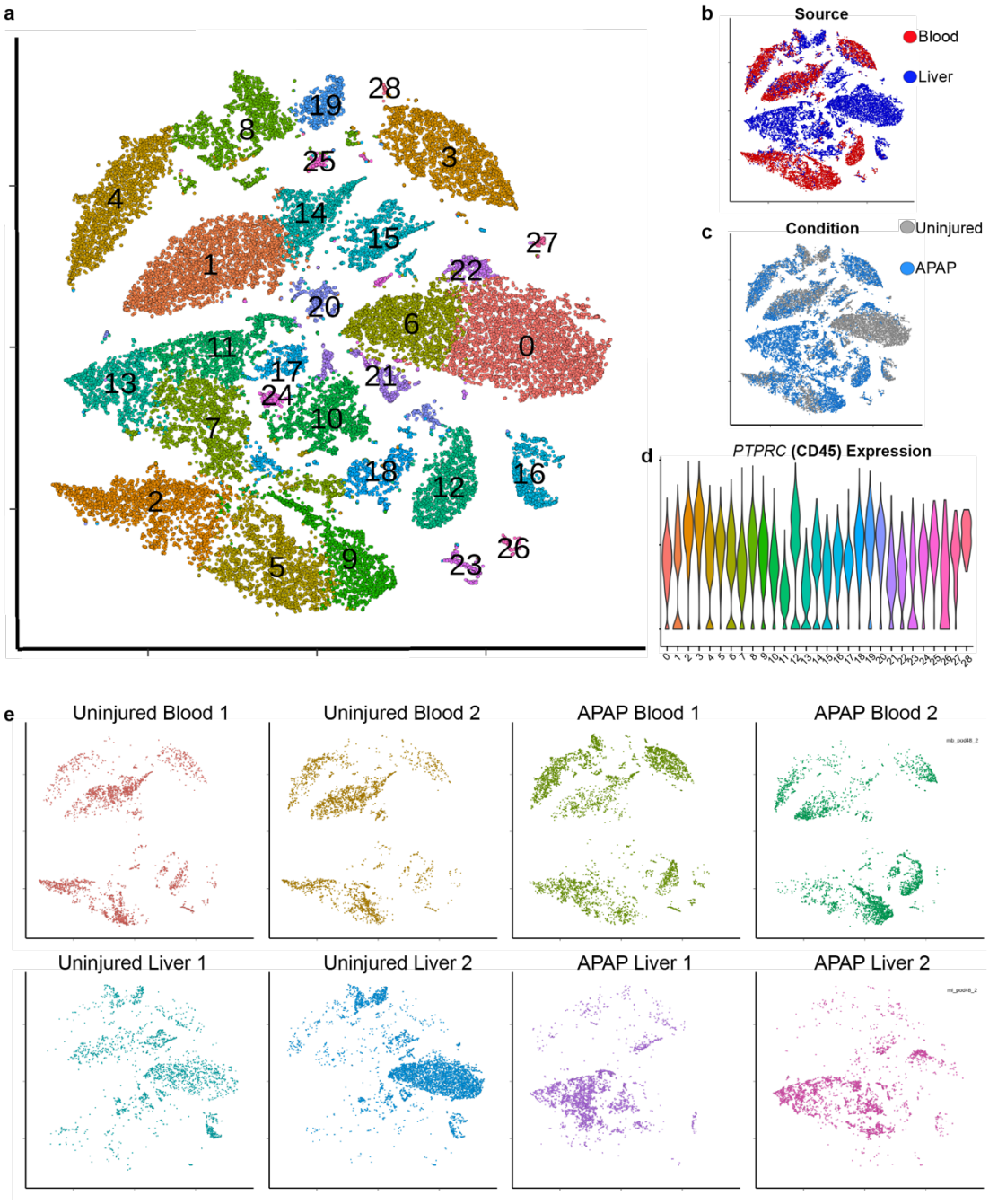

Figure 4.6 Unsupervised clustering of hepatic and systemic leucocytes. (**a**) t-SNE visualization clustering of hepatic and systemic leucocytes from uninjured and APAP samples. Cells labelled by their source (**b**) and condition (**c**). (**d**) Violin plot demonstrating the expression of *PTPRC* (CD45) genes expression across the clusters. (**e**) Cells labelled by individual samples.

4.2.5 Annotation of leucocyte lineages in the scRNA-seq dataset

Having performed initial clustering on these cells, the next aim was to annotate the clusters relying on known lineage specific marker genes. In order to do this, I collated a list of marker genes that could identify the different leucocyte lineages, based on a literature search. The expression of the selected genes across the clusters are shown in Figure 4.7b, the full list of genes used can be found in Appendix 4. Using this list, Dr. Wilson-Kanamori performed gene signature analysis on the cells, which facilitated annotation of all the expected cell lineages: mononuclear phagocyte (MP; clusters: 0, 2, 5, 6, 7, 9, 10,11, 13, 17, 18, 20, 21, 22, 24), plasmacytoid dendritic cell (pDC; cluster: 16), innate lymphoid cell (ILC; clusters: 6, 28), T cell (clusters: 4, 8, 19, 25), B cell (clusters:1, 14), Mast cell (cluster: 23), Neutrophil (cluster: 12) (Figure 4.7a, c). There was some red blood cell (RBC) contamination (cluster 26) but notably, very little contamination from mesenchymal or epithelial cells (Figure 4.7c). Clusters 21 and 28 revealed cell cycle gene signatures, which indicated a portion of MPs and ILCs, respectively, were proliferating (Figure 4.7c).

We identified cluster 15 as endothelial cells (Figure 4.7c), these group of cells expressed CD45 (*PTPRC*) (Figure 4.6c), along with endothelial specific genes such as: *PECAM1, ICAM2*, *CDH5*, and *KDR* (Figure 4.8b). Interestingly, they also expressed MP lineage genes, including *CD68* and *CSF1R* (Figure 4.8b). The endothelial cluster was composed of both uninjured and 48hrs-post APAP cells, from the broad clustering there was no indication of heterogeneity (Figure 4.8a). The genes which differentiated cluster 15 from the rest of the clusters were related to angiogenesis (*FLT1, ADGRL4*), matrix remodelling (*TIMP3*), proliferation (*IGFBP7, IL6ST*) and phagocytosis (*CLEC4G, STAB2*, *FCGR2B*). In comparison to other leucocytes, the endothelial cells had high transcriptional diversity (nGene), and transcriptional activity (nUMI) during basal conditions (Uninjured; grey), which increased following AILI (APAP; blue) (Figure 4.9b, c). Increased nGene and UMI suggested these cells might represent doublets rather than a true population.

Looking closely at the leucocyte lineages, the lymphocytes (T cells, B cells, ILCs) displayed low transcriptional diversity and activity both under basal conditions (Uninjured) and following injury (APAP) (Figure 4.9b, c). The T cell lineage contained both liver and blood cells that formed three separate clusters: 8,19 (Liver) and 4 (Blood), indicating hepatic and circulating T cells have distinct transcriptional profiles (Figure 4.7a, 4.9a). The blood T cell cluster (8) was dominated by APAP cells. B cells (clusters: 1,14) and ILCs (clusters 3, 28) were mainly from blood samples and did not have any injury specific clusters associated with them (Figure 4.7a, 4.9a). As this is very broad clustering, the differences between lineages are more dominant, than the subtle differences between subpopulations within a lineage. So, isolating these cells and re-analysing them will aid in gaining resolution into lymphocyte heterogeneity. Despite sorting based on CD45+ there were no hepatic neutrophils or eosinophils in the dataset, the neutrophils cluster (12) consisted of circulating neutrophils, primarily from APAP blood samples (Figure 4.7, 4.9a). Neutrophils also displayed very low transcriptional diversity and activity (Figure 4.9b, c). Cluster 16 was identified as pDC, mainly containing liver-resident cells (Figure 4.7, 4.9a) and clustered distant from the MP lineage which contained cDCs (Figure 4.7, 4.9). The MP lineage dominated the whole dataset and partitioned into 15 distinct clusters (Figure 4.7). MP lineage represented a very heterogenous group of cells, even at a very broad level of clustering, revealing injury (APAP) specific blood (9) and tissue clusters (13,7,11,17) (Figure 4.7). The number of genes per cell and the UMI count for MP clusters were higher in the APAP samples than uninjured samples (Figure 4.9b, c). To study these cells at a higher resolution, we isolated the MP cluster specifically and re-clustered the cells.

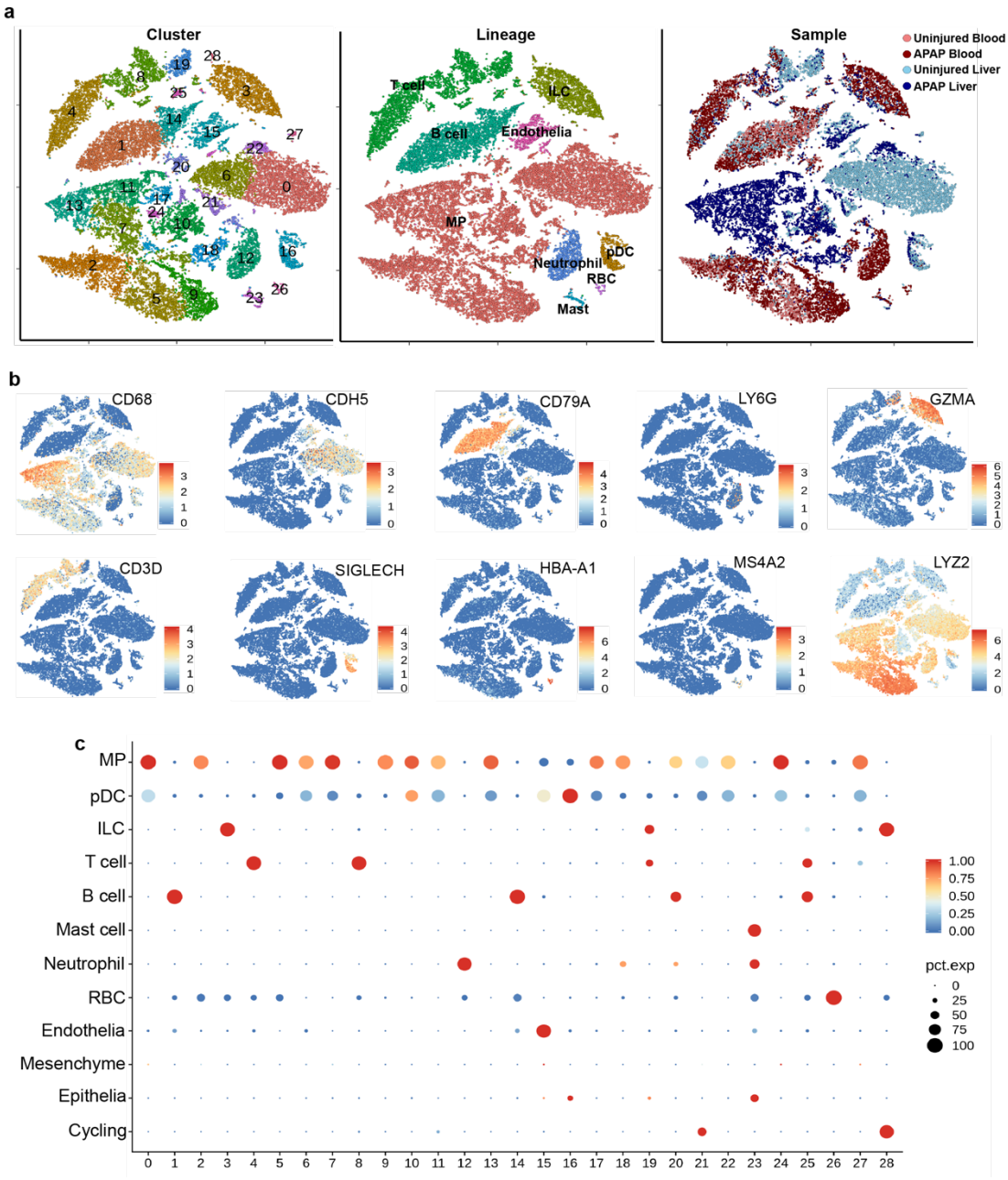

Figure 4.7 Annotation of clusters based on gene signature analysis. (**a**) t-SNE visualization of the cell based on clusters, lineage and source. (**b**) t-SNE plots showing the expression of stated genes, used for the annotation of cells, across the clusters, (red indicates high expression and blue indicates low expression) (**c**) Dotplot annotating liver and blood cell clusters by lineage signature. Circle indicated cell fraction expressing signature greater than mean; color indicates mean signature expression (red, high; blue, low).

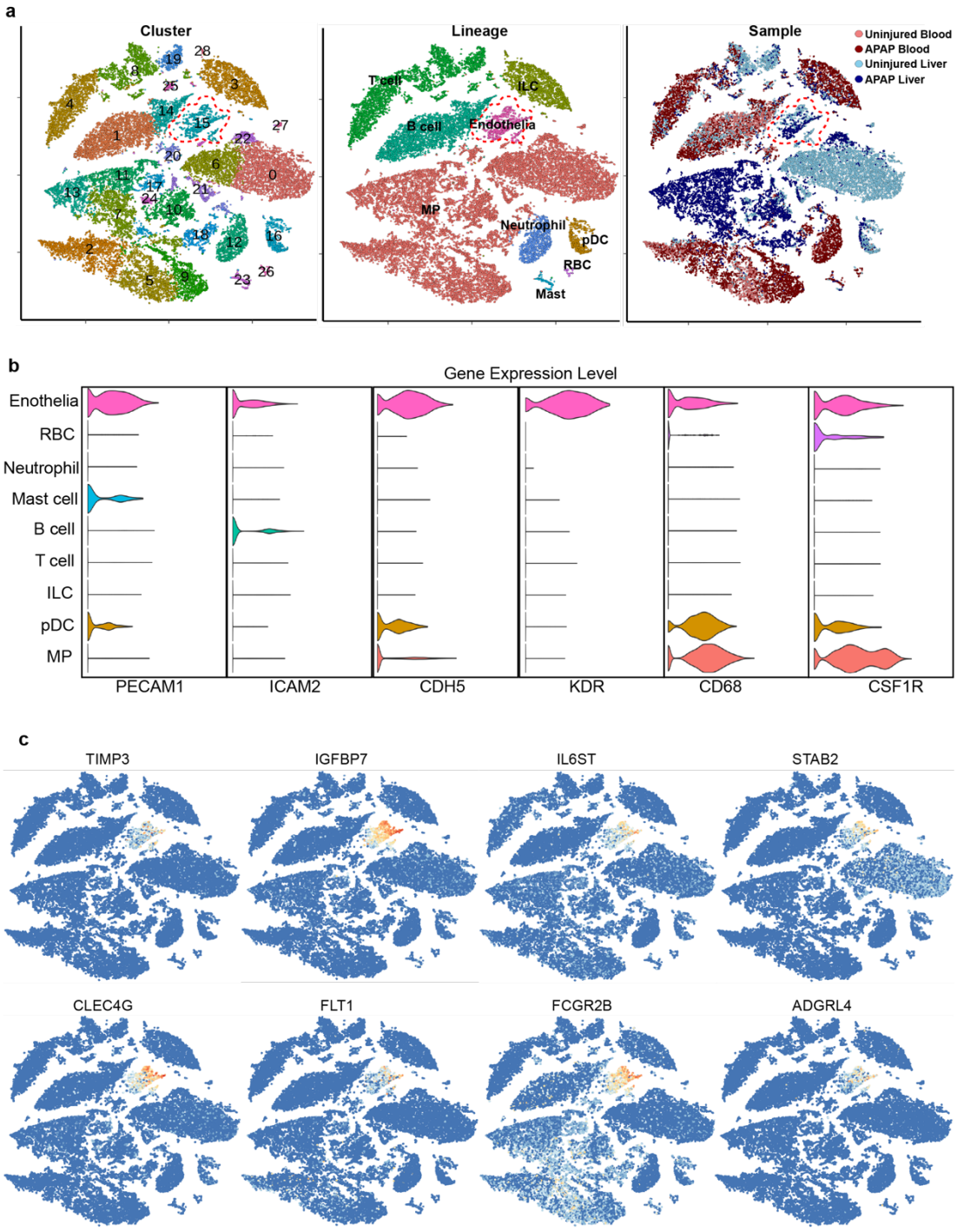

Figure 4.8 Endothelial cluster with macrophage markers (**a**) t-SNE visualization of the cell based on clusters, lineage and source. (**b)** Violin plots showing the expression of common endothelial -associated (*PECAM1, ICAM2, CDH5, KDR*) and macrophage-associated (*CD68*, *CSF1R*) genes across the identified lineages. (**c**) t-SNE plots showing the expression differentially expressed genes in cluster 15 (endothelia), red indicates high expression and blue indicated low expression.

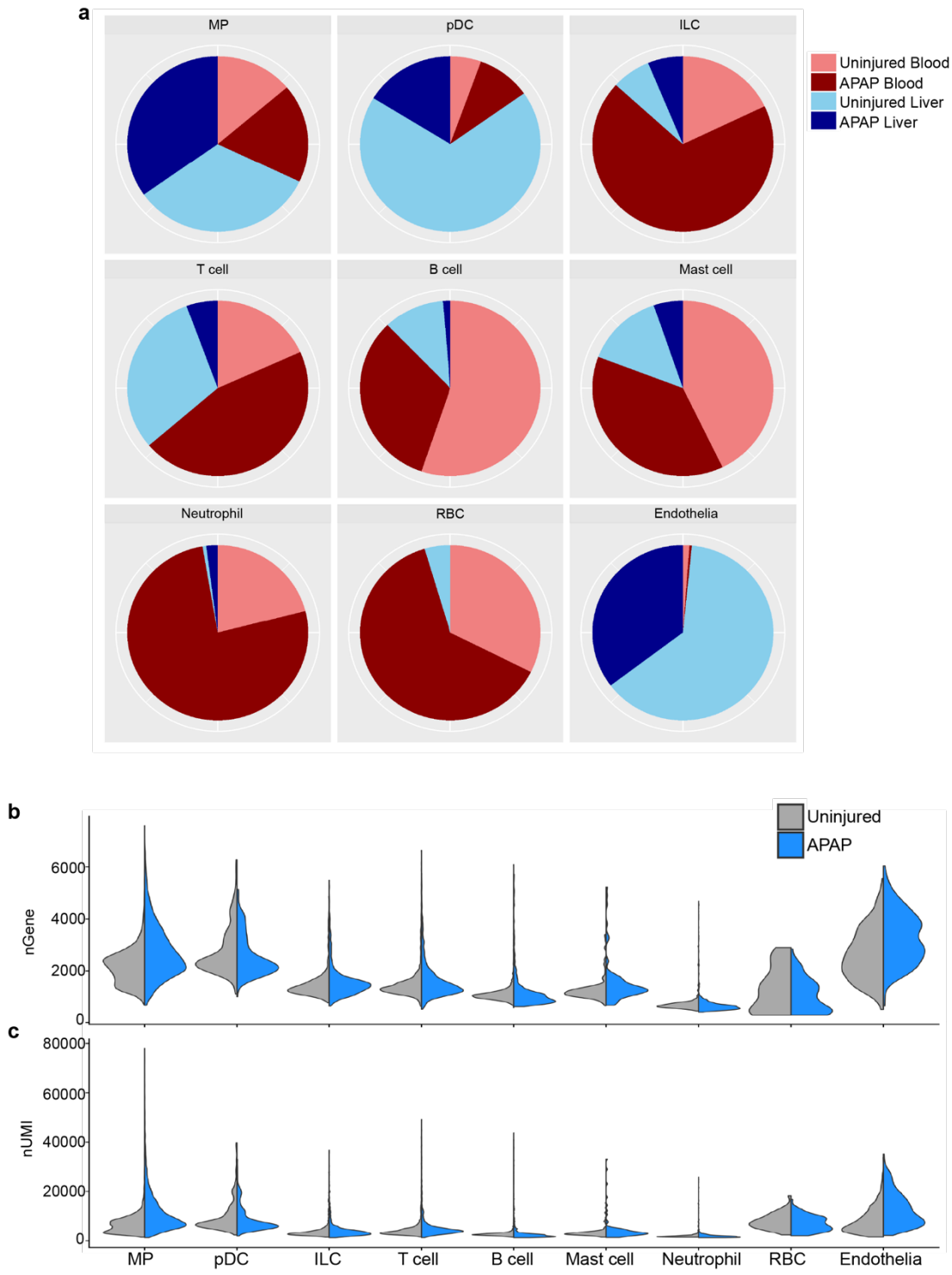

Figure 4.9 Proportional changes and transcript metrics for leucocyte lineages. (**a**) Pie charts showing the proportion of cells from liver and blood samples from uninjured and APAP animals in each cell lineage. Violin plots displaying the distribution and the total number of unique genes (nGene) (**b**) and total Unique Molecular Identifiers (UMIs) (**c**) expressed across the cell lineages in uninjured vs APAP livers.

4.2.6 Investigating heterogeneity within the mononuclear phagocyte compartment

Cells belonging to the MP lineage were re-clustered, 16,399 MPs from eight datasets (uninjured liver (n=2), APAP liver (n=2), uninjured blood (n=2), APAP blood (n=2)) partitioned into twelve distinct clusters (Figure 4.10a). Using the same principle as previously, based on known maker genes I annotated each cluster by major cell lineage. *MACRO*, *CD5L, CLEC4F* and *TIMD4* were highly expressed by cells in clusters: 0,12, and 8, therefore they were identified as Kupffer (Kupffer cells; KCs) (Scott *et al.*, 2016) (Figure 4.10, Appendix 6). Clusters 9 and 10 showed the highest expression of *H2-AA*, gene that encodes murine MHCII, indicating these cells might be conventional dendritic cells. The expression of *ITGAX* (CD11c) and *XCR1* facilitated annotation of cluster 9 as cDC1 and cluster 10 as cDC2 (Figure 4.10). Clusters 1, 2 and 6 were from blood samples and these clusters also exhibited increased expression of monocytic genes: *S100A4* and *LYZ2*, therefore I identified them as the monocytes (Figure 4.10) (Hoeffel *et al.*, 2015; Shi *et al.*, 2018). The remaining five clusters (3,4,5,7,11) consisted of cells exclusively from APAP Liver samples (Figure 4.10). These cells had high expression of *LYZ2*, a myelomonocytic marker, and *CSF1R,* a gene required for macrophage survival and maintenance (Pollard, 2009; Gow *et al.*, 2014; Shi *et al.*, 2018). Furthermore, varying expression of *CCR2*, *LY6C2* and *H2-AA* and the lack of expression of KC and DC related genes led me to annotate these cells as monocyte derived macrophages (MDM) (Figure 4.10). Overexpression of cell cycle genes such as: *STMN1*, *MKI67* in cluster 11, highlighted that a proportion of the MDMs were in cycle (Figure 4.10b). Examining the proportion of cells within each cluster that came from each sample (uninjured liver (n=2), APAP liver (n=2), uninjured blood (n=2), APAP blood (n=2) demonstrated that clusters (3,4,5,7,10,11) belonging to the MDM clusters are APAP specific (Figure 4.11a). and the most heterogenous population of cells (Figure 4 10a).

The MDM clusters also contained the most transcriptionally diverse and transcriptionally active cells during injury, indicated by the high number of number of genes and UMIs per cell seen in the cell from the APAP group (Figure 4.11b). Unsurprisingly, majority of the Kupffer clusters contained cells from uninjured livers, only small proportion of injury specific cells (APAP Liver) (Figure 4.10, 4.11). Despite this, based on the nUMIs and nGenes the APAP specific cells in the Kupffer lineage were more transcriptionally diverse and had more transcripts than cells from uninjured livers (Figure 4.11). They also formed a separate cluster (cluster 8) that is distinct to the uninjured Kupffer clusters (0,12) (Figure 4.10a). Clusters 9 and 10, belonging to the cDC1 and cDC2 lineage, respectively, contained a small fraction of blood cells, majority of the cells were liver cells from both APAP and uninjured samples (Figure 4.11a). Cells belonging to the cDC2 lineage (cluster 10) clustered more closely with MDMs (Figure 4.10a) and were more transcriptionally active following APAP induction, when compared to cDC1 (cluster 9) (Figure 4.11b). The monocyte clusters contained cell from blood samples, the small fraction of liver cells in this group were identified as contaminating blood cells in the liver samples, which survived the liver perfusion (Figure 4.11a). The close proximity of monocytes clusters to MDM clusters suggested a differentiation trajectory from blood into tissue (Figure 4.10a). There were no major differences in the number of genes and number of UMIs between Uninjured and APAP groups for the monocyte lineage (Figure 4.11b). Nevertheless, cluster 6 represented an injury specific population of circulating monocytes, which indicated transcriptional changes in the circulating monocytes at 48hrs post-APAP, prior to their entry into the liver (Figure 4.10a).

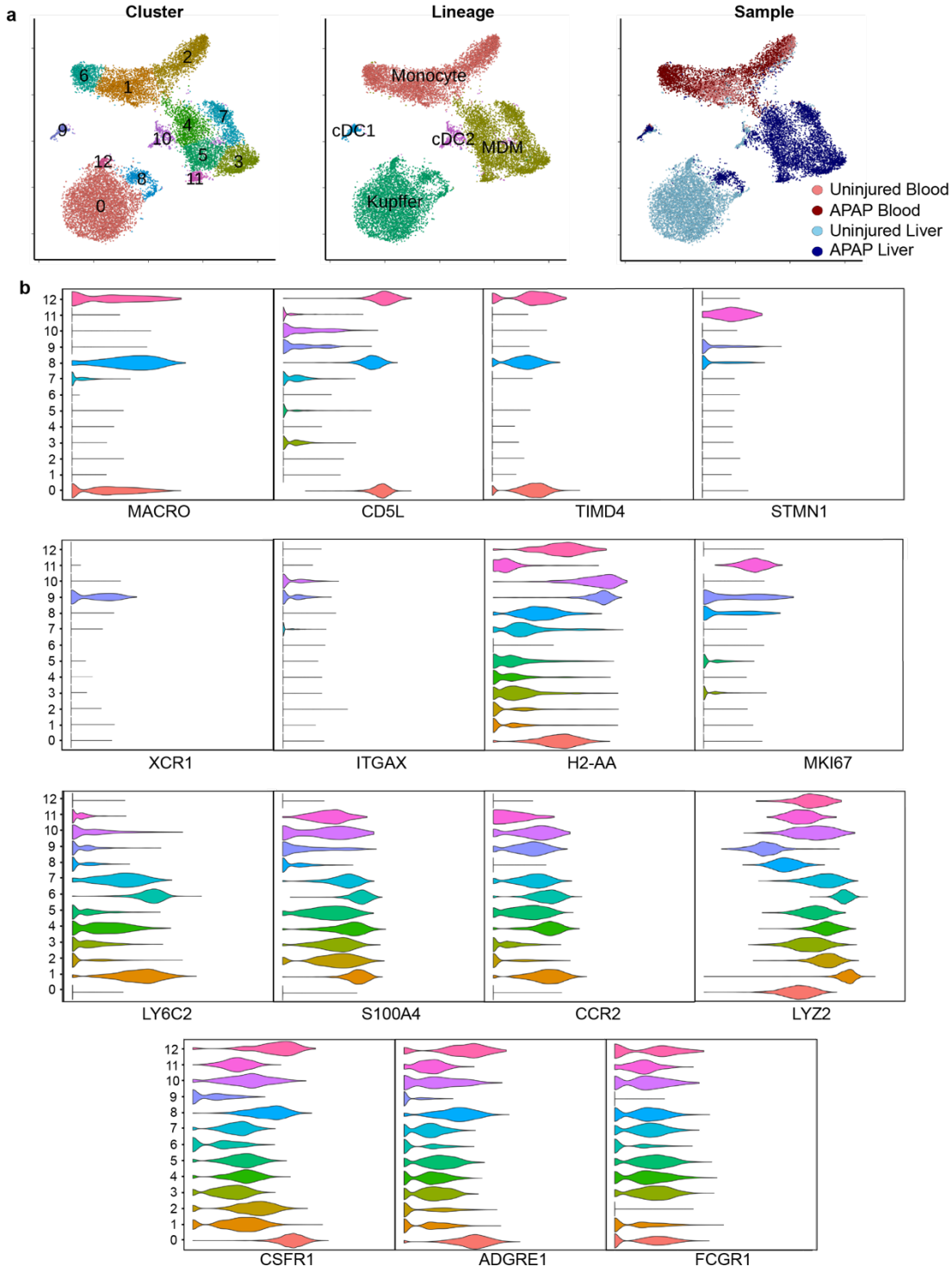

Figure 4.10 Unsupervised clustering of mononuclear phagocytes (**a**) t-SNE visualization of mononuclear phagocytes (MP) from uninjured and APAP liver and blood based on clusters, lineage and source. (**b**) Violin plots showing the expression of lineage specific markers, used for annotation, across the MP clusters.

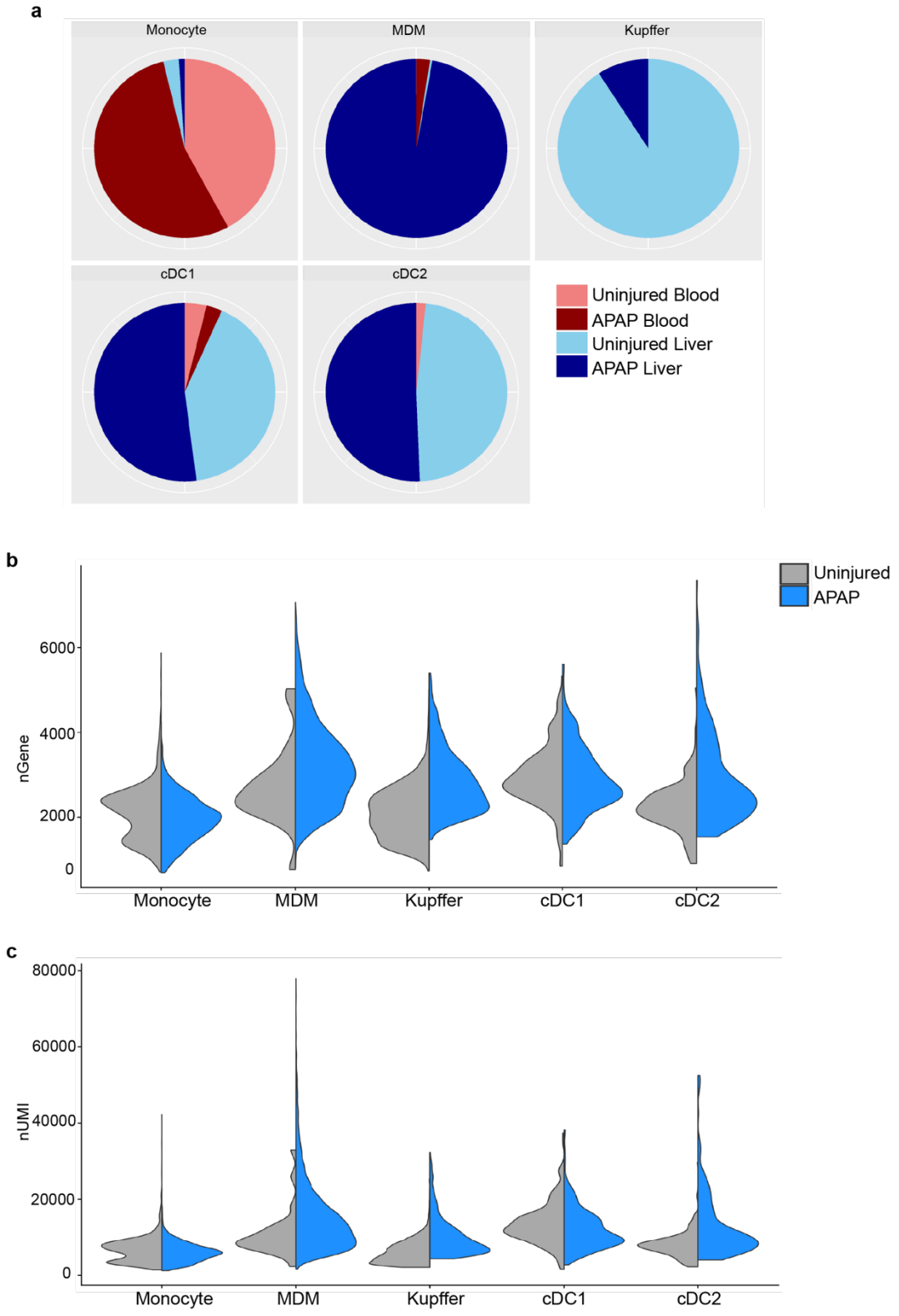
a
Monocyte
MDM
Kupffer
cDC1
cDC2
Uninjured Blood
APAP Blood
Uninjured Liver
APAP Liver
b
Uninjured
APAP
nGene
6000
4000
2000
0
Monocyte
MDM
Kupffer
cDC1
cDC2
c
nUMI
80000
60000
40000
20000
0
Monocyte
MDM
Kupffer
cDC1
cDC2

Figure 4.11 Proportional changes and transcript metrics for mononuclear phagocyte lineages (**a**) Pie charts showing the proportion of cells from liver and blood samples from uninjured and APAP animals in each MP lineage. Violin plots displaying the distribution and the total number of unique genes (nGene) (**b**) and total Unique Molecular Identifiers (UMIs) (**c**) expressed across the MP lineages in uninjured vs APAP livers.

Following the clustering of MPs and establishing the identity of the clusters I was interested in dissecting the heterogeneity within the different MP lineages. Performing differential gene expression (DE) analysis is one of the most common ways which enables the identification of specific genetic features which could indicate differences in phenotype and function. Gene expression in one cluster to another, as well as across all 12 clusters was analysed to identify differentially expressed genes (Appendix 5). The analysis was performed in Seurat (Methods) and only those genes with log-fold changes of at least 0.25 and expression in at least 20% of cells in the cluster under comparison were retained. Figure 4.12a displays DE analysis as a heatmap, where each column represents a single cell, and each row represents a gene. The 12 main clusters identified by the unsupervised clustering are represented at the top and on the left. The source (liver: blue, blood: red), and condition (Uninjured: grey, APAP: light blue) of the cells are represented on the top of the clusters. The expression of a certain gene is indicated by the colour red and absence by blue.

Firstly, the Kupffer cells (cluster 0,8,12) had a very differential gene expression profile to the other hepatic MP lineages (MDM, cDC) and to the circulating monocytes. A distinct set of genes such as: *TIMD4*, *VSIG4*, *FCNA* were exclusively expressed in the Kupffer clusters (Figure 4.12a). The genes which distinguished APAP Kupffer cells (cluster 8) from uninjured Kupffer cells (clusters: 0 and 12) were cell cycle related (*TK1*, *MCM3*) (Figure 4.12a, Appendix 6). This suggested that APAP induced local proliferation of Kupffer cells. We could not identify any non-cell cycle related genes which were exclusive to cluster 8. The DE analysis failed to generate any unique genes

for cluster 12 (Figure 4.12.a, Appendix 5, 6). Circulating monocytes (cluster 1,2,6) expressed a distinct set of genes to the tissue MPs, but they also shared some sets of genes with tissue MPs; cluster 7 in particular (Figure 4.12a, Appendix 7, 9). Amongst the MDM clusters, cluster 7 has the most distinct gene profile, compared to its liver counterparts. Genes such as *LCN2*, *WFDC21*, *VCAN*, *MCEMP1* were upregulated in cluster 7, interestingly these were also expressed by the APAP specific circulating monocyte cluster (6) (Figure 4.12a; Appendix 6). MDM clusters 3 and 4 displayed a relatively discrete transcriptional profile, whereas cluster 5 shared genes with 3 and 4, suggesting these cells might represent an intermediate phenotype (Figure 4.12a; Appendix 7). There were a select number of genes unique to each of the MDM clusters: cluster 3: *SPP1*, *IL7R*, *CCL7,* cluster 4: *NR4A2, IFIT1*, *IFIT3*: cluster 4, cluster 5: *STAB1*, *IGFBP4* and Cluster 7: *LCN2*, *CXCL2, CXCR2, RETNLG* (Figure 4.12a, Appendix 7). As noted before, cell cycle marker genes delineated cluster 11 from the other MDMs (Figure 4.12a). There were no other uniquely expressed genes in cluster 11. cDC1 cells could be easily delineated from the rest of the MPs; they distinctly expressed a number of dendritic cell (DC) marker genes (*XCR1, CD24, FLT3, CLEC9A*). Cells in cDC2 on the other hand had very limited number of unique DC related genes (*CD209A, CIITA*), furthermore, these cells shared a lot of features with MDMs, expression of *CD63*, *STAB1*, *MS4A7*, *SLAMF7* amongst various other macrophage related genes such as *CSFR1, ADGRE1* and *FCGR1* (Figure 4.12a; Appendix 7).

Figure 4.12 Differential gene expression analysis of mononuclear phagocytes. (**a**) Scaled heatmap (red, high expression; blue, low expression) showing MP cluster marker genes (color coded at the top by cluster, condition and source), exemplar genes labelled right. (**b**) Gene ontology enrichment analysis of APAP specific tissue MP clusters (3,4,5,7,8,9,10), showing exemplar genes (left), GO terms (right) for each cluster.

Following the identification of differentially expressed genes across the different MP clusters, my next aim was to interrogate whether the transcriptomic differences dictated any functional differences in the MP clusters during acetaminophen induced liver injury (AILI). Based on the marker gene list Dr Wilson-Kanamori generated, I performed Gene Ontology (GO) enrichment analysis for clusters: 3,4,5,7,8,9 and 10 to delineate the functional profile of the injury specific liver cells during AILI. MDMs in cluster 3 were enriched for ontology terms relevant to ribosomal assembly, cholesterol storage, response to IL-7, in addition to phagocytosis and tissue regeneration; terms associated with a pro-repair macrophage phenotype (Figure 4.12b). MDMs in cluster 4 were enriched for terms of macrophage and lymphocyte migration, responses to IFNβ, production of TNF and leucocyte differentiation, which are associated with a pro-inflammatory macrophage phenotype. Cluster 5 had similar GO terms to MDM cluster 4, consisting of TRAIL regulation, myeloid cell migration and response to IL-4, considering these clusters had a number overlapping genes this was unsurprising (Figure 4.12b). The GO terms for cluster 7 were related to phagocytic clearance, response to IL-8 and neutrophil aggregation. Notably, cluster 7 also showed enrichment for glutathione biosynthesis, these cells upregulated of genes such as *SLC7A11* and *NFE212* (figure 4.12b), required for glutathione production (Clemons *et al.*, 2017; Ryoo and Kwak, 2018). The injury specific Kupffer cluster 8 showed significant enrichment for GO terms involving cholesterol and iron homeostasis, complement activation, IL-6 synthesis and apoptotic cell clearance, which are all known functions of KCs in mice (Ju *et al.*, 2002; Zigmond *et al.*, 2014; Scott and Guilliams, 2018). Both of the cDC clusters gave expected GO terms, with cDC2 showing enrichment of genes relating to regulation of lymphocyte migration and survival (Figure 4.12b). Overall, the GO enrichment analysis of injury specific clusters revealed distinct GO terms for the injury specific MP clusters and revealed novel ontology terms of macrophages in the context of AILI.

4.2.7 APAP induces transcriptional changes in the circulating monocyte compartment

To study the transcriptional landscape of circulating monocytes in more depth cells were isolated from the "Monocyte" lineage from the MP clustering analysis, contaminating cells from Liver samples were removed and they were re-clustered. A total of 4896 cells gave three distinct clusters: 1,2,3 (Figure 4.13a). Labelling the cells according to the sample of origin revealed cluster 3 to be APAP specific, whereas cluster 1 and 2 contained both uninjured and APAP cells (Figure 4.13b). As previously discussed, murine monocytes are broadly categorized into two main subsets: Ly6C^{Hi} Monocytes (classical) and Ly6C^{Lo} (non-classical monocytes) (Yona *et al.*, 2013). All three clusters expressed *LYZ2*, which confirmed the cells belonged to the monocytic lineage. Furthermore, cells in cluster 1 and 3 exhibited high expression of *LY6C2* and *CCR2* (Figure 4.13c) and was therefore identified as Ly6C^{Hi} monocytes (labelled as: Ly6C^{Hi} mono1 and Ly6C^{Hi} mono2, respectively) (Figure 4.13a). Lack of *LY6C2* and *CCR2* expression and distinguished expression of *NR4A1*, identified cells in cluster 2 as Ly6C^{Lo} Monocytes (Figure 4.12a, c). Mildner et al, 2017 has shown the existence of a third murine monocyte subtype, termed Ly6C^{Int} monocytes, which shares transcriptomic signature with both Ly6C^{Hi} monocytes and Ly6C^{Lo} monocytes. Comparative DE analysis on three clusters revealed Ly6C^{Lo} mono (cluster 2) exhibited a unique gene profile that has previously been reported, which included upregulation of genes such as *NR4A1*, *CD36*, *CD9* and *TREML4* (Ingersoll *et al.*, 2009; Mildner *et al.*, 2017). Whereas, the Ly6C^{Hi} mono1 (cluster 1), had overlapping gene expression to Ly6C^{Hi} mono2 and Ly6C^{Lo} mono clusters (Figure 4.13d). Ly6C^{Hi} mono2 which consisted of cells solely from APAP blood displayed a very distinct gene profile to the other two clusters, with enrichment of neutrophil signature in these cells (*LCN2*, *MMP8*, *WFDC21*, *RENTLG*) (Nakamura *et al.*, 2018) (Figure 4.13d).

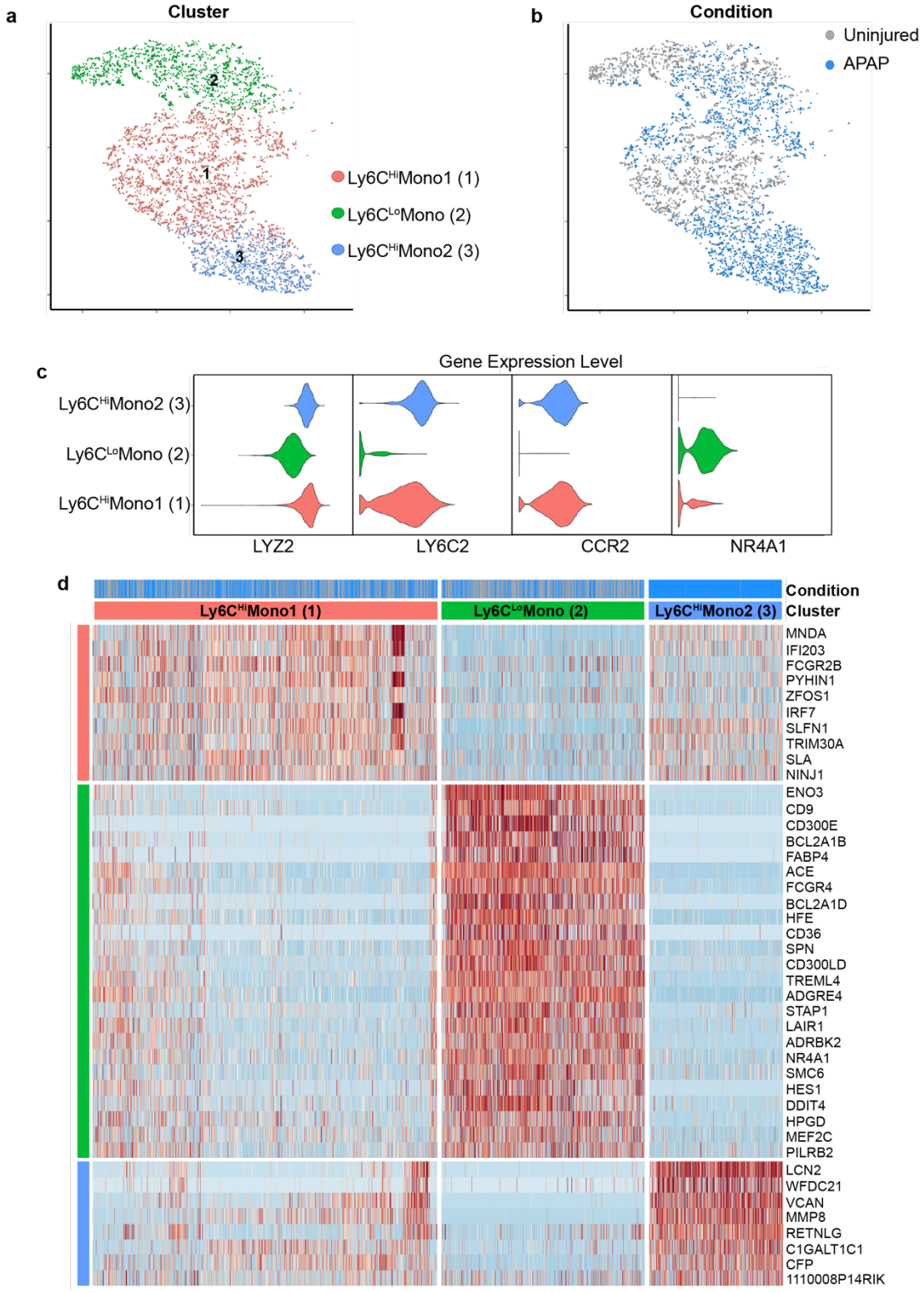
a
Cluster
2
1
3
Ly6C^HiMono1 (1)
Ly6C^LoMono (2)
Ly6C^HiMono2 (3)
b
Condition
Uninjured
APAP
c
Gene Expression Level
Ly6C^HiMono2 (3)
Ly6C^LoMono (2)
Ly6C^HiMono1 (1)
LYZ2
LY6C2
CCR2
NR4A1
d
Condition
Ly6C^HiMono1 (1)
Ly6C^LoMono (2)
Ly6C^HiMono2 (3)
Cluster
MNDA
IFI203
FCGR2B
PYHIN1
ZFOS1
IRF7
SLFN1
TRIM30A
SLA
NINJ1
ENO3
CD9
CD300E
BCL2A1B
FABP4
ACE
FCGR4
BCL2A1D
HFE
CD36
SPN
CD300LD
TREML4
ADGRE4
STAP1
LAIR1
ADRBK2
NR4A1
SMC6
HES1
DDIT4
HPGD
MEF2C
PILRB2
LCN2
WFDC21
VCAN
MMP8
RETNLG
C1GALT1C1
CFP
1110008P14RIK

Figure 4.13 Transcriptomic analysis of peripheral monocytes. (**a**) t-SNE visualization of circulating Monocyte clusters from uninjured and APAP samples. (**b**) Annotating clusters based on condition. (**c**) Conventional genes used for monocyte identification. (**d**) Heatmap (red, high expression; blue, low expression) showing differentially expressed marker genes in the monocyte cluster (color coded at the top by cluster and condition), genes labelled right.

4.3 Discussion

The goal of this body of work was to investigate the heterogeneity within murine hepatic and systemic monocytes and macrophages following acetaminophen induced liver injury (AILI), using scRNA-seq. A successful scRNA-seq experiment relies on efficient liberation of macrophages from uninjured and injured livers and subsequent generation of viable, single cell suspensions. The experiments in the previous chapter demonstrated that current digestion methods used in the field are inefficient at liberating Kupffer cells (KCs), from injured livers. Considering the success pronase had in the dissociation of mesenchymal cells from injured livers, I hoped a pronase-based digestion protocol (protocol 2), would increase the dissociation of KCs from injured livers. However, there was no significant differences in the percentages of total macrophages, KCs or MDMs liberated using protocol 2 compared to protocol 1 (collagenase-based) (Figure 4.2). In comparison to protocol 1, protocol 2 did generate more viable cells, which is crucial for scRNA-seq experiments (Figure 4.2a). Accepting the limitations associated with protocol 2 in liberating KCs from the liver post-APAP samples, I proceeded with a pronase-based digestion protocol for the scRNA-seq experiments, with the aim of gaining more resolution into the recruited macrophage subsets ($Ly6C^{Hi}$ monocytes, $Ly6C^{Lo}$ MDMs).

AILI is a highly dynamic model and macrophage transcriptome, proteome and function can vary over the course of AILI, consequently, timepoint selection for the scRNA-seq experiment was important. As shown in chapter 3 hepatocyte proliferation at 48hrs post-APAP is on an incline, thus increasing the chances of detecting pre-programming in macrophages towards a pro-repair

phenotype. It also represented a timepoint at which hepatocyte necrosis was minimal, but not completely absent (Figure 3.1). Given the link between phagocytosis and tissue repair following injury in various organs (Yang *et al.*, 2015; Woo *et al.*, 2016), including the liver (Campana *et al.*, 2018), I was interested in seeing potential changes in macrophage transcriptome that influenced their ability to phagocytose. Moreover, there was considerable heterogeneity observed within the Ly6C^{Lo} MDMs at this timepoint (Figure 3.7c). Based on these reasons 48hrs post-APAP was chosen as the timepoint for the scRNA-seq experiment.

Previous studies have selected a specific subset of monocyte/macrophage, based on cell surface markers such as: F4/80, CD11b, Ly6C, CCR2, CX3CR1 for their transcriptome analysis. Selection of particular subsets based on prior knowledge neglect cells which do not conform to these definitions, which can massively underestimate heterogeneity. For this reason, a broad, unbiased FACS gating strategy, based on CD45 expression was used to isolate hepatic and systemic leucocytes for scRNA-seq (Figure 4.3). Amongst the various scRNA-seq techniques available I decided to use a droplet-based approach using the 10x Genomics Chromium platform. As the 10x technology is based on a 3'-tag sequencing method, it generates partial transcripts, therefore the rate of "dropout" genes is high (Ziegenhain *et al.*, 2017). However, this technology was ideal for the question at hand, as it facilitated the capture of thousands of cells to give an aggregate view of transcriptional heterogeneity within cells. It also increased the chances of gaining transcriptomic information on rare, underrepresented cell types in the dataset, such as KCs from APAP livers.

The quality control (QC) checks before and after the 10x protocol indicated the protocol followed here generated good quality cells and resulting cDNA for sequencing. The stringent post-sequencing QC checks implemented by Dr. John Wilson-Kanamori filtered out any cells of low quality prior to downstream clustering analysis. Despite using a broad gating strategy to select for

leucocytes certain cell types such as hepatic neutrophils and eosinophils were underrepresented in the liver dataset. This could be because these cells are prone to RNA degradation or because the 10x scRNA-seq technique might not be best suited for these cells. All the other expected leucocyte lineages were identified and annotated.

The discovery of an endothelial signature (cluster 15) in the dataset was an interesting find but not a novel one. Liver sinusoidal cells (LSECs) with hematopoietic potential have been described before in rat livers, these CD45+ LSECs where shown to be important in liver regeneration following partial hepatectomy (Wang *et al.*, 2012). Lynch et al., 2018 report that endothelial cells can form aggregates with CD45+ cells, consequently contaminating macrophage liver preparations and highlights the importance of endothelial makers such as CD31 in removing these contaminants. As CD31 gets cleaved by pronase digestion, ICAM2 was used here, it was evident that there was a population of ICAM2+ CD45+ cells in the preparations (Figure 4.3b). These dual positive cells were included in the sorted samples to see whether scRNA-seq would permit their delineation. Cluster 15 had a very strong endothelial signature; however, these cells also expressed several other macrophage related genes such as: *LYZ2*, *CSF1R*. Cells in cluster 15 could represent doublets, though we did not find other leucocyte gene signatures except signatures for MPs in these cells. Given the “sticky” nature of macrophages, especially following injury, it is possible that macrophages preferentially form aggregates with endothelial cells. Conversely, it is also possible that these cells are truly derived from bone marrow derived hematopoietic progenitors, and display MP characteristics. In depth comparative analysis of these cells is needed to decipher this, as there was a small fraction of these cells in the dataset, we did not perform any further analysis.

MP clusters represented a highly heterogenous group of cells (Figure 4.10), apparent even at the very broad clustering stage. Isolating the MPs and performing unsupervised clustering we saw that much of the heterogeneity

was exhibited by blood monocytes and tissue macrophages. Identification of marker genes and DE analysis on the MP clusters allowed for annotation and delineation of these cells. Dendritic cell clusters (9,10) accounted for only a small fraction of MPs and consisted mainly of injury specific cells. While cDC2 cells showed enrichment for GO terms associated with DCs, they lacked *FLT3* expression, and displayed overlap in gene expression to MDM clusters (Figure 4.12). This suggests that these cells might be akin to the CD209+ monocyte-derived dendritic cell subtype reported by Menezes et al., 2016. Using a pronase-based protocol (protocol2) I managed to liberate KCs from APAP livers albeit not very many (Figure 4.10). These cells formed a distinct cluster (8) to the uninjured KCs (0,12). DE analysis highlighted cluster 8 upregulated cell cycle genes, indicating there is local proliferation of KCs during AILI. Data from chapter 3 demonstrated that KCs showed a dynamic behaviour and localized to repairing areas at 48hrs-post APAP (Figure 3.6), here transcriptomic analysis of KC from 48hrs post-APAP livers showed no upregulation of migratory genes. In fact, APAP specific KCs (cluster 8) had a very similar gene profile to uninjured KCs (0,12), and except for the cell cycle genes, did not display unique gene modules. A pronase-based protocol (protocol 2) used here and the other protocols reported in the literature (Holt, Cheng and Ju, 2008; Zigmond *et al.*, 2014; Bain *et al.*, 2016; Graubardt *et al.*, 2017; Lynch *et al.*, 2018; Krenkel *et al.*, 2019) are not efficient in liberating the true “injury specific KCs” seen around the repairing areas of the liver post-APAP. One of the ways the digestion protocol could be optimised in the future is by perfusing the liver *in situ* with enzyme cocktail, prior to dissection, this has been proven to yield more cells in the case of hepatic stellate cells (Mederacke *et al.*, 2015).

MDMs represented the most expanded MPs post-APAP, they were also the most heterogenous. Bulk RNA-seq and microarray analysis of monocytes/macrophages during AILI highlights two distinct gene profiles for these cells (Zigmond *et al.*, 2014; Graubardt *et al.*, 2017). Following scRNA-seq analysis they partition into four clusters. Three clusters (3,4,7) showing

very distinct profiles and one cluster (5) showing an intermediate gene expression profile (Figure 4.10). Clusters 4 and 7 upregulated various proinflammatory genes, and the expression of *LY6C2* and *CCR2* in these clusters (Appendix 7) indicated they might be akin to proinflammatory Ly6C^{Hi} CCR2^{Hi} CX3CR1^{Lo} monocytes reported in previous studies (You *et al.*, 2013; Zigmond *et al.*, 2014; Mossanen *et al.*, 2016; Graubardt *et al.*, 2017). They also expressed a range of discriminatory genes and the GO enrichment analysis also suggested these cells might have different functions (Figure 4.12). Cluster 4 exhibited macrophage migratory and pro-inflammatory cytokine response terms and cluster 7 had terms related to neutrophil aggregation and clearance. Regulation of neutrophil survival and clearance by Ly6C^{Hi} monocytes during AILI has been shown to promote a pro-repair phenotype (Graubardt *et al.*, 2017). Cluster 7 might represent a subpopulation of Ly6C^{Hi} monocytes responsible for this, furthermore these cells also preferentially upregulate apoptotic cell bridge molecules and receptors (*THBS1, CLEC4E, CLEC4D*). Cluster 5 had commonalities with cluster 4 and cluster 3, which to me suggests they represent cells on a differentiation trajectory from Ly6C^{Hi} monocytes to Ly6C^{Lo} MDMs (Appendix 7). Whereas, cluster 3 had a very distinct transcriptional profile to cluster 4, these cells showed enrichment for *IL7R*, *GPNMB*, *CLEC4D*, *SPP1, CD9, CD63, IGF1* thus, giving GO enrichment for term relating to IL7 signalling, tissue regeneration and phagocytosis.

Although there are many studies reporting on the transcriptome, proteome and function of monocytes while they are in the liver. To my knowledge, there are no studies which have interrogated these cells in the blood during AILI or in the context of other acute liver injuries. Here, scRNA-seq of circulating monocytes from uninjured and APAP samples permitted an in-depth transcriptomic analysis of murine monocytes during homeostasis and following AILI. I identified the two main subsets of murine monocytes during homeostasis: Ly6C^{Hi} monocytes and Ly6C^{Lo} monocytes as cluster 1 and 2, respectively. Both of the clusters exhibited expected gene signatures (Figure

4.13). The key observation from this analysis was the identification of cluster 3, composed of cells exclusively from APAP blood (Figure 4.13). These cells were counterparts of Ly6C^{Hi} monocytes, seen during homeostasis and expressed conventional genes *CCR2*, *LY6C2.* They also had a unique gene signature, showing enrichment of *S100A8, S100A9*, *RETNLG, LCN2, SELL, MCEMP1,* this gene expression profile was also evident in liver cluster 7 in the MP clustering analysis (Appendix 7). These cells exhibited gene expression modules akin to that seen in neutrophils, it is important to highlight that neutrophils were excluded following their identification based on gene signature analysis, therefore it is highly unlikely the signatures seen in cluster 3 (blood monocyte cluster) and cluster 7 (Liver MP cluster) are from contaminating neutrophils. These findings indicate that APAP induces an inflammatory transcriptional pre-programming in Ly6C^{Hi} monocytes prior to their entry into the liver. Injury induced pre-programming of Ly6C^{Hi} monocytes in the bone marrow has been reported before. Krenkel et al., 2019 demonstrates a metabolic transcriptional re-programming of Ly6C^{Hi} monocytes in the bone marrow during non-alcoholic fatty liver disease (NAFLD). Contrary to the inflammatory signature exhibited here (Figure 4.13), the “NAFLD myeloid phenotype” downregulated inflammatory genes such as *S100A8/A9*, demonstrating a distinct signature. Adoptive transfer of NAFLD monocytes had the capacity to modulate injury responses in mice during AILI, indicating this signature is stable even on changes to their micromilieu (Krenkel *et al.*, 2019). Ikeda et al., 2018 reports Ly6C^{Hi} monocyte transcriptional pre-programming to an immunoregulatory phenotype in a mouse model of colitis, these monocytes promoted tissue repair in the colon. (Ikeda et al., 2018). These studies and the findings reported here indicate tissue injury can have a wide systemic impact and further studies are needed to interrogate the functional relevance of the systemic transcriptional switching observed here.

In summary scRNA-seq of hepatic and systemic monocytes and macrophages in an unbiased manner revealed heterogeneity in circulating monocytes and hepatic macrophages following AILI. It is clear that a

dichotomous M1 (pro-inflammatory) and M2 (anti-inflammatory) phenotype classification is not sufficient to describe these cells. Injury specific MDM clusters showing enrichment for distinct GO terms highlights that monocytes and macrophages exists in different activation states and can have different functions following injury. While scRNA-seq analysis of cells allows to study their transcriptome at a great resolution, uncovering crucial details which were previously masked, it is critical to remember that gene expression in a cell is a stochastic process (Raj and van Oudenaarden, 2008). This coupled with the dropout transcripts, and technical artefacts can generate a very noisy data (Ziegenhain *et al.*, 2017; Haimon *et al.*, 2018). Therefore, in order to make reliable and relevant assumptions the findings from scRNA-seq analysis needs to be phenotypically and functionally validated.

5 Validation of scRNA-seq results to identify injury specific monocyte and macrophage subsets during AILI

5.1 Introduction

Monocytes and macrophages have been suggested as therapeutic targets for the treatment of acute and chronic liver diseases for some time now. One of the main challenges in developing macrophage-based therapies is that these cells are very dynamic, exhibiting a spectrum of phenotypes and functions based on their environmental cues (Guillot and Tacke, 2019). Generally, KCs and Ly6C^{Lo} MDMs are regarded as the pro-regenerative subsets and Ly6C^{Hi} monocytes are thought to be the pro-injury subset but recent transcriptomic analysis has revealed heterogeneity in these cells. For example Ly6C^{Hi} monocytes show upregulation of both proinflammatory and pro- regenerative genes, both in the context of AILI (Zigmond *et al.*, 2014; Graubardt *et al.*, 2017) and models of chronic liver injury (Ramachandran *et al.*, 2012). This highlights that monocyte and macrophage response following liver injury is multifaceted and although this heterogeneity has been acknowledged, thus far the existing studies have not attempted to dissect this during AILI.

Phagocytosis represents one of the mechanisms by which macrophage promote liver repair. In the context of AILI, studies have highlighted the role of Ly6C^{Lo} MDMs to mediate efferocytosis (clearance of apoptotic cells) of neutrophils (Graubardt *et al.*, 2017). Both Ly6C^{Hi} monocytes and Ly6C^{Lo} MDMs show upregulation of apoptotic bridging genes such as *Gas6,* complement complex genes, *Mertk* and *Axl*, which are necessary molecules for recognizing “find me” signals on apoptotic cells in both mice and humans (Fujimori *et al.*, 2015; Healy *et al.*, 2016; Graubardt *et al.*, 2017; Grabiec *et al.*, 2018). MerTK is upregulated at a protein level on monocytes and macrophages in murine models of AILI and in humans suffering from ALF (Triantafyllou *et al.*, 2017). MerTK deficient mice exhibit persistent liver injury

and inflammation during AILI, higher number of neutrophils and lower number of pro-reparative macrophages (defined as F4/80+ MHCII^{Hi} Ly6C^{Lo}) (Triantafyllou *et al.*, 2017). This highlights a role for efferocytic receptor MerTK in mediating tissue repair in AILI, via suppression of neutrophil activation and clearance (Triantafyllou *et al.*, 2017).

In addition to possessing efferocytic receptors, efficient efferocytosis also depends on the ability to process and degrade internalized cargo, a process referred to as phagosome maturation (Kinchen and Ravichandran, 2008; Hochreiter-Hufford and Ravichandran, 2013). The *in vivo* molecular mechanisms involved in phagosome maturation has not been studied as extensively as its preceding stages (recognition, binding and engulfment of particulates) (Kinchen and Ravichandran, 2008). Nevertheless, key features of this process have been highlighted. Phagosomes go through a series of progressive acidification steps, acquire different proteins which leads to its fusion with lysosome structures, containing hydrolytic enzymes necessary for the breakdown of internalised cargo. Acidification of the phagosome necessary to activate the hydrolytic enzymes, therefore it is commonly used as readout for successful degradation of cargo (Kinchen and Ravichandran, 2008). The role for phagosome maturation in promoting tissue repair has been demonstrated by a number of studies. Animals lacking glycoprotein non-metastatic protein B (GPNMB), a protein needed for phagosome maturation, demonstrate extensive tissue injury and increased mortality following acute kidney injury (Li, Castano, Hudson, Nowlin, S. L. Lin, *et al.*, 2010). Similarly, GPNMB deficient mice in the context of acute liver injury have higher necrosis and an impaired ability to generate pro-reparative macrophages (Campana *et al.*, 2018). These studies highlight the therapeutic potential of phagocytosis in modulating the repair process.

In my previous chapter I used scRNA-seq in an unbiased manner to study the transcriptional changes in mononuclear phagocytes (MPs), with a focus on monocyte and macrophages during AILI. The findings highlighted the major

changes in the gene expression profile of monocytes and macrophages, during the repair phase (48hrs post-APAP). The MDMs showed striking heterogeneity, they partitioned into 5 distinct clusters, demonstrating distinct gene signatures, namely for: inflammation, immune cell recruitment, tissue repair, phagocytosis. This chapter consists of validation of the tissue MP clusters identified via scRNA-seq at protein level. Firstly, by identifying the hepatic MP cell lineages (cDC1, cC2, KC, MDM), following this, delineating the heterogeneity within the MDMs based on specific marker genes identified through scRNA-seq, to find key pro-regenerative subsets that has the potential to drive liver repair and regeneration following AILI.

5.1.1 Aims

- To use a combination of unique markers generated through scRNA-seq and known biology to identify the MP lineages populating the liver during AILI via flow cytometry
- To use flow cytometry and immunohistochemistry to delineate the MDM clusters and define them on their protein expression
- To investigate the dynamics of any pro-regenerative subsets identified and phenotypically characterize them
- To interrogate the origin and function of specific pro-regenerative subsets

5.2 Results

5.2.1 Validation of conventional dendritic cell clusters

Unsupervised clustering of hepatic and systemic MPs identified various marker genes which facilitated the annotation of clusters into 5 main cell types: cDC1, cDC2, MDM, KC and Monocyte (Chapter 4). For the identification of tissue MP cell types, I isolated non-parenchymal cells (NPCs) from the livers of uninjured and 48hrs post-APAP (300mg/kg) C57BL/6 wild type mice and analyzed them via flow cytometry (Figure 5.1). As the pronase-based tissue dissociation protocol (protocol 2) cleaved many cell surface antigens, protocol 1 (Methods) was used for the validation experiments. The primary gating strategy remained the same as before, where single live cells (DAPI+) were analyzed for their expression of various surface markers. Leucocytes were identified based on CD45 expression, to define the MPs further, rest of the leucocytes were “dump gated” based on the expression of conventional lineage markers (Figure 5.1). Identification of MP lineages and the MDM clusters at a protein level relied on membranal antigens. Different antibody fluorophore combinations were tried alongside isotype FMOs, especially for the novel markers identified and antibodies were titrated to determine the optimal concentration for flow cytometric detection.

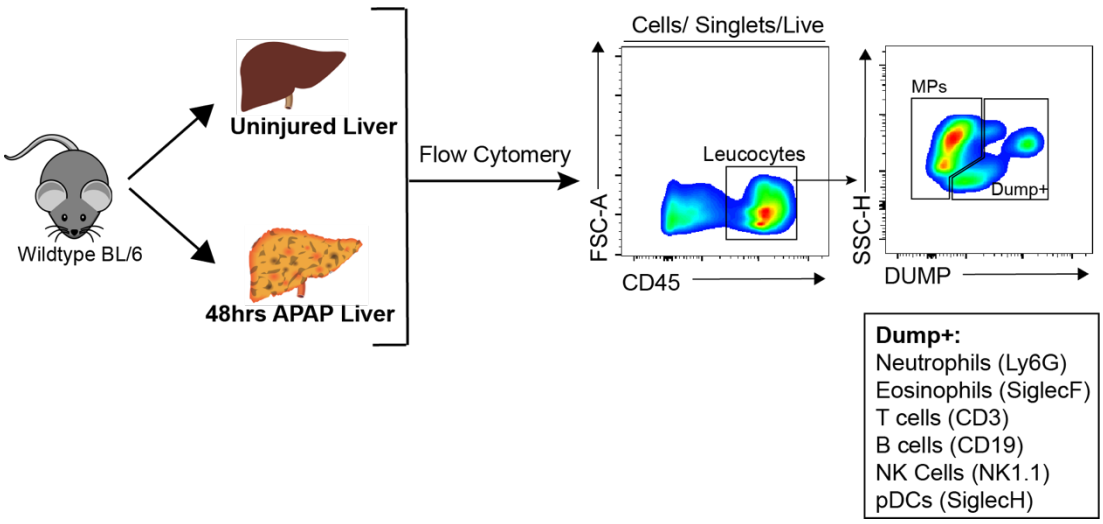

Figure 5.1 Methodology and gating strategy for flow cytometric validation of tissue MP clusters from scRNA-seq analysis.

Within the MPs, cluster 9 (cDC1) (Figure 5.2a) selectively expressed *XCR1* and had high expression of *CD24* and *ITGAX* (Figure 5.2b, c). Based on this XCR1+ CD24+ cells were identified as cDC1 via flow cytometry (Figure 5.2c), these cells also had higher levels of CD11c (*ITGAX*) expression when compared to the other MP lineages (Figure5.2d), confirming their identity as cDC1. Enumeration of cDC1 cells during homeostasis and at 48hrs post-APAP showed they expanded significantly following injury (Figure5.2e). Validating cDC2 (cluster 10) proved to be more challenging (Figure 5.3a), as they lacked unique cell surface markers. *CD209A* was one top marker genes identified by differential expression analysis, t-SNE visualization indicated *CD209A* to be selectively upregulated in cluster 10 (Figure 5.3b). However, the violin plots suggested the expression was low (Figure 5.3c). This translated across to protein expression, I failed to detect any CD209a+ cells in the liver at 48hrs-post APAP when compared to an isotype control antibody (Figure 5.3d). Cluster 10 (cDC) had higher transcript expression of *ITGAX* (CD11c) and *H2-AA* (MHCII) when compared to other MP lineages but as macrophages also upregulated MHCII and CD11c during inflammation (Yu *et al.*, 2016), I feared this gating strategy will include macrophages. Therefore, I used CD11c and F4/80 (a pan-macrophage marker) and identified $CD11c^{Hi}$ and $F4/80^{Lo}$ cells as

cDC2s (Figure 5.3e). Quantification of the number of cDC2 cells indicated an expansion of these cells post-APAP, though this was not significant (Figure 5.3f).

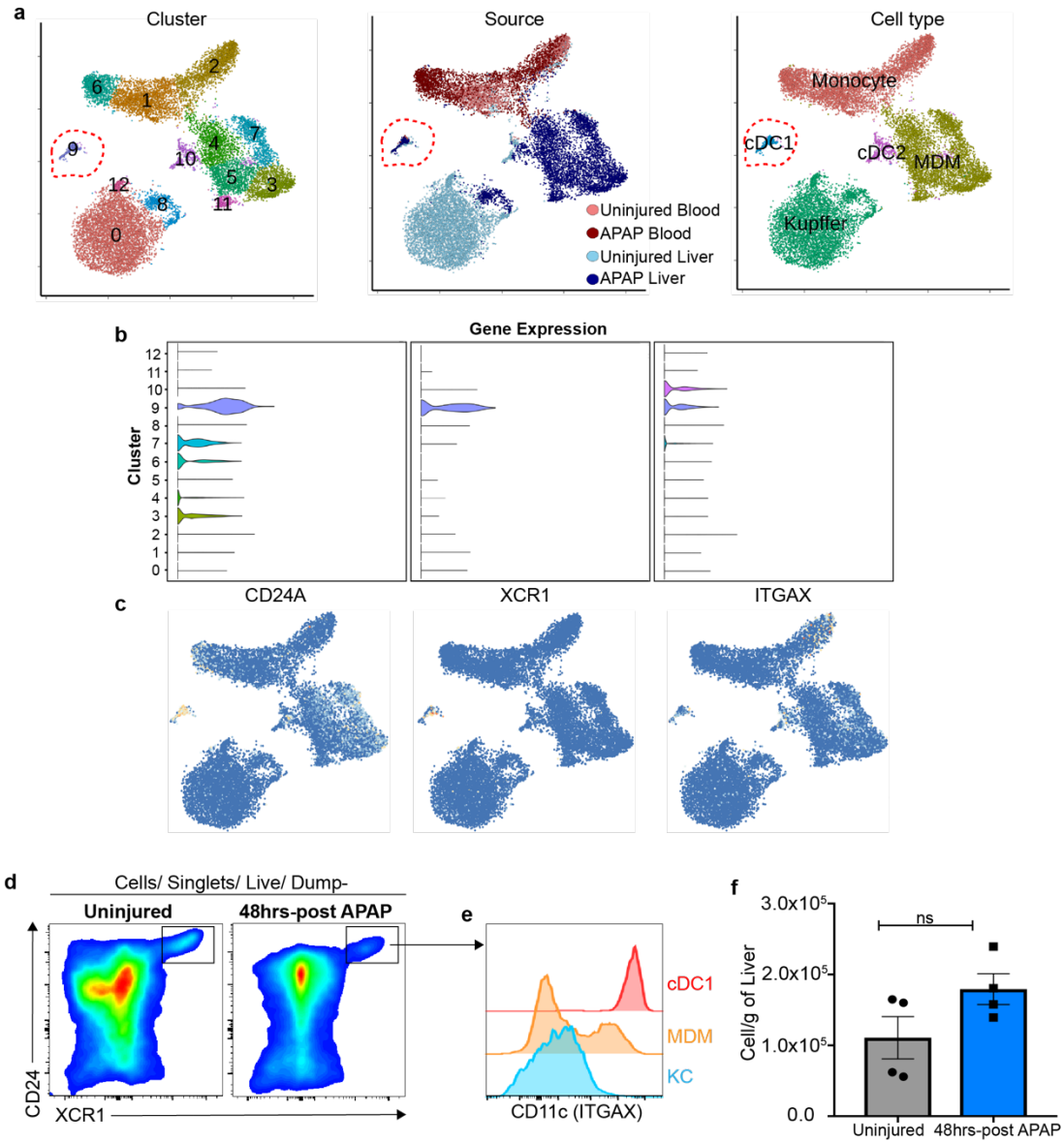

Figure 5.2 Identification of cDC1 cells in uninjured and APAP livers. (**a**) t-SNE visualization of mononuclear phagocyte (MP) by cluster, source and cell type, red dotted line indicates the cell type being validated. Violin plots (**b**) and t-SNE visualization (**c**) of top marker genes for cluster 9; cDC1. (**d**) Identification of cDC1 cells via flow cytometry. (**e**) Protein expression of CD11c on different MP lineages via flow cytometry. (**f**) Quantification of the changes in cDC1 cells during steady state (uninjured) and at 48hrs post-APAP. Data acquired from two independent experiments, n=4 per group. Mann-Whitney nonparametric paired t-Test. Data shown as Mean±S.E.M, * P<0.05.

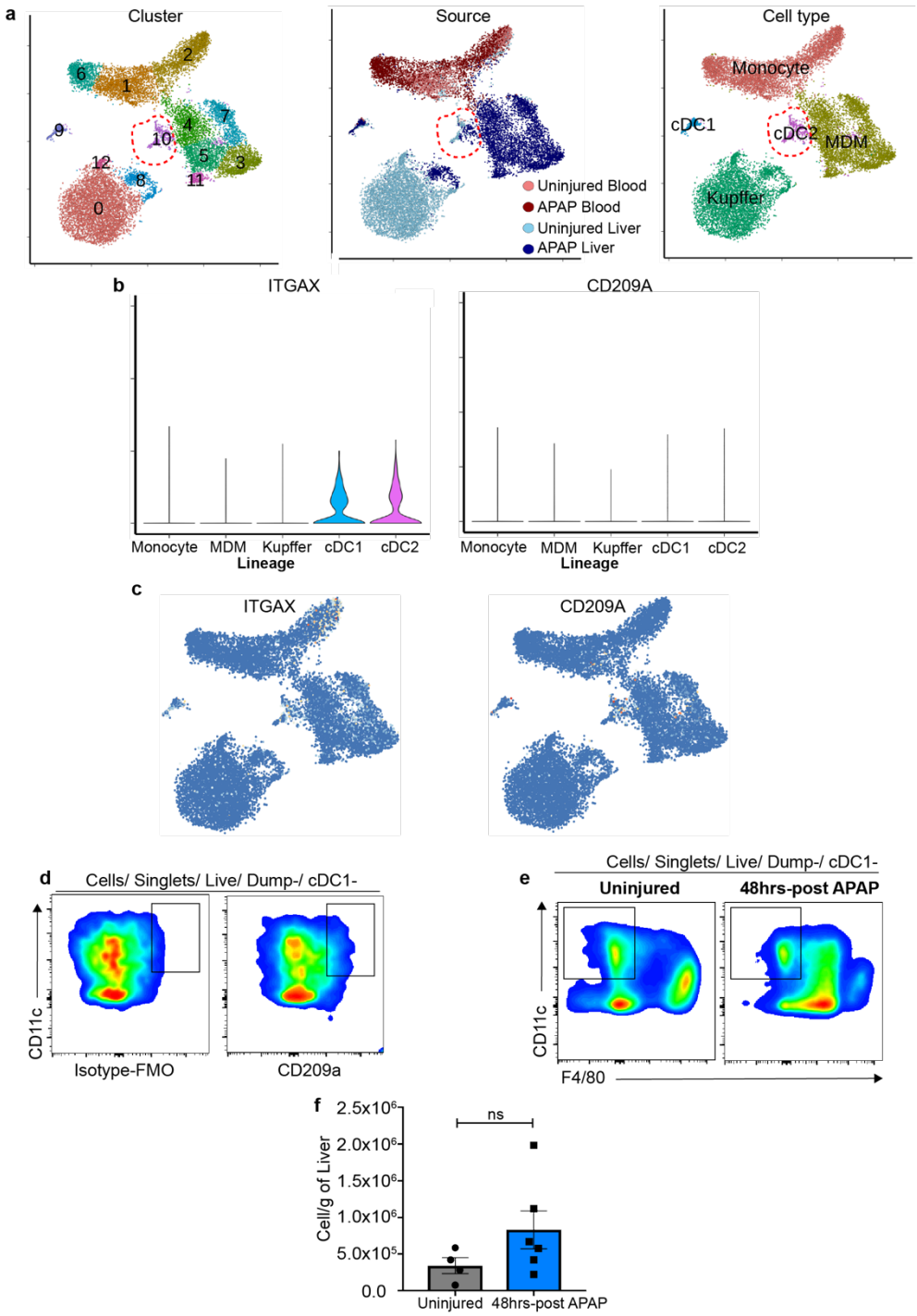

Figure 5.3 Identification of cDC2 cells in uninjured and APAP livers. (**a**) t-SNE visualization of mononuclear phagocyte (MP) by cluster, source and cell type, red dotted line indicates the cell type being validated. Violin plots (**b**) and t-SNE visualization (**c**) of top marker genes for cluster 10; cDC2. (**d**) Identification of cDC2 cells via flow cytometry on CD209a and CD11c expression (**e**) Identification of cDC2 cells via flow cytometry on F/480 and CD11c expression (**f**) Quantification of the changes in cDC2 cells during steady state (uninjured; grey) and at 48hrs post-APAP (blue). Data acquired from two independent experiments n=4-6 per group. Mann-Whitney nonparametric paired t-Test. Data shown as Mean±S.E.M.

5.2.2 Validation of kupffer cell clusters

Once cDC1 and cDC2 cells were identified and removed from subsequent analysis, I focused on delineating the MDM and KC compartment (Figure 5.4a). Macrophage associated genes such as *ADGRE1* (F4/80), *ITGAM* (CD11b) were expressed at high levels in MDM and Kupffer clusters (Figure 5.4b, c), therefore macrophages were isolated via flow cytometry based on their expression of F4/80 and CD11b (Figure 5.4d). In concordance with existing literature transcriptomic analysis revealed that KCs (Kupffer) had a very unique gene signature compared to MDMs, monocytes and cDCs (Chapter 4). As before, separation of KCs from MDMs relied on TIMD4 expression (Figure 5.4b, d). Quantification of absolute changes in KC ($TIM4^{+}/CD11b^{Lo}$) and MDM ($TIM4^{-}/CD11b^{Int/Hi}$) numbers in uninjured and 48hrs post-APAP supported my previous flow cytometry findings (Chapter 3) where, KC numbers declined and MDMs increased significantly post-APAP (Figure 5.4e, f).

The functional role of KCs during the initial phase of AILI has been characterized, they have been shown to release various chemokines and cytokines, which results in the recruitment of leucocytes, such as monocytes into the liver (You *et al.*, 2013; Ju and Tacke, 2016). However, their precise role during liver repair remains elusive, partly because flow cytometric analysis suggested their numbers declined during the repair phase (24hrs-48hrs post APAP), hence previous studies have focused more on the role of infiltrating monocytes and MDMs during the repair phase of AILI (You *et al.*, 2013; Zigmond *et al.*, 2014; Mossanen *et al.*, 2016; Graubardt *et al.*, 2017). One of the reasons for using a droplet-based scRNA-seq technique here was to increase the chances of gaining transcriptomic information on KCs during the repair phase of AILI (48hrs post-APAP). Albeit low in numbers, scRNA-seq analysis contained KCs from 48hrs post-APAP livers and these cells (cluster 8) clustered separately from uninjured KCs (cluster 0; Figure 5.4a). Differential gene expression analysis failed to detect any unique gene expression profiles

between these clusters, but t-SNE visualization of top marker genes for cluster 0 and 8 indicated that certain genes in cluster 8 were downregulated (*C3*, *TIMD4*), whereas genes such as *MARCO* was upregulated (Appendix6). Based on this observation I wanted to see if APAP induction resulted in any cell surface phenotypic changes during the peak regenerative phase of AILI (48hr-72hrs post-APAP, Figure 5.5). Therefore, expression of CD36, MerTK, and CD9, molecules which are known to mediate phagocytosis on macrophages (Huang, Febbraio and Silverstein, 2011; Healy *et al.*, 2016; Woo *et al.*, 2016), along with CD24, and antigen presenting molecules MHCII and CD11c on KCs were analyzed (Figure 5.5). APAP induced increased expression of both CD36 and CD24 following APAP compared to basal levels and as previously observed (chapter 3) MHCII expression was downregulated on KCs from APAP livers, whereas there were no major changes observed with CD11c expression (Figure 5.5). This suggested that at 72hr-post APAP there are noticeable phenotypic changes in KCs, the functional relevance of these changes warrants further experiments.

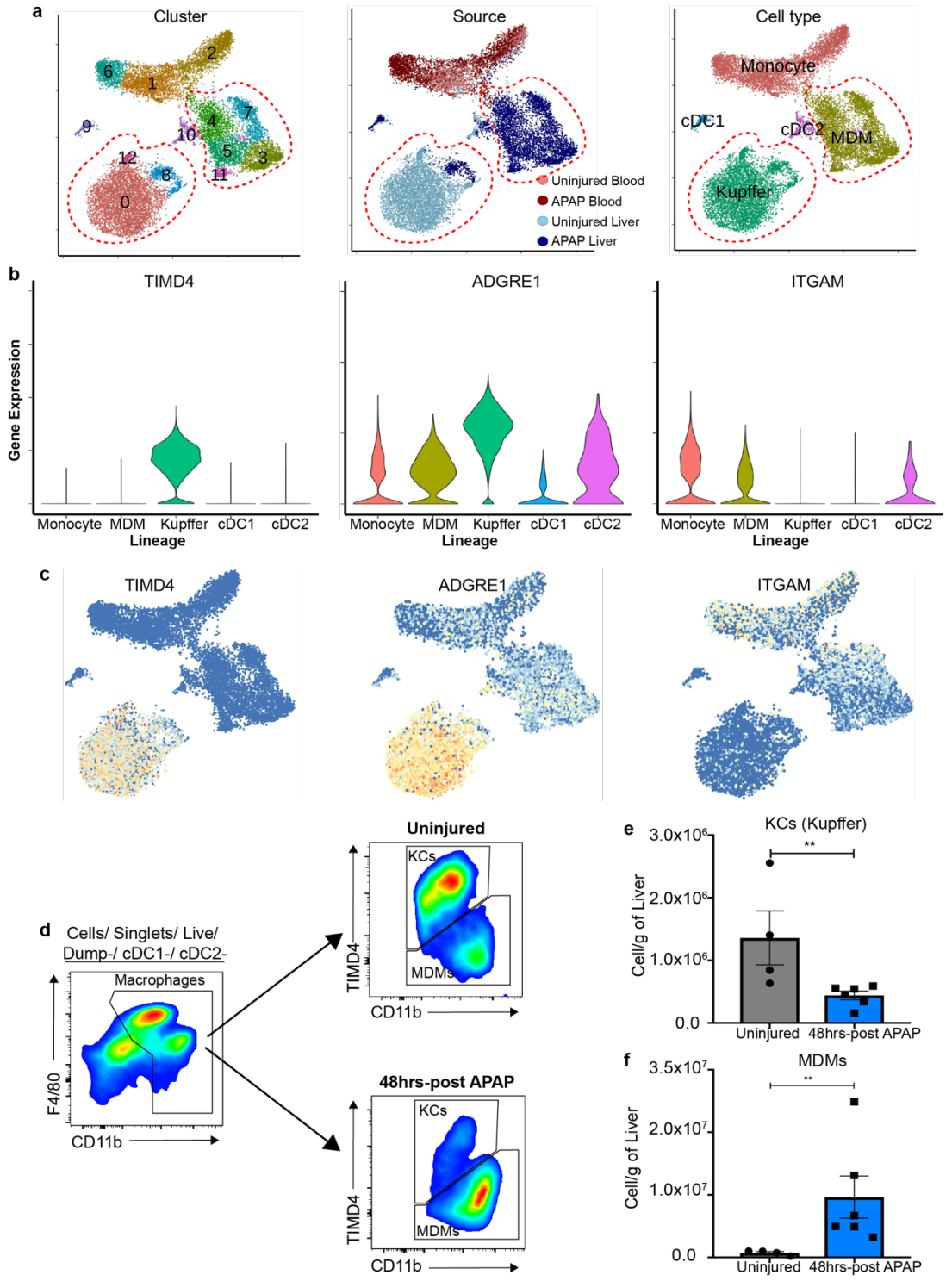
a
Cluster
Source
Cell type
Uninjured Blood
APAP Blood
Uninjured Liver
APAP Liver
Monocyte
cDC1
cDC2
MDM
Kupffer
b
TIMD4
ADGRE1
ITGAM
Gene Expression
Monocyte MDM Kupffer cDC1 cDC2
Lineage
c
d
Cells/ Singlets/ Live/
Dump-/ cDC1-/ cDC2-
Macrophages
F4/80
CD11b
Uninjured
48hrs-post APAP
KCs
MDMs
TIMD4
e
KCs (Kupffer)
Cell/g of Liver
Uninjured
48hrs-post APAP
f
MDMs

Figure 5.4 Identification of KCs and MDMs. (**a**) t-SNE visualization of mononuclear phagocyte (MP) by cluster, source and cell type, red dotted line indicates the cell types being validated. Violin plots (**b**) and t-SNE visualization (**c**) of top marker genes for KCs and MDMs. Macrophages were identified first, following this KCs and MDMs were defined (**d**). Quantification of KCs (**e**) and MDMs (**f**) in the liver at steady state (uninjured; grey) and at 48hrs post-APAP (blue). Data acquired from two independent experiments n=4-6 per group. Mann-Whitney nonparametric paired t-Test. Data shown as Mean±S.E.M, ***P*<0.01.

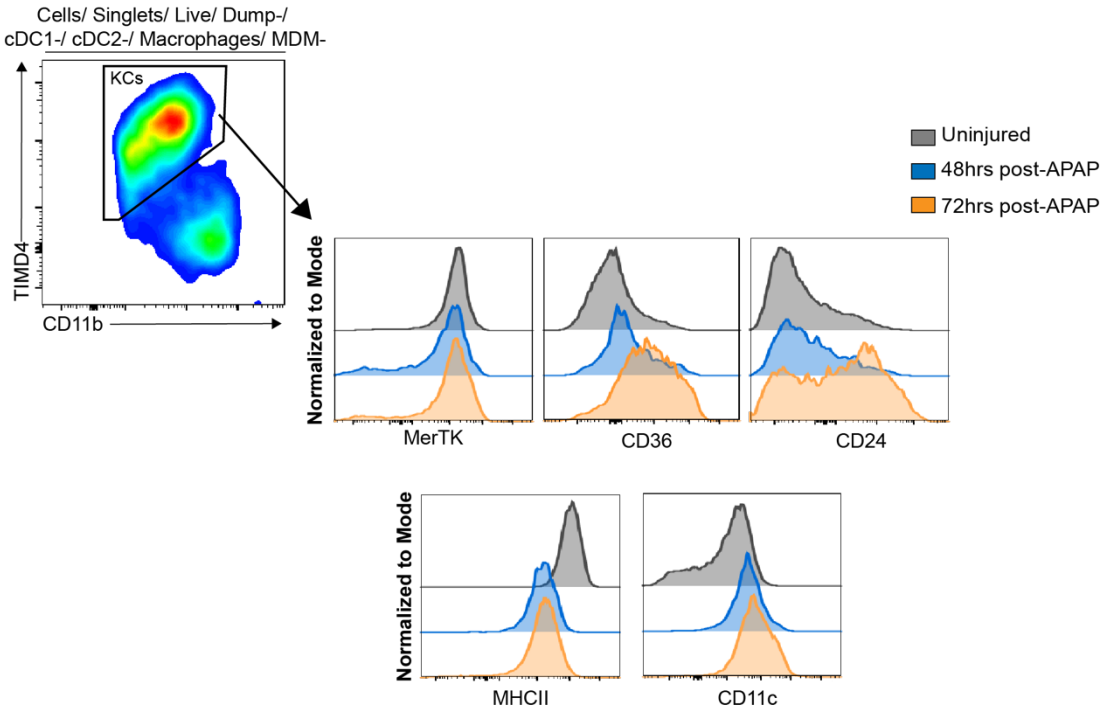

Figure 5.5 Phenotypic characterization of KCs. Steady state (grey), 48hrs (blue) and 72hrs (orange) post-APAP.

5.2.3 Identification of phenotypic heterogeneity in the Ly6C^{Hi} monocytes during AILI

The MDM lineage was composed of 5 clusters, cluster 11 as discussed in chapter 4 was identified to be cycling cells. Expression of *CCR2, LY6C2* and *CX3CR1* across the MDMs clusters indicated that cluster 4 and 7 represented the pro-inflammatory Ly6C^{Hi} CCR2^{Hi} CX3CR1^{Lo} monocytes whereas, 5 and 3 represented pro-reparative Ly6C^{Lo} CCR2^{Lo} CX3CR1^{Hi} MDMs, described by Zigmond et al., (2014). Here, relying on my previous gating strategy (Chapter 3) I isolated these cells via F4/80 and CD11b expression and negative expression of TIMD4 (Figure 5.4d). Using Ly6C in combination with CCR2 and CX3CR1 failed to effectively separate monocytes from MDMs but Ly6C against MHCII gave a clear distinction between Ly6C^{Hi} monocytes (Ly6C^{Hi} MHCII^{Lo}) and Ly6C^{Lo} MDMs and this gating strategy was followed for the subsequent experiments (Figure 5.6c). Quantitation of Ly6C^{Hi} monocytes and Ly6C^{Lo} MDMs showed that both populations increased significantly and Ly6C^{Lo} MDMs represented the principal subset at 48hrs-post APAP, confirming my previous findings in chapter 3 (Figure 5.6d, e).

Unsupervised clustering demonstrated heterogeneity within the hepatic Ly6C^{Hi} monocytes (cluster 4 and 7). Overall, cluster 4 and 7 shared a proinflammatory gene profile, expressing genes such as *CCR1, CCR2, CCL2* involved in recruitment and activation of inflammatory cells (Saiman and Friedman, 2012). However, cluster 7 also exhibited a unique granulocytic (*LCN2, RENTLG, VCAN, CXCR2*) and immune clearance (*CLEC4D, CLEC4E*) gene signature. To delineate this heterogeneity at a protein level I had to rely on markers genes in cluster 7, which encoded cell surface proteins and based on availability of antibodies for flow cytometry, CXCR2 was chosen. Expression of CXC chemokine receptor 2 (CXCR2) on hepatic Ly6C^{Hi} monocytes was analyzed, although there were subtle changes in CXCR2 expression compared to an isotype control (Figure 5.7c), it was not sufficient to distinctly subset the Ly6C^{Hi} monocytes (Figure 5.7b). Another gene that was selectively expressed in

cluster 7 was S*ELL* (CD62L) (Figure 5.7a) and analysis of CD62L expression on Ly6C^{Hi} monocytes showed a significant increase of CD62L+ Ly6C^{Hi} monocytes in the liver at 48hrs post-APAP (figure 5.d, e) and around 20% of the Ly6C^{Hi} monocytes expressed CD62L (Figure 5.7f).

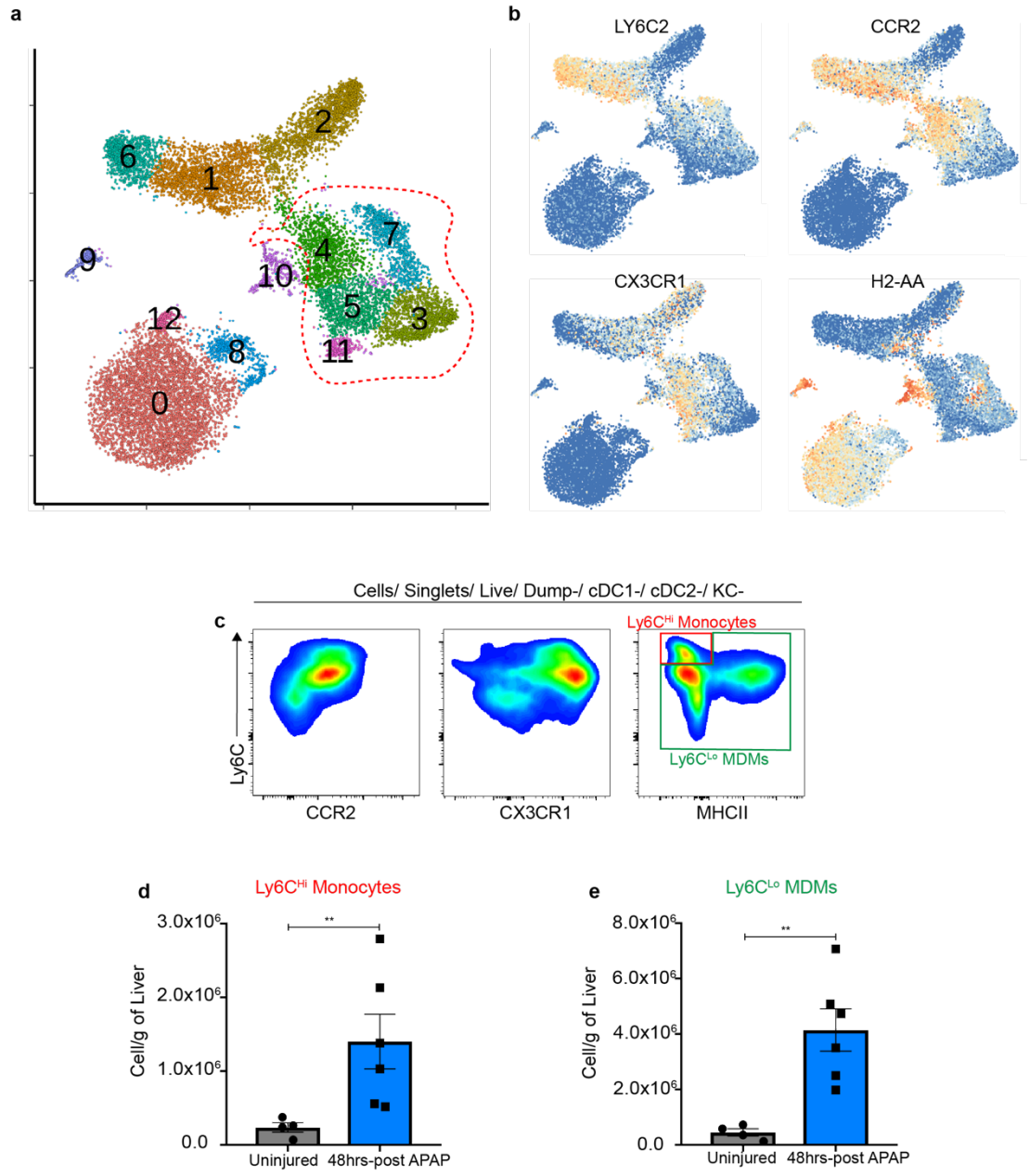

Figure 5.6 Identification of Ly6C^{Hi} monocytes and Ly6C^{Lo} MDMs in uninjured and APAP livers. (**a**) t-SNE visualization of mononuclear phagocyte (MP) by cluster, source and cell type, red dotted line indicates the clusters being validated. (**b**) t-SNE visualization of conventional marker genes for MDMs. (**c**) Defining the MDMs into Ly6C^{Hi} monocytes and Ly6C^{Lo} MDMs, based on Ly6C and MHCII expression. Quantification of Ly6C^{Hi} monocytes (Ly6C^{Hi} MHCII^{Lo}) (**d**) and Ly6C^{Lo} MDMs (Ly6C^{Lo} MHCII$^{Lo/Hi}$) (**e**) in the liver at steady state (uninjured; grey) and at 48hrs post-APAP (blue). Data acquired from two independent experiments n=4-6 per group. Mann-Whitney nonparametric paired t-Test. Data shown as Mean±S.E.M. $^{**}P<0.01$

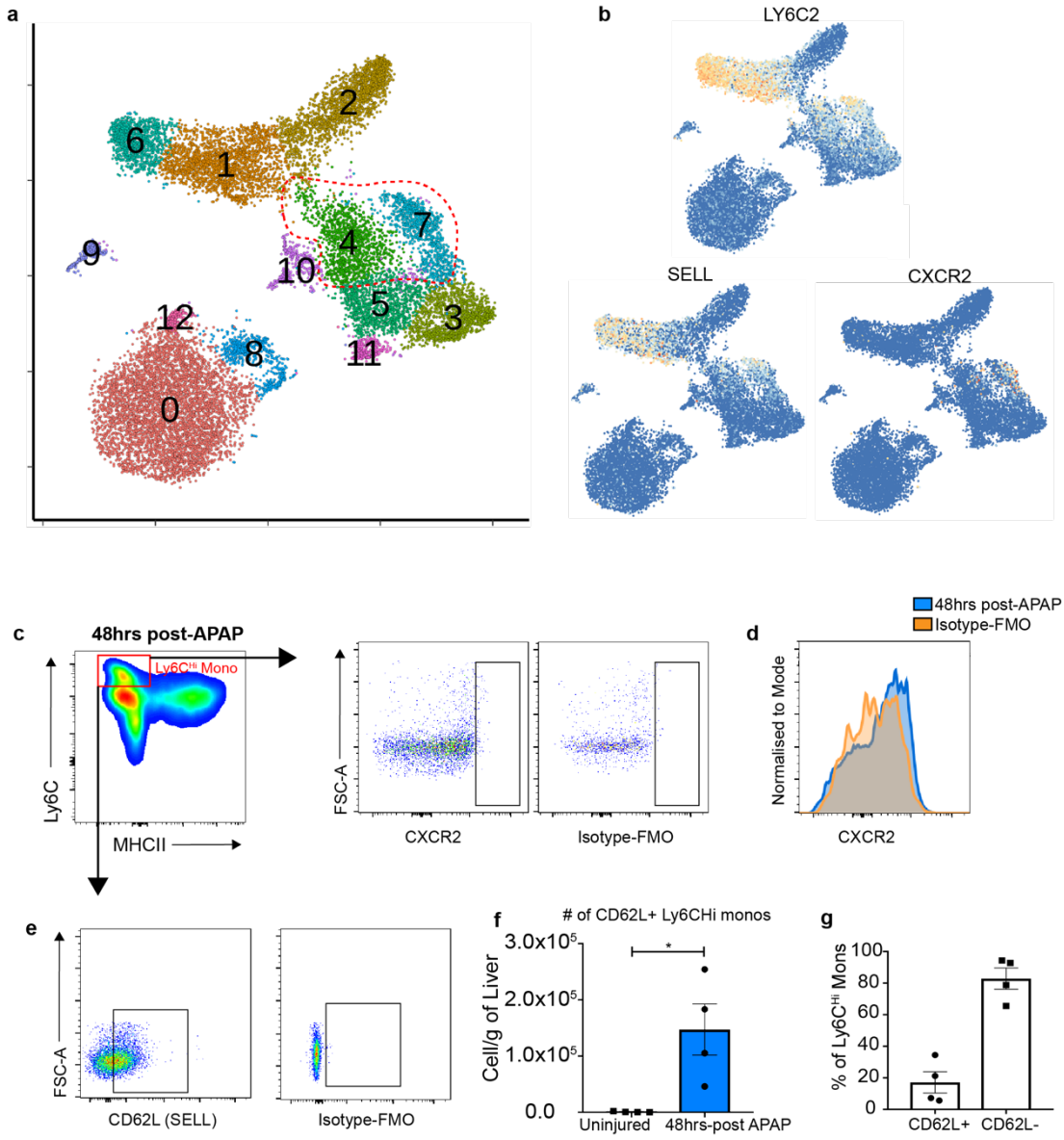

Figure 5.7 Validating heterogeneity in the Ly6C^{Hi} monocytes in uninjured and APAP livers. (**a**) t-SNE visualization of unsupervised clustering of mononuclear phagocytes (MPs), red dotted line indicates the clusters being validated. (**b**) t-SNE visualization of top marker genes for cluster 7. (**c**) Defining the Ly6C^{Hi} monocytes by CXCR2 expression. (**d**) Expression of CXCR2 on Ly6C^{Hi} monocytes at 48hrs post-APAP (blue), in comparison to an isotype FMO (orange). (**e**) Defining the Ly6C^{Hi} monocytes based on CD62L expression. (**f**) Quantification of CD62L+ Ly6C^{Hi} monocytes in the liver at steady state (uninjured; grey) and at 48hrs post-APAP (blue). (**g**) Proportion of CD62L+ and CD62L- cells in the Ly6C^{Hi} monocyte compartment. Data acquired from single experiment, n=4 per group. Mann-Whitney nonparametric paired t-Test. Data shown as Mean±S.E.M, * $P \leq 0.05$.

5.2.4 Identification of phenotypic heterogeneity within the Ly6CLo MDMs during AILI

Expression of conventional marker genes (*LY6C2, CX3CR1, CCR2*) suggested clusters 3 and 5 represented Ly6C^{Lo} MDMs (Figure 5.6a, b). My previous work characterizing Ly6C^{Lo} MDMs using MHCII and CD11c suggested heterogeneity within these cells, during the repair phase of AILI (Chapter 3). Here, they partitioned into two clusters, cluster 3 was of particular interest, as these cells did not fit the conventional criteria currently used to define hepatic MDMs. Cluster 3 cells downregulated genes such as *LY6C2* and *CCR2* but also had low expression of *CX3CR1*, a marker previously used to define Ly6C^{Lo} MDMs (Figure 5.6a, b). In order to delineate this heterogeneity, I relied on marker genes for cluster 3, as cluster 5 lacked uniquely expressed cell surface genes, which could be verified on protein level via flow cytometry. *CD63* expression, was primarily in cluster 3 cells, therefore this was used to delineate Ly6C^{Lo} MDMs (Figure 5.8a, b). CD63 belongs to the tetraspanin family, its functions are mainly associated with endosomal pathways and it can be expressed on exosomes, plasma membranes and endosomes (Pols and Klumperman, 2009). Though scRNA-seq analysis did not identify *H2-AA* (MHCII) and *ITGAX* (CD11c) as discriminatory markers for MDMs, quite possibly due to their expression in DCs, I observed that a subset of Ly6C^{Lo} MDMs cells also expressed *H2-AA* (MHCII). Therefore, I used MHCII in combination with CD63 to investigate heterogeneity within the Ly6C^{Lo} MDMs (Figure 5.8).

In an uninjured liver the Ly6C^{Lo} MDMs separated into two main subsets: MHCII+ and MHCII-, with MHCII- MDMs being the dominant subset (Figure 5.8d). In line with the scRNA-seq data, APAP induction resulted in an expansion of CD63+ Ly6C^{Lo} MDMs confirmed by an isotype-FMO (Figure 5.8c). Furthermore, at 48hrs post-APAP the Ly6C^{Lo} MDMs could be separated into four distinct subsets, based on CD63 and MHCII expression (Figure 5.8d). It is important to highlight that there is an overlap in marker expression between macrophages and cDC2 cells, currently there are no unique surface markers capable of accurately separate one from the other at protein level. The chances that DCs could be contributing to the CD63+ MHCII+ and CD63- MHCII+ subsets here is minimal, as cDCs were identified and gated out prior to selecting cells expressing F4/80 and CD11b. I discovered CD63- MHCII- MDMs (green) and CD63+ MHCII- MDMs (orange) expanded significantly at 48hrs post-APAP (three independent experiments, Figure 5.8d). ScRNA-seq analysis revealed a proportion of cells in cluster 3 expressed *IL7R*, and cluster 3 also showed ontology enrichment for IL-7 signaling. Therefore, I was interested in seeing if this expression translated across to protein levels, and indeed CD63+ macrophages expressed higher levels of IL7R (Figure 5.8e).

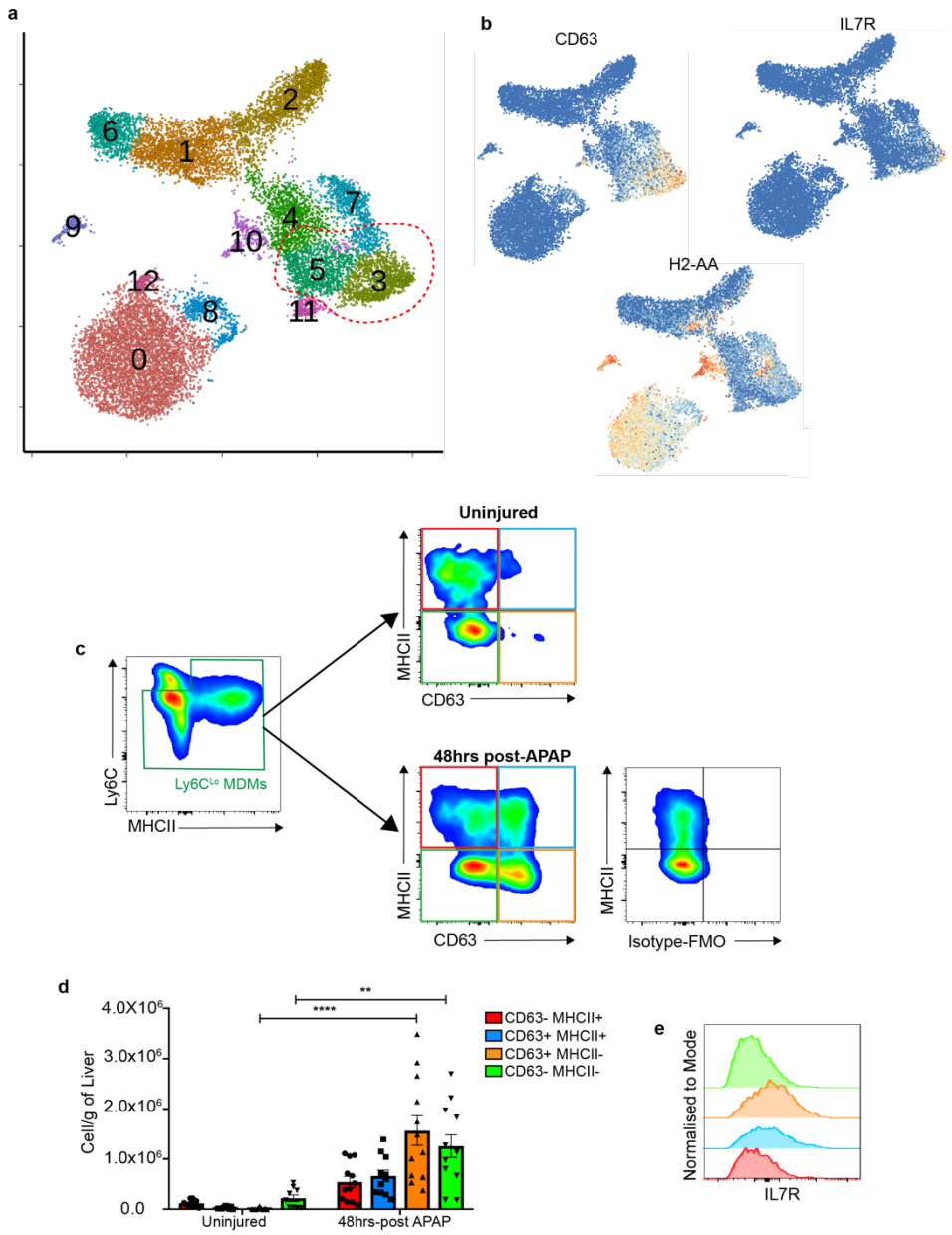

Figure 5.8 Identification of two distinct subsets of Ly6C^{Lo} MDMs populating the liver during the repair phase of AILI. (**a**) t-SNE visualization of MP clusters, red dotted line represents the clusters being validated. (**b**) t-SNE visualization of expression of two of the top marker genes for cluster 3 (*CD63, IL7R*) and *MHCII*. (**c**) Delineating Ly6C^{Lo} MDMs based on CD63 and MHCII expression on flow cytometry identified four distinct subsets of Ly6C^{Lo} MDMs at 48hrs post-APAP. (**d**) Quantification of the four subsets of Ly6C^{Lo} MDMs in the liver at steady state (uninjured) and at 48hrs post-APAP. (**e**) Upregulation of IL7R on CD63+ MDMs (orange and blue) at 48hrs post-APAP. Data acquired from three independent experiments, n= 9-12 per group. Ordinary Two-way ANOVA, using Tukey's multiple comparisons test. Data shown as Mean±S.E.M, $^{**}P \leq 0.01$, $^{****}P \leq 0.0001$.

5.2.5 Validation of Ly6C^{Lo} MDM heterogeneity using macrophage reporter mice

Following identification of two specific subsets of Ly6C^{Lo} that populated the liver during the repair phase in wild type mice (W/T). I wanted to confirm the existence and the identity of these subsets in a macrophage reporter mouse. To do this, I characterised the Ly6C^{Lo} MDMs in a MacGreen^{GFP} mice (Figure 5.9a), in these mice green florescent protein (GFP) expression is driven by the colony stimulating factor 1 receptor (CSFR1) promoter, which is expressed selectively in macrophage and trophoblast lineages (Sasmono *et al.*, 2003). NPC isolation and flow cytometry gating strategy were kept the same as before. Analysis of Ly6C^{Lo} MDM compartment in the MacGreen^{GFP} mice also showed significant expansion of CD63+ MHCII- (orange) and increase in CD63- MHCII- (green) MDMs at 48hrs-post APAP, though the changes were not deemed significant, due to the low-test subjects (Figure 5.9b, c). Importantly, all four subsets of MDMs were positive for GFP, confirming a MP lineage identity for these cells (Figure 5.9d, e). Furthermore, immunofluorescence staining also supported the presence of CD63+ macrophages in the liver at 48hrs post-APAP (white arrows; Figure 5.10b). These cells were localized to the regenerative niches (indicated by EdU+ proliferating cells) of the liver at 48hrs-post APAP (Figure 5.10a). There were also CD63+ cells which were negative for GFP, while the CD63+ GFP+ cells displayed a circular morphology, the CD63+ GFP- cells were elongated and spindle-shaped (Figure 5.10b) ScRNA-seq data of mesenchymal cells at 48hrs post-APAP from the Henderson lab demonstrated CD63 expression in mesenchymal cells therefore based on morphology, CD63+ GFP- cells are likely to be mesenchymal cells. Additionally, IL7R staining in MacGreen^{GFP} mice confirmed the presence of IL7R+ macrophages (IL7R+ MacGreen^{GFP}+) in the liver at 48hrs post-APAP (Figure 5.11a, b). Due to antibody availability and technical difficulties I was not able to confirm the expression of CD63 in IL7R+ macrophages. Nevertheless, IL7R+ macrophages were also localized

to the repairing areas of the liver, and similar to the CD63+ macrophages, they also had a circular shape (Figure 5.11a, b).

Zigmond et al., (2014) relied on GFP expression driven by fractalkine receptor C-X3-C motif chemokine receptor 1 (CX3CR1), to define the three subsets involved in AILI: KCs (CX3CR1^{Lo}), Ly6C^{Hi} monocytes (Ly6C^{Hi} CD11b^{Hi} MHCII- CX3CR1+) and Ly6C^{Lo} MDMs (CX3CR1^{Hi}, Ly6C^{Lo}). Here, the scRNA-seq data indicated that *CX3CR1* expression is downregulated in cluster 3, this might explain why heterogeneity in the Ly6C^{Lo} MDMs went undetected in the past (Figure 5.13a). Following the same methodology and gating strategy used for MacGreen^{GFP} mice, I used CX3CR1$^{GFP/+}$ mice to confirm the presence of two main Ly6C^{Lo} MDMs at 48hrs-post APAP AILI via flow cytometry and immunofluorescence (Figure 5.12a). As seen with W/T mice and MacGreen^{GFP} mice the MHCII- CD63+ (orange) and MHCII- CD63- (green) MDMs increased in numbers following APAP, when compared to their MDM counterparts and uninjured livers (Figure 5.12b). Future experiments with higher number of test subjects is needed to confirm any significant difference. In keeping with scRNA-seq data (Figure 5.13a), assessment of GFP expression at protein level showed that a subset of CD63+ MDMs (around 40%) did not express CX3CR1 (Figure 5.13b, c). This was supported by immunofluorescence, where both, dual positive CD63+ CX3CR1+ cells (white arrows) and single positive CD63+ cells (blue arrows) were seen localized to the repairing centrilobular areas of the liver (Figure 5.14). While I cannot be certain CD63+ GFP- here are macrophages, based on the circular morphology they are most likely to be the CD63+ macrophages seen in MacGreen^{GFP} mice.

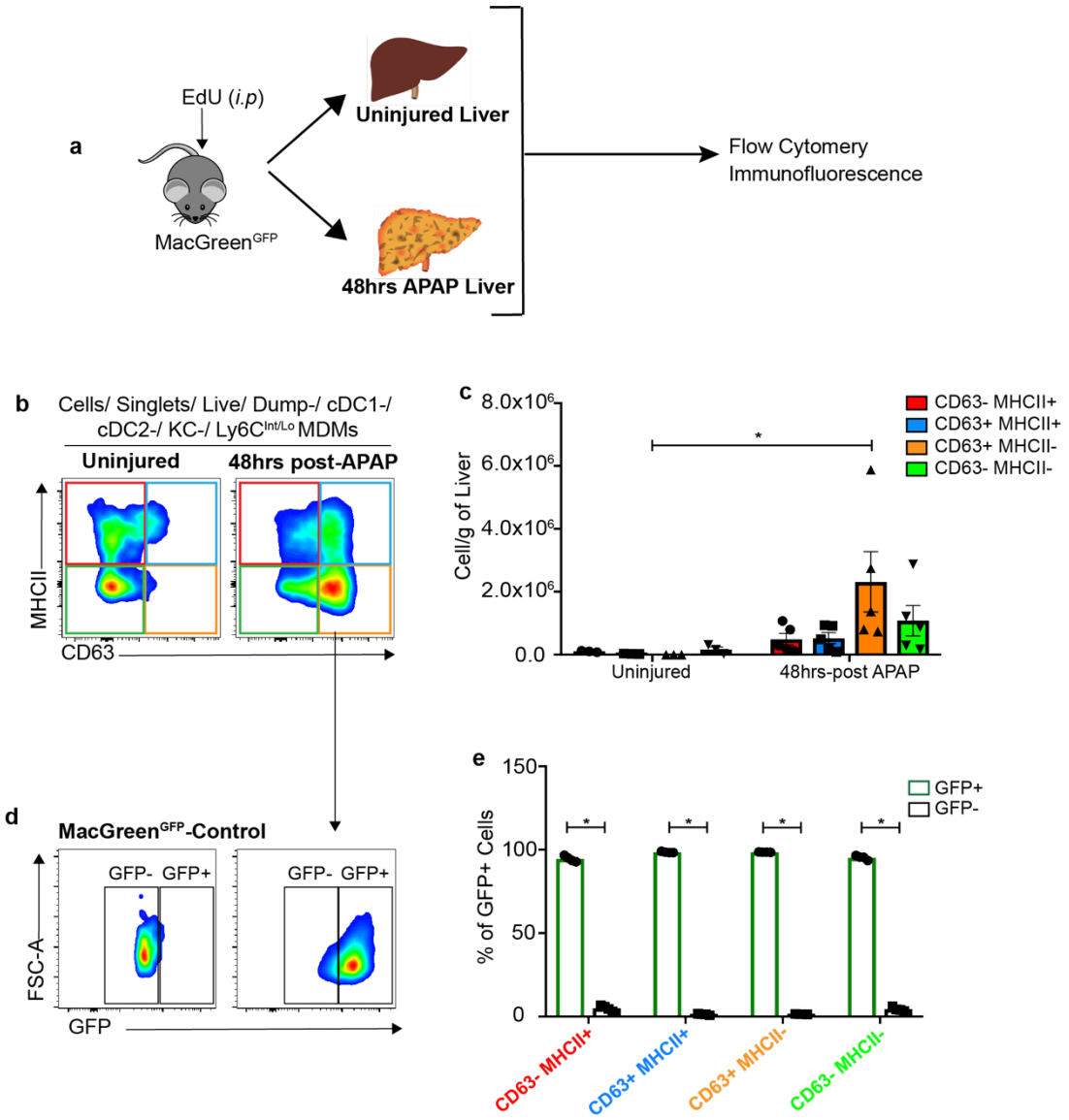

Figure 5.9 Validation of MDM clusters in MacGreen^{GFP} mice. (**a**) APAP was administered to MacGreen^{GFP} mice, EdU was injected to asses proliferation in the mice three hours prior to cull, livers were collected for flow cytometry and immunofluorescence analysis, uninjured MacGreen^{GFP} mice were used at controls. (**b**) Delineation of Ly6C^{Lo} MDMs on CD63 and MHCII expression. (**c**) Quantification of double negative (green), double positive (blue), CD63+ MHCII- (orange) and CD63- MHCII+ (red) MDMs at 48hrs post-APAP and at steady state (uninjured). (**d**) Representative plot of GFP expression in CD63+ MHCII- MDMs. (**e**) Proportion of GFP+ and GFP- cells in each of the four subsets of Ly6C^{Lo} MDMs. Data acquired from two independent experiments, n=3-5 per group. Mann-Whitney nonparametric paired t-Test. Data shown as Mean±S.E.M.
* $P \leq 0.05$

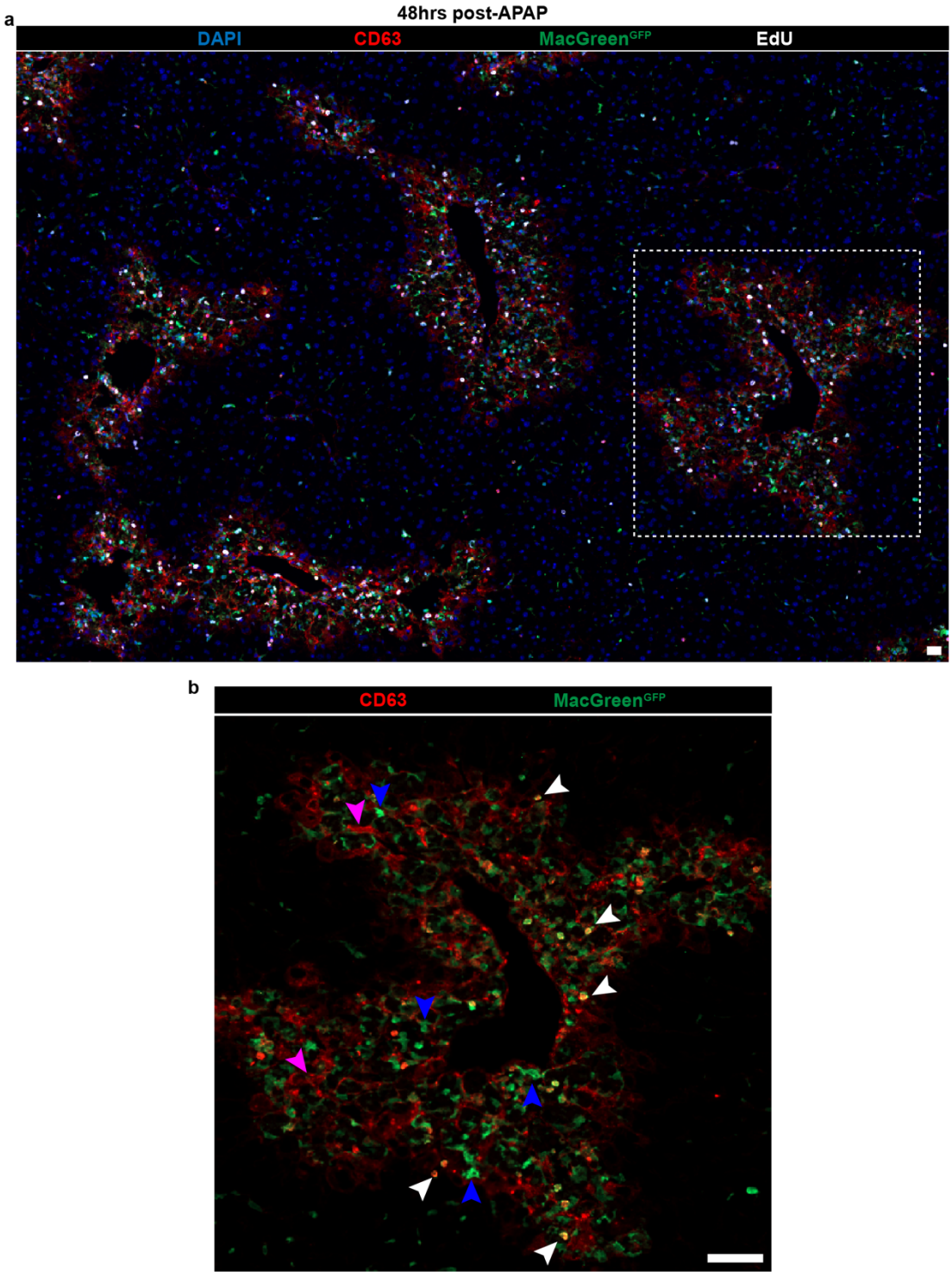

Figure 5.10 Localization of CD63+ MDMs to repairing areas of the liver at 48hrs post-APAP (**a**) Representative immunofluorescence images of MacGreen^{GFP} mice at 48hrs post-APAP, cells were stained for CD63 (red), GFP (macrophages), EdU (white) and DAPI (blue) was used for nuclear detection. (**b**) Magnified image of regenerative niche (white dotted square) where CD63+ GFP+ are seen (white arrows), along with CD63 single positive cells (pink arrows) and GFP single positive cells (blue arrows) (Scale bar=50μm).

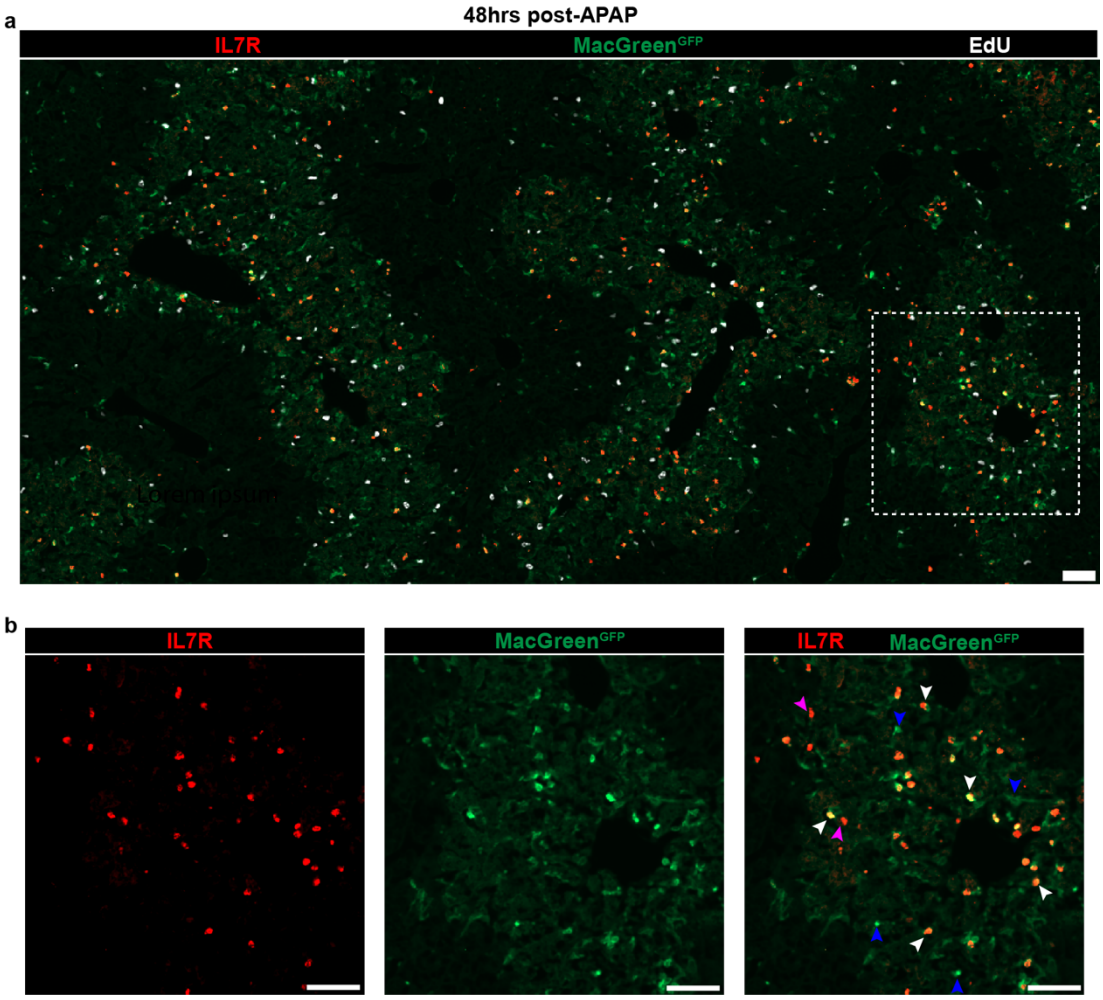

Figure 5.11 Localization of IL7R+ MDMs to repairing areas of the liver at 48hrs post-APAP (a) Representative immunofluorescence images of MacGreen^{GFP} mice at 48hrs post-APAP, cells were stained for IL7R (red), GFP (macrophages), EdU (white). (**b**) Magnified image of the regenerative niche (white dotted square) showed IL7R+ GFP+ macrophages (white arrows), along with IL7R- GFP+ macrophages (blue arrows) and IL7R+ GFP$^{-/Lo}$ cells (pink arrows; potentially lymphocytes) (Scale bar=50μm).

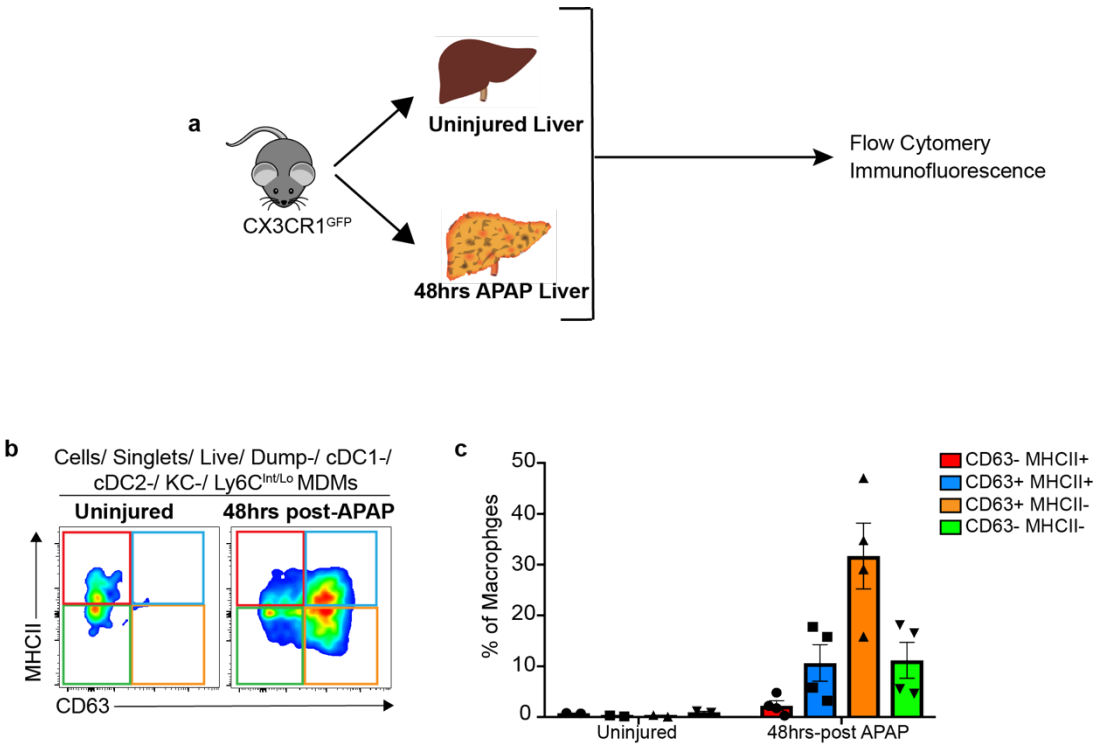

Figure 5.12 Validation of MDM clusters in CX3CR1$^{GFP/+}$ mice. (**a**) APAP was administered to CX3CR1^{GFP} mice, livers were collected for flow cytometry and immunofluorescence analysis, uninjured CX3CR1^{GFP} mice were used at controls. (**b**) Delineation of Ly6C^{Lo} MDMs on CD63 and MHCII expression via flow cytometry. (**c**) Quantification of the percentage of double negative (green), double positive (blue), CD63+ MHCII- (orange) and CD63+ MDMs (red) MDMs in 48hrs post-APAP and uninjured livers. Data acquired from single experiment, n=2-4 per group. Data shown as Mean±S.E.M.

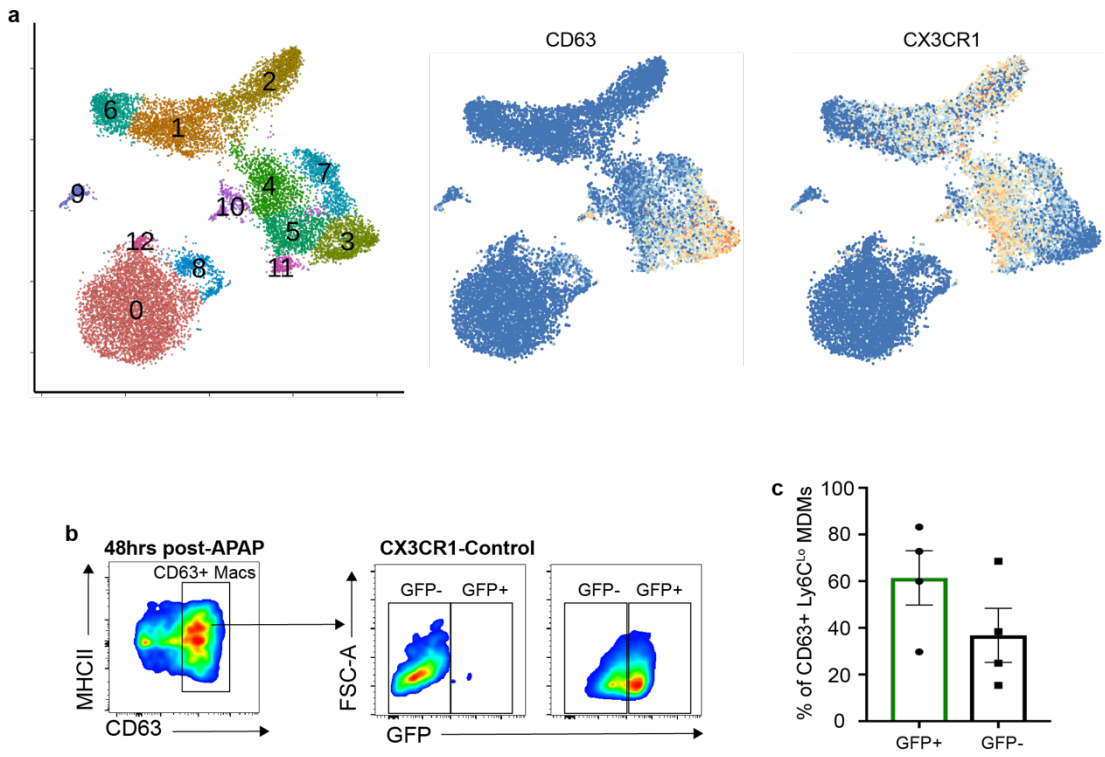

Figure 5.13 Validation of CX3CR1$^{GFP/+}$ expression in CD63+ MDMs. (**a**) t-SNE visualization of MP clusters, and the expression of CX3CR1 and CD63 across the MDM clusters. (**b**) Representative flow plots of GFP expression in CD63+ MHCII- MDMs, indicated the presence of GFP+ and GFP- subsets. (**c**) Proportion of GFP+ and GFP- CD63+ MDMs. Data acquired from two independent experiments, n=4 per group. Data shown as Mean±S.E.M.

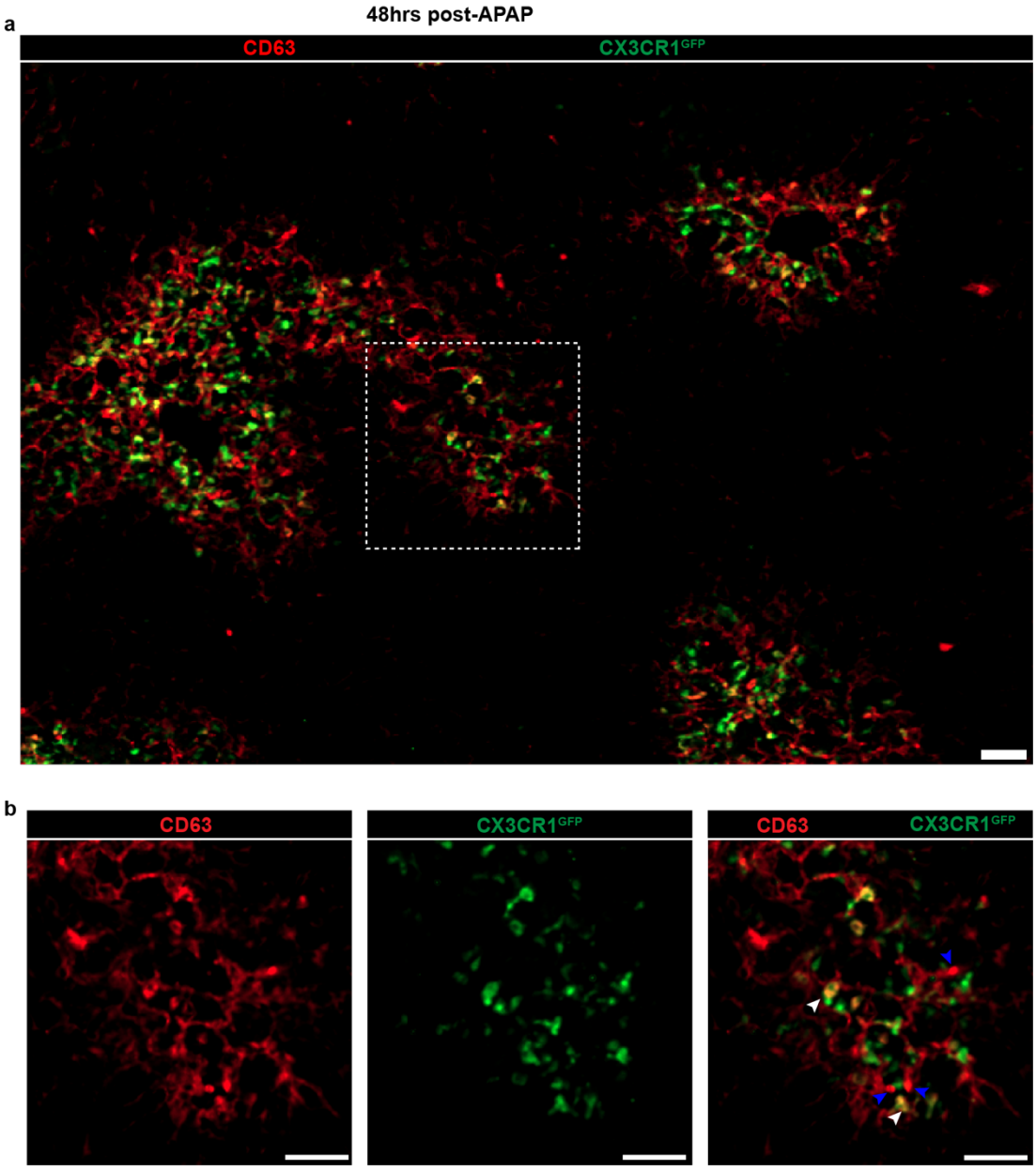

Figure 5.14 Identification of CX3CR1+ CD63+ MDMs and CX3CR1- CD63+ MDMs in the regenerative niche of the liver at 48hrs post-APAP (**a**) Representative immunofluorescence images of CX3CR1^{GFP} mice at 48hrs post-APAP, cells were stained for CD63 (red), GFP (macrophages). (**b**) Magnified image of the regenerative niche (white dotted square) showed CX3CR1+ CD63+ cells (white) and CX3CR1- CD63+ cells (blue) (Scale bar=50μm).

5.2.6 CD63+ MHCII- MDMs expand during the regenerative phase of the AILI

As discussed before, AILI is a highly dynamic model, and macrophages are plastic cells that change their phenotype according to their environment. In order to gain insight into the temporal changes in the $Ly6C^{Lo}$ MDMs, I performed a time course experiment. Mice were given APAP and livers were harvested at: 24hrs, 48hrs, 72hrs and 96hrs post-APAP (Figure 5.15). $Ly6C^{Hi}$ monocytes and $Ly6C^{Lo}$ MDMs were identified as discussed before and following this $Ly6C^{Lo}$ MDMs were assessed for their expression of MHCII and CD63 (Figure 5.15a). Following APAP induction all four subsets increased in numbers, during the inflammatory phase of AILI (24hrs) CD63- MHCII- MDMs were the primary subset (Figure 5.15b). However, during the peak regenerative phase of AILI (48 and 72hrs-post APAP) CD63+ MHCII- MDMs expanded the most and represented the predominant subset (Figure 5.15b). One of the gene ontology terms for cluster 3 was phagocytosis, C-type lectin genes (*CLEC4D*) and various phagolysosomal genes (*CD63, CD9, GPNMB*) were upregulated in cluster 3. Therefore, I assessed the expression of various scavenger receptors on CD63+ MHCII- MDMs when they expanded the most in the liver following APAP (48 and 72hrs post-APAP) and compared to the rest of the MDMs, to gain insight into the functional differences between them (5.16a, b). CD63+ macrophages as a whole had higher expression of scavenger receptors CD36 and MerTK, compared to the CD63- macrophages at 48hrs post-APAP and this expression was elevated at 72hrs post-APAP (Figure 5.16b). There were no major differences in the expression profile of CD9 and CD24 between the four subsets. CD63+ MDMs also had higher CD11c expression compared to the MHCII- CD63- MDMs at 48hrs post-APAP (Figure 5.16b). This highlighted the major phenotypic differences between the two main macrophage subsets: CD63+ MHCII- and MHCII- CD63- MDMs were the upregulation of scavenger receptors CD36 and MerTK on the former. Based on these results, I decided to assess functional capacity in these macrophages to phagocytose.

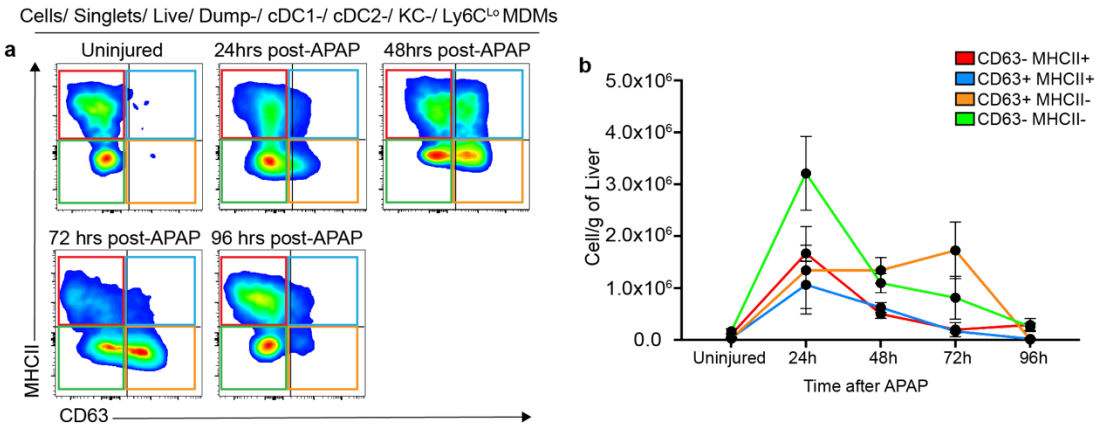

Figure 5.15 Dynamics of CD63+ MHCII- and CD63- MHCII- MDMs during AILI. (**a**) Representative flow plots of Ly6C^{Lo} MDMs at specific timepoints during AILI. (**b**) Quantification of the four subsets of Ly6C^{Lo} MDMs during AILI shows expansion of CD63+ MHCII- MDMs during peak liver regeneration (48hrs-72hrs post-APAP). Data acquired from three independent experiments, n=4-15. Data shown as Mean±S.E.M.

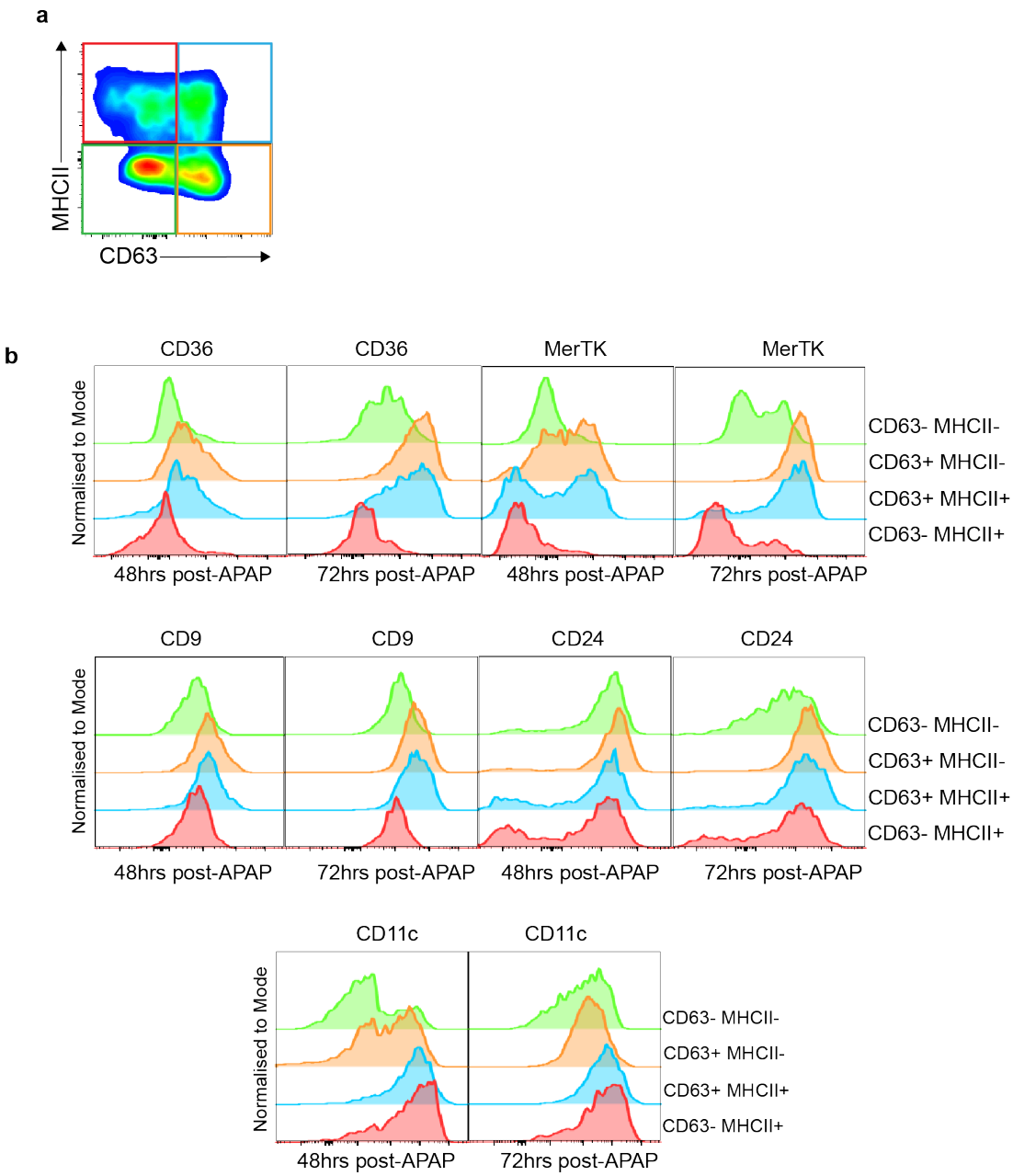

Figure 5.16 Phenotypic characterization of Ly6C^{Lo} MDMs. (**a**) The four subsets of Ly6C^{Lo} MDMs were identified on flow cytometry, based on CD63 and MHCII expression. (**b**) Representative histograms showing the expression of stated surface proteins with functional relevance on CD63- MHCII- (green), CD63+ MHCII- (orange), CD63+ MHCII+ (blue) and CD63- MHCII+ (red) macrophage subsets at 48hrs and 72hrs post-APAP.

5.2.7 CD63+ MHCII- MDMs show enhanced phagocytic capacity

I used two different phagocytosis assays to assess the phagocytic capacity of the macrophage subsets following APAP induction. PKH26PCL is a commercially available cell labelling dye which forms aggregates, that are selectively engulfed by phagocytic cells. Detection of dye via flow cytometry and/or immunofluorescence can be used as an indicator of phagocytic capacity of cells (Campana *et al.*, 2018). While *in vivo* administration of PKH26PCL can give you an indication of the phagocytic capacity of different cells, it does not tell you precisely which cells have actively phagocytosed during AILI. In order to address this, I used a low-pH sensing fluorescent probe, developed in Dr. Marc Vendrell's lab (CIR, QMRI), that enabled the detection of phagosomal acidification in cells of interest (Vázquez-Romero *et al.*, 2013). Two different fluorescent probes were acquired from Dr. Vendrell: PhagoGreen and PhagoRed, both of which operated on the same principle but had two different fluorophore conjugations. Optimization experiments were conducted to determine the optimal concentrations for each probe (Figure 5.17). Liver NPCs from uninjured and post-APAP mice were incubated with either PhagoGreen or PhagoRed at varying concentrations recommended by Dr. Vendrell and the dye incorporation in different leucocytes were assessed via flow cytometry (Figure 5.17). Comparing to the FMO sample the intensity of PhagoRed labelling was higher than PhagoGreen (Figure 5.17), however delineating positive cell labelling from background proved to be more challenging with PhagoRed (Figure 5.17a). For example, almost all of the CD45+ cells appeared to be positive for the dye (Figure 5.17a). Whereas, PhagoGreen labelling had a clear unlabeled population of leucocytes (CD45+ cells; Figure 5.17b) and non-phagocytic cells such as T and B cells were clearly separated from phagocytic cells (KCs and MDMs) in their expression of PhagoGreen (Figure 5.17c). Based on these results, I decided to use PhagoGreen, in conjunction with PKH26PCL for the assessment of phagocytosis.

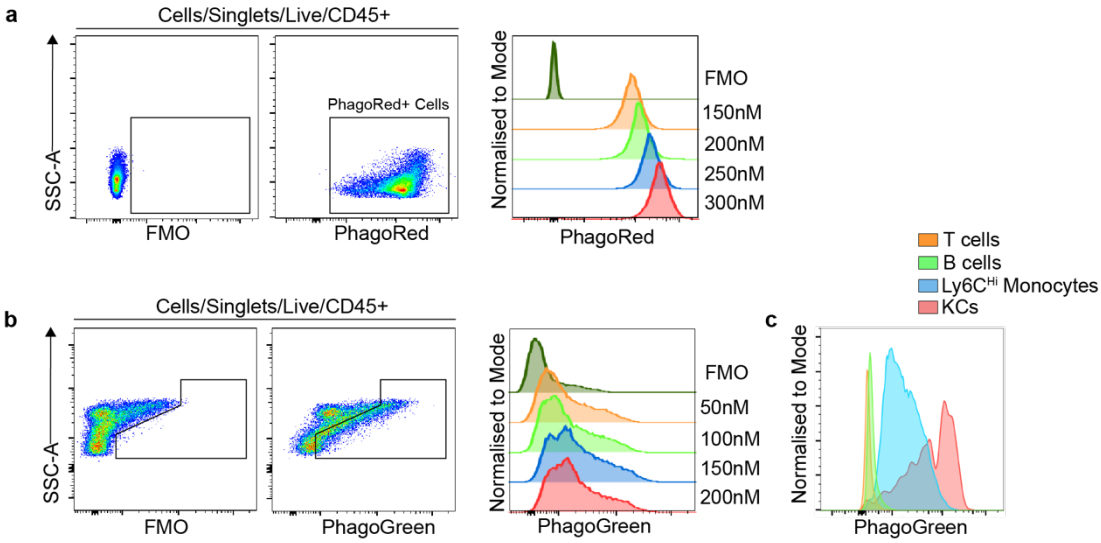

Figure 5.17 Optimisation of *ex vivo* phagocytosis assay. Representative flow plot of PhagoRed+ CD45+ cells (**a**) and PhagoGreen+ CD45+ cells (**b**) and the expression of dye+ CD45+ cells following incubation with different concentrations of the dye. (**c**) Delineation of phagocytic cells within the CD45 lineage using PhagoGreen.

PKH26PCL was injected intravenously into mice following APAP induction, 16hrs prior to tissue harvesting (72hrs post-APAP), when both liver regeneration and CD63+ MHCII- MDMs peaked in the liver (Figure 5.18a). Following NPC isolation, cells were incubated with PhagoGreen, stained with cell surface markers and then analyzed via flow cytometry (Figure 5.18a, b). Geometric mean fluorescence intensity (GMFI) for PKH26PCL and PhagoGreen in the four subsets of Ly6C^{Lo} MDMs were calculated by subtracting the GMFI of FMO controls. PKH26PCL and PhagoGreen fluorescence was the highest in CD63+ MHCII- MDMs and CD63+ MHCII+ MDMs, indicating these cells had high phagocytic capacity and increased acidified-phagosomal content compared to the CD63- MDMs (Figure 5.18c, d). As discussed previously, efficiency of KC liberation at 48hrs-post APAP is low, but at 72hrs KCs can be liberated efficiently from APAP livers (Chapter3). Therefore, I compared the phagocytic capacity of CD63+ MDMs to KCs, there was no significant difference in PKH26PCL detection between KCs, CD63+ MDMs and Ly6C^{Hi} monocytes (Figure 5.18e). PhagoGreen expression on the

other hand was significantly higher in CD63+ MHCII- MDMs compared to KCs (Figure 5.18f), indicating increased levels of phagosome acidification in these cells.

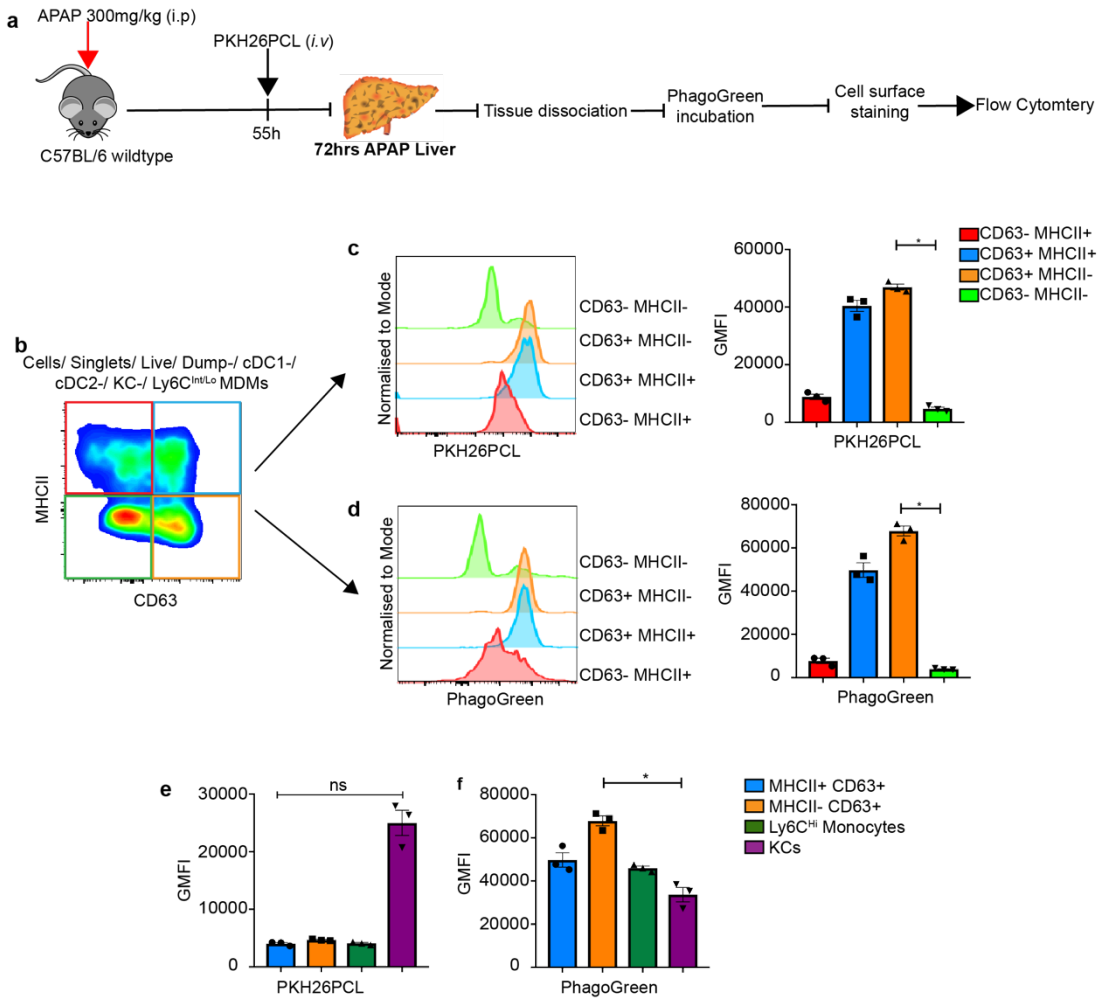

Figure 5.18 *In vivo* and *ex vivo* assessment of phagocytosis in macrophages. (**a**) Schematic of the methodology used for phagocytosis assessment of macrophages. (**b**) Flow gating strategy to subdivide the Ly6C^{Lo} MDMs. Flow histograms showing the detection of PKH26PCL (**c**) and PhagoGreen (**d**) in the four different subsets of Ly6C^{Lo} MDMs. To the right is the measurement of PKH26PCL (**c**) and PhagoGreen (**d**) detected in each subset based appropriate FMO controls, represented as geometric mean fluorescence intensity. (**e**) Comparison of PKH26PCL and PhagoGreen expression in CD63+ MHCII- (orange) and CD63+ MHCII+ (blue) MDMs in comparison to KCs (purple) and Ly6C^{Hi} monocytes (green). Data acquired from single experiment, n=3 per group. One-way ANOVA with Dunn's multiple comparisons test. Data shown as Mean±S.E.M, * $P \leq 0.05$.

5.2.8 Origin of CD63+ MHCII- macrophages

Having established there are four distinct subsets of Ly6C^{Lo} MDMs that populates the liver during the repair phase, I wanted to investigate the origin of these macrophages, as macrophage ontogeny can influence its function and behavior (Ginhoux and Guilliams, 2016). Hepatic macrophages can have one of two origins, they can be embryologically derived or and bone marrow derived. KCs have an embryological origin and it is thought the Ly6C^{Lo} MDMs, as the name indicates, are derived from bone marrow derived, circulating monocytes (Yona *et al.*, 2013; Ginhoux and Guilliams, 2016; Guilliams, Mildner and Yona, 2018). Here, I have defined CD63- MHCII+, CD63+ MHCII+, CD63+ MHCII- and CD63- MHCII- macrophages as "MDMs", as these cells clustered distinctly from KCs, and lacked KC specific markers at transcript (*CLEC4F, TIMD4, CD5L*) and protein (TIMD4) level (Appendix 6, Figure 5.4). However, this does not conclusively prove these cells are monocyte-derived, as transcriptional reprogramming of KCs to an "MDM phenotype" is also possible. One of the reasons for performing scRNA-seq on circulating MPs alongside tissue MPs was to use the transcriptional profile of these cells to assess the contribution of circulating monocytes to the ontogeny of hepatic macrophages, using *in silico* trajectory analysis. Unsupervised clustering on 16,399 MPs from eight different datasets (uninjured liver n=2, APAP liver n=2, uninjured blood n=2, APAP blood n=2), showed that indeed the circulating blood monocytes clustered next to tissue monocytes (MDM cluster 4), implying a differentiation trajectory from blood into tissue (Figure 5.19a). To interrogate the origin of CD63+ MHCII- and CD63- MHCII- macrophages, Dr. John Wilson-Kanamori performed Velocyto analysis on the dataset. Velocyto analysis essentially predicts the future transcriptional state of individual cells based on distinguishing spliced and unspliced precursor mRNAs ratios (RNA velocity) in a single cell and directionality of the differentiation process can be displayed by arrows (Manno *et al.*, 2018) (Figure 5.19b). Despite the blood monocytes clustering closely to liver Ly6C^{Hi} monocytes (cluster 4,7), there was no directionality from blood MPs to tissue MPs. The arrows from cluster 4,7, 5 and

11 towards CD63+ MDMs (cluster 3) indicated a differentiation trajectory from tissue monocytes to tissue resident CD63+ MDMs. More importantly, there was no differentiation trajectory observed from KCs (clusters; 0,8 and 12) to CD63+ MDMs (cluster 3; Figure 5.19b).

To confirm and validate the *in-silico* findings *in vivo*, I utilized a CCR2-/- transgenic mouse system, in which mice are deficient for the chemokine receptor CCR2, required for the recruitment of circulating Ly6C^{Hi} monocytes into the liver (Zigmond *et al.*, 2014; Mossanen *et al.*, 2016). CCR2 deficient mice have been used to model AILI to investigate the role of monocytes in the progression of liver injury (Mossanen *et al.*, 2016). The purpose of this study was to investigate the origin of CD63+ MHCII- and CD63- MHCII- MDMs, therefore the macrophage compartment in CCR2-/- mice (n=4) was compared to C57BL/6 W/T (n=3) mice, following APAP overdose (Figure 5.20a). Animals were culled at 48hrs-post APAP, blood was drawn for serum analysis and livers were harvested for flow cytometric analysis (Figure 5.20a). Serum ALT and AST levels of CCR2-/- mice at 48hrs post-APAP were lower in comparison to W/T mice, however this reduction was not significant (Figure 5.20b). Nevertheless, CCR2-/- have been reported to exhibit less liver injury than W/T mice, especially in the earlier phases of AILI (12-24hrs post-APAP) (Mossanen *et al.*, 2016). Differences in the composition of KCs and MDMs were analyzed on flow cytometry, using the standard gating strategy as described before (Figure 5.20c). This showed whilst the KC numbers between CCR2-/- and W/T groups are comparable (Figure 5.20c, d), CCR2-/- mice showed reduction in both Ly6C^{Hi} Monocytes and Ly6C^{Lo} MDMs (Figure 5.20e, f). Crucially, CD63+ MHCII- MDM numbers were significantly lower in CCR2-/- mice in comparison to the W/T group, additionally, they also had lower numbers of CD63- MHCII- MDMs. Collectively, the *in-silico* analysis and experiments in CCR2-/- mice supported CD63+ MHCII- and CD63- MHCII- MDMs were the progeny of bone-marrow derived circulating CCR2^{+} Ly6C^{Hi} monocytes.

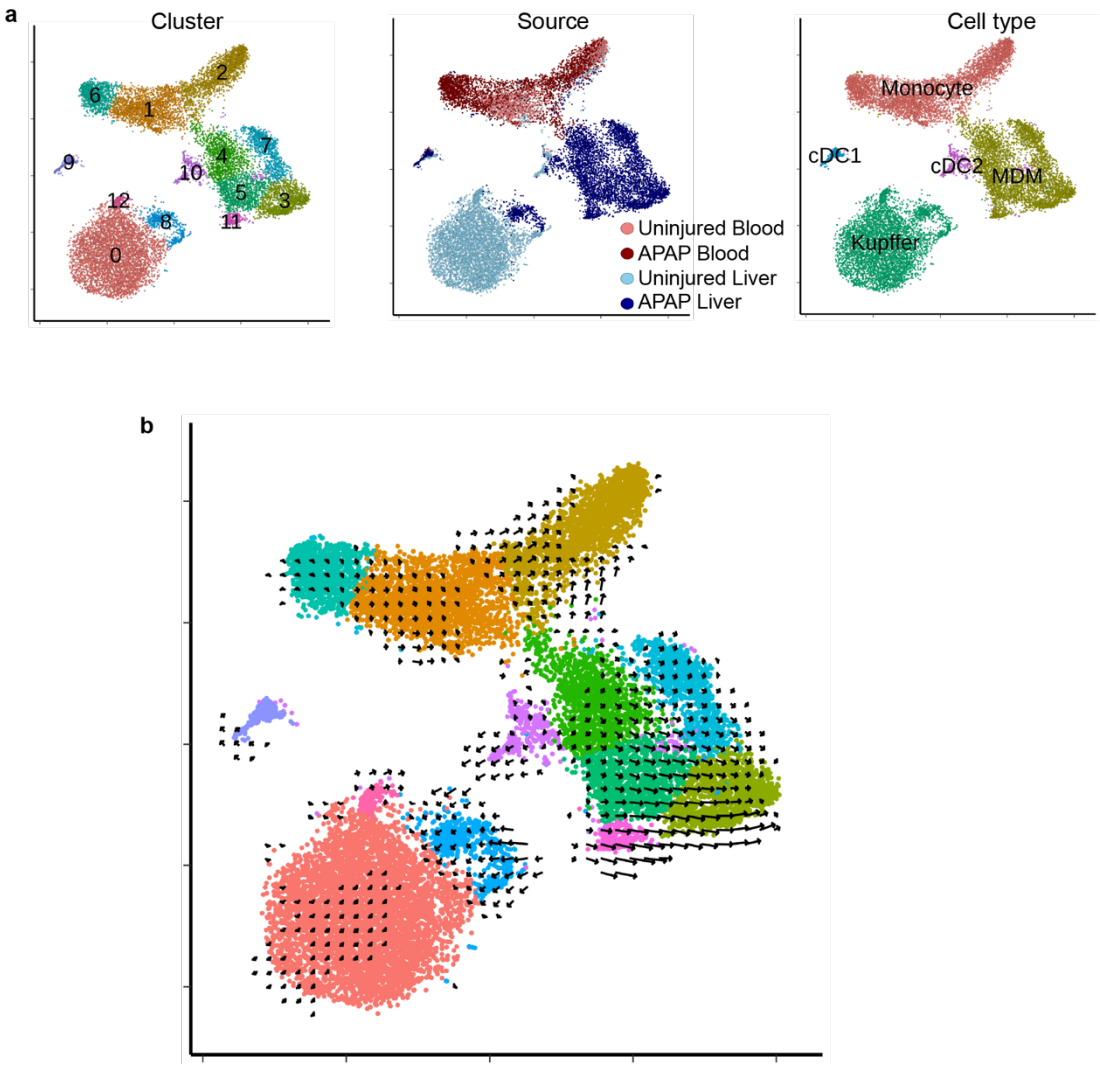

Figure 5.19 Computational analysis of differentiation trajectories in MP cluster via Velocyto (**a**) t-SNE visualization of mononuclear phagocyte (MP) by cluster, source and cell type, these cells were analyzed on Velocyto. (**b**) Velocyto results show no differentiation trajectory from blood monocytes to tissue MPs (indicated by the absence of arrows) but show differentiation trajectory from Ly6C^{Hi} Monocytes (cluster 4, 7) towards Ly6C^{Lo} MDMs (cluster 5 and 3).

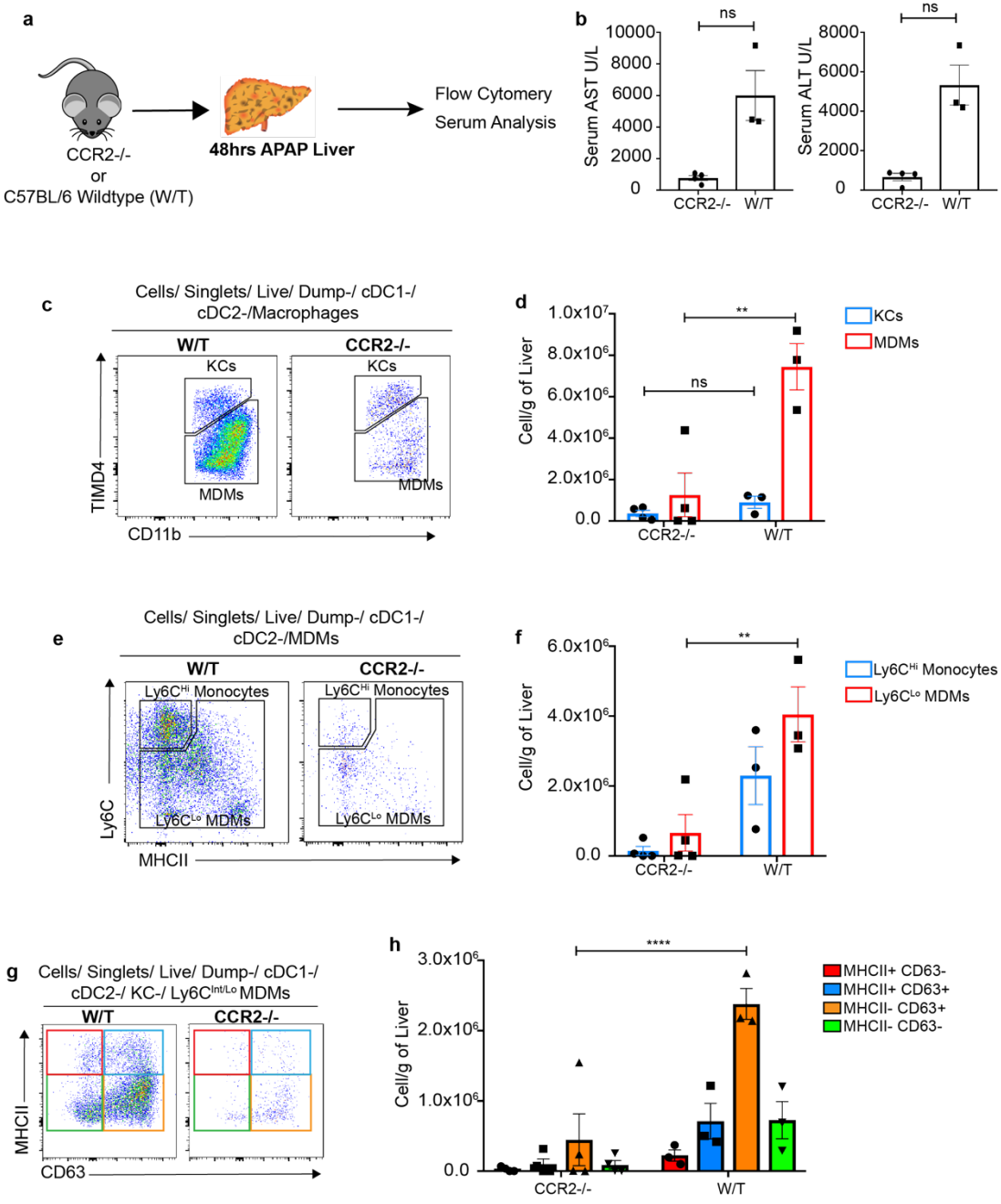
a
CCR2-/-
or
C57BL/6 Wildtype (W/T)
48hrs APAP Liver
Flow Cytomery
Serum Analysis
b
Serum AST U/L
Serum ALT U/L
ns
CCR2-/-
W/T
c
Cells/ Singlets/ Live/ Dump-/ cDC1-/
cDC2-/Macrophages
W/T
CCR2-/-
KCs
MDMs
TIMD4
CD11b
d
Cell/g of Liver
KCs
MDMs
**
ns
e
Cells/ Singlets/ Live/ Dump-/ cDC1-/
cDC2-/MDMs
Ly6C^Hi Monocytes
Ly6C^Lo MDMs
Ly6C
MHCII
f
Ly6C^Hi Monocytes
Ly6C^Lo MDMs
g
Cells/ Singlets/ Live/ Dump-/ cDC1-/
cDC2-/ KC-/ Ly6C^Int/Lo MDMs
MHCII
CD63
h
****
MHCII+ CD63-
MHCII+ CD63+
MHCII- CD63+
MHCII- CD63-

Figure 5.20 Assessing the origin to CD63+ MHCII- and CD63- MHCII- MDMs using CCR2 deficient mice (**a**) Methodology used to study the origin of hepatic CD63+ MHCII- and CD63- MHCII- MDMs consisted of administering APAP to CCR2-/- and wildtype (W/T) mice, prior to liver and serum analysis at 48hrs post-APAP. (**b**) Serum AST and ALT measurements of CCR2-/- and W/T mice at 48hrs post-APAP. Representative flow plots (**c**) and quantitative analysis (**d**) showing the differences in KCs and MDMs in CCR2-/- and W/T mice. Representative flow plots (**e**) and quantitative analysis (**f**) showing the differences in $Ly6C^{Hi}$ monocyte and $Ly6C^{Lo}$ MDM numbers in CCR2-/- and W/T mice. The $Ly6C^{Lo}$ MDMs were defined on CD63 and MHCII expression (**g**), and the four subsets of MDMs were quantified for both CCR2-/- and W/T mice (**h**). Data acquired from single experiment, n=3-4 per group. Mann-Whitney nonparametric paired t-Test. Data shown as Mean±S.E.M, $^{**}P \leq 0.01$, $^{****}P \leq 0.0001$.

5.2.9 Identification of $Ly6C^{Lo}$ MDM heterogeneity in other models of acute liver injury

Having identified heterogeneity within the $Ly6C^{Lo}$ MDMs and demonstrated the emergence of four distinct subsets $Ly6C^{Lo}$ MDMs during AILI, I wanted to see if a similar macrophage programming could be seen during other types of liver injury. To investigate this, I used two different models of liver injury: Carbon tetrachloride (CCl_4) and partial hepatectomy (PHx). CCl_4 is a standardly used model of liver cirrhosis, chronic iterative administration of CCl_4 leads to recurrent hepatocyte necrosis which results in fibrosis and cirrhosis. For the purposes of this study, animals were administered a single dose of CCl_4 to induce hepatocellular death and acute inflammation and livers were collected at stated timepoints (Figure 5.21a). PHx (70% surgical resection) was performed as previously described, and livers were harvested at 48hrs-following PHx (Figure 5.21a). Livers were also collected from uninjured and post-APAP animals for comparison (Figure 5.21a). Analysis of the $Ly6C^{Lo}$ MDMs demonstrated that MDMs during CCl_4 injury the $Ly6C^{Lo}$ MDMs adopted four distinct phenotypes similar to that seen during AILI (Figure 5.21b). Both CD63+ MHCII- (orange) and CD63- MHCII- MDMs (green) were significantly increased at 72hrs-post CCl4 in comparison to basal levels (Figure 5.21c). Whereas, there was no significant difference between the composition of

Ly6C^{Lo} MDMs following PHx versus uninjured livers (Figure 5.21b, c). Strikingly, expansion of both MDMs was more pronounced (around fourfold increase) following CCl_4 than APAP (Figure 5.21c). These findings suggested that macrophage differentiation and heterogeneity in the liver is heavily influenced by the type of liver injury.

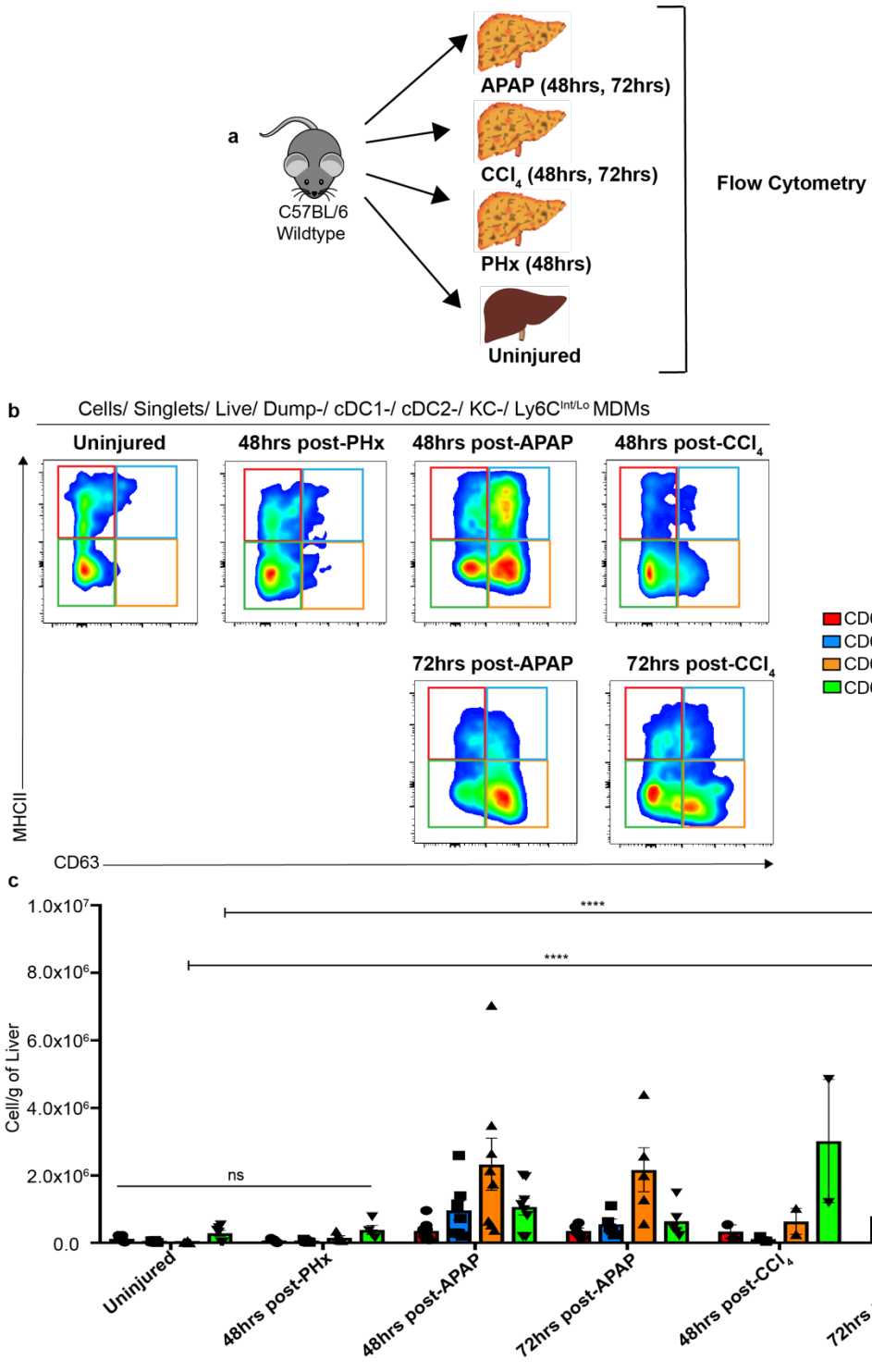
a
C57BL/6
Wildtype
APAP (48hrs, 72hrs)
CCl4 (48hrs, 72hrs)
PHx (48hrs)
Uninjured
Flow Cytometry
b
Cells/ Singlets/ Live/ Dump-/ cDC1-/ cDC2-/ KC-/ Ly6CInt/Lo MDMs
Uninjured
48hrs post-PHx
48hrs post-APAP
48hrs post-CCl4
72hrs post-APAP
72hrs post-CCl4
CD63- MHCII+
CD63+ MHCII+
CD63+ MHCII-
CD63- MHCII-
MHCII
CD63
c
Cell/g of Liver
1.0x10^7
8.0x10^6
6.0x10^6
4.0x10^6
2.0x10^6
0.0
****
****
ns
Uninjured
48hrs post-PHx
48hrs post-APAP
72hrs post-APAP
48hrs post-CCl4
72hrs post-CCl4

Figure 5.21 Characterizing the Ly6C^{Lo} MDM compartment on CD63 and MHCII expression in PHx and CCl_4 models of liver injury. (**a**) Mice were subjected to acute liver injury by one of the following ways: single administration of APAP, single administration of CCl_4 or 70% partial hepatectomy (PHx), livers were harvested and analyzed via flow cytometry at stated timepoints, following injury. (**b**) Representative flow plots from at Ly6C^{Lo} MDM compartment at stated specific time points following APAP, PHx and CCl_4, compared to uninjured groups. (**c**) Quantification of the Ly6C^{Lo} MDM subsets in each group. Data acquired from single experiment, n=3 per group. 3way ANOVA with Tukey's multiple comparisons test. Data represented as Mean±S.E.M. ****$P \leq 0.0001$.

5.3 Discussion

In this chapter I have attempted to validate the scRNA-seq findings at a protein level to dissect the heterogeneity within the MDM compartment during the repair phase of AILI, to identify specific pro-regenerative subpopulations of macrophages. Validation of broad MP lineages (cDC1, cDC2, KC and MDM) were made possible by the top marker genes generated through differential expression analysis. Defining of most of the lineages were relatively straight forward, though identifying cDC2 cells required prior knowledge (cDC2 cells). The significant expansion of MP lineages at 48hrs post-APAP, in comparison to uninjured livers highlighted the contribution from these cells during the repair phase of AILI. Transcriptional profile of KCs from uninjured and post-APAP livers indicated these cells are not dramatically different post-injury, they exhibited subtle changes in the degree of expression of certain genes rather than an on and off expression. That was not to say these subtle changes will not result in major phenotypical and functional differences in these cells and indeed there were changes in the expression of various cell surface proteins. Significant upregulation of *CD36* gene expression in KCs at 72hrs post-AILI has been reported previously (Graubardt *et al.*, 2017), here, I have shown CD36 expression is dramatically increased at protein level as well. CD36 on macrophages has been shown to promote inflammation resolution via promotion of phagocytosis (Woo *et al.*, 2016). CD24 also has a functional role in AILI, where they were shown to dampen tissue injury and damage to

promote an anti-inflammatory phenotype (Chen *et al.*, 2009). Timely upregulation of these molecules indicate KCs are programmed towards a pro-regenerative phenotype during the repair phase of AILI. Post-APAP KCs did not show any changes in the expression of MerTK, my findings indicate upregulation of MerTK by Ly6C^{Lo} MDMs (Figure 5.16) but not KCs (Figure 5.5). This was in contradiction with the observation made by Triantafyllou et al (2018), where the authors show a dramatic increase in MerTK+ KCs via flow cytometry, at 24 and 48hrs post-APAP. A possible reason of this disparity might be the differences in gating strategy, the lack of KC specific markers (TIMD4, CLEC4F) in their study could have led to the inclusion of MerTK+ F4/80+ Ly6C^{Lo} MDMs in their analysis (Triantafyllou *et al.*, 2017). Contrary to the general belief in the field that KCs are sessile cells localized to sinusoids, my previous findings (Chapter 3, Figure 3.6) revealed that KCs localize to the repairing areas of the liver during AILI. Additionally, in this chapter I have demonstrated that there are major phenotypic changes in the KCs during the repair phase of AILI. Collectively these findings call for future studies to interrogate the precise function of these cells.

Ly6C^{Hi} monocytes were long thought to be an injury promoting subset (Holt, Cheng and Ju, 2008), transcriptomic analysis showing an upregulation of angiogenic, wound healing and matrix remodelling genes in Ly6C^{Hi} monocytes and their role in promoting neutrophil apoptosis has painted them in a different light recently (Zigmond *et al.*, 2014; Graubardt *et al.*, 2017). Here, Ly6C^{Hi} monocytes split into two distinct clusters, gene ontology enrichment analysis in chapter 4 suggested that these two clusters might not only be transcriptionally distinct but functionally distinct. While cluster 7 showed enrichment of genes which regulated neutrophil recruitment, neutrophil clearance and, and glutathione biosynthesis, cluster 4 showed upregulation of genes relating to leucocyte migration and differentiation. What has been lacking until now is the distinction of this duality in Ly6C^{Hi} monocytes at a protein level, therefore I attempted to delineate this heterogeneity via flow cytometry. Characterization of Ly6C^{Hi} monocytes on CD62L expression

(unique to clusters 7) showed an expansion of CD62L+ Ly6C^{Hi} monocytes at 48hrs post-APAP, compared to steady state, however there was not a clear distinction between CD62L+ Ly6C^{Hi} monocytes and CD62L- Ly6C^{Hi} monocytes. Perhaps this is not surprising, as Ly6C^{Hi} monocytes are on a differentiation spectrum, where they undergo transcriptional programming towards a pro-restorative phenotype (Zigmond *et al.*, 2014; Mossanen *et al.*, 2016). Nevertheless, CD62L+ Ly6C^{Hi} monocytes represented 20% of the overall Ly6C^{Hi} monocyte subset in APAP mice. Future studies looking at expression of markers generated via scRNA-seq at both transcript and protein level in CD62L+ Ly6C^{Hi} monocytes vs CD62L- Ly6C^{Hi} monocytes could help delineate any functional differences in these cells.

Currently, Ly6C^{Lo} MDMs are broadly characterized as the “pro-reparative” subset showing ability to promote matrix remodelling, angiogenesis, and phagocytosis during AILI (Zigmond *et al.*, 2014; Graubardt *et al.*, 2017). ScRNA-seq of these cells has revealed heterogeneity, the distinct gene ontology terms associated with cluster 5 and 3 suggested functional differences in these cells. Phenotypically delineating cluster 5 and cluster 3 was more challenging, though cluster 3 had a range of discriminatory genes including *SYNGR, SPP1, GPNMB, ADAM8, LMNA, EMP1* (Appendix 7) identifying these targets via multi-parametric flow cytometry was challenging. This meant I had to rely on known biology, my previous data (chapter 3) indicated differentially expression of MHCII by Ly6C^{Lo} MDMs (Figure 3.7). Based on this, using MHCII in combination with CD63 I identified four distinct subsets of Ly6C^{Lo} MDMs.

The temporal dynamics of CD63- MHCII- and CD63+ MHCII- macrophages, whereby they expanded at 24hrs and 48hrs post-APAP suggests they might have distinct functions during AILI. The main functional difference between CD63+ MHCII- and CD63- MHCII Ly6C^{Lo} MDMs identified here was their ability to phagocytose. CD63+ MHCII- macrophages demonstrated a number of phagocytic characteristics, which has been associated to tissue repair. They upregulated MerTK and CD36 at 48 and 72hrs post-APAP. MerTK expressing

macrophages promote tissue resolution during ALF resulting from APAP overdose in both humans and murine models (Triantafyllou *et al.*, 2017). CD36 on the other hand is a scavenger receptor, which functions in oxidized low-density lipoprotein uptake and its role to promote efficient efferocytosis by both murine and human macrophages is well-known (Park, 2014; Greenlee-Wacker, 2016). CD36+ macrophages has also been shown to promote tissue resolution through phagocytosis in a murine model of ischemic stroke (Woo *et al.*, 2016). At transcript level CD63+ MDMs (cluster 3) expressed phagocytosis promoting genes such as *CLEC4D* and *GPNMB*. GPNMB functions to mediate phagosomal maturation and degradation of cargo in macrophages (Li, Castano, Hudson, Nowlin, S. L. Lin, *et al.*, 2010; Campana *et al.*, 2018). My data showed that PhagoGreen (detects phagosomal acidification) expression was significantly higher in CD63+ MHCII- MDMs than KCs at 72hrs-post APAP, this fits with the scRNA-seq data. These findings in addition to the topography of the CD63+ macrophages in liver, where they localize in the regenerative niche (Figure 5.10) suggests that these cells might function to clear necrotic and apoptotic debris. Notably, KCs also exhibit phagocytic features and are found within the repairing areas of the liver during AILI, therefore there might be functional redundancies between KCs and Ly6C^{Lo} MDMs. The role of CD63- MHCII- MDMs also needs to be addressed, the temporal dynamics suggested that these cells are involved in the repair process. Flow cytometric phenotypic characterizations demonstrate they are distinct to CD63+ MHCII- MDMs, however this was insufficient to interrogate the function of these cells.

Additionally, in line with the scRNA-seq data, the CD63+ MDMs (cluster 3) showed upregulation of IL7R at protein level and IL7R+ GFP+ cells were detected in the repairing areas of the liver at 48hrs post-APAP, these cells had a monocytic appearance (Figure 5.11). IL-7 signaling is commonly associated with lymphogenesis and very recently been associated with macrophages development (Fry and Mackall, 2009; Leung *et al.*, 2019). Their role in pathological conditions is limited to autoimmune conditions such as rheumatoid arthritis, where IL7R+ monocytes were shown to promote

inflammation via TNF-α production (Chen *et al.*, 2013). ScRNA-seq of synovial fluid of spondyloarthritis patients in a recent study identified a distinct subset of monocytes expressing IL7R+, the function of these cells is unknown (Al-mossawi *et al.*, 2018). Currently there is no evidence to show that they are involved in tissue repair and resolution.

Despite the transcriptional similarities in circulating Ly6C^{Hi} monocytes to tissue Ly6C^{Hi} monocytes, namely cluster 7, computational trajectory analysis of MPs failed to show directionality from blood monocytes to tissue monocytes and MDMs. One of the reasons for this could be because the dataset consisted of cells from a single time-point and infiltration of Ly6C^{Hi} monocytes into the liver occurred at earlier timepoints (Chapter3, Figure 3.5). However, the Velocyto analysis did show directionality from tissue Ly6C^{Hi} monocytes towards CD63+ Ly6C^{Lo} MDMs (Cluster 3). Experiments in CCR2 deficient mice suggests the four subsets of Ly6C^{Lo} MDMs are derived from CCR2+ Ly6C^{Hi} circulating monocytes and are not derived from resident KCs. However, I cannot deny the possibility that there might be tissue resident CCR2+ precursors in the liver that could give rise to Ly6C^{Lo} MDM subsets. In order to confirm a systemic origin, I would need to do additional experiments to trace circulating monocytes. For instance, the MacBlue^{CFP} transgenic reporter system, in which CFP expression is driven by truncated CSF1R promoter represents an effective tool to investigate this. In these tissue resident KCs do not express CFP, whereas circulating monocytes do (Sauter *et al.*, 2014). Additionally, labelling BM-derived circulating monocytes with DNA intercalators such as EdU or BrdU and then using proliferation as a readout is another way to prove or disprove origin from circulating cells in this context (Yona *et al.*, 2013).

The finding that CCR2-/- mice exhibit less injury than W/T mice is in keeping with existing literature, based on the study by Mossanen et al (2016). This reduction in injury is one of the main reasons why CCR2+ Ly6C^{Hi} monocytes have been considered to be a pro-injury subset during AILI, consequently, CCR2 blocking or inhibition has been suggested as a therapeutic strategy in the clinical setting. It is important to note that the effect of ablating CCR2+

Ly6C^{Hi} monocytes led to significant reduction in the pro-regenerative Ly6C^{Lo} MDM subset here. Furthermore, Yang et al. (2019) reports significantly lower hepatocyte proliferation in CCR2-/- mice, in comparison to wild type counterparts. Therefore, CCR2 inhibition represents a potential early therapeutic intervention, which might be ineffective in late-presenting cases in the clinical setting and while CCR2 inhibition dampens liver injury, it does not promote the regenerative capacity of the liver (Mossanen *et al.*, 2016).

There are a lot of similarities and differences in the characteristics and dynamics of MPs in the context of acute liver injury. In chapter 3 I showed the lack of contribution from bone-marrow derived Ly6C^{Hi} monocytes and MDMs during the regenerative phase of PHx, in comparison to AILI. This highlights that macrophage response during liver injury and regeneration is dependent on the type of injury inflicted. Similar to AILI, CCl_4 also show expansion of CD63+ MHCII- and CD63- MHCII- MDMs, whereas following PHx these populations did not expand and was similar to basal levels. Perhaps this is not surprising as both the hepatic and systemic environment is widely different in AILI and CCl4 compared to PHx and we know that macrophage phenotype is influenced by environmental cues. Both AILI and CCl_4 cause centrilobular necrosis, resulting in massive inflammatory response, while PHx represents a relatively non-inflammatory model, showing minimal systemic involvement. Further studies need to be carried out to determine the Ly6C^{Lo} phenotype in other models of injury and repair, where there is a systemic involvement, both in the liver and other organs. There is a lot of transcriptional and phenotypic overlap in the phenotype of CD63+ MHCII- MDMs identified here and the Ly6C^{Lo} MDM subset responsible for resolution of fibrosis, reported in Ramachandran et al. (2015). Namely, the upregulation of genes such as *IGF1*, *GPNMB, MerTK, CD36* and the increased capacity to phagocytose, additionally they share a common origin from circulating Ly6C^{Hi} monocytes. Although these cells share some phenotypic similarities, there are also differences between them, the matrix metalloproteinase signature displayed by the “pro-restorative Ly6C^{Lo} MDMs” reported in Ramachandran et al. (2012) is not observed in the Ly6C^{Lo} MDMs here.

Non-alcoholic steatohepatitis (NASH) is another model of characterized by the similar features seen in AILI; infiltration of CCR2+ Ly6C^{Hi} monocytes and their differentiation into Ly6C^{Lo} MDMs. Recently, scRNA-seq of myeloid cells during NASH revealed heterogeneity within the macrophages and a subset of these macrophages displayed a distinct anti-inflammatory metabolic gene signature, which the authors termed as “NAFLD gene signature” (Krenkel *et al.*, 2019). Collectively, these observations demonstrate the multitude of functional adaptations of circulating Ly6C^{Hi} monocytes to differentiate into phenotypically and functionally distinct Ly6C^{Lo} MDMs.

In this final chapter I have validated the scRNA-seq results, identified and characterized the broad MP lineages populating the liver during the repair phase of AILI (48hrs post-APAP). Centered around the markers identified through scRNA-seq and known markers I attempted to dissect the heterogeneity within the MDMs. This led to the discovery that following acute inflammation Ly6C^{Hi} monocytes can differentiate into four distinct macrophage populations, two of which are heavily involved in the injury and repair process (CD63+ MHCII- and CD63- MHCII- MDMs). Phenotypic characterization and functional assays suggest a phagocytic role for CD63+ MHCII- MDMs, while the role of CD63- MHCII- MDM subset remains unknown. While we are moving away from the M1 and M2 dichotomous classification, this chapter has highlighted that solely relying on predefined markers to classify and study monocytes and macrophages can massively underestimate functionally relevant heterogeneity in these cells. The findings presented here suggests CD63+ MHCII- Ly6C^{Lo} MDMs may represent a pro-reparative subset, future studies are needed to interrogate the functional relevance of these cells during AILI.

6 Discussion

In my doctoral studies I utilised scRNA-seq to investigate circulating and hepatic monocyte and macrophage heterogeneity in an unbiased manner during AILI, facilitating the identification of injury-specific subsets. Transcriptome analysis of circulating Ly6C^{Hi} monocytes revealed AILI-induced monocyte reprogramming towards a "granulocytic signature" prior to their entry into the liver and indicated heterogeneity within the hepatic Ly6C^{Hi} monocytes and Ly6C^{Lo} MDMs. Subsequent phenotypic validation delineated Ly6C^{Hi} monocytes into two subsets: CD62L^{+} and CD62L^{-}. It also led to the identification of four distinct subsets of Ly6C^{Lo} MDMs populating the liver during the repair phase of AILI, characterized by differential expression of CD63 and MHCII. This was confirmed in two different macrophage reporter mice (CX3CR1$^{GFP/+}$ and MacGreen^{GFP}). CD63+ MHCII- and CD63- MHCII- Ly6C^{Lo} MDMs were the predominant subsets in the liver during peak regeneration. The main functional difference between CD63+ MHCII- and CD63- MHCII- Ly6C^{Lo} MDMs was phagocytic ability. Tissue staining revealed CD63+ macrophages are localized to areas of repair within the liver, where they may be exposed to necrotic debris. *In vivo* and *ex vivo* phagocytic assays confirmed CD63+ macrophages exhibit increased phagocytic capacity and phagosome maturation in comparison to their CD63- Ly6C^{Lo} counterparts and KCs. Experiments in a CCR2 deficient system suggests the four subsets of Ly6C^{Lo} MDMs are a progeny of BM-derived CCR2+ circulating monocytes. The emergence and expansion of CD63+ MHCII- and CD63- MHCII- Ly6C^{Lo} MDMs during acute CCl_4 injury, but not partial hepatectomy, suggests these activation states result from an inflammatory cue in the liver. This body of work lays the foundation for future work that will investigate the functional relevance of these subsets during AILI.

Monocytes and macrophages have a dual role during AILI due to their ability to change phenotype based on microenvironmental cues, consequently

pinpointing precise therapeutic targets has been challenging. I used scRNA-seq, during AILI and homeostasis, to delineate specific injury and repair promoting subsets. In order to achieve this a broad characterisation of the AILI model was necessary to inform timepoint selection for scRNA-seq. When I began my PhD there were few studies that had extensively characterised leucocyte responses following AILI (You *et al.*, 2013; Zigmond *et al.*, 2014; Guillot and Tacke, 2019). As liver injury responses in mice can be influenced by a number of factors including strain background, APAP dose and route of administration (Mossanen and Tacke, 2015), I had to characterise leucocyte responses throughout the course of AILI in C57BL/6 mice. As shown in **Figure 3.1 and 3.2** 6hrs-24hrs post-APAP represented a necroinflammatory (injury) phase, characterised by significant necrosis and elevated serum liver enzyme levels. The repair phase was between 48hrs-168hrs, defined by a reduction in necrosis and restoration of tissue architecture. Hepatocyte proliferation peaked between 48hrs-72hrs post-APAP.

As described in chapter 1, the leucocyte response in the liver during AILI is not limited to monocytes and macrophages, with a wide range of innate and adaptive immune responses influencing liver injury and repair. Therefore, using multi-parametric flow cytometry, I simultaneously numerically characterized both innate and adaptive leucocytes in the same panel over the course of AILI for the first time **(Figure 3.3 and 3.4)**. This highlighted that macrophages are the most dominant subset in the liver during peak hepatocyte proliferation (48hrs-72hrs post-APAP). Utilizing CX3CR1$^{GFP/+}$ mice Zigmond et al, (2014) categorized monocytes and macrophages populating the liver during AILI into three distinct subsets: KCs, Ly6C^{Hi} monocytes and Ly6C^{Lo} MDMs. As shown in **Figure 3.5-3.7** these subsets were identified and characterized via flow cytometry. Further phenotypic characterization of these subsets revealed heterogeneity within Ly6C^{Lo} MDMs, which was previously reported as a homogenous population, emphasizing the need to study these cells at higher resolution.

In chapter 4, I optimised a digestion protocol which allowed isolation of a high percentage of viable cells, which is critical in the generation of high-quality scRNA-seq data (**Figure 4.1-4.3**). Previous gene expression studies in the context of AILI has relied heavily on known biology, to pre-define monocytes and macrophages prior to sequencing (Zigmond *et al.*, 2014; Mossanen *et al.*, 2016; Graubardt *et al.*, 2017; Triantafyllou *et al.*, 2017). I do believe this strategy can limit the identification of novel subtypes and activation states that do not conform to the conventional classifications. Therefore, a broad gating strategy (all CD45+ cells) was used in isolating cells for scRNA-seq, avoiding any front-end selection bias. One could argue this can result in monocytes and macrophages being underrepresented in the sample, however these cells represented the pre-dominant leucocytes in the liver at 48hrs-post APAP. Additionally, given that the number of cells sequenced via the 10X platform ranged in the tens of thousands, underrepresentation was unlikely. Indeed, broad clustering of CD45+ cells post-sequencing demonstrated the highest number of cells were within the mononuclear phagocyte (MP) lineage, which includes monocytes and macrophages.

In addition to developing laboratory skills in a cutting-edge technique, this body of work exposed me to computational analysis of large datasets. The *in silico* analysis was performed in collaboration with a post-doctoral bioinformatician, Dr. John Wilson Kanamori, who is based in the Henderson group. I was able to gain valuable insights into the different stages involved in scRNA-seq data analysis. As a result, I now have a greater understanding of data processing, the importance of QC steps and normalization and importantly, interpretation of scRNA-seq data.

One of the novel findings from my scRNA-seq data was the identification of an APAP-specific subset of Ly6C^{Hi} monocytes, characterized by a “granulocytic” signature (**Figure 4.13**). Transcriptional switching of circulating monocytes following tissue injury has been reported in several other studies (Yáñez *et al.*, 2017; Ikeda *et al.*, 2018; Krenkel *et al.*, 2019). Contrary to the transcriptional

switching seen during NAFLD injury, where monocytes downregulate inflammatory genes such as calprotectin genes *S100A8/A9* and *RTENLG* (Krenkel *et al.*, 2019), the observation here is akin to the emergence of distinct subset of monocytes seen during LPS-induced inflammation (Yáñez *et al.*, 2017; Ikeda *et al.*, 2018). Yanez et, (2017). In these instances, monocytes are derived from granulocyte myeloid precursors (GMPs) expressing a wide range of neutrophil genes such as *S100A8/A9, LCN2*, which is similar to the changes I have observed in my scRNA-Seq data. This finding raises a number of questions. What is the origin of these cells? Are they derived from cMoPs (common monocyte precursor) and then undergo transcriptional switching following AILI or are these cells the progeny of GMPs? What is the functional relevance of this transcriptional preprogramming? Ikeda *et al*, (2018) reported transcriptional switiching of Ly6C^{Hi} monocytes to an immunoregulatory phenotype, defined by YM1 expression, which drove tissue repair in a murine model of colitis. In the context of AILI are these "granulotyic" monocytes driving the repair process or promoting injury? In order to precisely address these questions markers are required which allow discrimination between the various Ly6C^{Hi} monocyte subsets. As most of the discriminatry markers (LCN, S100A8/A9, RTENLG) are intracellular proteins and show wide expression in both monocytes and neutrohpils, genetically modified Cre-based murine systems may be best suited for the future study of these cells.

As shown in **Figure 4.10, 4.12** scRNA-Seq of tissue monocytes and macrophages during AILI and homeostasis revealed heterogeneity, within KCs (Custer 0, 8 and 12), Ly6C^{Hi} (cluster 4 and 7) monocytes and Ly6C^{Lo} MDMs (cluster 5 and 3). One of the main unanswered questions in the field is the precise function of KCs during the repair phase of AILI. Although APAP specific KCs formed a distinct cluster compared to homeostatic KCs (**Figure 4.10, 4.12**), there were no differentially expressed markers which delineated the two clusters (Appendix 6). This might be a true biological observation, where any APAP-induced transcriptional changes occurring in KCs are subtle at gene level, perhaps with more profound post-transcriptional phenotypic and

functional changes. The low-read depth and high dropout rate associated with the 10X Genomics Chromium system could also have contributed to the lack of transcriptional changes between cluster 0 (homeostatic) and cluster 8 (APAP specific) (Appendix 6). The other more likely explanation is that the tissue digestion protocol did not efficiently liberate the “true” injury specific population of KCs. Based on immunofluorescence they migrate to areas of injury (**Figure 3.6**) at 48hrs APAP, however despite this no chemotaxis related genes were identified in the scRNA-seq analysis. As discussed in chapter 3, developing cell isolation protocols which liberate more KCs, in combination with imaging studies, are needed to study these cells during the repair phase of AILI.

My work in chapter 5 consisted of phenotypically and functionally validating scRNA-seq findings using novel marker genes to delineate the heterogeneity within Ly6C^{Hi} monocytes and Ly6C^{Lo} MDMs. ScRNA-seq data indicated that *SELL* (CD62L) marks cluster 7 but not cluster 4 (**Figure 5.7**). CD62L, also known as L-selectin is a type-I transmembrane glycoprotein which regulates monocyte trafficking and transmigration into tissue (Geissmann, Jung and Littman, 2003; Xu *et al.*, 2008). It is characteristically expressed by inflammatory Ly6C^{Hi} CCR2+ monocytes (Geissmann, Jung and Littman, 2003; Auffray, Sieweke and Geissmann, 2009), and I found that CD62L expression was present on a subset of Ly6C^{Hi} monocytes at 48hrs-post AILI (**Figure 5.7**). Gene ontology enrichment analysis in chapter 4 generated distinct terms for cluster 4 and cluster 7. The terms for cluster 4 (CD62L-) were associated with leucocyte migration and differentiation whereas cluster 7 (CD62L+) had terms related to immune complex clearance, neutrophil aggregation and clearance (**Figure 4.12**). Ly6C^{Hi} monocytes have a role in regulating neutrophil function and apoptosis during AILI (Graubardt *et al.*, 2017), and given the gene ontology terms associated with cluster 7, CD62L+ Ly6C^{Hi} monocytes may mediate this. Alternatively, this might represent a monocyte differentiation phenotype, i.e. newly recruited Ly6C^{Hi} monocytes express CD62L+ and subsequently downregulate CD62L expression, thus CD62L- Ly6C^{Hi}

monocytes could represent an intermediary subset during their reprogramming towards Ly6C^{Lo} MDMs (Zigmond *et al.*, 2014).

In the context of AILI, Ly6C^{Lo} MDMs are defined as a homogeneous pro-reparative macrophage subset, which are progeny of BM-derived Ly6C^{Hi} monocytes (Zigmond *et al.*, 2014; Mossanen *et al.*, 2016; Graubardt *et al.*, 2017). With the aid of scRNA-seq I have shown that Ly6C^{Lo} MDMs are heterogenous, and using MHCII expression in combination with CD63, I identified four distinct subpopulations of Ly6C^{Lo} MDMs populating the liver at 48hrs-post APAP (**Figure 5.8**).

- CD63+ MHCII-
- CD63+ MHCII+
- CD63- MHCII+
- CD63-MHCII-

Identification of these subsets in MacGreen^{GFP} and CX3CR1$^{GFP/+}$ reporter mice confirmed that these cells belong to the mononuclear phagocyte system (MPS) (**Figure 5.10-5.14**). The complexity between dendritic cells (DCs) and macrophages was mentioned in chapter 1, MHCII and CD11c expression is insufficient to faithfully isolate DCs from macrophages. As cDC1, cDC2 and pDCs subsets were removed during front-end analysis based on positive expression of XCR1, CD24, SiglecH, and CD11c, and negative expression of F4/80, it is unlikely that the MHCII expressing cells are derived from the common DC progenitor (cDP) lineage. Experiments in CCR2-/- mice (**Figure 5.20**) revealed Ly6C^{Lo} MDM subsets were deficient in this system, suggesting these cells are a progeny of CCR2+ Ly6C^{Hi} monocyte derived from cMoPs in the bone marrow (Serbina and Pamer, 2006; Mossanen *et al.*, 2016; Guilliams, Mildner and Yona, 2018). Studies have described the capacity of circulating monocytes to give rise to dendritic cells referred to as m-DCs (monocyte-derived DCs) (Serbina, Shi and Pamer, 2012; Menezes *et al.*, 2016; Mildner *et al.*, 2017). I cannot be certain that the MHCII expressing Ly6C^{Lo} MDM

subsets described here are not m-DCs as these cells also show expression for the classic macrophage markers CD64 and F4/80 (Guilliams and van de Laar, 2015). Currently, it is impossible to distinguish between m-DCs and MDMs solely based on marker expression. To definitively do this I would need to investigate their relative migration and T-cell interaction potential (Guilliams and van de Laar, 2015). Further studies will be required to fully elucidate the function of mDCs and MDMs during AILI.

The expansion of CD63+ MHCII- and CD63- MHCII- MDMs during peak hepatocyte regeneration suggests these cells may be involved in liver repair (**Figure 5.15**). The mechanism by which Ly6C^{Lo} MDMs drives liver repair has been attributed to phagocytosis; specifically the clearance of apoptotic neutrophils (efferocytosis) (Graubardt *et al.*, 2017; Triantafyllou *et al.*, 2017). Indeed, phagocytic capacity was a distinguishing feature between the two most dominant Ly6C^{Lo} MDM subsets, CD63+ MHCII- MDMs have significantly higher phagocytic capacity than CD63- MHCII- MDMs (**Figure 5.18**). Localisation of CD63+ macrophages to areas of repair in the liver would be consistent with this function, where they are likely to encounter apoptotic neutrophils and necrotic debris which they may phagocytose (**Figure 5.10**). We know that acidification of the phagolysosome is an indicator of phagosome maturation and thus successful cargo degradation (Kinchen and Ravichandran, 2008). In addition to *CD63,* which has a role in endosomal pathways, cluster 3 cells showed upregulation of *GPNMB* (Appendix 7), known to regulate phagosome maturation in phagocytic cells (Li, Castano, Hudson, Nowlin, S. L. Lin, *et al.*, 2010). In concordance, the PhagoGreen assay which detects acidified phagolysosomes demonstrated that both CD63+ Ly6C^{Lo} MDM subsets had increased acidified phagolysosome activity compared to CD63- Ly6C^{Lo} MDMs and KCs during the repair phase (72hrs-post APAP) (**Figure 5.18**). This lends weight to CD63+ MHCII- MDMs being the principle phagocytic subset in the liver during the repair phase of AILI.

The link between successful phagosome maturation and tissue repair has been demonstrated by several studies utilizing GPNMB deficient mice (Li, Castano, Hudson, Nowlin, S.-L. Lin, *et al.*, 2010; Campana *et al.*, 2018). GPNMB is a protein that is necessary for recruitment of autophagy protein LC3 to the phagosome, mediating lysosomal fusion with phagosomes containing apoptotic cargo (Li, Castano, Hudson, Nowlin, S. L. Lin, *et al.*, 2010). Therefore, GPNMB deficient mice have the ability to engulf but do not degrade phagocytosed cargo. Following acute kidney injury, GPNMB was upregulated in inflammatory monocytes and *GPNMB* mutant mice had a 5-fold increase in apoptotic cellular debris in comparison to wild type mice, which was also accompanied by an 85% increase in mortality (Li, Castano, Hudson, Nowlin, S. L. Lin, *et al.*, 2010). In the context of acute and chronic liver injury induced by APAP and CCl_4 respectively, successful phagocytic cargo degradation limited tissue injury, promoted polarization of macrophages and increased hepatocyte proliferation (Campana *et al.*, 2018). Here, CD63+ MHCII- Ly6C^{Lo} MDMs may serve to efficiently carry out phagocytosis to promote liver repair.

To fully understand the mechanism by which CD63+ MHCII- Ly6C^{Lo} MDMs may promote liver repair, there are number of questions that remain unanswered: Is liver regeneration induced by debris removal, where a niche is created for hepatocyte proliferation or can macrophage phagocytosis also release mitogens to directly induce hepatocyte proliferation? There have been reports to suggest that clearance of hepatocyte debris can induce Wnt3a, which acts on hepatocytes to promote liver regeneration following biliary liver injury (Boulter, Govaere and Bird, 2012). This begs the questions whether CD63+ MHCII- macrophages show preferential uptake of necrotic versus apoptotic debris? *In vitro* studies suggest apoptotic versus necrotic uptake by macrophages activate distinct signaling events (Reddy *et al.*, 2002). During AILI hepatocyte necrosis precedes neutrophil apoptosis. So, are there distinct macrophage subsets equipped to mediate necrotic and apoptotic cell clearance or are phagocytic macrophages equally capable of carrying out efferocytosis regardless of the nature of cellular debris? Data by Triantafyllou

et al, (2017) shows that secretory leucocyte protease inhibitor (SLPI), can promote MerTK expression on macrophages to induce efferocytosis when they are presented with apoptotic neutrophils, but not apoptotic and necrotic hepatocytes (Triantafyllou *et al.*, 2017). This supports the notion that there are distinct cues and outcomes involved in macrophage-mediated efferocytosis, interrogating these mechanisms may go a long way in the identification of precise macrophage-based targets to drive liver repair.

The four subsets of Ly6C^{Lo} MDMs were also identified during CCl_4 induced acute liver injury, but not partial hepatectomy (PHx). As with APAP a similar expansion was seen in CD63+ MHCII- and CD63- MHCII- macrophages at 48hrs and 72hrs post-CCl_4, but the increase was more profound in CCl_4 compared to APAP-induced liver injury (**Figure 5.21**). These results indicate inflammation is a key driver in dictating macrophage responses and activation states. PHx is a relatively non-inflammatory model where the mechanisms by which macrophages drive liver repair may be different to that in APAP and CCl_4-induced liver injury. As shown in chapter 3, there is very minimal inflammatory infiltrate such as neutrophils and Ly6C^{Hi} monocytes following PHx in comparison to APAP (**Figure 3.10-3.12**). It may be interesting to see if similar macrophage phenotypes are observed during chronic liver injury or in other models of tissue injury which involve inflammation as a primary stimulus.

One of the gene ontology terms for cluster 3 (CD63+ Ly6c^{Lo} MDMs) was IL-7 signaling and indeed a small population of cells in cluster 3 expressed *IL7R.* Validation via flow cytometry suggested a proportion of CD63+ Ly6C^{Lo} MDMs express interleukin 7 receptor (IL7R) at protein level as well (**Figure 4.12**). The role for IL7R on monocytes and macrophages in the context of tissue repair is unexplored. IL7R+ monocytes have been identified as a pathogenic subset during autoinflammatory conditions such as rheumatoid arthritis (Chen *et al.*, 2013) . A recent study demonstrated that both LPS and TNF-α can induce IL7R expression on peripheral blood mononuclear cells (PBMCs) monocytes *in vitro* (Al-mossawi *et al.*, 2018). These IL7R+ monocytes are sensitive to IL-

7 and this stimulation activates multiple transcriptional pathways including anti-apoptotic pathways (Al-mossawi *et al.*, 2018). Using scRNA-seq the authors identified a distinct population of IL7R+ monocytes from synovial fluid from spondyloarthritis patients, however the functional role of this monocyte population remains unknown (Al-mossawi *et al.*, 2018). I found that IL7R+ macrophages accumulate in areas of repair around the centrilobular veins at 48hrs-post APAP (Figure 5.11), whether this macrophage subpopulation regulates elements of the liver repair process remains to be seen.

Using scRNA-seq I was able to study monocyte and macrophage heterogeneity during liver homeostasis and post-AILI in a high throughput and unbiased manner. This identified heterogeneity within circulating and hepatic Ly6C^{Hi} monocytes and Ly6C^{Lo} MDMs and has opened up multiple avenues for the progression of this project.

6.1 Future Work

In order to validate APAP induced transcriptional switching of Ly6C^{Hi} monocytes to a granulocytic signature, marked by genes such as *S100A8*, *S100A9, RETNLG, LCN2, VCAN*, I propose to track these cells using a Cre-lox genetically modified system. A S100A8-cre mouse was acquired during the last few months of my PhD, and we are in the process of crossing this mouse to a TdTomato fluorescent reporter mouse line, which will drive TdTomato expression in S100A8+ cells. Future studies using this system, in conjuction with additonal markers such as Ly6C ad Ly6G (neutrophil marker), will allow tracking of S100A8+ Ly6C+ cells, and enable their charactersation and isolation via flow cytometry and FACS, giving insights into their function during AILI.

Hepatic Ly6C^{Hi} monocytes were delineated as CD62L+ and CD62L- Ly6C^{Hi} monocytes during AILI. Gene ontology enrichment suggests a role for CD62L+ Ly6C^{Hi} monocytes (cluster 7) in regulating neutrophil activity. *In vitro* experiments in which neutrophils are either cultured with CD62L+ or CD62L-

Ly6C^{Hi} monocytes from APAP livers and measuring neutrophil apoptosis or ROS production could inform their role in neutrophil regulation.

The predominant subsets in the liver during peak hepatocyte regeneration were the CD63+ MHCII- and CD63- MHCII- Ly6C^{Lo} MDMs, suggesting they have a key role during the liver repair process. CD63+ MHCII- Ly6C^{Lo} MDMs were found to be phagocytic, however the overall functional relevance of CD63- MHCII- Ly6C^{Lo} MDMs in the context of AILI liver injury is yet to be investigated. There are several ways I can address this; isolating these subsets via FACS and performing conventional gene expression analysis can facilitate identification of pro-mitogenic genes and pathways that are upregulated. Co-culturing hepatocytes with either CD63+ MHCII- or CD63- MHCII- cells and using EdU incorporation as a readout, will assess whether these cells have the capacity to directly induce hepatocyte proliferation. In order to investigate the efferocytic role of CD63+ MHCII- macrophages, they could be cultured with necrotic hepatocytes and apoptotic neutrophils, Subsequent analysis of supernatants from these cells may inform us as to whether efferocytosis induces release of pro-mitogenic factors.

One major drawback to *in vitro* experiments designed to further assess function of the macrophage subpopulations identified in my scRNA-Seq data is that these populations exhibit considerable plasticity when cultured *ex-vivo*. Nevertheless *in vitro* experiments are a useful starting point to interrogate function in the absence of precise transgenic *in vivo* tools. Importantly, to investigate the therapeutic potential of these newly identified subsets, *in vivo* experiments are necessary. One possible option is to use the CCR2 deficient mouse line. Following APAP-induced liver injury these mice show attenuated hepatic injury in the early phase (Mossanen *et al.*, 2016), followed by impaired hepatocyte proliferation (Yang *et al.*, 2019). Adoptively transferring specific subsets of monocytes and macrophages into CRR2-/- mice following APAP-induced liver injury, followed by assessment of hepatocyte necrosis, serum

liver enzyme levels and hepatocyte proliferation should inform whether any of these subsets have the capacity to modulate the injury and/or repair response.

Investigating the role of IL7R+ macrophages during liver injury and repair may be challenging, secondary to its expression on lymphocytes. For instance, a pan-blocking antibody against IL7R would also target T cells and B cells, and therefore any phenotype observed cannot be ascribed to IL7R function on monocytes and macrophages. An alternative to this would be to use RAG deficient mice, lacking T cell and B cells (Collins *et al.*, 1996), and analyze the effects of IL7R inhibition during AILI, but again this has many drawbacks. A more accurate way to interrogate this would be to specifically delete IL7R on macrophages during AILI. This could be achievable using a macrophage Cre line crossed to IL7R flox mice (Shi *et al.*, 2018).

The ultimate goal of therapeutic target identification is application of this within the clinical setting. It is imperative to consider the similarities and differences between murine models of AILI and the human disease in order to develop potent regenerative therapies for ALF. The work conducted here and in other studies that uses murine models of liver regeneration focusses mainly on understanding how the normal liver regenerates and much less attention is given to modelling the human clinical syndrome in completeness (Forbes and Newsome, 2016). Early endpoints and/or reduction in the degree of liver injury that facilitates spontaneous survival in murine models does not reflect clinically important scenarios of severe hepatic injury, impaired regeneration and fulminant hepatic failure seen in humans (Mossanen and Tacke, 2015; Guillot and Tacke, 2019). Additionally, the temporal dynamics seen in age, sex and strain-matched mouse models is incomparable to human AILI. Underlying health conditions, differences in age, sex, genetic factors, APAP dose and time of hospital admission could all influence the severity of AILI and progression of ALF in humans and consequently have an impact on the effectiveness of therapeutic interventions (Yoon *et al.*, 2016). That said, regenerative murine models do give us an insight into the cellular and molecular mechanisms

underpinning successful liver regeneration following AILI. In regard to monocytes/macrophages, despite the differences in their surface markers between mouse and human, many key aspects of macrophage activation, recruitment signals and functional activities following AILI appear to be conserved (Heymann and Tacke, 2016; Guillot and Tacke, 2019). Therefore, monocyte/macrophage-directed targets identified in this context have a tangible translational potential. Promising results from early phase clinical trials using macrophage-based therapies such as cenicriviroc; a CCR2/CCR5 inhibitor (Friedman *et al.*, 2018), and autologous macrophages (Moroni *et al.*, 2019) in patients with liver disease indicate that macrophage-targeted findings in murine models have the potential to be translated into the clinical setting (Ramachandran *et al.*, 2012; Lefebvre *et al.*, 2016).

The relevance of the findings in my doctoral work to human ALF has not been elucidated as yet. Assessment of explant livers from ALF patients could identify analogous subsets of monocytes/macrophages to those I have described here in murine models. Combining conventional techniques such as flow cytometry with immunohistochemistry would facilitate phenotypic, morphological and topographical characterization of cells. Applying novel techniques like scRNA-seq in the setting of human ALF could be powerful. For example, scRNA-seq of circulating leucocytes from ALF patients and heathy donors could be an excellent way to investigate the systemic inflammatory response (SIRS). Identifying key characteristics of monocyte and neutrophil phenotype in ALF could help with patient prognostication, as well as facilitating the identification of therapeutic targets. ScRNA-seq of explant livers is also possible, however the low frequency of viable cells in AILI ALF explant livers represents a significant technical challenge.

In summary, future studies in this area are likely to take a multimodal approach, combining conventional and cutting-edge techniques to enable in-depth study of monocyte and macrophage biology in the context of ALF, thereby accelerating the development of effective therapies.

7 Appendices

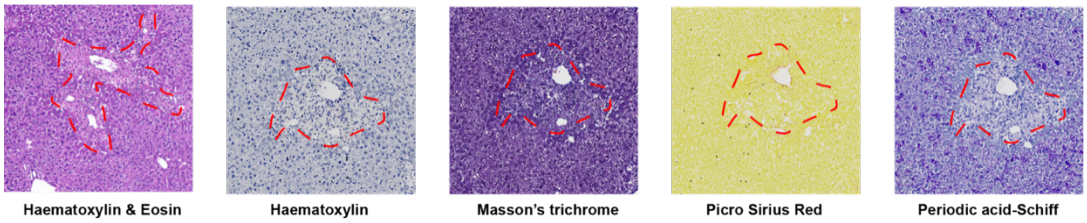

Appendix 1 Comparison of histology stains to visualize liver architecture. Mouse liver sections post-6hrs APAP overdose were stained with different types of histology stains to visualize liver architecture and hepatocyte necrosis. The red dotted line represents necrosis, the stain which gave the biggest contrast between necrotic and non-necrotic area was chosen (Periodic acid-Schiff) for the assessment of hepatocyte necrosis following AILI.

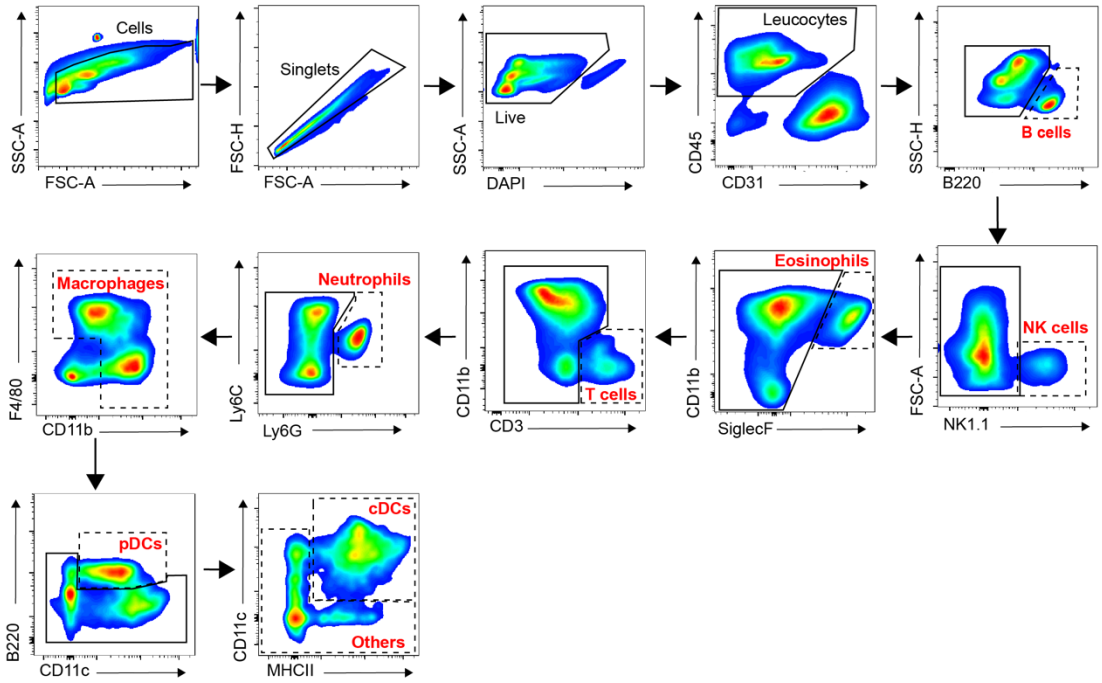

Appendix 2 Gating strategy for the identification of hepatic leucocytes following acute liver injury. Based on their expression of lineage specific, cell surface markers different types of hepatic leucocytes were isolated (black dotted line, red font), using the gating strategy shown above.

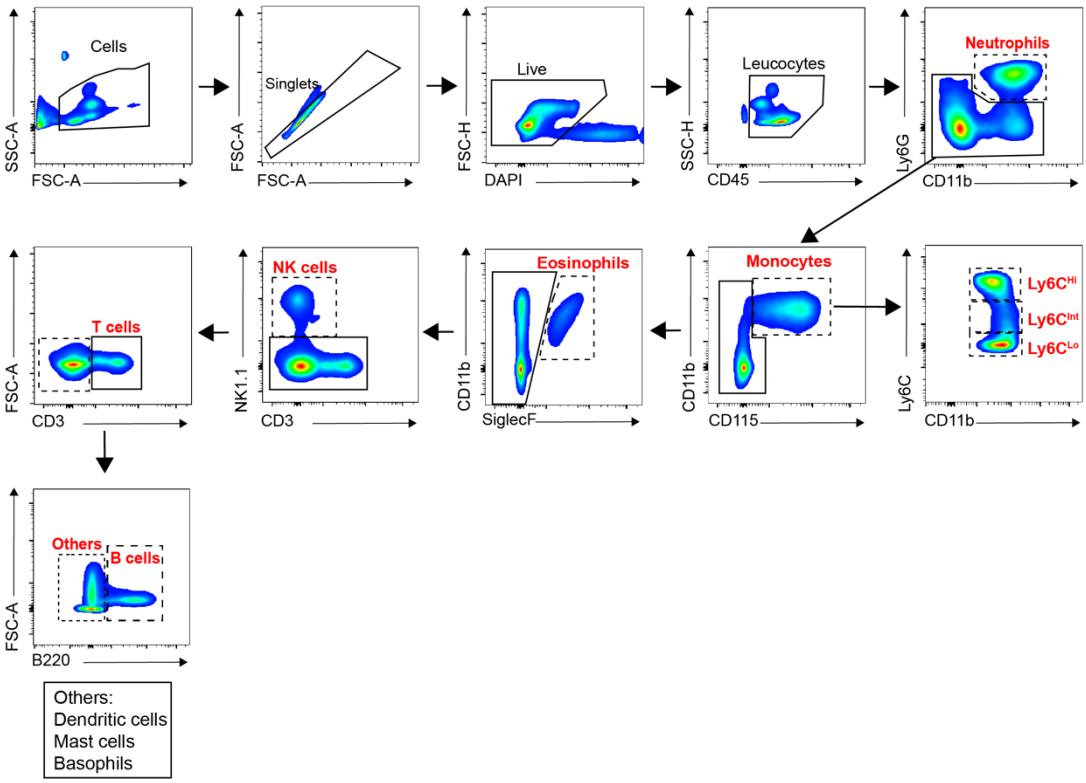

Appendix 3 Gating strategy for the identification of systemic leucocytes following acute liver injury. Based on their expression of lineage specific, cell surface markers different types of systemic leucocytes were isolated (black dotted line, red font), using the gating strategy shown above. The “others” group contained cells which were unaccounted for.

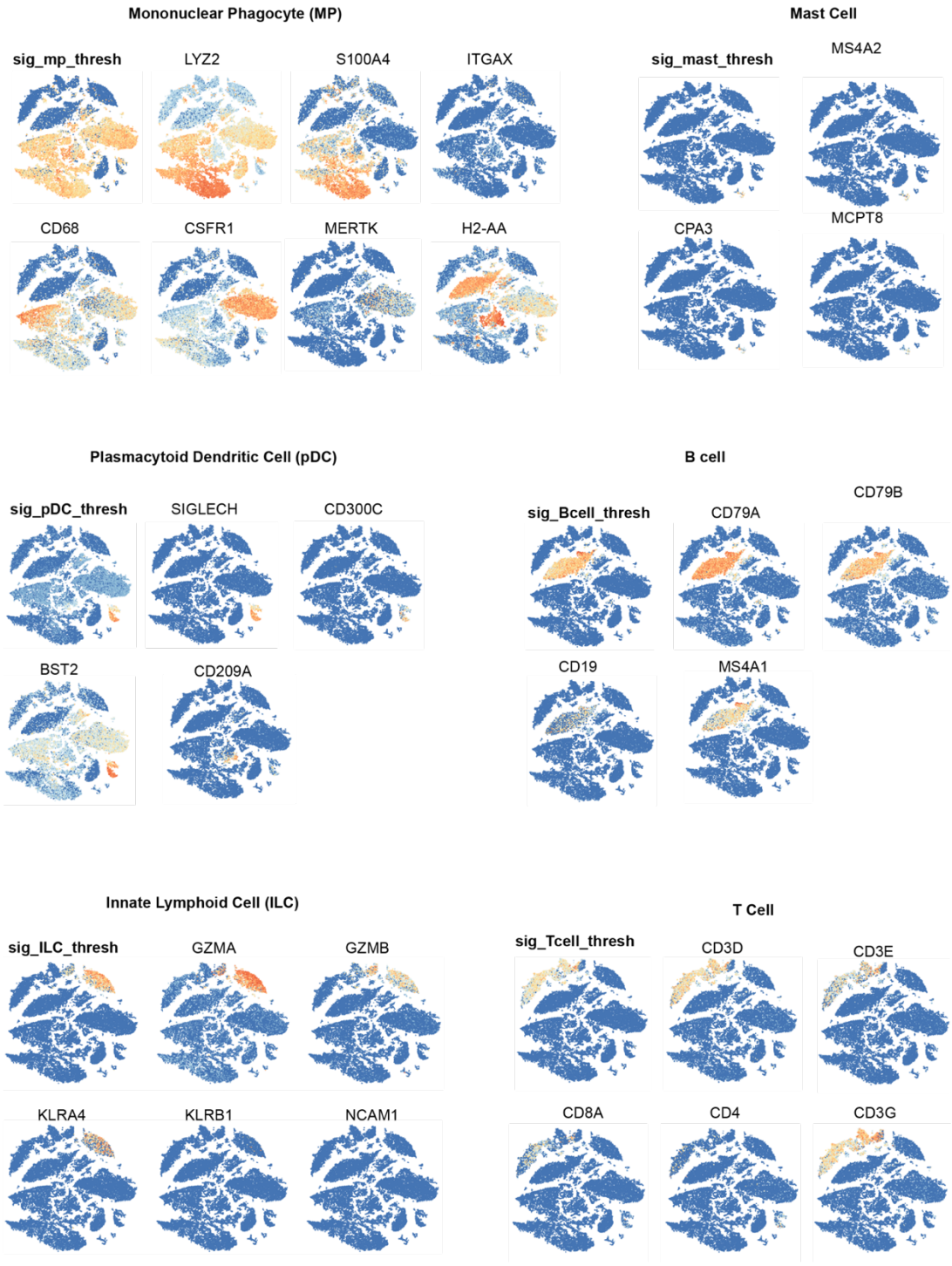
Mononuclear Phagocyte (MP)
sig_mp_thresh
LYZ2
S100A4
ITGAX
CD68
CSFR1
MERTK
H2-AA
Mast Cell
sig_mast_thresh
MS4A2
CPA3
MCPT8
Plasmacytoid Dendritic Cell (pDC)
sig_pDC_thresh
SIGLECH
CD300C
BST2
CD209A
B cell
sig_Bcell_thresh
CD79A
CD79B
CD19
MS4A1
Innate Lymphoid Cell (ILC)
sig_ILC_thresh
GZMA
GZMB
KLRA4
KLRB1
NCAM1
T Cell
sig_Tcell_thresh
CD3D
CD3E
CD8A
CD4
CD3G

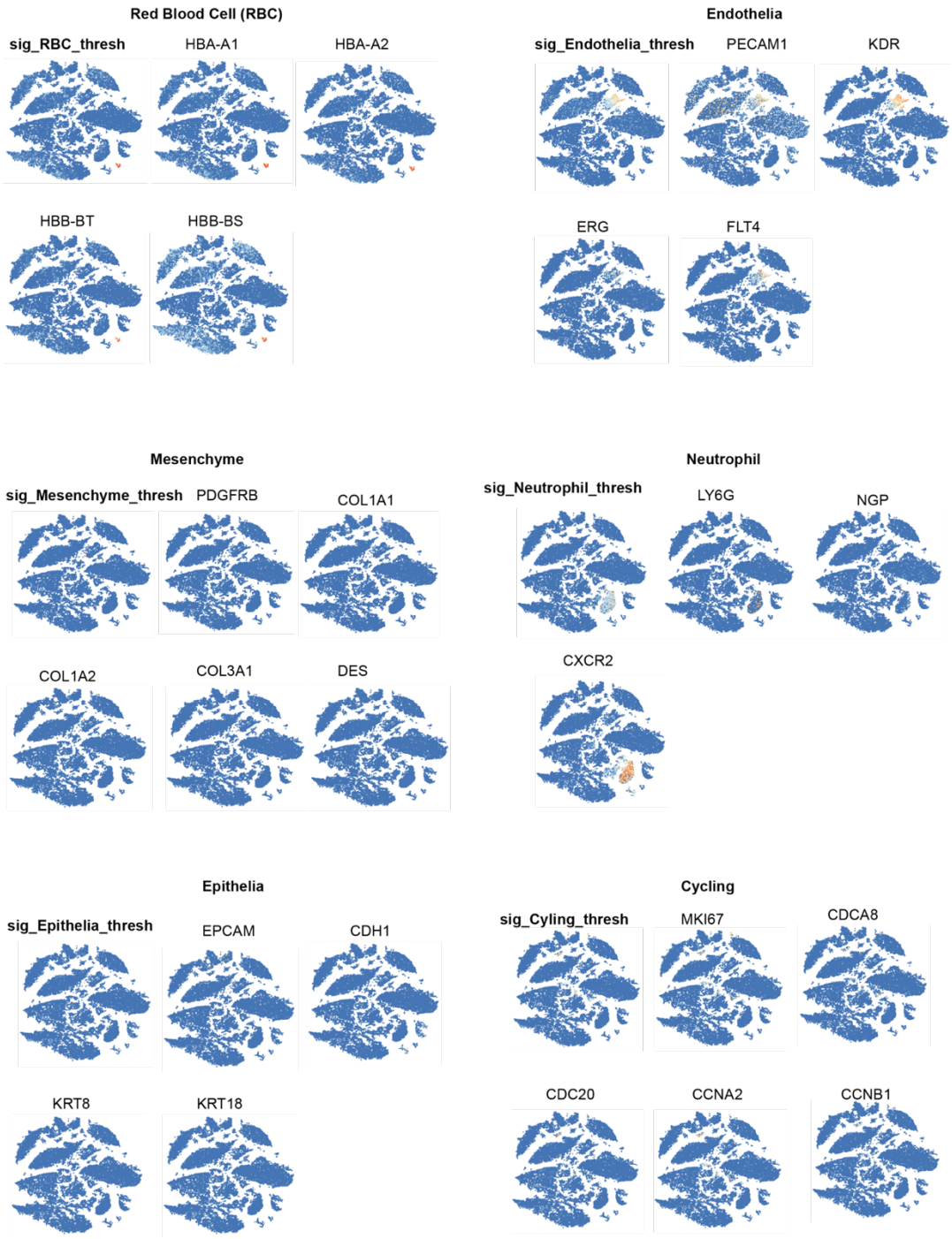

Appendix 4 Gene signature analysis. Lineage marker genes used for annotation of different clusters.

gene	avg_logFC	pct.1	pct.2	cluster
Cd5l	2.45655475	1	0.271	0
Clec4f	2.44001988	1	0.214	0
Apoc1	2.35842084	0.998	0.384	0
Vsig4	2.31330119	0.999	0.158	0
Fcna	2.21426212	0.994	0.172	0
Sdc3	2.17032632	0.997	0.553	0
Slc40a1	2.1099609	0.998	0.309	0
C1qa	1.98206211	1	0.466	0
AW112010	1.88106832	0.995	0.588	0
Folr2	1.87658307	0.971	0.211	0
Ly6c2	1.49168613	0.963	0.468	1
Plac8	1.28304401	0.998	0.935	1
Ms4a4c	1.24404742	0.948	0.488	1
Lyz2	1.20028056	1	1	1
Hp	1.19192389	0.971	0.389	1
Tmsb10	1.15431215	0.999	0.838	1
Vim	1.11985885	0.988	0.734	1
Emb	1.11950286	0.934	0.398	1
Hbb-bs	1.07984256	0.673	0.15	1
Mgst1	1.0780224	0.938	0.46	1
Pglyrp1	2.06991488	0.9	0.263	2
Ace	1.74616363	0.865	0.117	2
Eno3	1.7126095	0.768	0.109	2
Ear2	1.53588727	0.94	0.552	2
Spn	1.46618967	0.767	0.141	2
Hbb-bs	1.26948186	0.694	0.151	2
Agpat4	1.24053454	0.715	0.243	2
Cd9	1.22596158	0.729	0.317	2
Pou2f2	1.21903661	0.925	0.587	2
Ceacam1	1.19451535	0.716	0.207	2
Spp1	2.60976962	0.874	0.197	3
Fabp5	2.17162858	0.914	0.338	3
Gpnmb	2.14200509	0.971	0.207	3
Ccl7	1.83696357	0.815	0.178	3
Cd63	1.81711603	0.935	0.201	3
Ccl2	1.73188847	0.915	0.266	3
Plin2	1.67909828	0.998	0.694	3
Lgals1	1.6421731	1	0.659	3
Lgals3	1.49834252	1	0.958	3
Cdkn1a	1.35544856	0.901	0.319	3

Ccr2	0.91454342	0.96	0.499	4
Tpt1	0.55080549	1	0.999	4
Rps16	0.47452663	1	0.998	4
Rpl7	0.46100621	0.999	0.99	4
Rps15a	0.45029681	1	0.994	4
Eef1a1	0.44024885	1	1	4
Rpl23	0.42287958	1	0.999	4
Rpl26	0.40738651	1	0.997	4
Rps23	0.37408262	1	0.999	4
Rpl36	-0.64181209	0.99	0.993	4
Pf4	1.47919441	0.893	0.341	5
Trem2	1.00115622	0.979	0.47	5
Cd93	0.98308861	0.944	0.297	5
Lgals1	0.95588087	0.998	0.664	5
Stab1	0.65364869	0.807	0.281	5
Rps2	0.65103902	1	0.987	5
Rnase4	0.61091007	0.678	0.195	5
Gpnmb	0.56700306	0.789	0.23	5
Rps29	-0.86794746	1	1	5
Gpx1	-0.76444994	0.999	0.998	5
S100a8	2.15535183	0.996	0.65	6
Chil3	2.10426684	0.994	0.545	6
Lcn2	1.95927349	0.892	0.132	6
Fn1	1.72190821	0.988	0.343	6
Hp	1.70686082	0.996	0.425	6
Ly6c2	1.65590409	0.995	0.498	6
Tmsb10	1.58047511	1	0.848	6
Slpi	1.5130568	0.957	0.321	6
Wfdc21	1.51044666	0.638	0.101	6
Mgst1	1.42689164	0.99	0.487	6
Cxcl2	1.65467849	0.751	0.142	7
Ccl2	1.2736	0.867	0.282	7
Slpi	1.14862695	0.912	0.326	7
Clec4e	1.09903957	0.865	0.188	7
Ccl3	1.00313324	0.874	0.306	7
Fos	0.95871314	0.986	0.791	7
Atf3	0.87302482	0.933	0.379	7
Ptafr	0.8571625	0.844	0.283	7
Clec4d	0.84175274	0.9	0.252	7
F10	0.80243655	0.854	0.29	7
Marco	1.60388433	0.926	0.297	8

Ccdc148	0.46357102	0.488	0.069	8
Fabp7	1.12335081	0.971	0.411	8
Vcam1	0.92494878	0.885	0.289	8
Clec1b	0.80773018	0.952	0.332	8
Tk1	0.65210537	0.485	0.096	8
Lyz2	-1.56445465	1	0.999	8
Epb41l3	0.48407053	0.609	0.139	8
Hbegf	0.46248235	0.419	0.072	8
Ccl24	0.99126903	0.875	0.337	8
Cd24a	1.56578493	0.905	0.181	9
Xcr1	1.19222166	0.59	0.012	9
Tnni2	1.10868585	0.811	0.142	9
Sept_6	0.99576958	0.872	0.126	9
H2-Oa	0.94541111	0.703	0.04	9
Amica1	0.8578624	0.74	0.085	9
Flt3	0.85357772	0.746	0.039	9
Gpr171	0.85116606	0.581	0.03	9
H2-DMb2	0.7961426	0.672	0.089	9
Olfm1	0.74129343	0.688	0.099	9
Cd74	1.95243731	1	0.893	10
H2-Aa	1.9845549	0.99	0.72	10
H2-Eb1	2.1508667	0.99	0.631	10
H2-Ab1	1.98153361	0.998	0.762	10
H2-DMb1	1.14454725	0.959	0.567	10
Ciita	0.36698387	0.35	0.053	10
Mgl2	0.40404887	0.144	0.01	10
Ccnd2	0.653666	0.559	0.171	10
Tmem176a	0.96520949	0.755	0.325	10
H2-DMa	0.89037145	0.952	0.709	10
2810417H13Rik	1.82086736	0.982	0.064	11
Stmn1	1.78679578	1	0.18	11
Birc5	1.30693407	0.885	0.059	11
Top2a	1.21478972	0.845	0.064	11
Mki67	1.21327674	0.903	0.067	11
Cks1b	1.13976866	0.989	0.182	11
Smc2	1.12866165	0.968	0.142	11
Cdca3	1.05068616	0.835	0.043	11
Ube2c	0.98119494	0.683	0.051	11
Cdca8	0.79116517	0.813	0.051	11
Malat1	-2.30405907	0.869	1	12
Folr2	1.44452758	0.973	0.422	12

Vsig4	1.36021675	0.986	0.391	12
C1qb	1.34067447	1	0.67	12
C1qa	1.36483044	1	0.614	12
AW112010	1.40751751	0.991	0.701	12
C1qc	1.22409951	1	0.639	12
Cd5l	1.28871347	0.995	0.473	12
Clec4f	1.27367078	0.991	0.432	12
Apoc1	1.37394249	0.995	0.554	12

Appendix 5 Top 10 differentially expressed genes identified for MP clusters 0-12. (genes) name of the gene identified. (avg_log_FC) Fold-change of the average expression between the two groups, positive values indicate a gene is highly expressed in the first group. (pct.1) The percentage of cells where the gene is detected in the first group. (pct.2) The percentage of cells where the gene is detected in the second group. (cluster) MP cluster which the gene corresponds to.

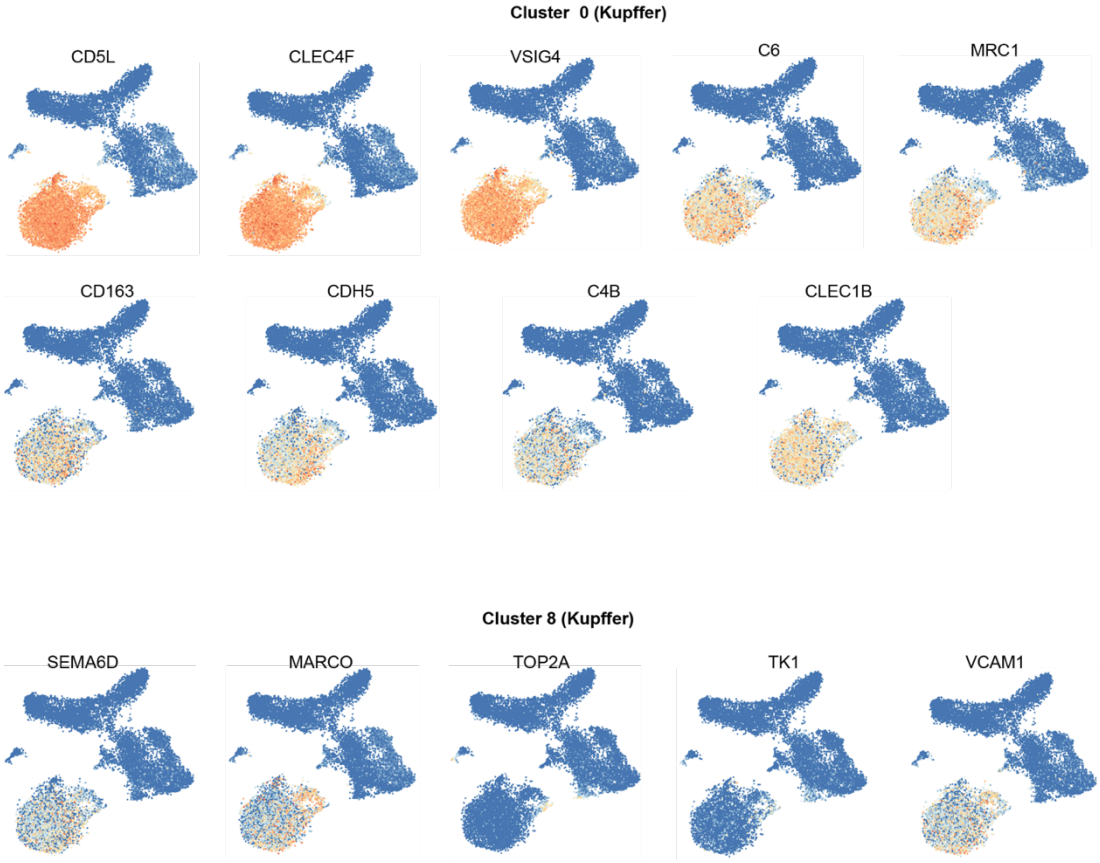

Appendix 6 t-SNE visualization of top markers genes identified for Kupffer clusters: 0, 8.

Cluster 3 (MDM)

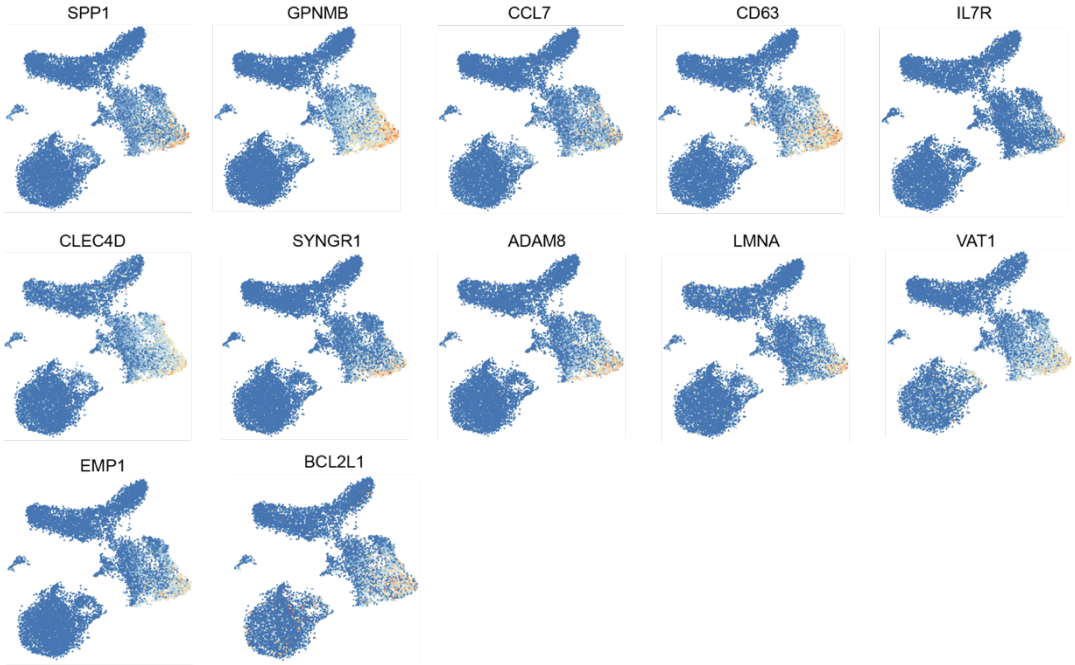

Cluster 4 (MDM)

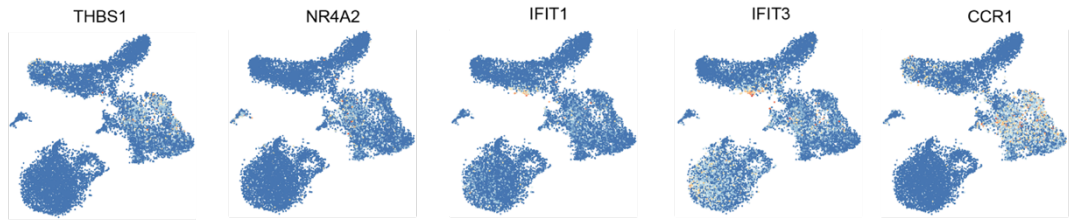

Cluster 5 (MDM)

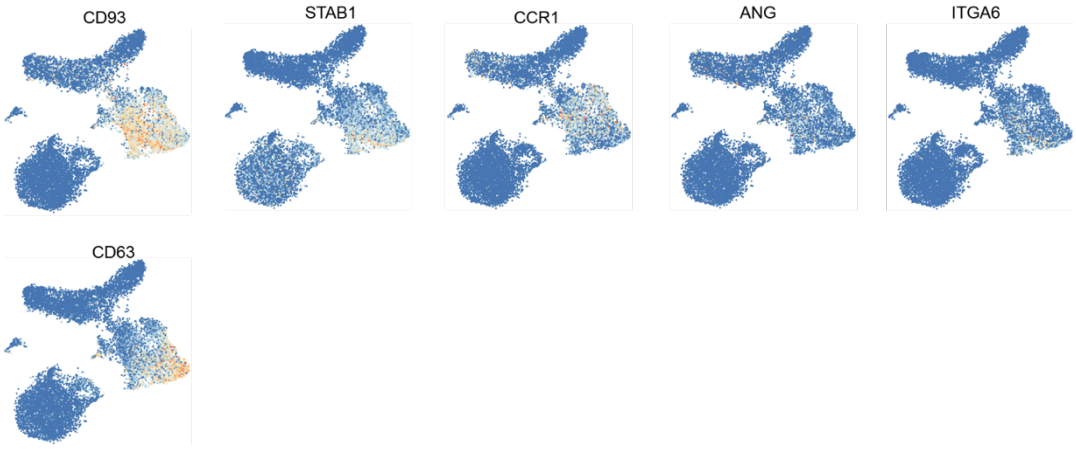

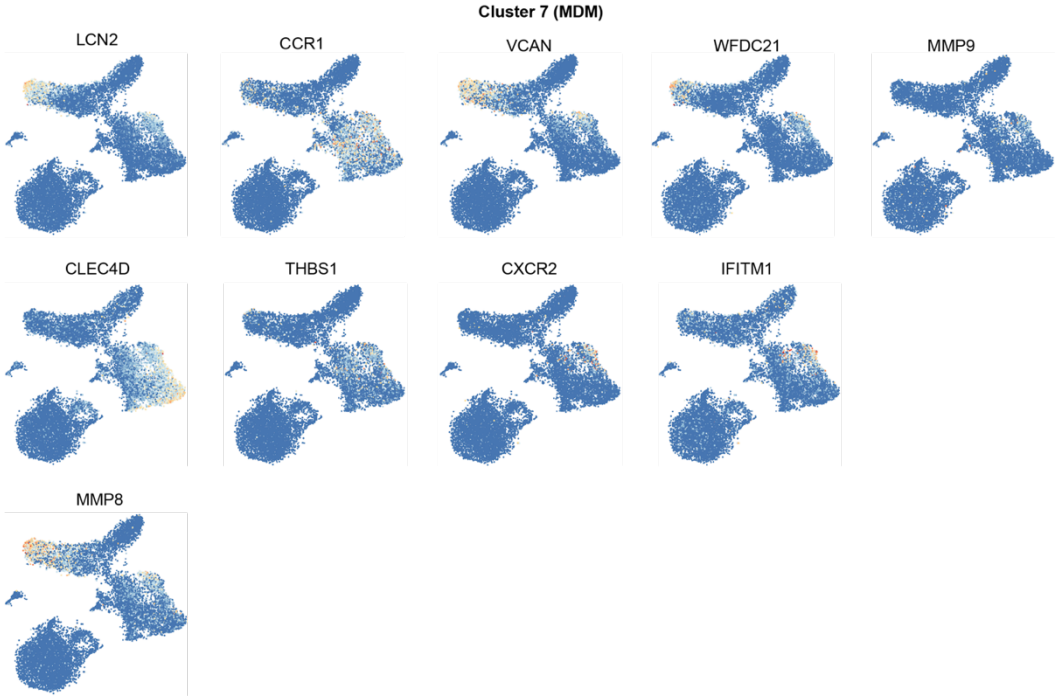

Appendix 7 t-SNE visualization of top marker genes for MDM clusters.

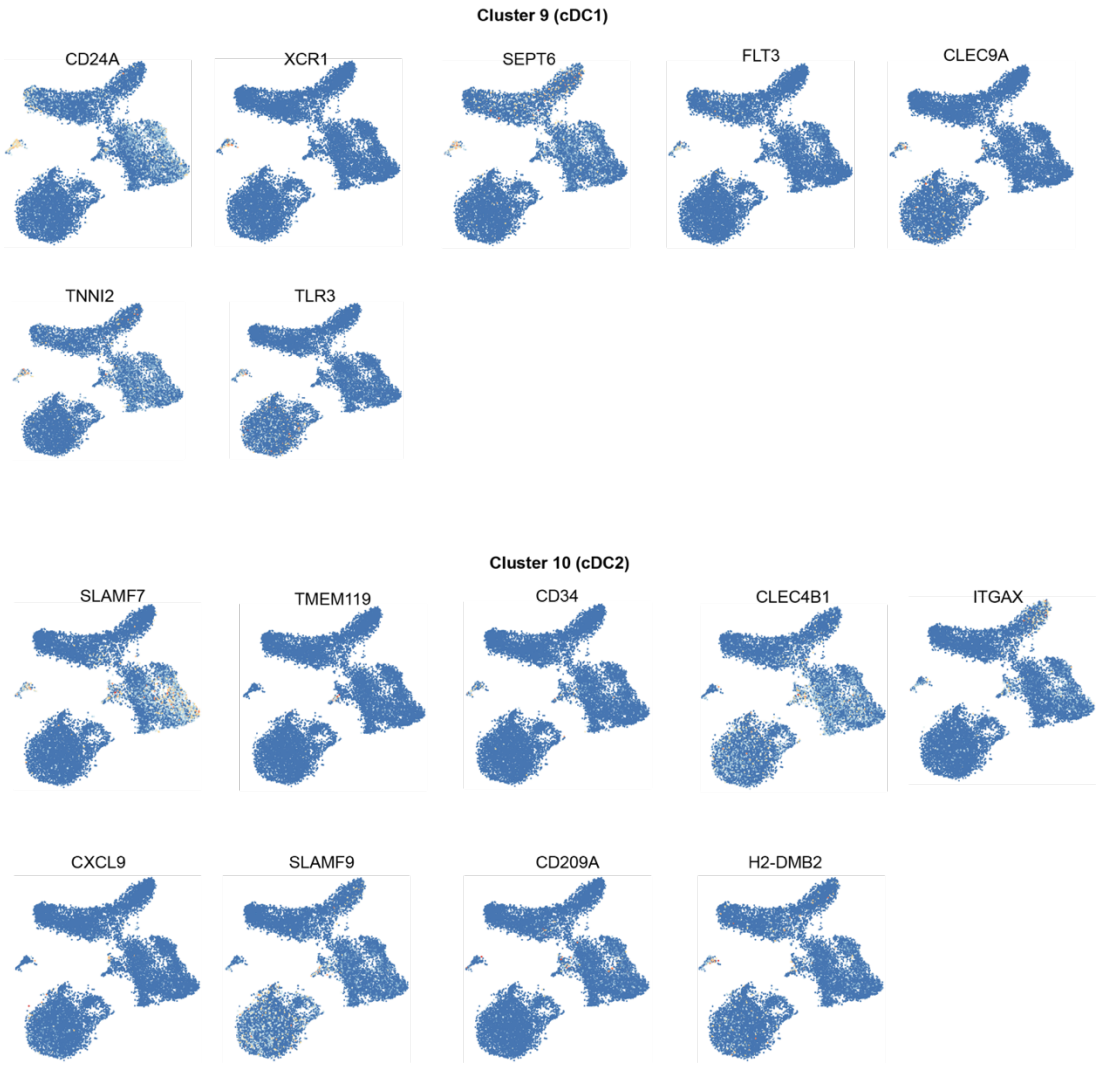

Appendix 8 t-SNE visualization of top marker genes for cDC1 and cDC2 clusters.

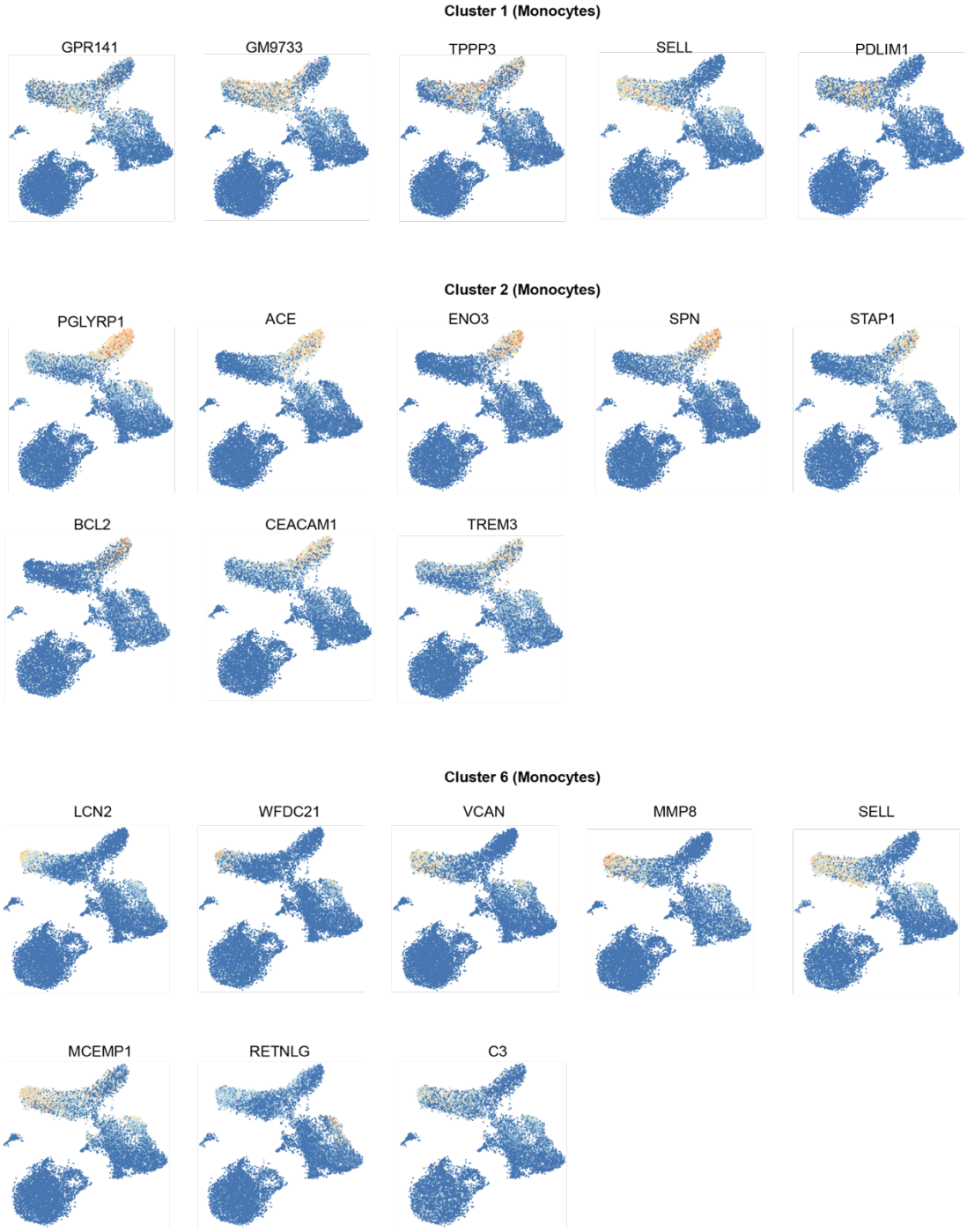

Appendix 9 t-SNE visualization of top marker genes for monocyte clusters

8 Bibliography

Abeles, R. D. *et al.* (2012) 'CD14, CD16 and HLA-DR reliably identifies human monocytes and their subsets in the context of pathologically reduced HLA-DR expression by CD14hi/CD16neg monocytes: Expansion of CD14hi/CD16pos and contraction of CD14lo/CD16pos monocytes in acute liver fail', *Cytometry Part A*, 81 A(10), pp. 823–834. doi: 10.1002/cyto.a.22104.

Aizarani, N. *et al.* (2019) 'A human liver cell atlas reveals heterogeneity and epithelial progenitors', *Nature*, pp. 5–10. doi: 10.1038/s41586-019-1373-2.

Ajami, B. *et al.* (2007) 'Local self-renewal can sustain CNS microglia maintenance and function throughout adult life', *Nature Neuroscience*, 10(12), pp. 1538–1543. doi: 10.1038/nn2014.

Al-mossawi, H. *et al.* (2018) 'Context-specific regulation of monocyte surface IL7R expression and soluble receptor secretion by a common autoimmune risk allele', *bioRxiv*. doi: https://doi.org/10.1101/262410.

Altin, M. *et al.* (1983) 'Neutrophil adherence in chronic liver disease and fulminant hepatic failure', *Gut*, 24(8), pp. 746–750. doi: 10.1136/gut.24.8.746.

Antoniades, C. G. *et al.* (2006) 'Reduced monocyte HLA-DR expression: A novel biomarker of disease severity and outcome in acetaminophen-induced acute liver failure', *Hepatology*, 44(1), pp. 34–43. doi: 10.1002/hep.21240.

Antoniades, C. G. *et al.* (2008) 'The importance of immune dysfunction in determining outcome in acute liver failure q', *Journal of Hepatology*. European Association for the Study of the Liver, 49(5), pp. 845–861. doi: 10.1016/j.jhep.2008.08.009.

Antoniades, C. G. *et al.* (2012) 'Source and Characterization of Hepatic Macrophages in Acetaminophen-Induced Acute Liver Failure in Humans', *Hepatology*, 56(2), pp. 735–746. doi: 10.1002/hep.25657.

Apte, U. *et al.* (2009) 'Beta-catenin activation promotes liver regeneration after acetaminophen-induced injury', *American Journal of Pathology*, 175(3), pp. 1056–1065. doi: 10.2353/ajpath.2009.080976.

Arnold, L. *et al.* (2007) 'Inflammatory monocytes recruited after skeletal muscle injury switch into antiinflammatory macrophages to support myogenesis', *Journal of Experimental Medicine*, 204(5), pp. 1057–1069. doi: 10.1084/jem.20070075.

Asrani, S. K. *et al.* (2019) 'Burden of liver diseases in the world', *Journal of Hepatology*. European Association for the Study of the Liver, 70(1), pp. 151–171. doi: 10.1016/j.jhep.2018.09.014.

Auffray, C. *et al.* (2017) 'Monitoring of Blood Vessels and Tissues by a Population of Monocytes with Patrolling Behavior', *Science*, 317(5838), pp. 666–670.

Auffray, C., Sieweke, M. H. and Geissmann, F. (2009) 'Blood monocytes: development, heterogeneity, and relationship with dendritic cells.', *Annual review of immunology*, 27, pp. 669–92. doi: 10.1146/annurev.immunol.021908.132557.

Bachmann, M., Pfeilschifter, J. and Mühl, H. (2018) 'A prominent role of interleukin-18 in acetaminophen-induced liver injury advocates its blockage for therapy of hepatic necroinflammation', *Frontiers in Immunology*, 9(161), pp. 1–7. doi: 10.3389/fimmu.2018.00161.

Bain, C. C. *et al.* (2014) 'Constant replenishment from circulating monocytes maintains the macrophage pool in the intestine of adult mice', *Nature Immunology*, 15(10), pp. 929–937. doi: 10.1038/ni.2967.

Bain, C. C. *et al.* (2016) 'Long-lived self-renewing bone marrow-derived macrophages displace embryo-derived cells to inhabit adult serous cavities', *Nature Communications*. Nature Publishing Group, 7(May), pp. 1–14. doi: 10.1038/ncomms11852.

Balmer, M. L. *et al.* (2014) 'The liver may act as a firewall mediating mutualism between the host and its gut commensal microbiota', *Science Translational Medicine*, 6(237), pp. 1–11. doi: 10.1126/scitranslmed.3008618.

Beattie, L. *et al.* (2016) 'Bone marrow-derived and resident liver macrophages display unique transcriptomic signatures but similar biological functions', *Journal of Hepatology*. European Association for the Study of the Liver, 65(4), pp. 758–768. doi: 10.1016/j.jhep.2016.05.037.

Bernal, W., Jalan, R., *et al.* (2015) 'Acute-on-chronic liver failure', *The Lancet*. Elsevier Ltd, 386(10003), pp. 1576–1587. doi: 10.1016/S0140-6736(15)00309-8.

Bernal, W., Lee, W. M., *et al.* (2015) 'Acute liver failure: A curable disease by 2024?', *Journal of Hepatology*. European Association for the Study of the Liver, 62(S1), pp. S112–S120. doi: 10.1016/j.jhep.2014.12.016.

Bernal, W. and Wendon, J. (2013) 'Acute liver failure', *N Engl J Med*, 369, pp. 2525–2534. doi: doi: 10.1056/NEJMra1208937.

Bernsmeier, C. *et al.* (2015) 'Patients with acute-on-chronic liver failure have increased numbers of regulatory immune cells expressing the receptor tyrosine kinase MERTK', *Gastroenterology*. Elsevier, Inc, 148(3), pp. 603-615.e14. doi: 10.1053/j.gastro.2014.11.045.

Bernsmeier, C., Antoniades, C. G. and Wendon, J. (2014) 'What ' s new in acute liver failure ?', *Intensive Care Medicine*, 40(10), pp. 1545–1548. doi: 10.1007/s00134-014-3350-4.

Bhushan, B. *et al.* (2014) 'Pro-regenerative signaling after acetaminophen-induced acute liver injury in mice identified using a novel incremental dose model', *American Journal of Pathology*. American Society for Investigative Pathology, 184(11), pp. 3013–3025. doi: 10.1016/j.ajpath.2014.07.019.

Bhushan, B. *et al.* (2017) 'Dual role of epidermal growth factor receptor in liver injury and regeneration after acetaminophen overdose in mice', *Toxicological Sciences*, 155(2), pp. 363–378. doi: 10.1093/toxsci/kfw213.

Bird, T. G. *et al.* (2018) 'TGFβ inhibition restores a regenerative response in

acute liver injury by suppressing paracrine senescence', *Science Translational Medicine*, 10(454), p. eaan1230. doi: 10.1126/scitranslmed.aan1230.

Bjornsson, E., Kalaitzakis, E. and Olsson, R. (2007) 'The impact of eosinophilia and hepatic necrosis on prognosis in patients with drug-induced liver injury', *Alimentary Pharmacology & Therapeutics*, 25(March), pp. 1411–1421. doi: 10.1111/j.1365-2036.2007.03330.x.

Blériot, C. *et al.* (2015) 'Liver-Resident Macrophage Necroptosis Orchestrates Type 1 Microbicidal Inflammation and Type-2-Mediated Tissue Repair during Bacterial Infection', *Immunity*, 42(1), pp. 145–158. doi: 10.1016/j.immuni.2014.12.020.

Blom, K. G. *et al.* (2009) 'Isolation of murine intrahepatic immune cells employing a modified procedure for mechanical disruption and functional characterization of the B, T and natural killer T cells obtained', *Clinical and Experimental Immunology*, 155(2), pp. 320–329. doi: 10.1111/j.1365-2249.2008.03815.x.

Bloomston, M. and Misih, A. (2010) 'Liver Anatomy', *Surg Clin North Am*, 90(4), pp. 1–17. doi: 10.1016/j.suc.2010.04.017.Liver.

Boulter, L., Govaere, O. and Bird, T. (2012) 'Macrophage derived Wnt signalling opposes Notch signalling in a Numb mediated manner to specify HPC fate in chronic liver disease in human and mouse', *Nature …*, 18(4), pp. 572–579. doi: 10.1038/nm.2667.Macrophage.

Bourdi, M. *et al.* (2002) 'Protection Against Acetaminophen-Induced Liver Injury and Lethality by Interleukin 10: Role of Inducible Nitric Oxide Synthase', *Hepatology*, 35(2), pp. 289–298. doi: 10.1053/jhep.2002.30956.

Camp, J. G. *et al.* (2017) 'Multilineage communication regulates human liver bud development from pluripotency', *Nature*. Nature Publishing Group, 546(7659), pp. 533–538. doi: 10.1038/nature22796.

Campana, L. *et al.* (2018) 'The STAT3–IL-10–IL-6 Pathway Is a Novel Regulator of Macrophage Efferocytosis and Phenotypic Conversion in Sterile Liver Injury', *The Journal of Immunology*, 200(3), pp. 1169–1187. doi: 10.4049/jimmunol.1701247.

Carlin, L. M. *et al.* (2013) 'Nr4a1-dependent Ly6Clow monocytes monitor endothelial cells and orchestrate their disposal', *Cell*. Elsevier Inc., 153(2), pp. 362–375. doi: 10.1016/j.cell.2013.03.010.

Carotta, S. *et al.* (2010) 'The transcription factor PU.1 controls dendritic cell development and Flt3 cytokine receptor expression in a dose-dependent manner', *Immunity*. Elsevier Ltd, 32(5), pp. 628–641. doi: 10.1016/j.immuni.2010.05.005.

Cassado, A. A., D'Império Lima, M. R. and Bortoluci, K. R. (2015) 'Revisiting mouse peritoneal macrophages: Heterogeneity, development, and function', *Frontiers in Immunology*, 6(MAY), pp. 1–9. doi: 10.3389/fimmu.2015.00225.

Castellaneta, A. *et al.* (2006) 'Functional modification of CD11c+ liver dendritic cells during liver regeneration after partial hepatectomy in mice', *Hepatology*, 43(4), pp. 807–816. doi: 10.1002/hep.21098.

Chen, G. Y. *et al.* (2009) 'CD24 and siglec-10 selectively repress tissue

damage - Induced immune responses', *Science*, 323(5922), pp. 1722–1725. doi: 10.1126/science.1168988.
Chen, H., Ye, F. and Guo, G. (2019) 'Revolutionizing immunology with single-cell RNA sequencing', *Cellular and Molecular Immunology*. Springer US, 16(3), pp. 242–249. doi: 10.1038/s41423-019-0214-4.
Chen, Z. *et al.* (2013) 'The novel role of IL-7 ligation to IL-7R in myeloid cells of rheumatoid arthritis and collagen induced arthritis', *J Immunol*, 190(10), pp. 5256–5266. doi: 10.1371/journal.pone.0178059.
Chiu, H. *et al.* (2003) 'Role of tumor necrosis factor receptor 1 (p55) in hepatocyte proliferation during acetaminophen-induced toxicity in mice', *Toxicology and Applied Pharmacology*, 193(2), pp. 218–227. doi: 10.1016/j.taap.2003.07.003.
Choi, Y. H. and Kim, J. K. (2019) 'Dissecting cellular heterogeneity using single-cell RNA sequencing', *Molecules and Cells*, 42(3), pp. 189–199. doi: 10.14348/molcells.2019.2446.
Clemons, N. J. *et al.* (2017) 'Inhibiting system xC− and glutathione biosynthesis–a potential Achilles' heel in mutant-p53 cancers', *Molecular and Cellular Oncology*. Taylor & Francis, 4(5), pp. 1–3. doi: 10.1080/23723556.2017.1344757.
Collins, C. *et al.* (1996) 'RAGl, RAG2 and pre-T cell receptor a chain expression by adult human hepatic T cells: evidence for extrathymic T cell maturation', *European journal of immunology*, 26, pp. 3114–3118.
Colonna, M. and Butovsky, O. (2017) 'Microglia Function in the Central Nervous System During Health and Neurodegeneration', *Annual Review of Immunology*, 35(1), pp. 441–468. doi: 10.1146/annurev-immunol-051116-052358.
Connolly, M. K. *et al.* (2011) 'Dendritic Cell Depletion Exacerbates Acetaminophen Hepatotoxicity', *Hepatology*, 54(3), pp. 959–968. doi: 10.1002/hep.24429.
Cressman, D. E. *et al.* (1996) 'Liver failure and defective hepatocyte regeneration in interleukin-6- deficient mice', *Science*, 274(5291), pp. 1379–1383. doi: 10.1126/science.274.5291.1379.
Dai, C. *et al.* (2018) 'Chloroquine ameliorates carbon tetrachloride-induced acute liver injury in mice via the concomitant inhibition of inflammation and induction of apoptosis', *Cell Death and Disease*. Springer US, 9(12). doi: 10.1038/s41419-018-1136-2.
Dai, X. M. *et al.* (2002) 'Targeted disruption of the mouse colony-stimulating factor 1 receptor gene results in osteopetrosis, mononuclear phagocyte deficiency, increased primitive progenitor cell frequencies, and reproductive defects', *Blood*, 99(1), pp. 111–120. doi: 10.1182/blood.V99.1.111.
DeKoter, R. P. and Singh, H. (2000) 'Regulation of B lymphocyte and macrophage development by graded expression of PU.1', *Science*, 288(5470), pp. 1439–1442. doi: 10.1126/science.288.5470.1439.
Duana, L. *et al.* (2016) 'Differential Susceptibility to Acetaminophen-Induced Liver Injury in Sub-Strains of C57BL/6 Mice: 6N versus 6J', *Food Chem Toxicol.*, 98, pp. 139–148. doi: 10.1016/j.physbeh.2017.03.040.
El-Serafi, I. *et al.* (2018) 'The effect of N-acetyl-l-cysteine (NAC) on liver toxicity

and clinical outcome after hematopoietic stem cell transplantation', *Scientific Reports*, 8(1), pp. 6–15. doi: 10.1038/s41598-018-26033-z.
Epelman, S. *et al.* (2014) 'Embryonic and adult-derived resident cardiac macrophages are maintained through distinct mechanisms at steady state and during inflammation', *Immunity*. Elsevier Inc., 40(1), pp. 91–104. doi: 10.1016/j.immuni.2013.11.019.
Fernández, A. and Vendrell, M. (2016) 'Smart fluorescent probes for imaging macrophage activity', *Chemical Society Reviews*, 45(5), pp. 1182–1196. doi: 10.1039/c5cs00567a.
Fisher, J. E. *et al.* (2013) 'Role of Kupffer cells and toll-like receptor 4 in acetaminophen-induced acute liver failure', *Journal of Surgical Research*. Elsevier Ltd, 180(1), pp. 147–155. doi: 10.1016/j.jss.2012.11.051.
Forbes, S. J. and Newsome, P. N. (2016) 'Liver regeneration-mechanisms and models to clinical application', *Nature Reviews Gastroenterology and Hepatology*, 13(8), pp. 473–485. doi: 10.1038/nrgastro.2016.97.
Friedman, S. L. *et al.* (2018) 'A randomized, placebo-controlled trial of cenicriviroc for treatment of nonalcoholic steatohepatitis with fibrosis', *Hepatology*, 67(5), pp. 1754–1767. doi: 10.1002/hep.29477.
Fry, T. J. and Mackall, C. L. (2009) 'Interleukin-7 : from bench to clinic Review article Interleukin-7 : from bench to clinic', *Blood*, 99(11), pp. 3892–3904. doi: 10.1182/blood.V99.11.3892.
Fujimori, T. *et al.* (2015) 'The Axl receptor tyrosine kinase is a discriminator of macrophage function in the inflamed lung', *Mucosal Immunology*, 8(5), pp. 1021–1030. doi: 10.1038/mi.2014.129.
Fujiyama, S. *et al.* (2018) 'Identification and isolation of splenic tissue-resident macrophage sub-populations by flow cytometry', *International Immunology*, 31(1), pp. 51–56. doi: 10.1093/intimm/dxy064.
Gao, B. (2016) 'Basic liver immunology', *Cellular and Molecular Immunology*. Nature Publishing Group, 13(3), pp. 265–266. doi: 10.1038/cmi.2016.09.
Geissmann, F. *et al.* (2010) 'Development of monocytes, macrophages and dendritic cells', *Science*, 327(5966), pp. 656–661. doi: 10.1126/science.1178331.Development.
Geissmann, F., Jung, S. and Littman, D. R. (2003) 'Blood Monocytes Consist of Two Principal Subsets with Distinct Migratory Properties', *Immunity*, 19, pp. 71–82.
Ginhoux, F. *et al.* (2010) 'Fate Mapping Analysis Reveals That Adult Microglia Derive from Primitive Macrophages', 330(6005), pp. 841–845.
Ginhoux, F. *et al.* (2016) 'New insights into the multidimensional concept of macrophage ontogeny, activation and function', *Nature Immunology*, 17(1), pp. 34–40. doi: 10.1038/ni.3324.
Ginhoux, F. and Guilliams, M. (2016) 'Tissue-Resident Macrophage Ontogeny and Homeostasis', *Immunity*. Elsevier Inc., 44(3), pp. 439–449. doi: 10.1016/j.immuni.2016.02.024.
Ginhoux, F. and Jung, S. (2014) 'Monocytes and macrophages: Developmental pathways and tissue homeostasis', *Nature Reviews Immunology*. Nature Publishing Group, 14(6), pp. 392–404. doi:

10.1038/nri3671.
Goh, Y. P. S. *et al.* (2013) 'Eosinophils secrete IL-4 to facilitate liver regeneration', *Proceedings of the National Academy of Sciences*, 110(24), pp. 9914–9919. doi: 10.1073/pnas.1304046110.
Gomez Perdiguero, E. *et al.* (2015) 'Tissue-resident macrophages originate from yolk-sac-derived erythro-myeloid progenitors', *Nature*. Nature Publishing Group, 518(7540), pp. 547–551. doi: 10.1038/nature13989.
Gow, D. J. *et al.* (2014) 'Characterisation of a novel fc conjugate of macrophage colony-stimulating factor', *Molecular Therapy*, 22(9), pp. 1580–1592. doi: 10.1038/mt.2014.112.
Grabiec, A. M. *et al.* (2018) 'Axl and MerTK receptor tyrosine kinases maintain human macrophage efferocytic capacity in the presence of viral triggers', *European Journal of Immunology*, 48(5), pp. 855–860. doi: 10.1002/eji.201747283.
Graubardt, N. *et al.* (2017) 'Ly6Chi Monocytes and Their Macrophage Descendants Regulate Neutrophil Function and Clearance in Acetaminophen-Induced Liver Injury', *Frontiers in immunology*, 8(626), pp. 1–17. doi: 10.3389/fimmu.2017.00626.
Greenhalgh, S. N., Conroy, K. P. and Henderson, N. C. (2015) 'Cre-ativity in the Liver: Transgenic Approaches to Targeting Hepatic Nonparenchymal Cells', *Hepatology*, 61(6), pp. 2091–2099. doi: 10.1002/hep.27606.
Greenlee-Wacker, M. (2016) 'Clearance of apoptotic neutrophils and resolution of inflammation', *Immunol Rev*, 273(1), pp. 357–370. doi: 110.1016/j.bbi.2017.04.008.
Grün, D. *et al.* (2015) 'Single-cell messenger RNA sequencing reveals rare intestinal cell types', *Nature*, 525(7568), pp. 251–255. doi: 10.1038/nature14966.
Guilliams, M. *et al.* (2013) 'Alveolar macrophages develop from fetal monocytes that differentiate into long-lived cells in the first week of life via GM-CSF', *Journal of Experimental Medicine*, 210(10), pp. 1977–1992. doi: 10.1084/jem.20131199.
Guilliams, M. (2014) 'Dendritic cells, monocytes and macrophages: a unified nomenclature based on ontogeny', *Nature Reviews Immunology*, 14(8), pp. 571–578. doi: 10.1016/j.physbeh.2017.03.040.
Guilliams, M. and van de Laar, L. (2015) 'A hitchhiker's guide to myeloid cell subsets: Practical implementation of a novel mononuclear phagocyte classification system', *Frontiers in Immunology*, 6(JUL), pp. 1–12. doi: 10.3389/fimmu.2015.00406.
Guilliams, M., Mildner, A. and Yona, S. (2018) 'Developmental and Functional Heterogeneity of Monocytes', *Immunity*. Elsevier Inc., 49(4), pp. 595–613. doi: 10.1016/j.immuni.2018.10.005.
Guillot, A. and Tacke, F. (2019) 'Liver Macrophages: Old Dogmas and New Insights', *Hepatology Communications*, 3(6), pp. 730–743. doi: 10.1002/hep4.1356.
Haghverdi, L. *et al.* (2016) 'Diffusion pseudotime robustly reconstructs lineage branching', *Nature Methods*, 13(10), pp. 845–848. doi: 10.1038/nmeth.3971.

Haimon, Z. *et al.* (2018) 'Re-evaluating microglia expression profiles using RiboTag and cell isolation strategies /631/1647/2017 /631/1647/2017/2079 technical-report', *Nature Immunology*. Springer US, 19(6), pp. 636–644. doi: 10.1038/s41590-018-0110-6.

Hashimoto, D. *et al.* (2013) 'Tissue-resident macrophages self-maintain locally throughout adult life with minimal contribution from circulating monocytes', *Immunity*, 38(4), pp. 792–804. doi: 10.1016/j.immuni.2013.04.004.

Healy, L. M. *et al.* (2016) 'MerTK Is a Functional Regulator of Myelin Phagocytosis by Human Myeloid Cells', *The Journal of Immunology*, 196(8), pp. 3375–3384. doi: 10.4049/jimmunol.1502562.

Hettinger, J. *et al.* (2013) 'Origin of monocytes and macrophages in a committed progenitor', *Nature Immunology*, 14(8), pp. 821–830. doi: 10.1038/ni.2638.

Heymann, F. and Tacke, F. (2016) 'Immunology in the liver — from homeostasis to disease', *Nature Publishing Group*. Nature Publishing Group, 13(2), pp. 88–110. doi: 10.1038/nrgastro.2015.200.

Hochreiter-Hufford, A. and Ravichandran, K. S. (2013) 'Clearing the dead: Apoptotic cell sensing, recognition, engulfment, and digestion', *Cold Spring Harbor Perspectives in Biology*, 5(1). doi: 10.1101/cshperspect.a008748.

Hoeffel, G. *et al.* (2015) 'C-Myb+ Erythro-Myeloid Progenitor-Derived Fetal Monocytes Give Rise to Adult Tissue-Resident Macrophages', *Immunity*, 42(4), pp. 665–678. doi: 10.1097/CCM.0b013e31823da96d.Hydrogen.

Hogaboam, C. M. *et al.* (2000) 'Exaggerated Hepatic Injury Due to Acetaminophen Challenge in Mice Lacking C-C Chemokine Receptor 2', *The American Journal of Pathology*. American Society for Investigative Pathology, 156(4), pp. 1245–1252. doi: 10.1016/S0002-9440(10)64995-4.

Holt, M. P., Cheng, L. and Ju, C. (2008) 'Identification and characterization of infiltrating macrophages in acetaminophen-induced liver injury', *J Leukoc Biol*, 84(6), pp. 1410–1421. doi: 10.1189/jlb.0308173.

Hosoya, S. *et al.* (2013) 'Innate immune responses involving natural killer and natural killer T cells promote liver regeneration after partial hepatectomy in mice.', *American journal of physiology. Gastrointestinal and liver physiology*, 304(3), pp. G293-9. doi: 10.1152/ajpgi.00083.2012.

Hu, J. *et al.* (2015) 'Efficacy and safety of acetylcysteine in "non-acetaminophen" acute liver failure: A meta-analysis of prospective clinical trials', *Clinics and Research in Hepatology and Gastroenterology*. Elsevier Masson SAS, 39(5), pp. 594–599. doi: 10.1016/j.clinre.2015.01.003.

Huang, W., Febbraio, M. and Silverstein, R. L. (2011) 'CD9 tetraspanin interacts with CD36 on the surface of macrophages: A possible regulatory influence on uptake of oxidized low density lipoprotein', *PLoS ONE*, 6(12). doi: 10.1371/journal.pone.0029092.

Hume, D. A. (2006) 'The mononuclear phagocyte system', *Current Opinion in Immunology*, 18(1), pp. 49–53. doi: 10.1016/j.coi.2005.11.008.

Hume, D. A. and MacDonald, K. P. A. (2012) 'Therapeutic applications of macrophage colony-stimulating factor-1 (CSF-1) and antagonists of CSF-1 receptor (CSF-1R) signaling', *Blood*, 119(8), pp. 1810–1820. doi: 10.1182/blood-2011-09-379214.

Hwang, B., Lee, J. H. and Bang, D. (2018) 'Single-cell RNA sequencing technologies and bioinformatics pipelines', *Experimental and Molecular Medicine*. Springer US, 50(8). doi: 10.1038/s12276-018-0071-8.

Ikeda, N. *et al.* (2018) 'Emergence of immunoregulatory Ym1+Ly6Chi monocytes during recovery phase of tissue injury', *Science Immunology*, 3(28), pp. 1–14. doi: 10.1126/sciimmunol.aat0207.

Imaeda, A. B. *et al.* (2009) 'Acetaminophen-induced hepatotoxicity in mice is dependent on Tlr9 and the Nalp3 inflammasome', *Journal of Clinical Investigation*, 119(2), pp. 305–314. doi: 10.1172/JCI35958.

Ingersoll, M. A. *et al.* (2009) 'Comparison of gene expression profiles between human and mouse monocyte subsets (Blood (2010) 115, 3 (e10-e19))', *Blood*, 115(3). doi: 10.1182/blood-2010-06-290122.

Ishida, Y. *et al.* (2002) 'A pivotal involvement of IFN-γ in the pathogenesis of acetaminophen-induced acute liver injury', *FASEB Journal*, 16(10), pp. 1227–1236. doi: 10.1096/fj.02-0046com.

Ishida, Y. *et al.* (2006) 'Opposite roles of neutrophils and macrophages in the pathogenesis of acetaminophen-induced acute liver injury', *European Journal of Immunology*, 36(4), pp. 1028–1038. doi: 10.1002/eji.200535261.

Jaeschke, H., Xie, Y. and Mcgill, M. R. (2014) 'Acetaminophen-induced Liver Injury : from Animal Models to Humans', *Journal of Clinical and Translational Hepatology*, 2(3), pp. 153–161. doi: 10.14218/JCTH.2014.00014.

James, L. P. *et al.* (2003) 'Interleukin 6 and hepatocyte regeneration in acetaminophen toxicity in the mouse', *Biochemical and Biophysical Research Communications*, 309(4), pp. 857–863. doi: 10.1016/j.bbrc.2003.08.085.

Jarido, V. *et al.* (2017) 'The emerging role of mast cells in liver disease', *American Journal of Physiology - Gastrointestinal and Liver Physiology*, 313(2), pp. G89–G101. doi: 10.1152/ajpgi.00333.2016.

Jenne, C. N. and Kubes, P. (2013) 'Immune surveillance by the liver', *Nature Immunology*, 14(10), pp. 996–1006. doi: 10.1038/ni.2691.

Ju, C. *et al.* (2002) 'Protective role of kupffer cells in acetaminophen-induced hepatic injury in mice', *Chemical Research in Toxicology*, 15(12), pp. 1504–1513. doi: 10.1021/tx0255976.

Ju, C. and Tacke, F. (2016) 'Hepatic macrophages in homeostasis and liver diseases: from pathogenesis to novel therapeutic strategies', *Cellular and Molecular Immunology*. Nature Publishing Group, 13(October 2015), pp. 1–12. doi: 10.1038/cmi.2015.104.

Keren-Shaul, H. *et al.* (2017) 'A Unique Microglia Type Associated with Restricting Development of Alzheimer's Disease', *Cell*. Elsevier, 169(7), pp. 1276-1290.e17. doi: 10.1016/j.cell.2017.05.018.

Kietzmann, T. (2017) 'Metabolic zonation of the liver: The oxygen gradient revisited', *Redox Biology*. Elsevier B.V., 11(December 2016), pp. 622–

630. doi: 10.1016/j.redox.2017.01.012.
Kinchen, J. M. and Ravichandran, K. S. (2008) *Phagosome maturation: Going through the acid test*, *Nature Reviews Molecular Cell Biology*. doi: 10.1038/nrm2515.
Knoll, P. *et al.* (1995) 'Human Kupffer cells secrete IL-10 in response to lipopolysaccharide (LPS) challenge', *Journal of Hepatology*, 22(2), pp. 226–229. doi: 10.1016/0168-8278(95)80433-1.
Koizumi, S. *et al.* (2007) 'UDP acting at P2Y6 receptors is a mediator of microglial phagocytosis', *Nature*, 446(7139), pp. 1091–1095. doi: 10.1038/jid.2014.371.
Krenkel, O. *et al.* (2019) 'Myeloid cells in liver and bone marrow acquire a functionally distinct inflammatory phenotype during obesity-related steatohepatitis', *Gut*, pp. 1–13. doi: 10.1136/gutjnl-2019-318382.
Kukurba, K. R. and Montgomery, S. B. (2015) 'RNA Sequencing and Analysis', *Cold Spring Harbor protocols*, 2015(11), pp. 951–69. doi: 10.1101/pdb.top084970.RNA.
Lauwerys, B. R. *et al.* (2000) 'Cytokine Production and Killer Activity of NK/T-NK Cells Derived with IL-2, IL-15, or the Combination of IL-12 and IL-18', *The Journal of Immunology*, 165(4), pp. 1847–1853. doi: 10.4049/jimmunol.165.4.1847.
Lefebvre, E. *et al.* (2016) 'Antifibrotic effects of the dual CCR2/CCR5 antagonist cenicriviroc in animal models of liver and kidney fibrosis', *PLoS ONE*, 11(6), pp. 1–19. doi: 10.1371/journal.pone.0158156.
Leung, G. *et al.* (2019) 'The lymphoid-associated interleukin 7 receptor (IL-7R) regulates tissue resident macrophage development', *bioRxiv*, p. 534859. doi: 10.1101/534859.
Lever, J. M. *et al.* (2019) 'Resident macrophages reprogram toward a developmental state after acute kidney injury', *JCI Insight*, 4(2). doi: 10.1172/jci.insight.125503.
Li, B., Castano, A. P., Hudson, T. E., Nowlin, B. T., Lin, S. L., *et al.* (2010) 'The melanoma-associated transmembrane glycoprotein Gpnmb controls trafficking of cellular debris for degradation and is essential for tissue repair', *FASEB Journal*, 24(12), pp. 4767–4781. doi: 10.1096/fj.10-154757.
Li, B., Castano, A. P., Hudson, T. E., Nowlin, B. T., Lin, S.-L., *et al.* (2010) 'The melanoma-associated transmembrane glycoprotein Gpnmb controls trafficking of cellular debris for degradation and is essential for tissue repair', *The FASEB Journal*, 24(12), pp. 4767–4781. doi: 10.1096/fj.10-154757.
Li, W. (2012) 'Eat-me signals: Keys to molecular phagocyte biology and "appetite" control', *J Cell Physiol.*, 227(4), pp. 1291–1297. doi: 10.1002/jcp.22815.Eat-me.
Liew, P. X., Lee, W. Y. and Kubes, P. (2017) 'iNKT Cells Orchestrate a Switch from Inflammation to Resolution of Sterile Liver Injury', *Immunity*. Elsevier Inc., 47(4), pp. 752-765.e5. doi: 10.1016/j.immuni.2017.09.016.
Limaye, P. B. *et al.* (2003) 'Calpain released from dying hepatocytes mediates progression of acute liver injury induced by model hepatotoxicants',

Toxicology and Applied Pharmacology, 191(3), pp. 211–226. doi: 10.1016/S0041-008X(03)00250-3.

Liu, Z. X. *et al.* (2006) 'Neutrophil depletion protects against murine acetaminophen hepatotoxicity', *Hepatology*, 43(6), pp. 1220–1230. doi: 10.1002/hep.21175.

Lu, W. Y. *et al.* (2015) 'Hepatic progenitor cells of biliary origin with liver repopulation capacity', *Nature Cell Biology*, 17(8), pp. 973–983. doi: 10.1038/ncb3203.

Lundbäck, P. *et al.* (2016) 'A novel high mobility group box 1 neutralizing chimeric antibody attenuates drug-induced liver injury and postinjury inflammation in mice', *Hepatology*, 64(5), pp. 1699–1710. doi: 10.1002/hep.28736.

Lynch, R. W. *et al.* (2018) 'An efficient method to isolate Kupffer cells eliminating endothelial cell contamination and selective bias', *Journal of Leukocyte Biology*, 104(3), pp. 579–586. doi: 10.1002/JLB.1TA0517-169R.

Macaulay, I. C. *et al.* (2016) 'Single-Cell RNA-Sequencing Reveals a Continuous Spectrum of Differentiation in Hematopoietic Cells', *Cell Reports*. The Authors, 14(4), pp. 966–977. doi: 10.1016/j.celrep.2015.12.082.

MacDonald, R. A. (1961) '" Lifespan " of Liver Cells Autoradiographic Study Using Tritiated Thymidine in Normal, Cirrhotic, and Partially Hepatectomized Rats', *Archives of Internal Medicine*, 107(3), pp. 335–343.

MacParland, S. A. *et al.* (2018) 'Single cell RNA sequencing of human liver reveals distinct intrahepatic macrophage populations', *Nature Communications*, 9(1), pp. 1–21. doi: 10.1038/s41467-018-06318-7.

Manno, G. La *et al.* (2018) 'RNA velocity of single cells', *Nature*, 560(7719), pp. 494–498. doi: 10.1038/s41586-018-0414-6.RNA.

Mantovani, A. *et al.* (2002) 'macrophase polarization TAMS paradigm for polarized M2 mononuclear phagocytes', *TRENDS in Immunology*, 23(11), pp. 549–556. Available at: http://immunology.trends.com.

Markose, D. *et al.* (2018) 'Immune cell regulation of liver regeneration and repair', *Journal of Immunology and Regenerative Medicine*. Elsevier Ltd, 2, pp. 1–10. doi: 10.1016/j.regen.2018.03.003.

Marques, P. E. *et al.* (2012) 'Chemokines and Mitochondrial Products Activate Neutrophils to Amplify Organ Injury During Mouse Acute Liver Failure', *Hepatology*, 56(5), pp. 1971–1982. doi: 10.1002/hep.25801.

Marques, P. E. *et al.* (2015) 'Hepatic DNA deposition drives drug-induced liver injury and inflammation in mice', *Hepatology*, 61(1), pp. 348–360. doi: 10.1002/hep.27216.

Martin-Murphy, B. V., Holt, M. P. and Ju, C. (2010) 'The role of damage associated molecular pattern molecules in acetaminophen-induced liver injury in mice', *Toxicology Letters*. Elsevier Ireland Ltd, 192(3), pp. 387–394. doi: 10.1016/j.toxlet.2009.11.016.

Mass, E. *et al.* (2016) 'Specification of tissue-resident macrophages during organogenesis', *Science (New York, N.Y.)*, 353(6304). doi: 10.1126/science.aaf4238.

Masubuchi, Y., Sugiyama, S. and Horie, T. (2009) 'Th1 / Th2 cytokine balance as a determinant of acetaminophen-induced liver injury', *Chemico-Biological Interactions*, 179(2–3), pp. 273–279. doi: 10.1016/j.cbi.2008.10.028.

McGill, M. R. (2016) 'The past and present of serum aminotransferases and the future of liver injury biomarkers.', *EXCLI journal*, 15, pp. 817–828. doi: 10.17179/excli2016-800.

Mederacke, I. *et al.* (2015) 'High-yield and high-purity isolation of hepatic stellate cells from normal and fibrotic mouse livers', *Nature Protocols*, 10(2), pp. 305–315. doi: 10.1016/j.physbeh.2017.03.040.

Menezes, S. *et al.* (2016) 'The Heterogeneity of Ly6Chi Monocytes Controls Their Differentiation into iNOS+ Macrophages or Monocyte-Derived Dendritic Cells', *Immunity*, 45(6), pp. 1205–1218. doi: 10.1016/j.immuni.2016.12.001.

Merad, M. *et al.* (2002) 'Langerhans cells renew in the skin throughout life under steady-state conditions', *Nature Immunology*, 3(12), pp. 1135–1141. doi: 10.1038/ni852.

Michael, S. L. *et al.* (1999) 'Pretreatment of mice with macrophage inactivators decreases acetaminophen hepatotoxicity and the formation of reactive oxygen and nitrogen species', *Hepatology*, 30(1), pp. 186–195. doi: 10.1002/hep.510300104.

Michalopoulos, G. K. (2007) 'Liver regeneration', *Journal of Cellular Physiology*, 213(2), pp. 286–300. doi: 10.1002/jcp.21172.

Michalopoulos, G. K. (2017) 'Hepatostat: Liver regeneration and normal liver tissue maintenance', *Hepatology*, 65(4), pp. 1384–1392. doi: 10.1002/hep.28988.

Mildner, A. *et al.* (2017) 'Genomic Characterization of Murine Monocytes Reveals C/EBPβ Transcription Factor Dependence of Ly6C− Cells', *Immunity*, 46(5), pp. 849-862.e7. doi: 10.1016/j.immuni.2017.04.018.

Mills, C. D. *et al.* (2000) 'M-1/M-2 Macrophages and the Th1/Th2 Paradigm', *The Journal of Immunology*, 164(12), pp. 6166–6173. doi: 10.4049/jimmunol.164.12.6166.

Miragaia, R. J. *et al.* (2019) 'Single-Cell Transcriptomics of Regulatory T Cells Reveals Trajectories of Tissue Adaptation', *Immunity*, 50(2), pp. 493-504.e7. doi: 10.1016/j.immuni.2019.01.001.

Mitchell, C. and Willenbring, H. (2008) 'A reproducible and well-tolerated method for 2/3 partial hepatectomy in mice', *Nature Protocols*. Nature Publishing Group, 3(7), pp. 1167–1170. doi: 10.1038/nprot.2008.80.

Mohar, I. *et al.* (2014) 'Acetaminophen-induced liver damage in mice is associated with gender-specific adduction of peroxiredoxin-6', *Redox Biology*. Elsevier, 2(1), pp. 377–387. doi: 10.1016/j.redox.2014.01.008.

Moles, A. *et al.* (2014) 'A TLR2/S100A9/CXCL-2 signaling network is necessary for neutrophil recruitment in acute and chronic liver injury in the mouse', *Journal of Hepatology*. European Association for the Study of the Liver, 60(4), pp. 782–791. doi: 10.1016/j.jhep.2013.12.005.

Moore, J. K. *et al.* (2017) 'Patients with the worst outcomes after paracetamol (acetaminophen)-induced liver failure have an early monocytopenia', *Alimentary Pharmacology and Therapeutics*, 45(3), pp. 443–454. doi:

10.1111/apt.13878.
Moroni, F. *et al.* (2019) 'Safety profile of autologous macrophage therapy for liver cirrhosis', *Nature Medicine*. Springer US, 25(10), pp. 1560–1565. doi: 10.1038/s41591-019-0599-8.
Mossanen, jc and Tacke, f. (2015) 'Acetaminophen-induced acute liver injury in mice', *Laboratory Animals*, 49, pp. 30–36. doi: 10.1177/0023677215570992.
Mossanen, J. C. *et al.* (2016) 'Chemokine (C-C Motif) Receptor 2–Positive Monocytes Aggravate the Early Phase of Acetaminophen-Induced Acute Liver Injury', *Hepatology*, 64(5), pp. 1667–1682. doi: 10.1002/hep.28682.
Mota, M. *et al.* (2017) 'IL-33 signalling in liver immune cells enhances drug-induced liver injury and inflammation', *Inflammation Research*. Springer International Publishing, (0), p. 0. doi: 10.1007/s00011-017-1098-3.
Nagasue, N. *et al.* (1987) 'Human liver regeneration after major hepatic resection. A study of normal liver and livers with chronic hepatitis and cirrhosis', *Annals of Surgery*, 206(1), pp. 30–39.
Nahrendorf, M. *et al.* (2007) 'The healing myocardium sequentially mobilizes two monocyte subsets with divergent and complementary functions', *Journal of Experimental Medicine*, 204(12), pp. 3037–3047. doi: 10.1084/jem.20070885.
Nakamura, K. *et al.* (2018) 'Dysregulated IL-18 Is a Key Driver of Immunosuppression and a Possible Therapeutic Target in the Multiple Myeloma Microenvironment', *Cancer Cell*, 33(4), pp. 634-648.e5. doi: 10.1016/j.ccell.2018.02.007.
Nelson, J. E. and Kowdley, K. V. (2010) 'N-Acetylcysteine on Its Way to a Broader Application in Patients with Acute Liver Failure', *Hepatology*, 51(1), pp. 336–338. doi: 10.1002/hep.23459.
Nguyen, A. *et al.* (2018) 'Single cell RNA sequencing of rare immune cell populations', *Frontiers in Immunology*, 9(JUL). doi: 10.3389/fimmu.2018.01553.
Nishiyama, K. *et al.* (2015) 'Mouse CD11b+Kupffer cells recruited from bone marrow accelerate liver regeneration after partial hepatectomy', *PLoS ONE*, 10(9), pp. 1–16. doi: 10.1371/journal.pone.0136774.
Okabe, Y. and Medzhitov, R. (2014) 'Tissue-Specific Signals Control Reversible Program of Localization and Functional Polarization of Macrophages', *Cell*, 157(4), pp. 832–844. doi: 10.1038/jid.2014.371.
Paranjpe, S. *et al.* (2016) 'Combined systemic elimination of MET and EGFR signaling completely abolishes liver regeneration and leads to liver decompensation', *Hepatology*, 64(5), pp. 1711–1724. doi: 10.1016/j.physbeh.2017.03.040.
Park, Y. M. (2014) 'CD36, a scavenger receptor implicated in atherosclerosis', *Experimental and Molecular Medicine*. Nature Publishing Group, 46(6), pp. e99-7. doi: 10.1038/emm.2014.38.
Patel, A. A. *et al.* (2017) 'The fate and lifespan of human monocyte subsets in steady state and systemic inflammation', *Journal of Experimental Medicine*, 214(7), pp. 1913–1923. doi: 10.1084/jem.20170355.
Patricia Fitzgerald-Bocarsly, Dai, J. and Singh, S. (2008) 'Plasmacytoid

dendritic cells and type I IFN: 50 years of convergent history', *Cytokine Growth Factor Review*, 19(1), pp. 3–19. doi: 10.1038/jid.2014.371.
Paul, F. *et al.* (2015) 'Transcriptional Heterogeneity and Lineage Commitment in Myeloid Progenitors', *Cell*. Elsevier Inc., 163(7), pp. 1663–1677. doi: 10.1016/j.cell.2015.11.013.
Pollard, J. W. (2009) 'Trophic macrophages in development and disease', *Nature Reviews Immunology*, 9(4), pp. 259–270. doi: 10.1038/nri2528.
Pols, M. S. and Klumperman, J. (2009) 'Trafficking and function of the tetraspanin CD63', *Experimental Cell Research*. Elsevier Inc., 315(9), pp. 1584–1592. doi: 10.1016/j.yexcr.2008.09.020.
Raj, A. and van Oudenaarden, A. (2008) 'Nature, Nurture, or Chance: Stochastic Gene Expression and Its Consequences', *Cell*, 135(2), pp. 216–226. doi: 10.1016/j.cell.2008.09.050.
Ramachandran, P. *et al.* (2012) 'Differential Ly-6C expression identifies the recruited macrophage phenotype, which orchestrates the regression of murine liver fibrosis', *Proceedings of the National Academy of Sciences of the United States of America*, 109(46), pp. 3186–95. doi: 10.1073/pnas.1119964109.
Ravichandran, K. S. and Lorenz, U. (2007) 'Engulfment of apoptotic cells: Signals for a good meal', *Nature Reviews Immunology*, 7(12), pp. 964–974. doi: 10.1038/nri2214.
Reddy, S. M. *et al.* (2002) 'Phagocytosis of Apoptotic Cells by Macrophages Induces Novel Signaling Events Leading to Cytokine-Independent Survival and Inhibition of Proliferation: Activation of Akt and Inhibition of Extracellular Signal-Regulated Kinases 1 and 2', *The Journal of Immunology*, 169(2), pp. 702–713. doi: 10.4049/jimmunol.169.2.702.
Regev, A. *et al.* (2017) 'The Human Cell Atlas AND HUMAN CELL ATLAS MEETING PARTICIPANTS', *eLIFE*, pp. 1–30. Available at: https://doi.org/10.7554/eLife.27041.001.
Rostom, R. *et al.* (2017) 'Computational approaches for interpreting scRNA-seq data', *FEBS Letters*, 591(15), pp. 2213–2225. doi: 10.1002/1873-3468.12684.
Ryan, P. M. *et al.* (2012) 'Endogenous interleukin-4 regulates glutathione synthesis following acetaminophen-induced liver injury in mice', *Chemical Research in Toxicology*, 25(1), pp. 83–93. doi: 10.1021/tx2003992.
Ryoo, I. geun and Kwak, M. K. (2018) 'Regulatory crosstalk between the oxidative stress-related transcription factor Nfe2l2/Nrf2 and mitochondria', *Toxicology and Applied Pharmacology*. Elsevier, 359(June), pp. 24–33. doi: 10.1016/j.taap.2018.09.014.
Saiman, Y. and Friedman, S. L. (2012) 'The role of chemokines in acute liver injury', *Frontiers in Physiology*, 3 JUN(June), pp. 1–12. doi: 10.3389/fphys.2012.00213.
Sakamoto, T. *et al.* (1999) 'Mitosis and apoptosis in the liver of interleukin-6-deficient mice after partial hepatectomy', *Hepatology*, 29(2), pp. 403–411. doi: 10.1002/hep.510290244.
Salazar-Mather, T. P., Orange, J. S. and Biron, C. A. (1998) 'Early murine cytomegalovirus (MCMV) infection induces liver natural killer (NK) cell

inflammation and protection through macrophage inflammatory protein 1α (MIP-1α)-dependent pathways', *Journal of Experimental Medicine*, 187(1), pp. 1–14. doi: 10.1084/jem.187.1.1.

Sarin, S. K. and Choudhury, A. (2016) 'Acute-on-chronic liver failure: Terminology, mechanisms and management', *Nature Reviews Gastroenterology and Hepatology*. Nature Publishing Group, 13(3), pp. 131–149. doi: 10.1038/nrgastro.2015.219.

Sasmono, R. T. *et al.* (2003) 'A M-CSF green fluorescent protein transgene is expressed throughout the mononuclear phagocyte system of the mouse.', *Gene*, 101(3), pp. 1155–1163. doi: 10.1182/blood-2002-02-0569.Supported.

Satoh, T. *et al.* (2017) 'Identification of an atypical monocyte and committed progenitor involved in fibrosis', *Nature*. Nature Publishing Group, 541(7635), pp. 96–101. doi: 10.1038/nature20611.

Sauter, K. A. *et al.* (2014) 'The MacBlue Binary Transgene (csf1r-gal4VP16/UAS-ECFP) provides a novel marker for visualisation of subsets of monocytes, macrophages and dendritic cells and responsiveness to CSF1 administration', *PLoS ONE*, 9(8). doi: 10.1371/journal.pone.0105429.

Scaffidi, P., Misteli, T. and Bianchi, M. E. (2002) 'Release of chromatin protein HMGB1 by necrotic cells triggers inflammation', *Nature*, 418(6894), pp. 191–195. doi: 10.1038/nature00858.

Schneider, C. *et al.* (2014) 'Induction of the nuclear receptor PPAR-γ 3 by the cytokine GM-CSF is critical for the differentiation of fetal monocytes into alveolar macrophages', *Nature Immunology*, 15(11), pp. 1026–1037. doi: 10.1038/ni.3005.

Scholten, D. *et al.* (2015) 'The carbon tetrachloride model in mice', *Laboratory Animals*, 49, pp. 4–11. doi: 10.1177/0023677215571192.

Scott, C. L. *et al.* (2016) 'Bone marrow derived monocytes give rise to self-renewing and fully differentiated Kupffer cells', *Nature communications*, 7(10321), pp. 1–10. doi: 10.1038/ncomms10321.

Scott, C. L. *et al.* (2018) 'The Transcription Factor ZEB2 Is Required to Maintain the Tissue-Specific Identities of Macrophages', *Immunity*. Elsevier Inc., 49(2), pp. 312-325.e5. doi: 10.1016/j.immuni.2018.07.004.

Scott, C. L. and Guilliams, M. (2018) 'The role of Kupffer cells in hepatic iron and lipid metabolism', *Journal of Hepatology*. European Association for the Study of the Liver, 69(5), pp. 1197–1199. doi: 10.1016/j.jhep.2018.02.013.

See, P. *et al.* (2017) 'Mapping the human DC lineage through the integration of high-dimensional techniques', *Science*, 356(6342). doi: 10.1126/science.aag3009.

See, P. *et al.* (2018) 'A single-cell sequencing guide for immunologists', *Frontiers in Immunology*, 9(OCT), pp. 1–13. doi: 10.3389/fimmu.2018.02425.

Sekine, S. *et al.* (2007) 'Liver-specific loss of β-catenin results in delayed hepatocyte proliferation after partial hepatectomy', *Hepatology*, 45(2), pp. 361–368. doi: 10.1002/hep.21523.

Selzner, N. *et al.* (2003) 'ICAM-1 triggers liver regeneration through leukocyte recruitment and Kupffer cell-dependent release of TNF-α/IL-6 in mice', *Gastroenterology*, 124(3), pp. 692–700. doi: 10.1053/gast.2003.50098.

Serbina, N. V. and Pamer, E. G. (2006) 'Monocyte emigration from bone marrow during bacterial infection requires signals mediated by chemokine receptor CCR2', *Nature Immunology*, 7(3), pp. 311–317. doi: 10.1038/ni1309.

Serbina, N. V., Shi, C. and Pamer, E. G. (2012) 'Monocyte-mediated immune defense against murine listeria monocytogenes infection', *Advances in Immunology*, 113, pp. 119–134. doi: 10.1016/B978-0-12-394590-7.00003-8.

Shaw, T. N. *et al.* (2018) 'Tissue-resident macrophages in the intestine are long lived and defined by Tim-4 and CD4 expression', *Journal of Experimental Medicine*, 215(6), pp. 1507–1518. doi: 10.1084/jem.20180019.

Shi, J. *et al.* (2018) 'Cre Driver Mice Targeting Macrophages', *Methods Mol Biol*, 1784. doi: 10.1007/978-4-431-55855-2_10.

Sierro, F. *et al.* (2017) 'A Liver Capsular Network of Monocyte-Derived Macrophages Restricts Hepatic Dissemination of Intraperitoneal Bacteria by Neutrophil Recruitment', *Immunity*, 47(2), pp. 374-388.e6. doi: 10.1016/j.immuni.2017.07.018.

Singhal, R., Ganey, P. E. and Roth, R. A. (2012) 'Complement activation in acetaminophen-induced liver injury in mice', *J Pharmacol Exp Ther*, 341(2), pp. 377–385. doi: 10.1124/jpet.111.189837.

Stanger, B. Z. (2015) 'Cellular Homeostasis and Repair in the Mammalian Liver', *Annu Rev Physiol.*, 77, pp. 179–200. doi: 10.1126/science.1249098.Sleep.

Stolz, D. B. *et al.* (1999) 'Growth factor signal transduction immediately after two-thirds partial hepatectomy in the rat', *Cancer Research*, 59(16), pp. 3954–3960.

Surewaard, B. G. J. and Kubes, P. (2017) 'Measurement of bacterial capture and phagosome maturation of Kupffer cells by intravital microscopy', *Methods*, 128, pp. 12–19. doi: 10.1016/j.ymeth.2017.05.004.

T'Jonck, W., Guilliams, M. and Bonnardel, J. (2018) 'Niche signals and transcription factors involved in tissue-resident macrophage development', *Cellular Immunology*. Elsevier, 330(February), pp. 43–53. doi: 10.1016/j.cellimm.2018.02.005.

Tacke, F. and Zimmermann, H. W. (2014) 'Macrophage heterogeneity in liver injury and fibrosis', *Journal of Hepatology*. European Association for the Study of the Liver, 60(5), pp. 1090–1096. doi: 10.1016/j.jhep.2013.12.025.

Tamoutounour, S. *et al.* (2013) 'Origins and functional specialization of macrophages and of conventional and monocyte-derived dendritic cells in mouse skin', *Immunity*, 39(5), pp. 925–938. doi: 10.1016/j.immuni.2013.10.004.

Tan, X. *et al.* (2006) 'Conditional Deletion of β-Catenin Reveals Its Role in Liver Growth and Regeneration', *Gastroenterology*, 131(5), pp. 1561–1572. doi: 10.1053/j.gastro.2006.08.042.

Taub, R. (2004) 'Liver regeneration: From myth to mechanism', *Nature Reviews Molecular Cell Biology*, 5(10), pp. 836–847. doi: 10.1038/nrm1489.

Taylor, N. J. *et al.* (2013) 'Circulating neutrophil dysfunction in acute liver failure', *Hepatology*, 57(3), pp. 1142–1152. doi: 10.1002/hep.26102.

Thornley, T. B. *et al.* (2014) 'Fragile TIM-4–expressing tissue resident macrophages are migratory and immunoregulatory', *Journal of Clinical Investigation*, 124(8), pp. 3443–3454. doi: 10.1172/JCI73527.Introduction.

Togo, S. *et al.* (2004) 'Mechanism of liver regeneration after partial hepatectomy using mouse cDNA microarray', *Journal of Hepatology*, 40(3), pp. 464–471. doi: 10.1016/j.jhep.2003.11.005.

Trefts, E., Gannon, M. and Wasserman, D. H. (2017) 'The liver', *Current Biology*, 27(21), pp. R1147–R1151. doi: 10.1016/j.cub.2017.09.019.

Triantafyllou, E. *et al.* (2017) 'MerTK expressing hepatic macrophages promote the resolution of in fl ammation in acute liver failure', *Gut*, doi:10.113, pp. 1–15. doi: 10.1136/gutjnl-2016-313615.

Triantafyllou, E. *et al.* (2018) 'The Role of Monocytes and Macrophages in Acute and Acute-on-Chronic Liver Failure', *Frontiers in immunology*, 9(December), p. 2948. doi: 10.3389/fimmu.2018.02948.

Tumanov, A. V *et al.* (2009) 'T Cell-Derived Lymphotoxin Regulates Liver Regeneration', *Gastroenterology*. AGA Institute American Gastroenterological Association, 136(2), pp. 694-704.e4. doi: 10.1053/j.gastro.2008.09.015.

Vázquez-Romero, A. *et al.* (2013) 'Multicomponent reactions for de novo synthesis of bodipy probes: In vivo imaging of phagocytic macrophages', *Journal of the American Chemical Society*, 135(43), pp. 16018–16021. doi: 10.1021/ja408093p.

Villani, A.-C. *et al.* (2017) 'Single-cell RNA-seq reveals new types of human blood dendritic cells, monocytes and progenitors', 356(6335). doi: 10.1002/cncr.31084.Talking.

Villani, A. *et al.* (2017) 'Single-cell RNA-seq reveals new types of human blood dendritic cells, monocytes, and progenitors', *Science*, 16. doi: 10.1126/science.aah4573.

Wang, J. and Kubes, P. (2016) 'A Reservoir of Mature Cavity Macrophages that Can Rapidly Invade Visceral Organs to Affect Tissue Repair', *Cell*. Elsevier Inc., 165(3), pp. 668–678. doi: 10.1016/j.cell.2016.03.009.

Wang, L. *et al.* (2009) 'Disruption of the transcription factor recombination signal-binding protein-Jκ (RBP-J) leads to veno-occlusive disease and interfered liver regeneration in mice', *Hepatology*, 49(1), pp. 268–277. doi: 10.1002/hep.22579.

Wang, Lin *et al.* (2012) 'Liver sinusoidal endothelial cell progenitor cells promote liver regeneration in rats', *Journal of Clinical Investigation*, 122(4), pp. 1567–1573. doi: 10.1172/JCI58789.

Wang, X. *et al.* (2013) 'High-mobility group box 1 (HMGB1)-Toll-like receptor (TLR)4-interleukin (IL)-23-IL-17A axis in drug-induced damage-associated lethal hepatitis: Interaction of γδ T cells with macrophages', *Hepatology*, 57(1), pp. 373–384. doi: 10.1002/hep.25982.

Wang, X. *et al.* (2015) 'Regulatory T cells ameliorate acetaminophen-induced immune-mediated liver injury', *International Immunopharmacology*. Elsevier B.V., 25(2), pp. 293–301. doi: 10.1016/j.intimp.2015.02.008.

Watkins, S. K. *et al.* (2007) 'IL-12 Rapidly Alters the Functional Profile of Tumor-Associated and Tumor-Infiltrating Macrophages In Vitro and In Vivo', *The Journal of Immunology*, 178(3), pp. 1357–1362. doi: 10.4049/jimmunol.178.3.1357.

Williams, R. *et al.* (2018) 'Disease burden and costs from excess alcohol consumption, obesity, and viral hepatitis: fourth report of the Lancet Standing Commission on Liver Disease in the UK', *The Lancet*. Elsevier Ltd, 391(10125), pp. 1097–1107. doi: 10.1016/S0140-6736(17)32866-0.

Williams, R. and Horton, R. (2013) 'Liver disease in the UK: A Lancet Commission', *The Lancet*. Elsevier Ltd, 382(9904), pp. 1537–1538. doi: 10.1016/S0140-6736(13)62152-2.

Woo, M. S. *et al.* (2016) 'Cell surface CD36 protein in monocyte/macrophage contributes to phagocytosis during the resolution phase of ischemic stroke in mice', *Journal of Biological Chemistry*, 291(45), pp. 23654–23661. doi: 10.1074/jbc.M116.750018.

Woolbright, B. L. and Jaeschke, H. (2017a) 'Role of the inflammasome in acetaminophen-induced liver injury and acute liver failure', *Journal of Hepatology*. doi: 10.1016/j.jhep.2016.11.017.

Woolbright, B. L. and Jaeschke, H. (2017b) 'Role of the Inflammasome in Acetaminophen-induced Liver Injury and Acute Liver Failure', *Journal of Hepatology*, 66(4), pp. 836–848. doi: 10.1126/science.1249098.Sleep.

Wyke, R. J. *et al.* (1982) 'Serum stimulatory activity and polymorphonuclear leucocyte movement in patients with fulminant hepatic failure', *Clinical and Experimental Immunology*, 50(2), pp. 442–449.

Wyler, S. L. *et al.* (2016) 'Monocyte chemoattractant protein-1 is not required for liver regeneration after partial hepatectomy', *Journal of Inflammation*. Journal of Inflammation, 13(28), pp. 1–8. doi: 10.1186/s12950-016-0136-1.

Xiong, X. *et al.* (2019) 'Landscape of Intercellular Crosstalk in Healthy and NASH Liver Revealed by Single-Cell Secretome Gene Analysis', *Molecular Cell*, 75(3), pp. 644-660.e5. doi: 10.1016/j.molcel.2019.07.028.

Xu, C. P. *et al.* (2007) 'Dynamic changes and mechanism of intestinal endotoxemia in partially hepatectomized rats', *World Journal of Gastroenterology*, 13(26), pp. 3592–3597.

Xu, H. *et al.* (2008) 'Critical but divergent roles for CD62L and CD44 in directing blood monocyte trafficking in vivo during inflammation', *Blood*, 112(4), pp. 1166–1174. doi: 10.1182/blood-2007-06-098327.

Xue, J. *et al.* (2014) 'Transcriptome-Based Network Analysis Reveals a Spectrum Model of Human Macrophage Activation', *Immunity*. Elsevier Inc., 40(2), pp. 274–288. doi: 10.1016/j.immuni.2014.01.006.

Yamada, Y. *et al.* (1997) 'Initiation of liver growth by tumor necrosis factor: Deficient liver regeneration in mice lacking type I tumor necrosis factor

receptor', *Proceedings of the National Academy of Sciences of the United States of America*, 94(4), pp. 1441–1446. doi: 10.1073/pnas.94.4.1441.

Yan, M. *et al.* (2018) 'Mechanisms of acetaminophen-induced liver injury and its implications for therapeutic interventions', *Redox Biology*. Elsevier B.V., 17(March), pp. 274–283. doi: 10.1016/j.redox.2018.04.019.

Yáñez, A. *et al.* (2017) 'Granulocyte-Monocyte Progenitors and Monocyte-Dendritic Cell Progenitors Independently Produce Functionally Distinct Monocytes', *Immunity*, 47(5), pp. 890-902.e4. doi: 10.1016/j.immuni.2017.10.021.

Yang, L. *et al.* (2015) 'KIM-1 – mediated phagocytosis reduces acute injury to the kidney', 125(4), pp. 1620–1636. doi: 10.1172/JCI75417.tors.

Yang, W. *et al.* (2019) 'Neutrophils promote the development of reparative macrophages mediated by ROS to orchestrate liver repair', *Nature Communications*. Springer US, 10(1). doi: 10.1038/s41467-019-09046-8.

Yang, Y. A. *et al.* (2006) 'Smad3 reduces susceptibility to hepatocarcinoma by sensitizing hepatocytes to apoptosis through downregulation of Bcl-2', *Cancer Cell*, 9(6), pp. 445–457. doi: 10.1016/j.ccr.2006.04.025.

Yee, S. B. *et al.* (2007) 'Hepatoprotective role of endogenous interleukin-13 in a murine model of acetaminophen-induced liver disease', *Chemical Research in Toxicology*, 20(5), pp. 734–744. doi: 10.1021/tx600349f.

Yona, S. *et al.* (2013) 'Fate Mapping Reveals Origins and Dynamics of Monocytes and Tissue Macrophages under Homeostasis', *Immunity*. Elsevier, 38(1), pp. 79–91. doi: 10.1016/j.immuni.2012.12.001.

Yoon, E. *et al.* (2016) 'Acetaminophen-Induced Hepatotoxicity: a Comprehensive Update', *Journal of Clinical and Translational Hepatology*, 4(2), pp. 131–142. doi: 10.14218/jcth.2015.00052.

You, Q. *et al.* (2013) 'Role of hepatic resident and infiltrating macrophages in liver repair after acute injury', *Biochemical Pharmacology*. Elsevier Inc., 86(6), pp. 836–843. doi: 10.1016/j.bcp.2013.07.006.

Yu, Y. R. A. *et al.* (2016) 'A protocol for the comprehensive flow cytometric analysis of immune cells in normal and inflamed murine non-lymphoid tissues', *PLoS ONE*, 11(3), pp. 1–23. doi: 10.1371/journal.pone.0150606.

Zhang, C. *et al.* (2018) 'Macrophage-derived IL-1α promotes sterile inflammation in a mouse model of acetaminophen hepatotoxicity', *Cellular and Molecular Immunology*, 15(11), pp. 973–982. doi: 10.1038/cmi.2017.22.

Zhang, H. *et al.* (2013) 'Hepatic B cells are readily activated by Toll-like receptor-4 ligation and secrete less interleukin-10 than lymphoid tissue B cells', *Clinical and Experimental Immunology*, 173(3), pp. 473–479. doi: 10.1111/cei.12126.

Zhang, N. *et al.* (2019) 'Expression of factor V by resident macrophages boosts host defense in the peritoneal cavity', *The Journal of experimental medicine*, 216(6), pp. 1291–1300. doi: 10.1084/jem.20182024.

Zheng, C. *et al.* (2017) 'Landscape of Infiltrating T Cells in Liver Cancer Revealed by Single-Cell Sequencing', *Cell*. Elsevier, 169(7), pp. 1342-

1356.e16. doi: 10.1016/j.cell.2017.05.035.
Zheng, G. X. Y. *et al.* (2017) 'Massively parallel digital transcriptional profiling of single cells', *Nature Communications*. Nature Publishing Group, 8, pp. 1–12. doi: 10.1038/ncomms14049.
Zhu, X. and Uetrecht, J. (2013) 'A novel T(H) 17-type cell is rapidly increased in the liver in response to acetaminophen-induced liver injury : T(H) 17 cells and the innate immune response', *Journal of immunotoxicology*, 10(3), pp. 287–91. doi: 10.3109/1547691X.2012.724730.
Ziegenhain, C. *et al.* (2017) 'Comparative Analysis of Single-Cell RNA Sequencing Methods', *Molecular Cell*, 65(4), pp. 631-643.e4. doi: 10.1016/j.molcel.2017.01.023.
Zigmond, E. *et al.* (2014) 'Infiltrating Monocyte-Derived Macrophages and Resident Kupffer Cells Display Different Ontogeny and Functions in Acute Liver Injury', *Journal of immunology*, 193(1), pp. 344–53. doi: 10.4049/jimmunol.1400574.
Zimmerman, H. J. and Maddrey, W. C. (1995) 'Acetaminophen (paracetamol) hepatotoxicity with regular intake of alcohol: Analysis of instances of therapeutic misadventure', *Hepatology*, 22(3), pp. 767–773. doi: 10.1016/0270-9139(95)90295-3.
Zimmermann, H. W., Trautwein, C. and Tacke, F. (2012) 'Functional role of monocytes and macrophages for the inflammatory response in acute liver injury', *Frontiers in Physiology*, 3 OCT(October), pp. 1–18. doi: 10.3389/fphys.2012.00056.
Zou, Y. *et al.* (2012) 'Four waves of hepatocyte proliferation linked with three waves of hepatic fat accumulation during partial hepatectomy-induced liver regeneration', *PLoS ONE*, 7(2). doi: 10.1371/journal.pone.0030675.
Zywitza, V. *et al.* (2018) 'Single-Cell Transcriptomics Characterizes Cell Types in the Subventricular Zone and Uncovers Molecular Defects Impairing Adult Neurogenesis', *Cell Reports*. ElsevierCompany., 25(9), pp. 2457-2469.e8. doi: 10.1016/j.celrep.2018.11.003.